Global Precipitation Measurement (GPM) Science Implementation Plan
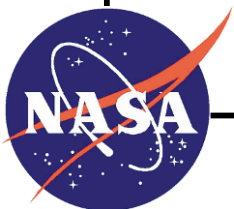
Date: April 2, 2013

Goddard Space Flight Center
Greenbelt, Maryland 20771
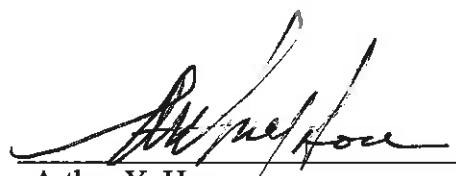
Signature Page

Approvals:

_____ 4/5/13   _____ 4/5/2013
Jack Kaye   Date   Ramesh Kakar   Date
Associate Director for Research   TRMM/GPM Program Scientist
Earth Science Division   Earth Science Division
Science Mission Directorate   Science Mission Directorate
NASA Headquarters   NASA Headquarters
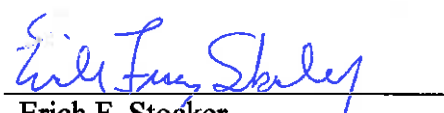
Concurrences:

_____ 4/26/13   _____ 4/19/2013
Arthur Y. Hou   Date   Gail Skofronick-Jackson   Date
GPM Project Scientist   GPM Deputy Project Scientist
Earth Science Division   Earth Science Division
Goddard Space Flight Center   Goddard Space Flight Center

_____ 4/19/13   _____ 4/23/2013
Erich F. Stocker   Date   Walter A. Petersen   Date
GPM Deputy Project Scientist   GPM Ground Validation
   for Data and Precipitation   Science Manager
   Processing System Project   Earth Sciences Office
   Manager   Wallops Island Facility
Earth Science Division   Goddard Space Flight Center
Goddard Space Flight Center

CONTENTS

Executive Summary

Water is fundamental to life on Earth. It transitions between gaseous, liquid, and solid states, dominating the behavior of the weather, climate, and ecological systems. The transport of water in all three phases is a powerful mechanism, helping to regulate the Earth's energy budget. As climate forcing changes, precipitation - which converts atmospheric water into rain or snow - can profoundly alter the global energy balance through its coupling with clouds, water vapor, atmospheric circulation, ocean circulation, soil moisture, and surface albedo. Precipitation also has a direct impact on our everyday life. It is the primary source of freshwater and has tremendous socio-economical impact through natural hazards such as hurricanes, floods, droughts, and landslides. Accurate knowledge of when, where, and how much it rains and snows is essential for improving understanding of how the Earth system functions and for making better predictions of weather, climate, natural hazard events, and freshwater resources.

The Global Precipitation Measurement (GPM) Mission is an international space network of satellites designed to provide the next generation precipitation observations around the world every 2 to 4 hours. The GPM concept centers on the deployment of a Core Observatory carrying an advanced radar/radiometer system in a non-Sun-synchronous orbit. The GPM Core Observatory will serve as a "physics observatory" to gain insights into precipitation systems and as a "reference standard" to unify and improve precipitation estimates from a constellation of research and operational satellites. GPM is a science discovery mission with integrated applications goals to advance the understanding of the Earth's water and energy cycles and extend current capabilities in a range of precipitation-related applications to directly benefit society.

The GPM Mission is currently a partnership between the National Aeronautic and Space Administration (NASA) and Japan Aerospace and Exploration Agency (JAXA), with additional partnerships with other space agencies both confirmed and under development. NASA and JAXA will provide the GPM Core Observatory. The GPM core will provide "asynoptic" observations that fill the temporal gaps between the observations made by polar-orbiting satellites at fixed local times, thereby improving the accuracy of time-integrated rain accumulation estimation and monitoring the development of storms and hurricanes in near realtime. The GPM Core Observatory is scheduled for launch in February 2014.

This document establishes the science drivers for the GPM mission, describes the mission architecture and observation requirements, provides high-level NASA implementation plans and schedules for GPM science algorithm and data system development, places GPM science activities in the context of other international missions and programs, and concludes with a list of GPM science deliverables and schedule in Section 10. Appendices are used to convey and archive details of supporting investigations, while gpm.nasa.gov provides ongoing information.

List of Contributors

Dr. Robert Adler, University of Maryland
Prof. Emmanouil Anagnostou, University of Connecticut
Prof. Ana Barros, Duke University
Dr. Peter Bauer, European Centre for Medium-Range Weather Forecasts
Dr. Thomas Bell, NASA/Goddard Space Flight Center
Prof. Ralf Bennartz, University of Wisconsin, Madison
Dr. Wesley Berg, Colorado State University
Prof. Rafael Bras, University of California, Irvine
Dr. Scott Braun, NASA/Goddard Space Flight Center
Prof. Venkatachalam Chandrasekar, Colorado State University
Dr. Ralph Ferraro, NOAA/National Environmental Satellite Data Information Service
Prof. Efi Foufoula-Georgiou, University of Minnesota
Dr. Mircea Grecu, NASA/Goddard Space Flight Center
Dr. Ziad Haddad, NASA/Jet Propulsion Laboratory
Prof. Robert Houze, University of Washington
Dr. George Huffman, NASA/Goddard Space Flight Center
Dr. Benjamin Johnson, NASA/Goddard Space Flight Center
Prof. Linwood Jones, University of Central Florida
Dr. Chris Kidd, University of Maryland
Dr. Dalia Kirschbaum, NASA/Goddard Space Flight Center
Prof. Christian Kummerow, Colorado State University
Dr. William Lau, NASA/Goddard Space Flight Center
Prof. Dennis Lettenmaier, University of Washington
Dr. Xin Lin, NASA/Goddard Space Flight Center
Prof. Guosheng Liu, Florida State University
Dr. Robert Meneghini, NASA/Goddard Space Flight Center
Dr. Stephen Joseph Munchak, NASA/Goddard Space Flight Center
Dr. William Olson, NASA/Goddard Space Flight Center
Dr. Christa Peters-Lidard, NASA/Goddard Space Flight Center
Prof. Grant Petty, University of Wisconsin, Madison
Dr. Franklin Robertson, NASA/Marshall Space Flight Center
Prof. Christopher Ruf, University of Michigan
Prof. Steven Rutledge, Colorado State University
Prof. Marshall Shepherd, University of Georgia
Dr. James Shiue, NASA/Goddard Space Flight Center
Dr. Eric Smith, Climatek, Inc.
Prof. Soroosh Sorooshian, University of California, Irvine
Prof. David Staelin, Massachusetts Institute of Technology
Dr. Wei-Kuo Tao, NASA/Goddard Space Flight Center
Dr. Joe Turk, NASA/Jet Propulsion Laboratory
Dr. Fuzhong Weng, NOAA/National Environmental Satellite Data Information Service
Prof. Thomas Wilheit, Texas A&M University
Prof. Eric Wood, Princeton University
Prof. Edward Zipser, University of Utah

1.   Introduction

Precipitation affects many aspects of our everyday life and is a key component of the Earth's water and energy cycle. It is the primary source of freshwater and has a tremendous impact on society through extreme weather events such as hurricanes, floods, droughts, and landslides. Long-term records of high-quality global precipitation estimates at small temporal and spatial scales are vital for understanding the Earth system under changing climatic conditions and for improved societal applications ranging from freshwater resource management to predictions of high-impact weather events.

While the need is great, accurate and timely information on global precipitation is difficult to obtain due to the large space-time variability of precipitating systems, the limited rainfall networks over land, and the impracticality of making extensive measurements over oceans. It follows that a comprehensive description of the space-time variability of global precipitation can only be achieved from the vantage point of space. The Global Precipitation Measurement (GPM) mission will measure precipitation on a global basis with sufficient Earth coverage, spatial resolution, temporal sampling, retrieval accuracy, and microphysical acuity to permit improved predictions of the Earth's climate, weather, and hydrometeorological processes as enabled by improved physical measurements and models of the water cycle across varied space and time scales.

The GPM Mission is an international space network of satellites designed to provide the next generation precipitation observations around the world every 2 to 4 hours. It is a science mission with integrated applications goals. The GPM concept (Figure 1-1) centers on the deployment of a Core Spacecraft carrying advanced active and passive microwave sensors to function as a physics observatory to gain physical insights into precipitating systems and to serve as a reference standard to improve global precipitation estimates from a constellation of research and operational microwave sensors capable of precipitation measurements. The GPM constellation buildup follows a progressive strategy to take advantage of partner satellites that carry microwave sensors such as a conical-scanning imager or a cross-track-scanning sounder.

Building upon the success of the U.S.-Japan Tropical Rainfall Measuring Mission (TRMM), GPM is a currently a partnership between the National Aeronautic and Space Administration (NASA) and the Japan Aerospace and Exploration Agency (JAXA), with additional partnerships with other space agencies either confirmed or under development. NASA will provide the Core Spacecraft with a multi-channel microwave imager with high-frequency capabilities and JAXA will provide a dual-frequency precipitation radar at Ka and Ku bands for quantitative microphysical measurements and increased sensitivity to light rain and snow relative to TRMM, as well as providing launch services for the Core Spacecraft. The GPM Core Observatory is scheduled for launch in 2014. The GPM Mission represents a major international endeavor to provide more accurate and more frequent global precipitation observations to advance scientific understanding of the Earth's water and energy cycle and to directly benefit society by extending current capabilities in weather/climate forecasting, weather-related natural hazard prediction, and freshwater resource management.
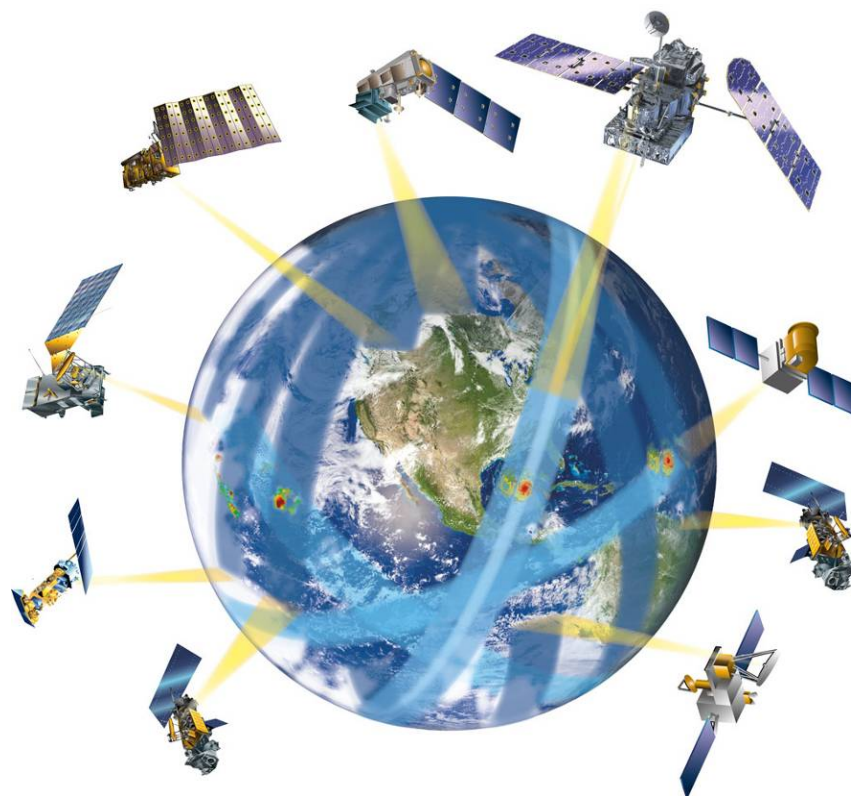
Figure 1-1: The GPM Mission concept, shown with the Core Observaory (upper right corner).

1.1   *Precipitation Measurements in the Context of Earth Observations*

Water is fundamental to the life on Earth. Its phase transitions among the gaseous, liquid, and solid states dominating the behavior of the weather, climate, and ecological systems. The movement of water in all three phases is a powerful vehicle for regulating the energy budget of the Earth system. As climate forcing varies, precipitation can profoundly alter the global energy balance through coupling with clouds, water vapor, atmospheric circulation (through latent heat release), ocean circulation (by modulating ocean salinity), soil moisture, and surface albedo (via snow cover). A better understanding of how precipitation interacts with these basic components of the Earth system is vital for gaining physical insights into climate sensitivity, advancing climate prediction capabilities, monitoring freshwater availability, and forecasting floods and landslides. Knowing when, where, and how much it rains or snows around the world is essential in taking on these challenges.

The GPM Mission will address these challenges by providing key measurements to advance the objectives of a host of international scientific programs and activities. These include the Global Energy and Water Cycle Experiment (GEWEX) established under the World Climate Research Program (WCRP) to understand the global hydrological cycle and energy fluxes through observations and modeling of the atmosphere, the land surface and upper oceans (see GEWEX 2007). The Integrated Global Water Cycle Observations (IGWCO) is an activity directed by the Integrated Global Observation Strategy (IGOS) Partners at the request of the United Nations to provide comprehensive information about the global environment to guide

policy-making for sustainable development and environmental protection. The International Precipitation Working Group (IPWG), is an international body cosponsored by the World Meteorological Organization (WMO) and the Coordination Group for Meteorological Satellites (CGMS) to improve space-based precipitation measurements and their utilization in research and applications. GPM observations are of interest to these activities and programs.

Within the United States, the GPM Mission is the Earth Science community's response to the urgent need to decipher how the water cycle changes in a changing climate and the desire to enhance a broad range of societal applications (NRC 2007a). As NASA's flagship mission focusing on the Global Water and Energy Cycle (GWEC) research and applications, GPM is an important contribution to the U.S. Climate Change Science Program and the U.S. Weather Research Program. While GPM measurements are essential for understanding the global water/energy cycle, precipitation information must be used synergistically with complementary observations to gain physical insights into the complex interactions between water and other components of the Earth system from the overlapping of different types of measurements. For instance, the processes that govern the onset of precipitation may be gleaned from the combination of GPM measurements with observations of water vapor, clouds, and aerosols. These observations may be provided by other satellite sensors including those under development by JAXA and the European Space Agency (ESA) such as the EarthCARE mission. Similarly, soil moisture information, when combined with precipitation, can be used to improve forecasts of droughts and floods. The same synergy exists between GPM and possible future missions targeting snow and cold surface processes for understanding how melting snow affects soil moisture and runoff. Recognizing that the global precipitation distribution provides a context in which to interpret the causes and consequences of local variations in water-related observations, the Earth Sciences Decadal Survey identified GPM as the first in a series of missions targeting the Earth's water and energy cycle in the coming decade (NRC 2007b). The GPM validation program, through its connection to atmospheric and surface modeling and observations, will have a key role in relating observations from diverse sources into a coherent framework.

Internationally, GPM has been identified in 2002 as an outstanding example of peaceful uses of space in the United Nations Program on "Remote Sensing for Substantive Water Management in Arid and Semi-Arid Areas". The GPM concept is currently serving as the scientific cornerstone for developing a multi-national satellite constellation to monitor global precipitation by the Committee on Earth Observation Satellites (CEOS) under the auspices of the Global Earth Observing System of Systems (GEOSS), an inter-governmental effort to provide comprehensive, long-term, and coordinated observations of the Earth. During its mission life, GPM is envisioned to be a mature realization of the CEOS Precipitation Constellation.

1.2   *GPM Mission Architecture*

GPM is an international satellite mission specifically designed to unify and advance global precipitation measurements from a heterogeneous set of research and operational microwave sensors to provide next-generation precipitation measurements from space around the world every 2 to 4 hours. Under the GPM partnership between NASA and JAXA, the two agencies are jointly developing a GPM Core Observatory carrying advanced active and passive precipitation sensors in a non-Sun-synchronous orbit at 65° inclination to serve as a reference

standard for the inter-calibration of constellation microwave radiometers. The Core Observatory will carry the first space-borne Ku/Ka-band Dual-frequency Precipitation Radar (DPR) and a multi-spectral (10 to 183 GHz) GPM Microwave Imager (GMI). The GMI is designed with special attention to instrument accuracy and stability to unify radiometric measurements by a constellation of microwave sensors. In addition, the DPR and GMI on the Core Observatory will together function as a precipitation physics observatory to provide 3-dimensional complementary information from active and passive sensors to improve the physical fidelity of precipitation algorithms for the GPM Core and constellation sensors. The increased sensitivity of the DPR relative to the TRMM radar, together with the high-frequency channels on the GMI, will give GPM new capabilities to take on the challenge of measuring light rain and falling snow, which account for large fractions of precipitation occurrences outside the Tropics, especially in winter seasons over land. The GPM Core Observatory is scheduled for launch in February 2014 from Tanegashima Island, Japan, with a prime mission life of 3 years and consumables sized for a minimum of 5 years of operation.

The GPM constellation design follows a "rolling wave" strategy with a flexible architecture to take advantage of satellites of opportunity capable of precipitation measurements. Each constellation member may have its unique scientific or operational objectives but contributes microwave brightness temperature measurements to GPM for the generation and dissemination of uniform constellation-based global precipitation products to worldwide user communities. In addition to DPR and GMI, sensors that will contribute data to GPM include (1) the Special Sensor Microwave Imager/Sounder (SSMIS) instruments on the U.S. Defense Meteorological Satellite Program (DMSP) satellites (Kunkee et al. 2008), (2) the Advanced Microwave Scanning Radiometer-2 (AMSR-2) on JAXA's Global Change Observation Mission - Water (GCOM-W1) satellite (Shimoda 2005), (3) the Multi-Frequency Microwave Scanning Radiometer (MADRAS) and the multi-channel microwave humidity sounder (SAPHIR) on the French-Indian Megha-Tropiques satellite (Desbois et al. 2003), (4) the Microwave Humidity Sounder (MHS) instrument on the NOAA-19 satellite, (5) the MHS on European MetOp satellites (Edward and Pawlak 2000), (6) the Advanced Technology Microwave Sounder (ATMS) instruments on the National Polar-orbiting Operational Environmental Satellite System (NPOESS) Preparatory Project (NPP) satellite, (7) the ATMS instruments on the Joint Polar Satellite System (JPSS) satellites (Bunin et al. 2004), and (8) a microwave imager in the planning stage by the Department of Defense as a DMSP follow-on. As more nations contribute to precipitation observations from space, it is envisioned that GPM sampling can be further augmented by additional microwave radiometers such as the Chinese FY-3 series (ASM 2008) and the Russian "MTVZA" sounder/imagers (Cherny et al. 2002). GPM will continue to establish throughout its mission additional partnerships with international space agencies to enhance the GPM constellation's coverage and sampling, and collaborate with research and operational organizations to build a worldwide network of robust ground validation (GV) sites and foremost international science teams.

The GPM Core satellite instrumentation and orbit is designed to relate a database of possible precipitation profile structures as the physical basis for interpreting radiometric measurements by members of the GPM constellation. This additional *a priori* information from the GPM Core simplifies the assumptions used in the retrievals for the constellation members. Thus the Core satellite with a design life of 3 years or more will improve constellation retrievals not only from the past, but also for decades to come when only constellation radiometers exist by reprocessing all existing precipitation radiometer data using the GPM transfer standard database.

For mission operations, product validation, and data dissemination, the GPM Mission is supported on the ground by (1) a NASA-provided mission operations system for the operation of the GPM Core Observatory, (2) a Ground Validation System (GVS) consisting of an array of dedicated and cooperative ground validation sites provided by NASA, JAXA, and GPM partners, and (3) a NASA-provided Precipitation Processing System (PPS) and a JAXA-provided data system to provide - in coordination with other GPM partner data processing centers - near-real-time and standard global precipitation products. The GPM data products will include three levels of processing: Level 1 processing of radar power/microwave radiances, Level 2 processing of instantaneous geophysical parameters; and Level 3 processing of spatially/temporally averaged geophysical parameters from one or more GPM constellation instruments.

1.3 *GPM Science Organization*

The NASA Precipitation Measurement Missions (PMM) Science Program, which supports both TRMM and GPM, is administered by the TRMM/GPM Program Scientist at NASA Headquarters. The program comprises three elements: (1) a PMM Science Team, which supports algorithm development, evaluation, and improvements for TRMM and GPM data products, and conducts precipitation science research, (2) a designated PMM Algorithm Team, which is responsible for implementing all algorithm codes and delivering them to the NASA PPS for the processing of GPM data products, and (3) PMM ground-based facility instruments supporting NASA satellite missions and field experiments pertaining to precipitation.

The PMM Science Team is competitively selected and periodically renewed through NASA's Research Opportunities in Space and Earth Sciences (ROSES) announcements. The PMM Algorithm Team comprises members of the PMM Science Team assigned by the TRMM/GPM Program Scientist to serve as lead developers to implement and deliver Level 2, 3, and 4 algorithm codes to the PPS on an established schedule (Level 1 codes are provided by the instrument developers). After launch, the PMM Algorithm Team is responsible for data calibration and validation of GPM standard data products. During the mission life, the PMM Algorithm Team will provide additional deliveries of science software for calibration updates and algorithm improvements, as necessary.

All GPM science activities in the United States, including the PMM Science Team, PMM Algorithm Team, PMM Ground Validation Facility Instruments, and PPS development, are led by the GPM Project Scientist under the direction of the GPM Program Scientist. PPS development, under direction of the GPM Project Scientist, is delegated to the GPM Deputy Project Scientist for Data. The GPM Flight Project provides the GPM Project Scientist the necessary resources to manage and coordinate PMM science activities to meet all GPM Project science requirements. GPM science activities in Japan are carried out in parallel under the direction of JAXA GPM Project Scientist and program managers.

As a key element of the NASA GPM program, the PPS implements the PMM-delivered science algorithm software into data production code, and provides the data processing equipment required by GPM. The PPS Team works closely with the PMM Algorithm Team to ensure that algorithms perform as designed throughout the data processing stream. The PPS is sized to handle all data from the NASA Core Observatory and partner data sets. During operations the PPS Team produces the standard data products, integrates new versions of science software as required, reprocessing data when new software requires it. The PPS is central to

NASA's creation of measurement-based data systems to process precipitation data products focused on the measurements rather than specific missions.

NASA and JAXA have agreed to pursue joint GPM Level 2 algorithm development, under the direction of NASA and JAXA GPM Project Scientists. This agreement does not preclude NASA and JAXA to pursue the development of non-standard GPM algorithms and data products. The selection of GPM Level 2 standard data products is the responsibility of the NASA-JAXA Joint PMM Science Team (JPST) co-chaired by the NASA and JAXA GPM Program Scientists.

GPM Ground Validation (GV) is implemented as an integrated element between the PMM Science Program and the GPM Flight Project. The PMM Science Program provides a number of facility ground instruments supporting GPM GV activities under the management of the TRMM/GPM Program Scientist at NASA/HQ, supported by the GPM Project Scientist at NASA/Goddard. The GPM Flight Project provides the GPM Ground Validation System (GVS) comprising GPM-specific ground instruments (e.g., the Dual-frequency Dual-polarized Doppler Radar (D3R) Ka-Ku-Band ground radar) and is responsible for the operation and maintenance of GPM field campaigns and GV data processing under the management of the GPM Project Manager at NASA/Goddard within the purview of the GPM Program Executive at NASA/HQ. The GPM Project Scientist provides high-level supervision and is supported by the GPM GV Science Manager and the GPM Project GVS Manager in the planning and implementation of all aspects of GPM GV activities. The GV Science Manager reports directly to the GPM Project Scientist and leads the coordination of members of the PMM Science Team and the GPM GV Advisory Panel in developing and implementing requisite science requirements and data collections for precipitation retrieval algorithm development and evaluation. The GPM Flight Project is responsible for the development and operations of the GPM GVS. The GPM Project GVS Manager has budget and management responsibilities for GVS observational hardware, data collection, processing, and storage funded under the GPM Project. The GPM Project GVS Manager takes directions from the GPM Project Scientist on all GV science matters but reports directly to the GPM Project management on matters relating to GVS budget and systems engineering.

1.4   *International and Interagency Science Collaboration*

Satellite partners associated with GPM include those listed in Section 1.2 GPM Mission Architecture. These satellite partners are United States domestic partners (NOAA, DOD) with international partners from EUMETSAT (European Organisation for the Exploitation of Meteorological Satellites) and ISRO/CNES (India/France).

International scientific investigators submit no-cost proposals to the NASA PMM Science Program to establish joint research projects that complement existing PMM Science Team activities in support of algorithm development, ground validation, and data utilization for the GPM Mission. Proposals from international investigators may be submitted at any time to the GPM Program Scientist at NASA Headquarters, together with a copy of the proposal sent to the GPM Project Scientist. Investigators of successful proposals become members of the NASA PMM Science Team. In early 2013, GPM had 22 active joint science projects with Principal Investigators from 13 countries (Argentina, Australia, Brazil, Canada, Ethiopia, Finland, France, India, Israel, Italy, South Korea, Spain, Switzerland, and the United Kingdom) as well as with

ECMWF. GPM also has an established scientific relationship with NOAA scientists with the majority of the funding supplied by NOAA for approved joint precipitation activities.

The PMM Science Program continues to seek to establish additional leveraged collaborations with international and U.S. agencies to conduct joint GV field experiments and scientific research in support of the GPM Mission.

2.   GPM Science Drivers

2.1   *New Reference Standards for Global Precipitation Measurement from Space*

Accurate knowledge of how precipitation is distributed in space and time is essential for understanding how the global water cycle interacts with other climate parameters. The current generation of multi-satellite rain products is built largely on the algorithm development and validation activities of TRMM, focusing on medium-to-heavy rainfall in the Tropics and subtropics. Outside the Tropics, light rain and snowfall account for nearly half of the precipitation events (Mugnai et al. 2007). Measurements of light rainfall and cold-season solid precipitation in the mid and high latitudes require not only more capable sensors but also new retrieval algorithms. Over land, current microwave rainfall algorithms are semi-empirical with little physical basis. GPM will provide an advanced space-borne radar/radiometer system on a Core Observatory to establish a transfer standard to unify constellation sensor measurements and provide a comprehensive description of the space-time variability of precipitation around the globe.

The GPM dual-frequency radar on the Core Observatory will provide quantitative information on microphysical properties such as particle size distribution, which can be used to reduce *a priori* assumptions in radar and radiometer retrieval algorithms. By employing a differential attenuation correction made possible by having dual frequencies, the DPR will provide more accurate precipitation estimates relative to the TRMM PR, and provide a benchmark for GPM radiometric retrievals in middle and high latitudes. Microphysical measurements provided by the DPR will also facilitate the development of more physically-based algorithms to retrieve precipitation signals from passive microwave radiometers over land. In particular, the combination of the DPR and the GMI high-frequency channels will present new opportunities for algorithm advances in the passive microwave retrieval of light rain rates and snowfall rates, especially over snow-covered land surfaces. Finally, combined DPR and GMI measurements on the Core Observatory will provide a common cloud/radiance database for passive microwave radiometer retrievals, which is the key to uniting the GPM constellation radiometers into one consistent framework to produce uniform global precipitation products. Altogether, GPM will is expected to deliver more accurate and frequent global precipitation estimates than what is available today through improvements in instantaneous retrievals, space-time coverage, and inter-satellite calibration, especially outside the Tropics.

2.2   *Improved Knowledge of Global Water Cycle Variability and Its Links to Climate Change*

The globally averaged temperature has been increasing over the past century (Trenberth et al. 2007), but the impact of climate change on life is realized most acutely at local scales

(Shepherd et al. 2002). A key question is how do precipitation characteristics (*i.e.*, amount, frequency, intensity, duration, and type) change regionally in a changing climate? Current global climate models predict increased heavy rain events in the next century but disagree with respect to moderate and light rain spectra. Studies using satellite observations suggest that there are indications of increased rainfall over certain regions (tropical ocean; Adler et al., 1998) and even increased intensity in heavy rain events and in certain regions such as the Tropics (Adler et al. 2007, Lau and Wu 2007). GPM will provide global precipitation measurements with improved accuracy, coverage, and dynamic range for detecting changes in precipitation characteristics, especially in light rain and solid precipitation, to provide insights towards answering these questions.

Since precipitation is related to the latent heat released in an atmospheric column above the surface, a major motivation for quantitative precipitation measurement is to estimate the latent heat release from precipitation processes, which redistribute the differential solar energy received at the Earth's surface into the atmospheric interior to drive the large-scale circulation. A major impetus for TRMM was to quantify the intensity and variability of the latent heating released by tropical precipitation systems, which play a crucial role in global monsoon systems, the Madden-Julian Oscillation (MJO), the Inter-tropical Convergence Zone (ITCZ), and large-scale circulation systems such as the Hadley and Walker circulations. Improved accuracy in the spatial and seasonal climatological rainfall in the tropics has been attained with TRMM (Adler et al., 2009) through the use of its active and passive microwave observations and GPM will provide improved observations, with increased accuracy, of the mean and variability of tropical rainfall and latent heating associated with these Tropical climate features and El Nino Southern Oscillation (ENSO) events to understand the influence of tropical processes on the weather and climate in the middle and high latitudes. On intra-seasonal time scales, the intensity and propagation of tropical precipitation systems associated with MJO's have been a continuing challenge for global climate models and analysis systems to replicate. GPM will provide detailed observations of the spatial structure, temporal evolution, and characteristic stages of the MJO (Morita et al. 2006) and their interaction with tropical waves (Masunaga et al. 2006), as well as help clarify the role of convective systems in climate feedback processes (Back and Bretherton 2005, Del Genio et al. 2005).

In addition to model evaluation, GPM precipitation data can be assimilated into global or regional analysis/forecast systems to provide atmospheric analyses that are dynamically consistent with the observed precipitation and latent heating (e.g., Hou and Zhang 2007) and to improve operational numerical weather forecasts, as will be discussed in the next section. The continued improvement of dynamic precipitation analyses within the global data assimilation framework in the GPM era will provide the necessary tools for diagnosing the relationships between tropical heating anomalies associated with ENSO and variations in the North Atlantic Oscillation (NAO), the Pacific-North America (PNA) teleconnection pattern, and extra-tropical storm tracks.

GPM measurements will also directly improve our understanding of the cycling and variability of global terrestrial water. The utility of current satellite precipitation products in estimating spatially distributed runoff and renewable freshwater supplies is still limited (Fekete et al., 2004). With improved measurement accuracy and sampling over land and new capabilities in monitoring snowfall (a major freshwater source for large portions of the world in the form of seasonal snowpack), GPM will enable hydrologists to better understand how changing precipitation patterns at multiple scales translate into changes in hydrologic fluxes and states –

e.g., runoff, evapotranspiration, soil moisture, and groundwater recharge – both directly and through land data assimilation (Rodell et al. 2004).

2.3 *New Insights into Storm Structures, Cloud Microphysics, and Mesoscale Dynamics*

Over oceans, where conventional observations are sparse, multi-satellite precipitation estimates have enabled us to map changes in the horizontal structure of precipitation over the life cycle of a storm, offering insights into storm dynamics such as the eye-wall replacement process in hurricanes (e.g., Braun 2007). GPM observations will continue to improve our understanding of internal structural changes of storms over their life cycles. GPM observations of 3-dimensional precipitation structures will permit us to track, for the first time, structural changes of tropical storms as they undergo the transition into mid-latitude frontal systems, offering the observational basis for investigating why some, but not all, storms intensify during this transition and what factors may contribute to the changes in intensity. GPM radar and radiometer data will also extend the development of the Precipitation Feature database (initiated with TRMM; Zipser et al. 2006) for examining the properties and regional variations of mesoscale convective systems. The enhanced 3-dimensional sensitivity of DPR and high-frequency GMI channels to light-intensity precipitation (including snowfall) will improve the determination of convective/stratiform structures and their geographic and seasonal variations. The DPR will provide observations of the 3-dimensional structure of precipitation, including the detection of convective hot towers that may affect the subsequent rapid intensification of tropical storms (Halverson and Simpson et al. 1998, Kelley et al. 2004).

Mounting evidence from satellite observations suggest that the onset of precipitation may be influenced by the presence of aerosols (Rosenfeld 2000, Ramanathan et al. 2001); the GPM dual-frequency radar will provide microphysical measurements to improve the understanding of microphysical variability in precipitation systems under different environmental conditions. For example, these data will allow us to investigate, in conjunction with ancillary aerosol data, the possible effects of aerosols on the mean precipitation particle diameter in storms affected by Saharan air mass or industrial pollution relative to those particles formed in clean air.

The dual frequency capability of the DPR is instrumental in providing observations and insights into storm structures, cloud microphysics, and mesoscale dynamics. The overlapping data from the Ka and Ku radar bands will allow the detection of presence of mixed phase precipitation, more robust PSD profiles, and detection of falling snow. Furthermore, the coverage of GPM to higher latitudes, provides spaceborne radar data for extra-tropical storms, including hurricanes, and cold higher latitude winter cyclones as well as the lighter rainfall events in mid-latitudes.

Furthermore, numerical models of storm structures, cloud microphysics and mesoscale dynamics can all be improved with the precipitation data sets available from GPM.

2.4 *Improved Understanding of Climate Processes and Prediction of Future Climate*

Precipitation acts as a coupler between the rapidly varying atmospheric processes and the slower components of the climate system such as soil moisture, ocean salinity, and land hydrology. GPM will help improve climate prediction skill by providing better estimates of

surface water inputs, cloud/precipitation microphysics and latent heat release in the Earth's atmosphere. Furthermore, GPM will reduce a major source of uncertainty in the global water and energy budget by quantifying the rate of transfer of water from the atmosphere to surface at regional and global scales.

At cloud scales, the DPR will provide information on bulk precipitation microphysics, for which systematic variations with the environmental state are important to understand. For instance, how are variations in microphysics related to boundary layer thermodynamics, CAPE, and updraft velocity structure? How does precipitation efficiency depend on cloud microphysics? DPR measurements of precipitation microphysical properties will complement available cloud and aerosol observations to provide a better understanding of the processes that determine the conversion of suspended cloud particles into precipitating liquid or ice under different environmental conditions. Knowledge of precipitation processes that control the cloud-rain partition under different climatic conditions is key to understanding climate sensitivity since cloud-moisture-radiation feedbacks and dynamical transport associated with latent heat release represent two very different feedback loops in the climate system, and together determine the global energy balance.

Satellite precipitation observations have been used in conjunction with other data to identify rainfall anomalies that may be associated with human impacts on the environment, including the effects of aerosols from pollution or biomass burning (e.g., Rosenfeld 2000, Ramanathan et al. 2001, Rosenfeld et al. 2001, Andreae et al. 2004, Bell et al. 2008), land-use (Cotton and Pielke 2007, Douglas et al. 2007), deforestation (Wang et al. 2000, Negri et al. 2004, Avissar and Werth 2005), and urban environment on precipitation (Shepherd et al. 2002, Shepherd 2005, Mote et al. 2007, Bell et al. 2007). By providing new microphysical measurements from the DPR to complement cloud and aerosol observations, GPM will play a key role in quantifying how precipitation processes may be affected by human activities.

At diurnal time scales, the best case scenario of 1 to 2 hour sampling by the GPM constellation (see Table 5-3 and better than the mission objectives of 3-hour sampling) will permit more accurate characterizations of the diurnal variability of precipitation over land and oceans, which is an important metric for assessing the physical fidelity of climate models (Dai et al. 1999, Lin et al. 2000). Furthermore, GPM measurements used in concert with observations or analyses of the atmospheric states such as winds, temperature, and moisture provide a wealth of information about moist physical processes; the representation of these processes in climate and forecast models is a major limiting factor of model performance. GPM offers the opportunity to reduce a major source of uncertainty in climate models by pursuing innovative strategies such as diagnosing model deficiencies or optimizing model physics parameters using precipitation information within the general framework of data assimilation (e.g., Hou and Zhang 2007).

3.   Societal Applications Drivers

During the TRMM era, it has been demonstrated that by making observations available in near realtime, a research satellite can provide valuable data for operational use in a range of societal applications. The capability to disseminate data in near realtime is an integral part of the GPM mission design. GPM is expected to make notable contributions in the following applications areas:

3.1   *Extending Current Capabilities in Monitoring Hurricanes and Other Extreme Weather Events*

The advantage of microwave instruments over infrared and visible sensors is their ability to see through clouds to reveal hurricane eyewalls and spiral rainbands within tropical cyclones. The Air Force Weather Agency in Omaha, Nebraska, has been using brightness temperature images from microwave sensors to provide near real-time tropical cyclone position fixes to the Department of Defense's Joint Typhoon Warning Center, NOAA's Tropical Prediction Center, and other operational centers to track the development of tropical cyclones and hurricanes. The GMI, with its 1.2 m antenna, is capable of providing measurements at the highest spatial resolution among all constellation radiometers (see Table 5-2), which will be crucial for obtaining accurate fixes of storm centers for track predictions. Precipitation measurements provided by the GPM constellation sensors will extend the current capabilities in monitoring and predicting severe storms and other extreme weather events such as floods and droughts around the globe.

Hurricane intensification has been tied to the presence and increasing number of hot towers occurring in and near the eyewalls of the tropical cyclones (e.g., Simpson et al 1998, Kelley et al 2004, Kelley and Halverson 2011). DPR has been designed to capture hot towers reaching up to 19 km in altitude. DPR's measurements of hot towers along with GMI's wide swath precipitation retrievals are important measurements for monitoring hurricanes and other extreme weather events. Furthermore, GPM is capable of estimating extreme rain rates up to 110 mm hr^{-1}.

3.2   *Improved Numerical Weather Prediction Skills*

Assimilation of precipitation information into global and regional analysis and forecast systems has been shown to improve atmospheric analyses and short-range forecasts under a variety of situations (Treadon et al. 2002, Zupanski et al. 2002, Marecal et al. 2003, Aonashi et al. 2004, Hou et al. 2001, Bauer et al. 2006a, 2006b). Precipitation data from microwave sensors (both brightness temperatures and rain retrievals) are currently being used at NWP centers to improve operational forecasts. By providing more accurate and frequent precipitation data accessible in near real-time (3 hours or less), GPM will enable NWP centers to continue improving weather forecasts via assimilation of rain-affected microwave brightness temperatures or precipitation retrievals. For microwave radiance assimilation, the DPR will also provide a valuable dataset for verifying precipitation forecasts. In addition, a major focus of GPM GV activities is to provide better error characterizations of GPM measurements, which is crucial for making effective use of precipitation information in NWP systems. Currently, the techniques for assimilating precipitation information in NWP systems are still in early development stages: the use of GPM data for improving NWP skills in the GPM era is expected to benefit from the continued development of advanced assimilation techniques such as ensemble data assimilation and precipitation assimilation using the forecast model as a weak constraint (e.g., Hou et al. 2004).

In addition to atmospheric data assimilation, GPM precipitation observations can be used in land data assimilation (Mitchell et al. 2004) either as inputs into land surface models (LSM's) to provide better soil moisture, temperature, snowpack, and vegetation initial conditions for

coupled NWP forecasts, or integrated into Land Information Systems (Kumar et al. 2006) to improve operational Land Data Assimilation Systems (LDAS) such as the Air Force Weather Agency's AGricultural METeorology model (AGRMET) or that in use at NOAA's National Centers for Environmental Prediction (NCEP) for improved weather forecasting and land hydrology applications at global and regional scales. Three-hour uniformly calibrated GPM global precipitation estimates would greatly enhance the AGRMET snow and other hydrometeorological products to serve hydrological customers worldwide.

3.3 *Improved Forecasting Capabilities for Floods, Landslides, and Freshwater Resources*

GPM will provide precipitation measurements over land roughly every 1 to 2 hours (see Table 5-3), significantly exceeding the minimum requirement of 3 hours for hydrometeorological modeling and applications (Nijssen and Lettenmaier 2004). Since uncertainties in the prediction of streamflow and other hydrological fluxes (e.g. soil moisture, evaporation) depend nonlinearly on uncertainties in precipitation estimates used as inputs (Steiner et al. 2004, Hossain and Anagnostou 2004), the improved sampling over land in the GPM era is expected to advance the detection and prediction capabilities for floods and landslides, as well as the assessment and forecasting of freshwater resources at medium to large basin scales. This GPM capability will be especially useful in developing nations, where in situ precipitation gauge networks are sparse (Hossain and Lettenmaier 2006). Within the United States, the GPM Mission is establishing cooperative research with NOAA's HMT program (http://hmt.noaa.gov/) to improve the use of satellite precipitation data to augment ground-based measurements in operational hydrometeorological applications at small basin scales. For general hydrological applications, NASA plans to produce high-resolution (1-2 km and sub-hourly) precipitation products through statistical downscaling and CRM-based dynamical precipitation analyses. Within Japan, GPM data will also be used develop a flood warning system such as the International Flood Network (IFNET 2008), which is expected to be operational in the GPM era.

4.   GPM Science Objectives

In view of the scientific and societal needs of precipitation measurements described in the previous section, GPM was conceived to be a science mission with integrated application goals. As a science mission, GPM aims to improve understanding of the microphysics and the space-time variability of global precipitation to characterize changes in the cycling of water in the Earth system. For societal applications, GPM will provide estimates of freshwater fluxes, as well as advance predictive capability for precipitation-related natural hazards and extreme weather events. GPM has been identified in NASA's Science Plan (Asrar et al. 2001, NASA 2007) as a priority systematic measurement mission to answer the question: "How is the Earth changing and what are the consequences for life on Earth?" The GPM Science Objectives follow an integrated approach to research and applications as shown in Table 4-1. Equally important, by making precipitation data available in near real-time to operational agencies and stakeholders beyond the traditional science community, GPM can also facilitate the use of space-based precipitation observations in a wide range of practical applications to directly benefit society. With these goals

in mind, the GPM Science Plan encompasses not only scientific discovery but also application-oriented research and development.

Table 4-1. GPM Science Objectives	
Science Driver	Mission Objectives
Advancing precipitation measurement from space	• Provide measurements of microphysical properties and vertical structure information of precipitating systems using active remote-sensing techniques over a broad spectral range. • Combine active and passive remote-sensing techniques to provide a reference standard for unifying and improving global precipitation measurements by a constellation of dedicated and operational microwave sensors.
Improving knowledge of precipitation systems, water cycle variability, and freshwater availability	• Provide 4-dimensional measurements of space-time variability of global precipitation to better understand storm structures, water/energy budget, freshwater resources, and interactions between precipitation and other climate parameters
Improving climate modeling and prediction	• Provide estimates of surface water fluxes, cloud/precipitation microphysics, and latent heat release in the atmosphere to improve Earth system modeling and analysis.
Improving weather forecasting and 4-D climate reanalysis	• Provide accurate and frequent measurements of precipitation-affected radiances and instantaneous precipitation rates with quantitative error characterizations for assimilation into weather forecasting and data assimilation systems.
Improving hydrological modeling and prediction	• Provide high-resolution precipitation data through downscaling and innovative hydrological modeling to advance predictions of high-impact natural hazard events (e.g., flood/drought, landslide, and hurricanes).

5.   GPM Observation Requirements

5.1 *Current Capabilities*

The TRMM satellite, launched in late 1997 by NASA and JAXA, is expected to operate until 2014 or beyond. TRMM is known as the world's foremost satellite for the study of precipitation and associated storms and climate processes in the tropics. TRMM's success is directly a result of the pairing of active and passive instruments that jointly provide three-dimensional views of the structure of precipitating events. The precessing, low inclination orbit (35°) of TRMM has allowed it to focus on tropical (liquid rain) precipitation. TRMM has met and exceeded its original goal of advancing our understanding of the distribution of tropical rainfall and its relation to the global water and energy cycles.

Comparison of the TRMM passive (TMI) and active (PR) rain rate estimates has led to increased understanding of differences between, and therefore improvements to, these retrievals and those for all passive microwave sensors (e.g., Berg et al. 2006; Nesbitt et al. 2004, Masunaga and Kummerow 2005, Shige et al. 2008). These new oceanic rain rate estimates from TRMM have improved the precision and accuracy of the estimates. Figure 5-1 shows the estimated TMI random error (precision) and the random deviation between the TMI and PR estimates. In Fig. 5-2, the PR to ground validation data biases (accuracy) are shown. These figures show that

precision and accuracy can be as low as 25% for rain rates of 10 mmh^{-1}; a tremendous improvement in retrieval performance in the TRMM lifetime.
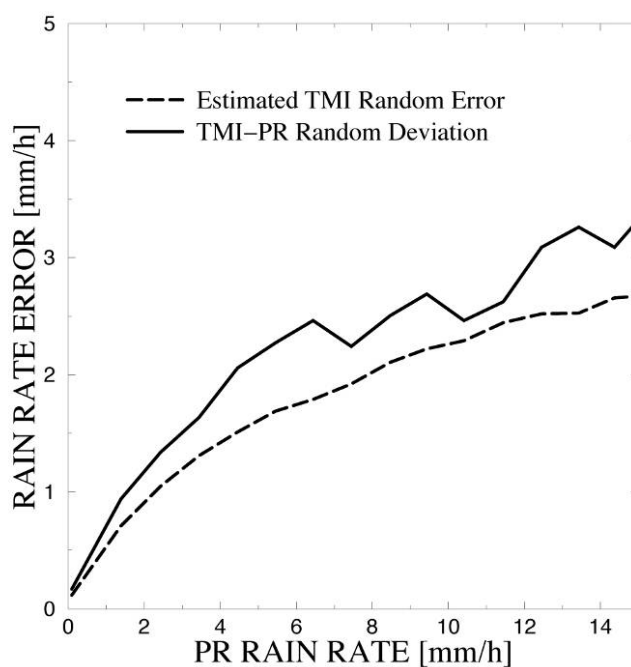
Figure 5-1. This figure shows that the expected precision (random error) of surface rain rate estimates from the V6 TMI algorithm are roughly 50% at 1 mmh^{-1} and 25% at 10 mm h^{-1} at 0.5 degree resolution. The <25-50% range from 1-10 mmh^{-1} is obtained from the results shown on this plot. Note that the dashed curve in the plot is a (Bayesian) algorithm-based estimate of the uncertainty, propagated to 0.5 degree resolution. [From Olson et al 2006]
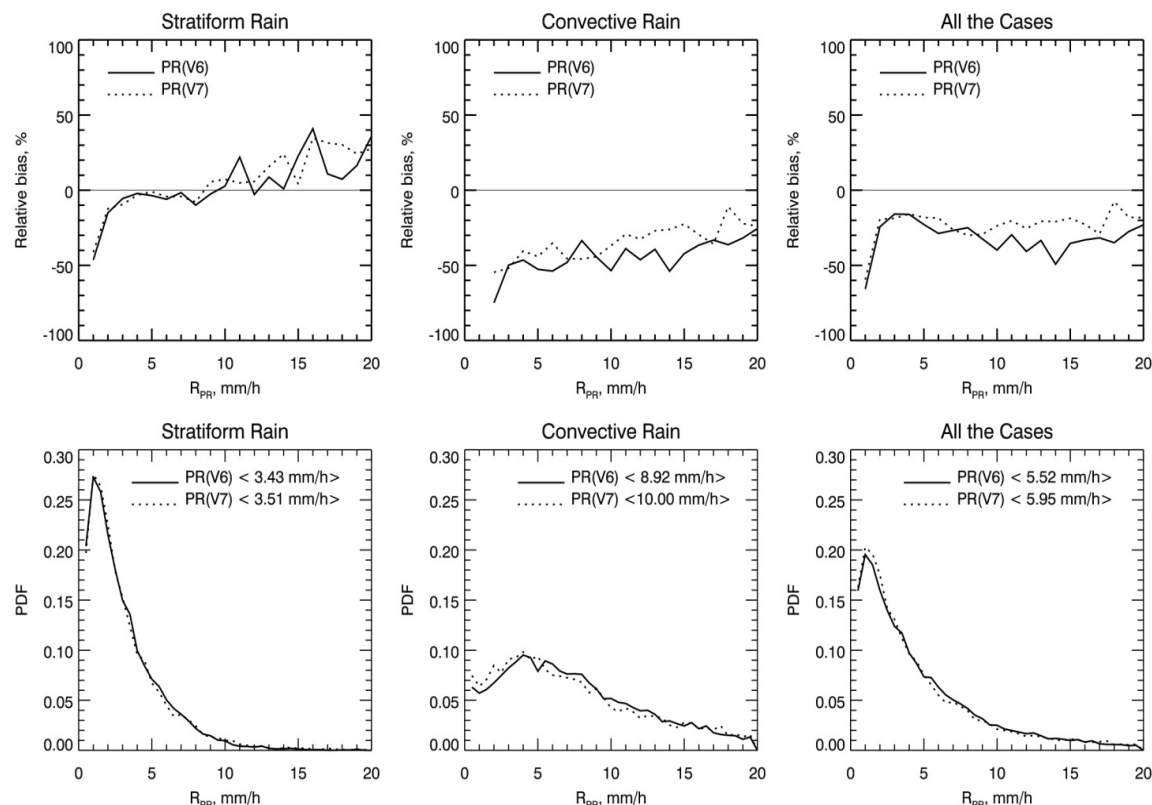
Figure 5-2: The PR normalized biases (top) as derived from the PR version-6 (solid lines) and version-7 (dashed lines) algorithms relative to the estimates from the ground-based WSR-88D for the stratiform, convective and all-rain cases for the Melbourne, Florida site. The probability density functions (bottom) are also plotted. The mean rain rates are provided in the brackets. The top right panel with all cases shows that the error at 1mm/h is about 50% while at 10mmh^{-1}, the error is closer to 25%.

While TRMM has made great strides in satellite-based measurements of tropical precipitation, the scientific community strives to meet additional research needs such as improving precipitation retrieval over land, retrieving mid-latitude precipitation (e.g., light rain and falling snow), advancing integrated applications (e.g., hydrology), and assimilating precipitation estimates into 4-D models.

5.2 *New Frontiers in Space-based Precipitation Observations*

The precipitation science drivers and societal application drivers of the GPM mission point to the new science frontiers of GPM over the existing TRMM mission. New discovery areas for GPM include, for example, estimating light-intensity rainfall, detecting falling snow events, improving retrievals over land, and assessing the 4-dimensional distribution of precipitation over large portions of the globe. To provide the measurements for these new science investigations, GPM will need advanced instrumentation capabilities relative to TRMM, as discussed in Section 5.3. The GPM Level 1 and Level 2 Mission Requirements shown in Appendix A reflect the instrument needs for these new science endeavors.

One of the mission requirements is that GPM will measure rain rates between 0.2 and 110 mm h^{-1} over land and ocean. The minimum detection, 0.2 mm h^{-1}, provides a significant fraction of the total precipitation accumulation in certain regions at mid-latitudes (e.g. NW US and NW

Europe) and is more sensitive than TRMM, which has a minimum detection of 0.5 mm h^{-1}. Figure 5-3 shows that the TRMM PR misses roughly 10% of the total rain volume at the light-rain end of the spectra, as verified against the more sensitive CloudSat radar at 94 GHz (Berg et al., 2009).
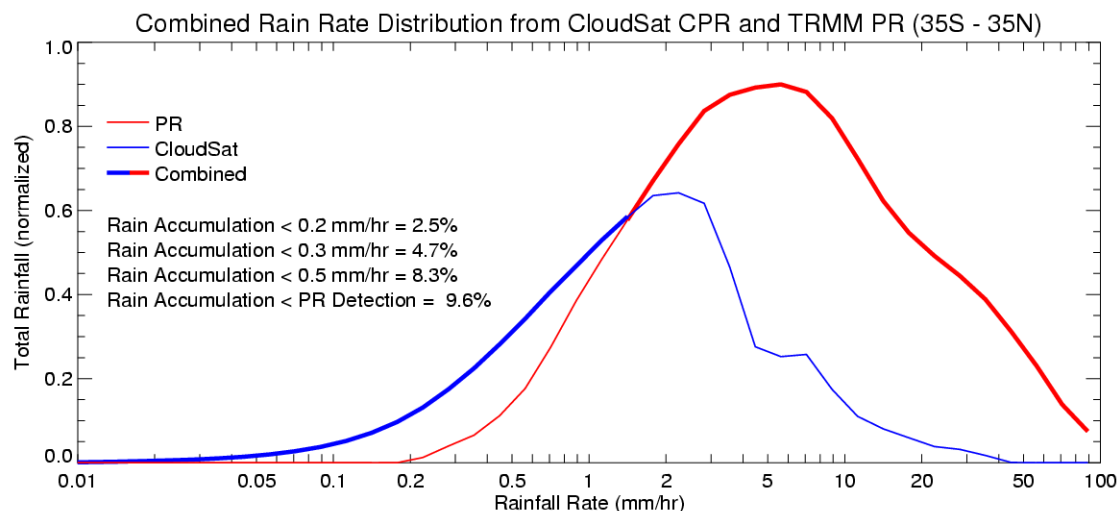
Figure 5-3. The contribution of rainfall by volume as a function of rainfall intensity derived from a combination of rain rate estimates from TRMM PR and CloudSat Cloud Profiling Radar (CPR) over tropical and extra-tropical oceans (35°S – 35°N). The CPR estimates have been adjusted to the 5 km PR spatial resolution. Since both the PR and CPR are sensitive to rain rates between 1 and 2 mm h^{-1}, the combined distribution uses the CPR/PR estimates below/above 1.5 mm h^{-1} respectively.

For a more complete observation of the atmospheric water cycle, GPM measurements must capture a wider spectrum of precipitation intensity and types, including the detection of falling snow over land and ocean surfaces, so that both liquid and frozen precipitation amounts can be monitored. While it is possible for a space-borne radar to achieve high detection threshold at the expense of spatial coverage (e.g., the CloudSat CPR), radar capabilities inevitably reflect a practical trade between measurement sensitivity and swath coverage. In that regard, microwave radiometers, which typically have wider swaths relative to spaceborne radars, play an important role in providing the spatial coverage and temporal sampling needed for global precipitation measurement. Over land, radiometer-based precipitation estimation algorithms have been limited because of contamination of the brightness temperatures from land surface emissions. GPM has added important channels (beyond those used for TRMM) to facilitate over-land retrievals and will develop physically-based retrieval algorithms over land (that will account for surface variations).

To improve hydrological modeling and prediction, the mission will measure precipitation three dimensionally at a 5 km horizontal resolution and 0.25 km vertical resolution between ±65° latitude. GPM will have the capability to determine the instantaneous 3D structure of precipitation, to estimate the distribution of the particle diameters, and to supply 3D estimates of latent heating. These measurements are also important for advances in understanding the microphysical processes of precipitation. Over time, the 3D estimates will provide the 4-dimensional distributions of precipitation. To improve the near-real time knowledge of precipitation systems for societal applications such as landslides and flood forecasting, GMI is

expected to have swath data latencies (publically available precipitation products) of 1 hour, 90% of the time, for the radiometer products of the Core and Low Inclination Observatories.

GPM precipitation products will need to be accurate and precise for providing a well-calibrated reference standard for use with constellation radiometers and also for assimilation into weather forecasts and climate reanalysis models. Accuracies with respect to well-calibrated ground validation data with biases less than 25% (at 10 mmh^{-1} rain rate) and 50% (at a 1 mmh^{-1} rain rate) are needed to improve over the TRMM estimates. Precision with random errors less than 25% (for rain rates of 10 mmh^{-1}) and 50% (for rain rates at 1 mmh^{-1}) are needed at a 50 km resolution. GPM will also provide error characterization estimates for the instantaneous rain rates, brightness temperatures, and radar reflectivities. Finally, the careful calibration of the Core instruments and the development of a reference standard for retrieving uniform precipitation information from the constellation sensors are required in order to insure consistency of 3-hourly precipitation rate estimates used in societal and science studies.

5.3   *GPM Measurement Capabilities*

To achieve the scientific objectives and new frontiers of the GPM mission, a Core Observatory will be developed with a dual-frequency radar and wideband radiometer. The GPM Core will fly in a unique non-Sun-synchronous orbit at 65$^{\rm o}$ inclination (407 km altitude at the Equator) to provide coincident measurements with all constellation radiometers to facilitate inter-sensor calibration - both in terms of radiometric measurements and precipitation retrievals - using data from the Core sensor as the reference. The 65$^{\rm o}$ inclination was selected to achieve a broad latitudinal coverage (without being locked into a Sun-synchronous polar orbit) while maintaining a relatively short precession period to sample the diurnal cycle within a season.

The GPM instrument design builds upon the highly successful rain-sensing package of TRMM augmented by enhanced capabilities to measure light rain (less than 0.5 mmh^{-1}) and solid precipitation, which account for significant fractions of precipitation occurrences in the middle and high latitudes. The increased sensitivity needed for light rain and snow detection, especially over land, drives the designs of the GPM radar and radiometer, as detailed below.

5.3.1   *Dual-frequency Precipitation Radar (DPR)*

The DPR instrument consists of a Ka-band precipitation radar (KaPR) at 35.5 GHz and a Ku-band precipitation radar (KuPR) at 13.6 GHz. The KuPR and the KaPR will be co-aligned such that their 5 km footprints coincide on the Earth surface, with cross-track swath widths of 245 km and 125 km, respectively (see Fig. 5-4). The DPR needs to be able to measure hurricane updrafts (hot towers) that penetrate into the lower stratosphere, hence there is a 19 km echo top requirement. The DPR will have a vertical range resolution of 250 m, except when the KaPR is operating in the high-sensitivity, spatial over-sampling mode, in which case the resolution is 500 m. A 250 m range resolution provides vertical information at scales needed to resolve cloud structures (e.g., the melting layer). The variable pulse repetition frequency technique is also expected to increase the number of samples at each Instantaneous Field-Of-View (IFOV) to achieve a detection threshold of ~12 dBZ for the Ka band and a ~18 dBZ minimum detectable signal level for the Ku-band. Although the CloudSat W-Band radar has a much lower minimum

detectable signal of -29 dBZ, CloudSat is a nadir-only viewing instrument that achieves higher sensitivity at the expense of reduced Earth coverage and higher attenuation.

The active radar channel at 13.6 GHz is required for measuring moderate to heavy precipitation rates. The heritage of the Ku-band radar is TRMM PR, which has a minimum detectable signal level of 18 dBZ, corresponding to a rain rate of approximately 0.5 mmh^{-1}. A $\pm$1 dBZ accuracy (based on TRMM heritage) at the Ku minimum detectable Z gives rain rates from 0.42 to 0.56 mmh^{-1}, which can help define the error at the minimum signal level. The Ka-band provides greater measurement sensitivity to signatures of falling snow and light rain rates (down to 0.2 mmh^{-1} using $Z = 200R^{1.6}$ with a minimum detectable signal level of 12 dBZ) relative to the Ku-band. A $\pm$1 dBZ accuracy (to match the Ku band) at the Ka minimum detectable Z gives rain rates from 0.18 to 0.23 mmh^{-1}, thus achieving the mission requirement of 0.2 mmh^{-1}.

With dual frequencies, rain/snow measurements are expected to be more accurate by using a retrieval technique based on the differential attenuation between the two frequencies. In addition to offering a greater dynamic range and improved retrievals relative to TRMM as shown in Fig. 5-5, the overlapping Ka/Ku-band measurements will provide information on rain/snow drop size distributions over the mid-range of precipitation intensities (from a few to about 15 mmh^{-1}). The dual-frequency returns also provide insight into microphysical processes (evaporation, collision/coalescence, aggregation) and allow us to better distinguish regions of liquid, frozen and mixed-phase precipitation, in addition to providing bulk properties of the precipitation such as water flux (rain rate) and water content in the measurement column. The improved accuracy and more detailed microphysical information from the dual-wavelength radar can also be used to constrain the *a priori* database to be used in simultaneous precipitation retrievals from the brightness temperature measurements by the radiometer on the GPM Core Spacecraft. These improvements are transferable to the constellation radiometers via similar *a priori* Bayesian databases. The DPR instrument was developed and built by JAXA and the National Institute of Information and Communications Technology (NICT) of Japan. It was shipped to NASA Goddard for integration onto the spacecraft bus and tested at Goddard prior to return shipment (in October 2013) to Japan for launch in 2014 from Tanegashima Island, Japan.
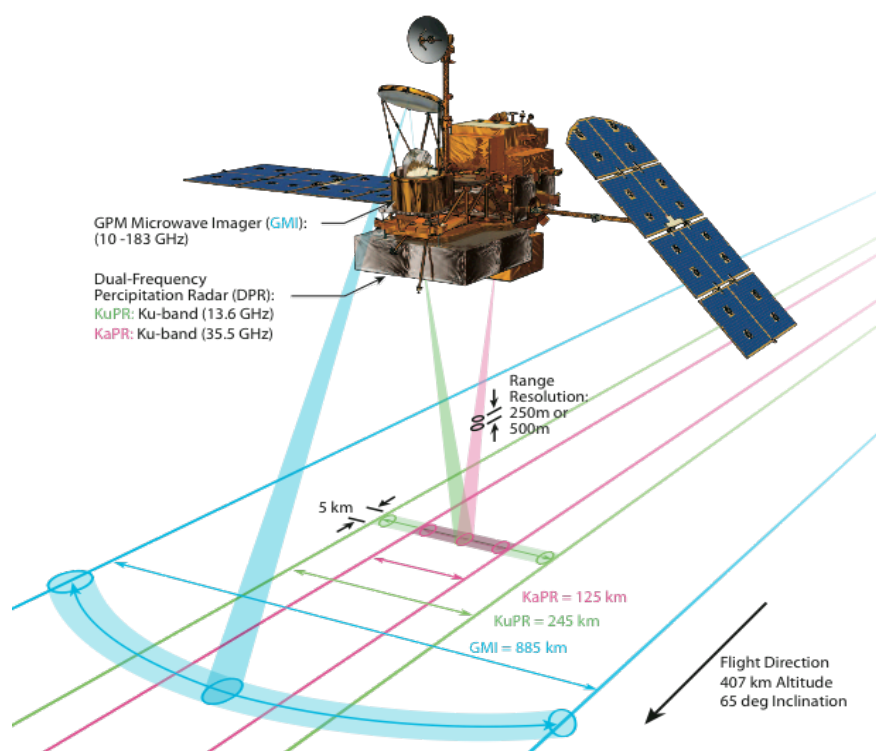
Fig. 5-4: The GPM Core Observatory with the DPR and GMI instruments
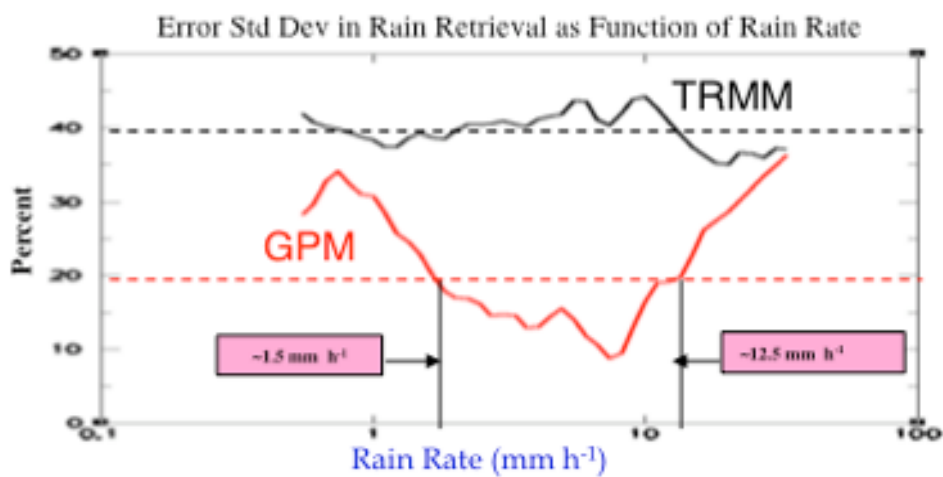
Figure 5-5: Increased sensitivity of Ka radar channel over Ku radar channel with respect to rain rate retrieval ranges. (Courtesy of Ziad Haddad.)

5.3.2   GPM Microwave Imager (GMI)

The GMI instrument is a multi-channel, conical-scanning, microwave radiometer characterized by thirteen channels ranging in frequency from 10 GHz to 183 GHz (Table 5-1). The channel selection is designed to meet scientific objectives with frequency-dependent specifications traceable to the heritage instruments of SSM/I, TMI, AMSR-E, WINDSAT and SSMIS. The selection of the high frequency channels added to the TMI channels for GMI was determined, in part, with the help of a trade-off that maximizes sensitivity to falling snow in the atmosphere while minimizing sensitivity to surface contamination (see Appendix C). The channels were selected with the following rationales:

- The 10 GHz channels are needed for retrieving heavy precipitation rates (>10 mmh^{-1}) encountered in the tropics. Dual polarizations (vertical-V and horizontal-H) are needed to differentiate surface emissivity effects from precipitation signals over oceans. The TMI instrument added the 10 GHz channels after noticing that the SSMI, its predecessor, without the 10 GHz channel, suffered from saturation in heavy tropical rain events.

- The 18.7 GHz V and H channels are needed for retrieving moderate to light precipitation rates over ocean. The 10 and 19 GHz channels provide Nyquist-sampled data as an integral part of the multi-channel retrieval algorithm.

- The 23.8 GHz channel is needed to correct for the absorption of water vapor in the other channels in multi-channel retrievals. Only V polarization is needed because the polarization signature is not very pronounced at frequencies around 22 GHz.

- The 36.5 GHz channels are used in tandem with 19 GHz channels to measure moderate and light precipitation over ocean. The 36 GHz V and H channels are critical in the multi-channel retrieval algorithm to estimate moderate rain rates at 15 km resolution and are used in conjunction with the 35.5 GHz channel of the KaPR to produce combined radar-radiometer precipitation retrievals.

- The 89 GHz V and H channels are used in the multi-channel retrievals, where their small Field of View (FOV) are essential to separate convective from stratiform precipitation and thus correct for nonlinearities introduced by rainfall heterogeneity. The 89 GHz frequencies are the main channels for TRMM retrievals over land, where only ice scattering can be detected over radiometrically warm backgrounds.

- The 165.5 GHz channels (together with the 89 and the 183 GHz channels) are needed for determining light precipitation rates encountered in frontal situations outside the tropics.

- The 183 GHz channels are needed for detecting scattering signals from small ice particles, which are used to estimate light rain and snowfall rates over snow-covered land (radiometrically cold backgrounds). Only V polarization is needed because the surface polarization signature is not very pronounced at frequencies around 183 GHz (mainly because of the water vapor absorption).

Table 5-1. The required frequencies, polarizations, footprints, beamwidths, and NEΔT values for the GMI instrument on the Core Observatory. (See Appendix A.)

	10.65 V & H	18.7 V & H	23.8 V	36.5 V & H	89.0 V & H	166 V & H	183.31 ±3 V	183.31 ±7 V
Resolution (km)	19.4 x 32.2	11.2 x 18.3	9.2 x 15.0	8.6 x 15.0	4.4 x 7.3	4.4 x 7.3	4.4 x 7.3	4.4 x 7.3
Sample NEDT[1] (K)	0.96	0.84	1.05	0.65	0.57	1.5	1.5	1.5
Sample NEDT[2] (K)	0.93	0.76	0.73	0.52	0.41	0.92	0.76	0.67
Beam NEDT[1] (K)	0.53	0.61	0.82	0.52	0.65	1.72	1.72	1.72
Beam NEDT[2] (K)	0.51	0.55	0.40	0.42	0.47	1.05	0.87	0.77
Beam Efficiency[2] (%)	91.1	91.2	93.0	97.8	96.8	96.5	95.2	95.2
Uncertainty[1] (K)	1.35	1.35	1.35	1.35	1.35	1.5	1.5	1.5
Uncertainty[2] (K)	0.99	1.05	0.71	0.53	0.69	0.69	0.66	0.66
Pass-band Bandwidth (MHz)	100	200	400	1000	6000	4000	3500	4500
Antenna 3 dB beamwidth [Max]	1.75°	1.0°	0.9°	0.9°	0.4°	0.4°	0.4°	0.4°
Sampling interval (ms)	3.6							
Incidence angles	Nominal Earth incidence = 52.8° Off-nadir angle = 48.5°				Earth Incidence = 49.19° Off-nadir angle = 45.36°			
Data Rate, Power, Mass	30 kbps, 162 Watts, 166kg, deployed size=1.4m x 1.5m x 3.5m							
Antenna Size, Swath width	1.2 m, 885 km							

[1]GMI Requirements
[2]Flight performance values measured prior to shipment from Ball to GSFC for I&T

The GMI has a large 1.2 m diameter antenna to provide better spatial resolution than TMI (~65 cm antenna at 402 km altitude) and AMSR (1.6 m antenna at 705 km altitude). Given the 3-dB beamwidths reported in Table 5-1 for each channel and the orbital altitude of the GPM Core Observatory, the footprint resolutions are as shown in Table 5-1. The small ~7 km IFOVs of the 89, 165 and 183 GHz channels take precedence over contiguous sampling considerations for these channels. TMI has shown that footprint gaps in the cross-scan direction of up to 60% of the scene are acceptable for precipitation retrievals at 89 GHz. The resolution of the 166 and 183

GHz channels is chosen to match that of the 89 GHz channels based on trade-off considerations between spatial resolution and coverage.

The Noise Equivalent Delta Temperature (NEΔT) values presented in Table 5-1 represent the Temperature Sensitivity of each channel. Temperature Sensitivity (or Radiometric Temperature Sensitivity) is the end-to-end radiometric resolution of a microwave radiometer; it is defined as the Standard Deviation (S.D.) of the radiometer measurement, and it includes all the components of the noises that affect the measurement, from the input signal (photon noise), to the output analog-to-digital (A/D) quantization noise. But the dominant component of the NEΔT is determined by NEΔT = Ts/sqrt(BW*τ), where Ts is the system temperature (which includes both the radiometer receiver internal noise and the Antenna Temperature - taken to be 300K), BW is the receiver passband bandwidth, and τ is the sampling period. The NEΔT values are provided in terms of (1) the Beam NEΔT (when the integration time is the time it takes for a scanning radiometer to scan across one full beam width, in the along-scan direction) and (2) the Sample NEΔT (when the integration time is the sample-time; e.g. the GMI set the sample-time of 3.6 ms for all its 13 channels). These NEΔTs are scientifically acceptable for ensuring accurate rain rate retrievals and detecting falling snow conditions (see Appendices D and E). Another consideration of defining the high frequency channels includes specifying the receiving pass-BW of these channels. Analyses show that different passbands lead to minor changes in brightness temperature values for selected snowing cases (see Appendix G). Included in Table 5-1 are the NEΔT values based on the requirements as well as the NEΔT values based on flight performance prior to shipment from Ball to Goddard Space Flight Center for integration and test.

The GMI has an off-nadir-viewing angle of 48.5 degrees, which corresponds to an earth-incidence-angle of 52.8 degrees. Maintaining a similar geometry with the predecessor TMI instrument, the GMI main reflector will rotate at 32 rpm to collect microwave radiometric brightness measurements over a 140 degree sector centered on the spacecraft ground track, giving a cross-track swath of 885 km on the Earth's surface for the Core Observatory (Figure 5-1). The central portion of the GMI swath overlaps the radar swaths (with an approximately 67-second lag between the GMI and radar observation times due to geometry and spacecraft motion). The measurements within the overlapping swath portions of the DPR and GMI are important for improving precipitation retrievals, especially the combined radar-radiometer and the radiometer-based retrievals.

As a radiometric reference for other radiometers in the GPM constellation, the GMI is designed to have a wide frequency range to encompass the frequency ranges on constellation sensors. The GMI also achieves greater instrument accuracy and stability by employing noise diodes in addition to the hot load and the cold-sky reflector to perform a "four-point" calibration to remove sensor nonlinearity under nominal conditions and as a backup calibration reference during hot load anomalies due to solar intrusion (Hou et al., 2008) with additional engineering features (e.g. a lip to limit solar intrusions). The GMI was developed and built by the Ball Aerospace and Technology Corporation in Boulder, Colorado, under contract with NASA Goddard Space Flight Center. GMI was shipped to NASA Goddard for integration onto the spacecraft bus and will be tested at Goddard prior to shipment to Japan for launch in 2014 from Tanegashima Island, Japan.

5.4 *Coverage and Sampling*

In order to achieve several of the Science Objectives in Table 4-1, temporally frequent rain rate estimates are needed on the order of near 3-hour coverage. In addition to the Core, GPM will rely on additional partner satellite observations to obtain the <3 hour coverage. The initial concept of the GPM constellation was envisioned to comprise conical-scanning radiometers; these have been the mainstay for rainfall estimation from space, especially over oceans where the contrast is strong between warm rain emissions and reflectively cool and uniform ocean surfaces. Over land, imagers rely on indirect high frequency ($\geq$ 85 GHz) measurements of ice scattering from cloud layers above the rain in order to have a high contrast between the rain signal (cooler TBs from ice scattering) and the surface signal (warm and variable land surface emissions). These indirect signatures from ice scattering must to be converted to surface precipitation estimates. This requires that additional information about the environmental state (surface characterization, water vapor profiles, etc.) be available. Over land, this information is more readily assessable than during TRMM operations and will be used to further improve retrieval approaches over land for both imagers and sounders in the GPM mission timeframe. Microwave sounder instruments, whose precipitation signal is also of the ice scattering variety, were originally not included in the GPM mission design. As retrieval algorithms for microwave sounders continued to improve in recent years, the quality of current rainfall retrievals from AMSU-B with channels between 89 and 183 GHz has been shown to be comparable to those from conical-scanning radiometers over land (Lin and Hou 2008). In keeping with these algorithm advances, the baseline GPM constellation was reconfigured in 2006 to include microwave sounder instruments (MHS on NOAA and MetOp and ATMS on NPP and JPSS) to augment the sampling by conical-scanning radiometers over land. Microwave sounders with quality rain algorithms and estimates over oceans will also be used in the sampling coverage of the GPM mission. The high-frequency sounding channels on GMI will provide a bridge in using GPM Core sensor measurements to further improve sounder retrievals in the GPM constellation.

As discussed in Section 2, the build-up of the GPM constellation follows a "rolling wave" strategy with a flexible architecture to take advantage of satellites of opportunity to provide the best possible sampling and coverage with assets provided by participating partners. The timeline of potential constellation sensors (both conically scanning imagers and cross-track scanning temperature/humidity sounders) expected during the GPM Core Observatory operational period (2014-2022) timeframe are summarized in Figure 5-5.
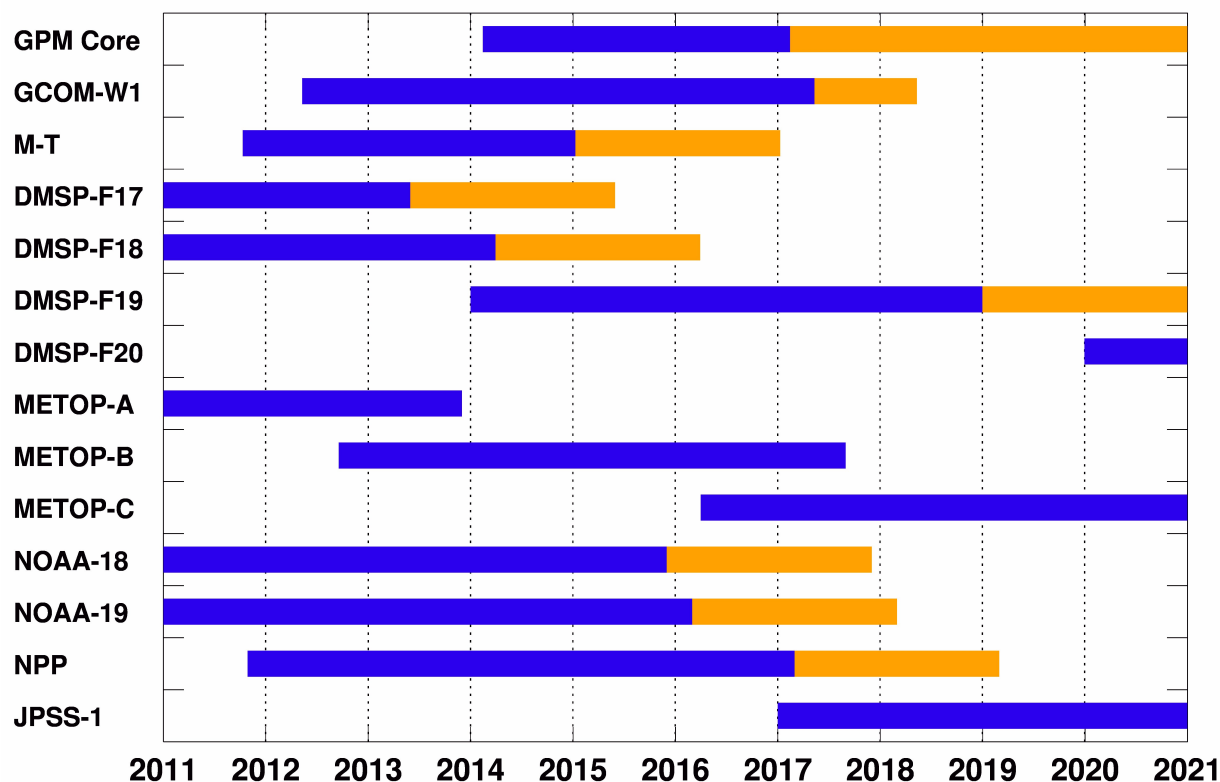
Figure 5-6: GPM constellation schedule based on current estimates. Blue indicates the primary mission phase and yellow the extended mission phase. GPM operations beyond the primary mission phase are subject to science and satellite performance evaluation after launch.

Table 5-2 lists the sensor characteristics of the planned GPM constellation. Despite many similarities among these sensors, significant differences exist in terms of center frequencies, viewing geometries and spatial resolutions, which must be reconciled in order to produce uniform global precipitation estimates. The inter-satellite calibration (at both radiance and precipitation retrieval levels) using GPM-Core sensor measurements as reference standards within a consistent framework will be a key contribution of the GPM Mission to global, unified precipitation products.

The GPM constellation performance is a function of the partner assets in orbit. For the constellation assets listed in the Table 5-2, the expected mean revisit times and coverage over different regions for the first 5 years of the expected GPM Core operating period are 1-2 hours and significantly exceeds the minimum requirement of 3-h revisit time for hydrological applications (Nijssen and Lettenmaier 2004). The sampling times reported in (Table 5-3) reflect the incorporation of operational sounder radiometers in the GPM constellation.

Table 5-2. Passive microwave radiometer sensor capabilities expected in the GPM era									
Channel[1]	6-7 GHz	10 GHz	19 GHz	23 GHz	31-37 GHz	50-60 GHz	89-91 GHz	150-167 GHz	183-190 GHz
GMI		10.65 V/H	18.70 V/H	23.80 V	36.50 V/H		89.0 V/H	165.6 V/H	183.31±3 V 183.31±8 V
Resolution[2]		26km	15km	12km	11km		6km	6km	6km
AMSR 2	6.925/7.3 V/H	10.65 V/H	18.70 V/H	23.80 V/H	36.5 V/H		89.0 V/H		
Resolution[2]	62/58km	42km	22km	26km	12km		5km		
SSMIS			19.35 V/H	22.235 V	37.0 V/H	50.3-63.28 V/H	91.65 V/H	150 H	183.31±1 H 183.31±3 H 183.31±7 H
Resolution[2]			59km	59km	36km	22km	14km	14km	14km
MADRAS			18.7 V/H	23.80 V	36.5 V/H		89.0 V/H	157 V/H	
Resolution[2]			40km	40km	40km		10km	6km	
MHS							89 V	157 V	183.31±1 H 183.31±3 H 190.311 V
Resolution[2]							17km	17km	17km
ATMS				23.8	31.4	50.3-57.29	87-91	165.5 H	183.31±1 H 183.31±1.8 H 183.31±3 H 183.31±4.5 H 183.31±7 H
Resolution[2]				74km	74km	32km	16km	16km	16km

[1]Channel Center Frequency (GHz): V–Vertical Polarization, H-Horizontal Polarization, no V/H indicates mixed polarization for cross-track scanners.

[2]Mean spatial resolution (km)

Note that GMI is at a 65-degree non-sun-synchronous orbital inclination, MADRAS is at a 20 degree non-sun-synchronous orbital inclination, while the other sensors are in polar orbits.

Table 5-3. Expected GPM Constellation Sampling over ocean and land										
	Average Revisit Time (hr)					Coverage of Mean Revisit Times ≤ 3 hr (%)				
Year *	2013	2014	2015	2016	2017	2013	2014	2015	2016	2017
	Land					Land				
Tropics	1.9	1.9	1.9	2.2	2.1	100	100	100	100	100
Extratropics	1.3	1.3	1.3	1.6	1.5	100	100	100	100	100
Globe	1.6	1.6	1.6	1.9	1.8	100	100	100	100	100
	Ocean					Ocean				
Tropics	1.9	1.9	1.9	2.1	2.1	100	100	100	100	100
Extratropics	1.5	1.5	1.5	1.8	1.7	100	100	100	100	100
Globe	1.7	1.7	1.7	2.0	1.9	100	100	100	100	100
	Land and Ocean					Land and Ocean				
Tropics	1.9	1.9	1.9	2.1	2.1	100	100	100	100	100
Extratropics	1.4	1.4	1.4	1.8	1.7	100	100	100	100	100
Globe	1.6	1.6	1.6	2.0	1.9	100	100	100	100	100
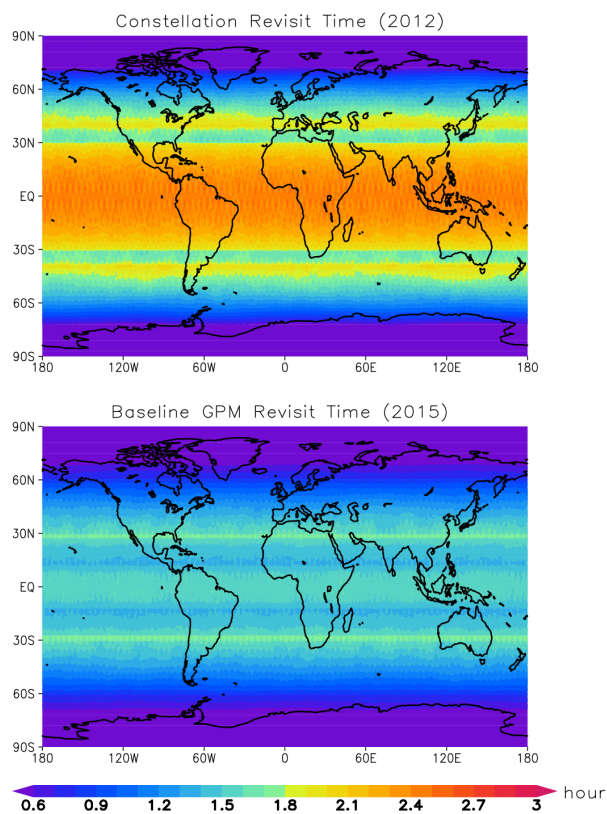
Figure 5-7. Comparison of mean revisit times by the GPM constellation in 2015 (bottom) with current capabilities (top).
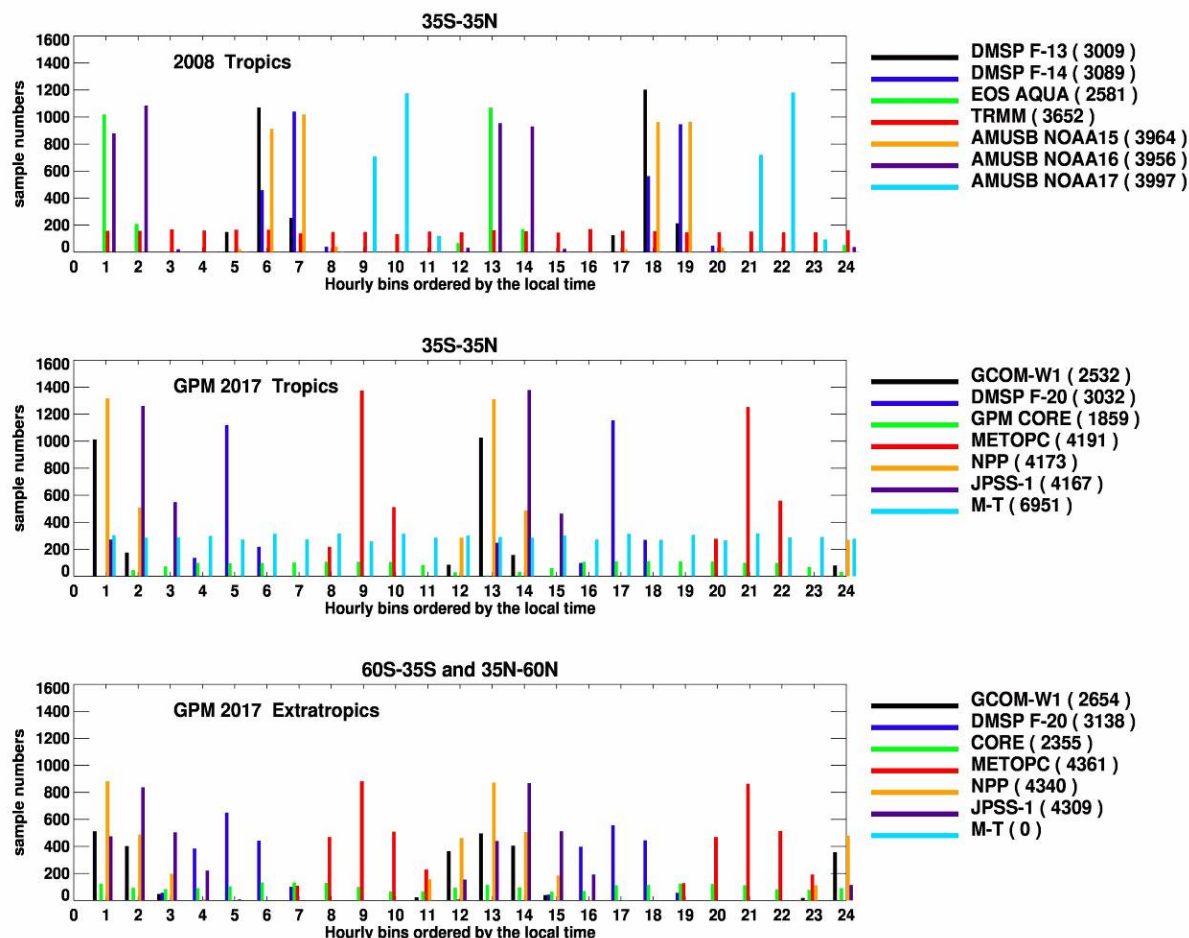
Figure. 5-8. Number of observations by different satellites over a month in hourly 1°x1^{o} bins centered at the local time. Top: Observation counts between 35S and 35N (the TRMM domain) at the 1° bin centered at 0E in 2008. Middle: Observation counts in the GPM era over the same 0E domain in 2017. Bottom: Observation counts in the extratropics for the 1° bin centered at 0E by the GPM constellation in 2017. Counts provided in the legend within parentheses is the sum over all hours for a month for that 1° bin centered at 0E for the specific sensor, latitude range, and year of observation.

Like TRMM, the GPM Core is in an inclined, non-Sun-synchronous, precessing orbit that provides the asynoptic observations needed to quantify the diurnal variation of precipitation over the globe and to monitor in near realtime the development of storms and hurricanes. The crucial role of asynoptic observations provided by TRMM and GPM in filling the temporal gaps between observations by polar satellites at fixed local times is illustrated in Fig. 5-8.

The importance of operational use of asynoptic observations in fixing tropical cyclone positions has been demonstrated by TRMM. In a typical year, nearly 16 percent of all position fixes made by the Joint Typhoon Warning Center are from TMI data (NRC 2005). The GPM Core will also provide, for the first time, asynoptic observations in the middle and high latitudes.

Asynoptic observations provided by the GPM Core and Megha-Tropiques have a large impact on GPM constellation sampling and estimations of time-integrated rain accumulation, especially over the tropics. Analyses in Appendix B show the benefits of an enhanced mission by adding an additional low inclination observatory in a non-sun-synchronous orbit at 40° inclination. Appendix B discusses that the additional asynoptic observations from such an low-

inclination observatory (1) would increase GPM's ability to provide < 3 h sampling (a requirement for hydrological applications, Hossain and Lettenmaier 2006) by 20-50% over land and 60-70% over ocean (assuming MW sounder measurements are not used over ocean), (2) decrease errors in rainfall accumulation by 40-60% in localized areas over the continental United States, improving the utility of GPM data for basin-scale water resource management and other hydrological applications, and (3) decreases errors in monthly-mean rate rain estimates by 20-60% over large portions of oceans, which would lead to more accurate estimates of global water and energy budgets.

6.   Radiometer Inter-Calibration Algorithms

A principal goal of the GPM mission is to unify and advance measurements from a heterogeneous constellation of microwave radiometers within a consistent framework to produce next-generation, inter-calibrated global precipitation products. Quantifying and reconciling differences among constellation radiometers to provide self-consistent multi-satellite global precipitation estimates requires a three-layer process: (1) calibration of individual instruments, (the responsibility of the manufacturers and instrument providers), (2) cross-calibration of radiometric measurements of constellation sensors, and (3) inter-calibration of precipitation retrievals. The GPM Radiometer Inter-satellite Calibration Algorithm Team, which focuses on the second layer of this process, is responsible for developing procedures for producing consistent, inter-calibrated radiances from GPM constellation radiometers, which are a necessary basis for consistent precipitation estimates. Since most of GPM constellation radiometers are expected to be in polar orbits, a radiometer on a non-Sun-synchronous satellite is needed to provide coincident measurements with constellation members over a wide range of latitudes. The strategy is to convert observations of the non-Sun-synchronous satellite to virtual observations of all other constellation satellites while making proper allowance for differences in radiometric characteristics (viewing geometry, bandwidth, center frequency, etc.). The GPM Core Observatory carrying the GMI is designed for such a purpose.

The GMI channel frequencies and radiometric sensitivities (Table 5-2) are selected based on two broad considerations: (1) they must provide measurements over sufficient spectral range to quantify precipitation rates that are commonly encountered in the tropics, mid-latitudes, and high latitudes, and (2) they must have sufficient accuracy and stability to serve as a radiometric reference to remove the relative biases among constellation radiometers for the purpose of generating uniform constellation-based global precipitation products. In this regard, it is important to recognize two things: (1) the GPM inter-calibrated (Level 1C) brightness temperatures are not meant to replace the officially calibrated Level 1B radiance products provided by GPM partners, but are strictly for generating consistent Level 2 precipitation retrievals from partner radiometers, and (2) the inter-calibration uses physical and statistical modeling to reconcile design differences among radiometers to uncover and correct calibration inconsistencies.

In comparing GMI performance to other conically-scanning radiometers (using a normalization process) we find that normalized NEΔT for channels 10–183 GHz are comparable for GMI versus SSMIS and TMI, with the exception of 183±3 GHz which has NEΔT about 0.4K higher on GMI than on SSMIS (see Appendix D). For cross-track scanners at high frequencies, the GMI is approximately 50 to 100% higher than the normalized ATMS NEΔT values (see

Appendix E). ATMS instruments need these better NEΔT values for the retrieval of water vapor profiles; on the other hand, GMI does not need such precision for the retrieval of snow. GMI channels do have sufficient spectral range to determine precipitation rates over the latitude range observed by the GPM Core Observatory. The GMI channel performance is also accurate and stable enough to serve as the radiometric reference to reduce the relative biases among the constellation sensors.

6.1 *Inter-calibration Procedures*

Achieving brightness temperature consistency through inter-satellite calibration requires multiple steps. A summary of the process is provided here with details provided in the ATBD (http://pps.gsfc.nasa.gov/atbd/atbd.html). First, each instrument provider is responsible for providing well-calibrated brightness temperature products according to established standards. Based on the standard brightness temperature products provided by partners, as part of a pre-screening step, GPM will perform consistency calibration that examines the data to find and remove pixel-to-pixel biases, which can be caused by pitch and roll errors, spacecraft interactions and more subtle causes. For conical scanners, detecting such biases is conceptually straightforward: the average of each beam position should be the same. Biases due to latitude and small incidence angle anomalies are readily removed (Gopalan, et al. 2009). For cross-track scanners detecting and correcting for biases to achieve self-consistency is much more difficult because the dependence on incidence angle must be very accurately modeled.

Once an instrument is shown to be self-consistent in a scan, it must be self-consistent through the orbit and statistically over days and months. For this purpose, environmental data such as Global Data Assimilation System (GDAS) will be used to compute brightness temperatures for non-raining oceanic pixels throughout the orbit. While these calculations may not be adequate for absolute calibration, they are suitable for identifying brightness temperature anomalies. If a consistent pattern of anomalies is detected, a function will be generated to correct for them. Special tests will also be applied to instruments to search for other issues that may arise during their self-calibration process.

Once individual instrument brightness temperatures are self-consistent, the multiple radiometers in the constellation are inter-calibrated among the various platforms to produce a uniform global brightness temperature product (Level 1C) within a consistent framework. To this end, Core GMI observations are spatially and temporally matched to multiple constellation sensors. For the matched data sets, algorithm development is preceding along two approaches (1) a system wherein collocated brightness temperatures are translated to a common basis and compared (Hong et al., 2009), and (2) deriving limiting values for each radiometer independently and comparing them vicariously through a model (Ruf 2000, Brown et al. 2004, Brown et al., 2005, Ruf et al., 2006). Corrections indicated by these matched comparisons are appropriately applied to constellation brightness temperatures. The aim of the inter-satellite calibration is to make the corrections required at Levels 2 and 3 small and credible.

Algorithm codes for inter-satellite calibration will be provided to PPS as they become available (not necessarily following the delivery requirements of the Level 2 algorithms) and as they are approved by the JPST. PPS and JPST reserve the right to make timing decisions on the implementation of the updates (e.g., during the next version and reprocessing stream or immediately).

7. Precipitation Algorithms

The PMM Precipitation Algorithm Teams are responsible for developing Level 2 (geolocated, geophysical) retrievals at the IFOV for the radar, combined radar-radiometer, and for microwave radiometer instruments (Figure 7-1). In addition, algorithms are produced for Level 3 retrievals that merge Level 2 precipitation estimates into time and space sampled products, including latent heating estimates. The algorithm development efforts are divided into core and constellation satellite products. Most critical in this hierarchy are the dual frequency radar algorithms, which serve as the basis for the combined radar-radiometer algorithm for the Core Satellite. The combined algorithm provides a common, fully representative inventory of naturally occurring cloud states that can be used as the *a priori* database for radiometer-only retrievals. While the technique does not entirely eliminate the need for assumptions, it does concentrate them at the Core Observatory level instead of requiring less-capable radiometers to make the assumptions independently.

The radar, combined, and radiometer algorithms are linked both in terms of observing/retrieving the same precipitation occurrence and in terms of providing a common basis for transferring knowledge gained by the GPM Core Observatory to the constellation radiometer observatories. Such linkages require that the algorithm-approach for these three retrievals be developed in coordination and with common elements within a consistent physical framework. Since the microphysics and the underlying state of the cloud environment will be the same for the views of the radar and radiometer observations, common microphysical representations (e.g., particle size distributions, frozen precipitation characteristics, vertical structure) are adopted, to the extent possible, across all three algorithms. Coordination for these common elements occurred early and often during the algorithm development process with oversight by the algorithm team leads and the Project Scientist.
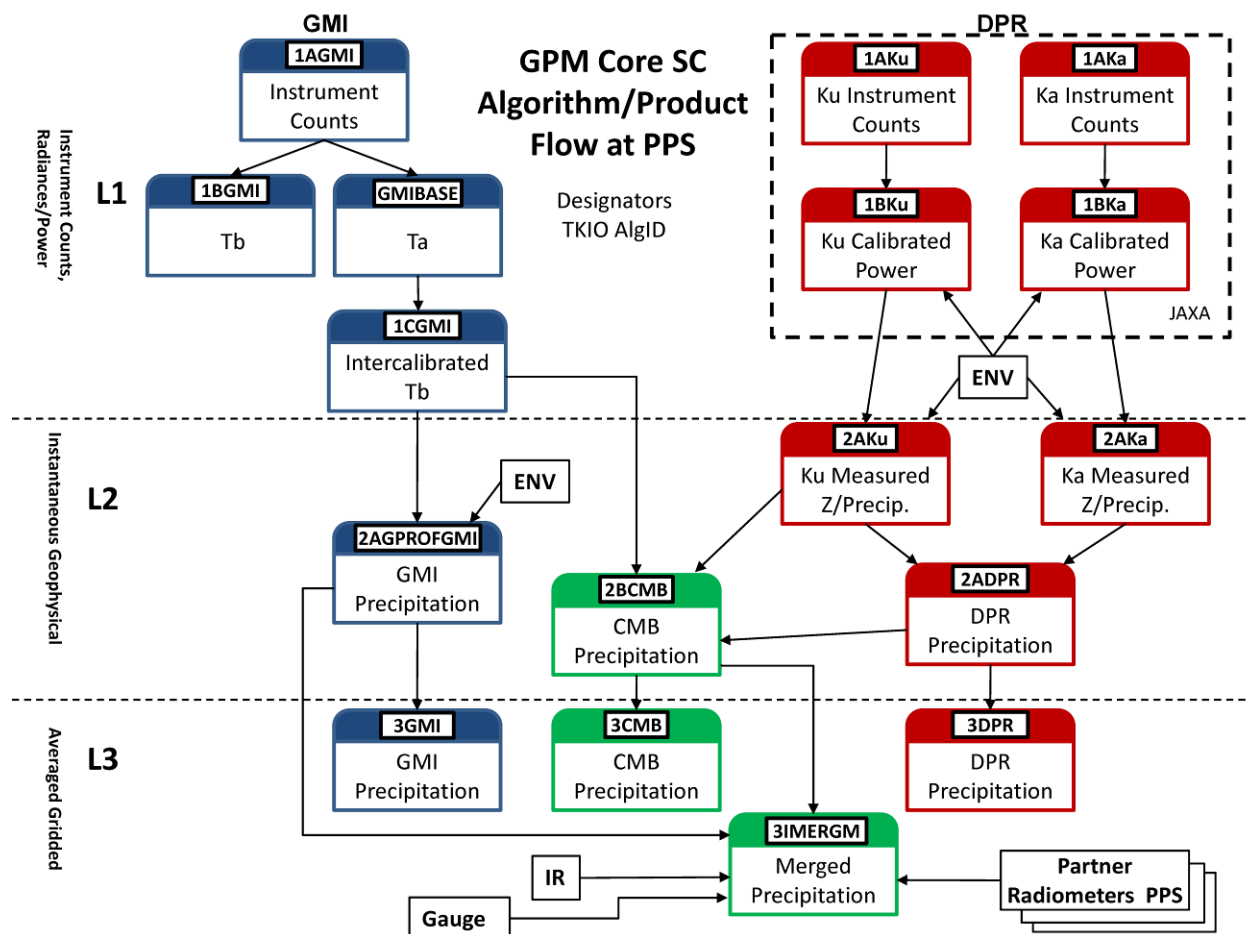
Fig. 7-1: Relationships between the Level 1-3 products and the radiometer (GMI), Combined (CMB) and radar (DPR) products.

Each algorithm will have an Algorithm Theoretical Basis Document (ATBD) delivered to the GPM Project Scientist and the PPS lead (GPM Deputy Project Scientist for Data) by the algorithm team leads as written by the algorithm developers. The ATBD will be required for not only the Level 2 and Level 3 precipitation algorithms listed above, but also for the Level 1 products from DPR, GMI, and the inter-satellite calibration process for Level 1C products. The ATBD has dual functionality. First it provides the scientific basis of the algorithm, its strengths, assumptions, and any known issues, as well as a detailed description of the algorithm software architecture, procedures, linkages with other algorithms, and any attendant databases that support the algorithm. Second, the ATBD provides the information necessary such that a knowledgeable user/science programmer could duplicate the retrieval and perhaps modify the code to investigate other approaches. The ATBD is expected to be a living document with version 1 fixed when the At-launch algorithms are submitted. Later versions of the ATBD will be required with each new PPS reprocessing of a new algorithm version. The current ATBDs will be available at http://pps.gsfc.nasa.gov/atbd/atbd.html.   The schedule and milestones of the algorithm development and linkages with ground validation efforts and PPS deliverables are documented in Section 10.

7.1 *Radar Algorithms*

The main objective of the Level 2 DPR algorithms is to generate from the Level 1 DPR (calibrated radar echo power) products calibrated reflectivities and radar-only derived meteorological quantities on an IFOV basis. The general idea behind the algorithms is to determine general characteristics of the precipitation, correct for attenuation and estimate profiles of the liquid water content, rainfall rate and, when dual-wavelength data are available, information on the particle size distributions in rain and snow.

The dual frequency radar can, in principle, be used to determine two parameters of the drop size distribution at each range bin in the near-vertically sampled profile. This is a significant step forward, even in relation to many surface based radars that must rely on a single frequency and an assumed drop size distribution. Particularly important, dual-wavelength data will provide better estimates of rainfall and snowfall rates than the TRMM PR data by using the particle size information and the capability of estimating, even in convective storms, the height at which the precipitation transitions from solid to liquid.

A major source of error in the rainfall estimates from the TRMM/PR comes from the uncertainty in the conversion of radar reflectivity into rainfall rate. This uncertainty originates in the variations of the drop size distribution (DSD) of rainfall that changes by region, season and rain type. One of the reasons for adding the Ka-band frequency channel to the DPR is to provide information on the DSD that can be obtained from non-Rayleigh scattering effects at the higher frequency. Another reason for the new Ka-band channel is to provide more accurate estimates of the phase-transition height in precipitating systems. This information is very important not only in increasing the accuracy of rain rate estimation by the DPR itself, but in improving rain estimation by passive microwave radiometers. The third reason for the Ka-band channel arises from the fact that the GPM core satellite will provide coverage up to about 65 degrees latitude; by increasing the sensitivity of this channel, a larger fraction of snow and light-rain events will be detected.

Since the Ku-band channel of the DPR is very similar to the TRMM PR, the principal challenge in the development of the DPR level 2 algorithms is to combine the new Ka-band data with the Ku-band data to achieve the objectives mentioned above. Practical considerations such as sensor noise or less than perfect alignment among the radar beams, however, complicate the retrieval and can lead to numerical instabilities if the algorithm is not properly constrained. These are priority items being addressed by the GPM algorithm development team, along with retrieval methods for both very light rainfall cases (where the Ku band radar will lose sensitivity) and very heavy rainfall cases (where the Ka band signal is likely to be lost due to attenuation).

There are three kinds of Level 2 algorithms for the DPR: DPR algorithm, Ku-only (KuPR) algorithm, and Ka-only (KaPR) algorithm. The latter two are single-frequency (SF) algorithms. The DPR algorithm is a dual-frequency (DF) algorithm. A draft of the DPR algorithm flow is shown in Fig. 7-1. The retrieval process is carried out in the Solver module, but the preparation of equations is shared by the other six modules. The path-integrated attenuation (PIA) is estimated in the surface reference technique (SRT) module. The DSD module provides look-up tables that relate radar quantities, such as normalized backscattering and attenuation coefficients, to parameters of the size distribution, such as characteristic particle size and number concentration, for different precipitation types (rain, snow and mixed phase) as

determined by the Classification module. The measured reflectivity factor, Z_m, is converted from Z_{m0} through attenuation correction for non-precipitation particles in the Vertical Profile module and Z_{m0} is converted from received echo power in the Preparation module. GANAL is the Japanese Global Analysis model data used to provide atmospheric environmental conditions.

For data in the inner swath an additional objective is to provide information on the particle size distributions in the rain and snow layers.
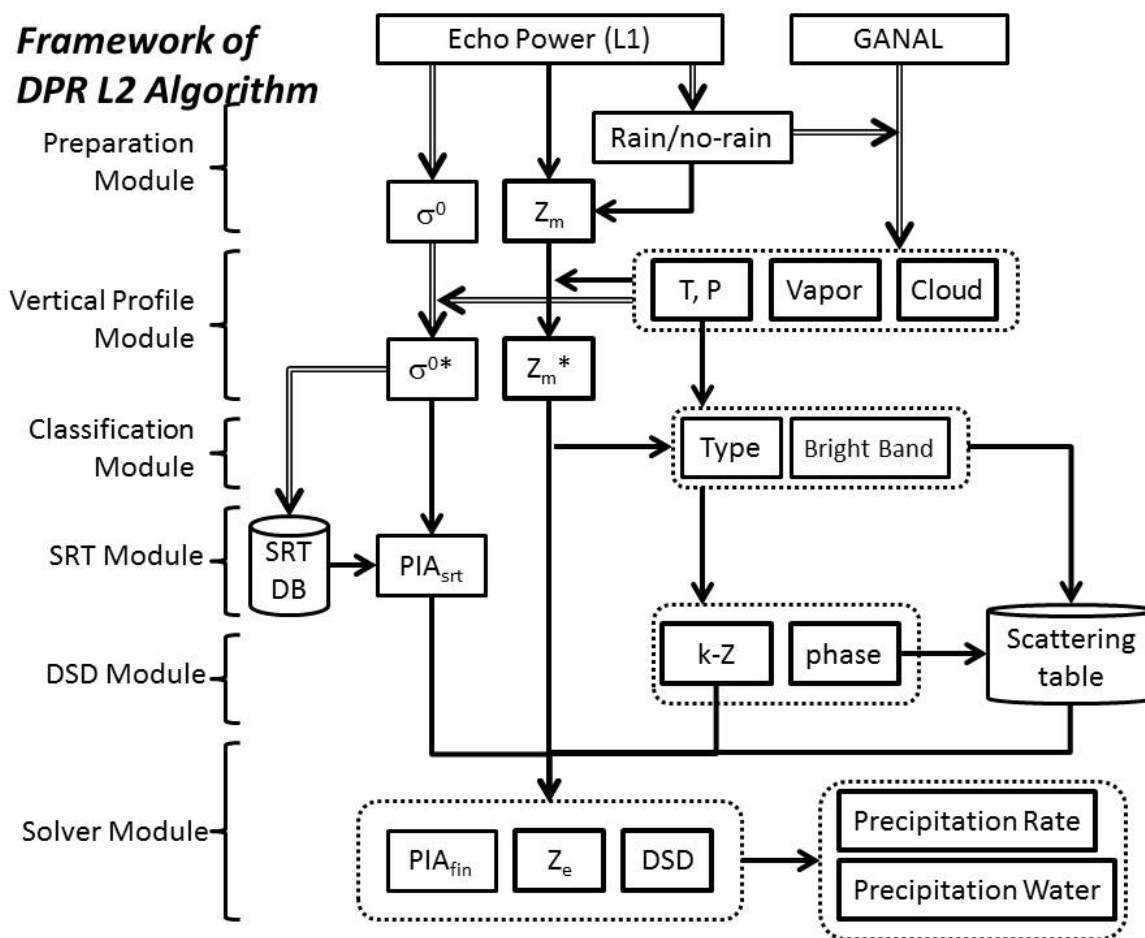
Fig. 7-2: DPR Algorithm flow chart.
Fig. 7-1: DPR algorithm flow chart.

7.2   Combined Radar+Radiometer Algorithms

The GPM combined radar-radiometer algorithm performs two basic functions: first, it provides, in principle, the most accurate, high resolution estimates of surface rainfall rate and precipitation vertical distributions that can be achieved from a spaceborne platform, and it is therefore valuable for applications where information regarding instantaneous storm structure are vital. Second, a global, representative collection of combined algorithm estimates will yield a single common reference dataset that can be used to cross-calibrate rain rate estimates from all of the passive microwave radiometers in the GPM constellation. Through the passive microwave radiometer estimates, the transfer standard from GPM to these constellation radiometers, can

ultimately be applied to the GPM infrared-microwave multi-satellite estimates of surface rainfall via the multisatellite Level 3 algorithms. The combined algorithm can be viewed as having two components. The *radar algorithm component* will draw heavily from the TRMM PR heritage algorithm, and this algorithm will be augmented to include dual-wavelength DPR precipitation observations (see section 7.1). An ensemble of precipitation estimates consistent with the radar data will be derived using this algorithm component. The *radiometer algorithm component* will essentially filter the radar algorithm precipitation estimates to obtain better agreement with coincident radiometer observations from GMI. The algorithm architecture is largely consistent with the successful TRMM combined algorithm design, but it has been updated and modularized to take advantage of improvements in the representation of physics, new climatological background information, and model based analyses that may become available at any stage of the mission.

The current GPM combined radar-radiometer algorithm architecture is descended from a rich heritage of algorithms that were developed for the TRMM mission, as well as other algorithms developed and applied to airborne radar-radiometer data. In TRMM, only Ku-band radar observations were available from the PR, and only lower-frequency (≤ 85 GHz) brightness temperature measurements were available from TMI. One of the broad challenges in GPM combined algorithm development is the creation of updated physical parameterizations that have greater accuracy at higher latitudes. Since freezing levels will be lower at these latitudes, there is a need for better identification of the altitudes where the transitions from liquid to mixed-phase to ice-phase precipitation occur, in both convective and stratiform precipitation regions. In addition, improved descriptions of the extinction and scattering of ice and mixed-phase precipitation that are applicable to the 10–183 GHz frequency range will be required. The development of improved physical parameterizations in the GPM pre-launch era will be aided by field campaign instrument "simulators", including the APR-2, HIWRAP, CoSSIR, CoSMIR and AMPR. The improved precipitation physical parameterizations will affect both the radar and radiometer components of the algorithm. The GPM combined algorithm takes advantage of the additional information provided by the Ka band radar channel to glean more specific information about the precipitation size distribution and associated attenuation in each gate. The estimation of precipitation size distribution parameters is further aided by precipitation attenuation information from the GMI channels, which have an extended spectral range relative to the TMI. However, if the Ka band reflectivities do not provide additional information due to very light rain (Rayleigh limit), or they are severely attenuated in heavy precipitation, then the combined algorithm must make a natural transition to a single-frequency, Ku band solution in which a more approximate estimation of precipitation size distribution parameters is performed.

Regardless of whether or not the Ka band data are applicable, however, information from the GMI brightness temperatures can be used to make further adjustments of path attenuation due to non-precipitating cloud liquid water and water vapor, which are not directly sensed by the DPR. In addition, there are precipitation microphysical parameters, such as the intercept of the particle size distribution and the density of ice-phase precipitation that may be adjusted using radiometer information.

Ultimately, the degree to which any precipitation or environmental parameters can be adjusted is limited by the information content of the DPR and GMI observations and any additional information provided by *a priori* data, such as the natural ranges of particle size distribution parameters, cloud water contents, etc., and how these parameters co-vary spatially.

The current algorithm design is based upon an Ensemble Kalman Filtering (EnKF) approach for inverting the DPR reflectivities and GMI brightness temperatures to estimate precipitation profiles; see Anderson (2003) for a general description of EnKF approaches. The general architecture of the GPM combined algorithm is illustrated in Fig. 7.3. There are three primary modules in the combined algorithm: an Environment Module, which establishes the environmental background of the precipitation distributions to be estimated, a Radar Module, which produces ensembles of radar-consistent precipitation profile solutions at each DPR footprint location, and a Radiometer Module, that modifies the radar-derived precipitation ensembles to be more consistent with the GMI observations. The outputs of the algorithm are the mean (best estimate) and standard deviation (uncertainty of estimate) of the DPR-GMI filtered ensemble of estimated precipitation profiles at each DPR footprint location.

Post-launch validation of GPM combined algorithm products will be in two parts: First, well-calibrated polarimetric radars, operating in conjunction with vertical radar profilers and collocated disdrometers during GPM field campaigns, will provide comparative data for detailed microphysical validation of GPM DPR+GMI vertical profiles. These comparative data will be augmented by spatially extensive radar network data that will test the coherence of retrieved precipitation distributions and identify any algorithm failures. The second validation component will be to validate computed microwave radiances based upon the DPR+GMI retrieved precipitation distributions. This will be accomplished by comparing DPR+GMI simulated radiances to coincident radiances observed by a given GPM constellation radiometer during swath crossovers. The second component of validation is critical, since the retrieved precipitation profiles and simulated radiances will be used to construct the databases for cross-calibrating the constellation radiometer precipitation algorithms.
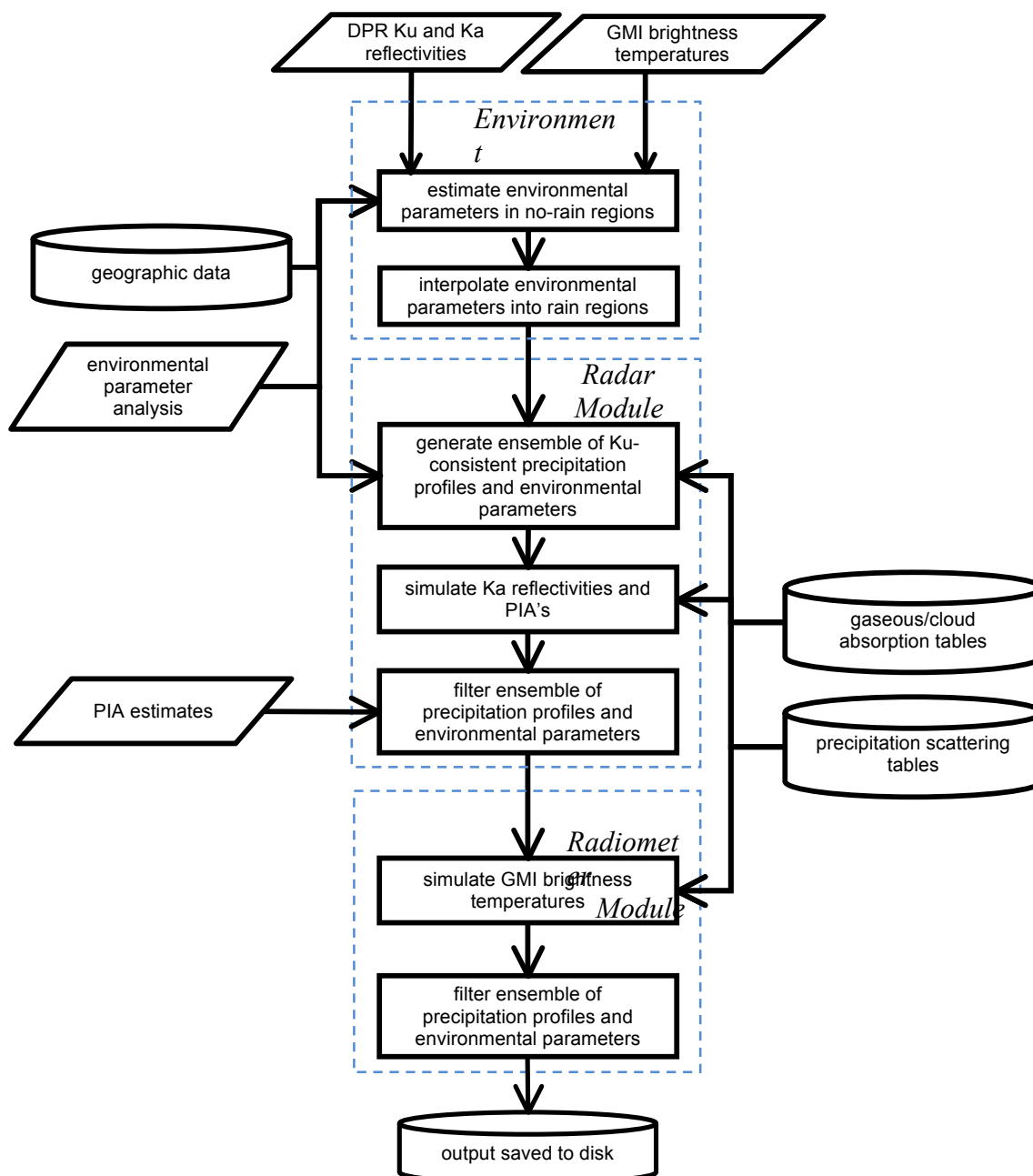
Fig. 7-3: Basic architecture of the GPM Combined Radar-Radiometer Algorithm

7.3 *Radiometer Algorithms*

The passive microwave rainfall algorithm is a parametric algorithm for the retrieval of liquid and solid precipitation profiles from the GMI and GPM constellation radiometers (see Table 5-2). The passive microwave algorithm is designed to take advantage of the Core observatory to define *a-priori* databases of observed precipitation profiles and their associated

brightness temperature signals. These databases are then used in conjunction with Bayesian inversion techniques to build consistent retrieval algorithms for each of the GPM constellation satellites. The dual frequency radar is the key to the success of this methodology and hence why we call this a radar-enhanced radiometer algorithm.

The at-launch algorithm will be known as GPROF_2014 to indicate that the algorithm uses an *a priori* database that was created before a climatology of the GPM Core satellite was available. The climatology used in GPROF_2014 is a combination of available satellite observations and cloud resolving models.   Three data sources are used to simulate the Core satellite as best as possible. Over the continental US, we use SSMIS observations with surface based radar derived rainfall from NMQ. This dataset is complemented over the tropics by using TRMM TMI and PR derived rainfall. Coincident AMSR-E and MHS coupled to CloudSat rain is used over the extra-tropics. These Tb and rainfall rates are then matched to a global Cloud Resolving Model to select profiles that match the observed Tb and rainfall rates in each of the three data sets. These profiles are finally used to compute Tb to each of the constellation sensors to construct the database used in the individual retrievals.

After launch, this procedure is simplified by using the combined algorithm as a basis for the *a priori* database. Because the DPR profiles will be developed to be consistent with GMI observations, it is anticipated that these profiles will be equally consistent with other radiometers. Forward calculations through the combined algorithm output at 4 km spatial resolution will be used to construct *a priori* databases for each of the constellation sensors once the combined algorithm is stable and available for roughly one year.

The retrieval itself uses a Bayesian foundation that has been well described in the literature (e.g., Evans et al. 1995, Kummerow and Giglio 1994, Kummerow et al. 1996, 2001; Marzano et al. 1999, Smith et al. 1994a,b; Bauer et al. 2001). These methods differ from what is proposed for GPM only in the steps they had to take in order to deal with non-robust global a-priori databases available prior to the launch of GPM. The early radiometer algorithms in the TRMM era were dominated by schemes using cloud-resolving models (CRMs) to produce *a priori* databases of cloud profiles. The ability of the *a priori* databases to faithfully reproduce and fully represent the actual microphysics structure of observed storms is one of the essential conditions for most of these algorithms to give reliable results. Using a finite and typically small number of these models to represent all raining environments led to a lack of representativeness.

Version 7 of the TRMM oceanic algorithm implemented in 2011 represented a significant advance in that the TRMM radar and radiometer were used in conjunction with the cloud-resolving model to (a) bring in only those cloud model profiles that simultaneously match the radar and radiometer observations (thus ensuring that the physics is nominally correct) and (b) to populate the Bayesian database with profiles that match the naturally observed occurrence as seen by PR and TMI. Version 7 also eliminates the need to determine the freezing level by organizing then subsequently searching the *a priori* database only within the appropriate sea surface temperature (SST) and total precipitable water (TPW) bin (Kummerow et al., 2009; Berg et al., 2006).   Version 7 of TRMM provides significant heritage for algorithm development for GPM-era algorithms.

Following the positive improvements seen in TRMM TMI V7 over oceans, GPROF_2014 will assign all entries in the *a priori* cloud profile database to specific surface temperature, TPW and land surface classes. Ten land classes have been identified using the Prigent and Aires emissivity classes (Aires et al., 2011, Prigent et al., 1997, Prigent et al., 2008),

shown in Fig. 7-4. These classes will also be tagged with additional information related snow cover following the work of Munchak and Skofronick-Jackson (2012).
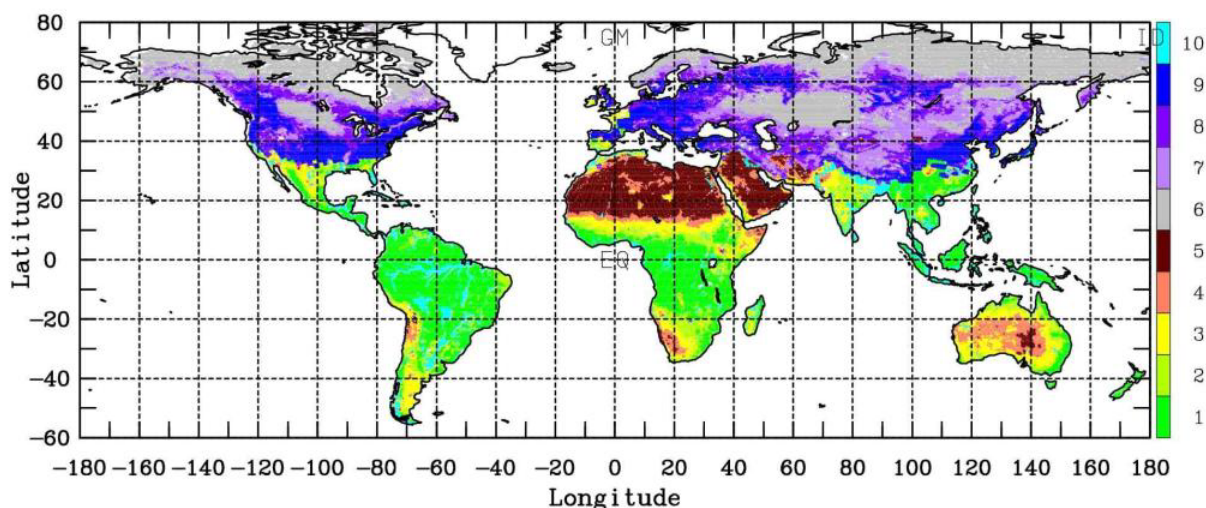
Fig. 7-4: Land surface clusters using a K-means or Kohonen methods algorithm in order to classify the surface based on the emissivity information. Here, the globe is classified into 10 classes for January (Prigent *et al*. 2008). In this example, class ten is for water-covered pixels, classes 6 to 9 are for snow/ice-covered pixels and classes 1 to 5 are for increasing vegetation cover. It is proposed to reproduce such a global classification for each location/month. The goal is to obtain 15-25 classes.

It is noted that for some precipitation occurrences and some locations, classifying into 10 land classes will not be useful. Therefore, the GPROF_2014 algorithm has been further broken into three algorithm approaches based on knowledge of surface emissivity:

S0: Emissivity is not known and/or corrupts TB signals. Retrieval uses a channel combination that is insensitive to the surface (Petty and Li, 2013, Petty 2013)

S1: Emissivity is not known but can be identified from land surface cluster maps. Retrieval searches Bayesian profiles of self-similar emissivity classes

S2: Emissivity is known by physical models of the surface features. Retrieval searches a-priori database with same surface properties

In general, two retrievals (either S0 and S1 or S1 and S2) will be run in parallel and results compared in the output. Full details of the output variables and formats can be found in the algorithm theoretical basis document (ATBD) available at http://rain.atmos.colostate.edu/ATBD or at http://pps.gsfc.nasa.gov/atbd/atbd.html.

7.4   *Algorithm Readiness Test Plan for PPS Delivery*

7.4.1   *Introduction*

The Radar, Combined, and Radiometer Level 2 algorithms being developed by the algorithm teams will require acceptance testing both before and after delivery to the Precipitation Processing System (PPS). The scheduling for algorithm submittal and verification follows the Integrated Algorithm-GV-PPS Schedule and Milestones given in Section 10. Appendix M reports the testing plans for each PPS delivery (V1; November 2011 and V2; November 2012) and algorithm (radar, combined, radiometer). Each test plan includes datasets used to validate the algorithm, tests performed, and measures of success/checklists of performance requirements.

At this point, the focus is on GPM pre-launch algorithm testing. While there will be ongoing post-launch evaluation of GPM DPR and GMI products resulting from the delivered algorithms (and updated post-launch versions), the priority is to ensure that test plans for pre-launch algorithm code delivery are adequate to demonstrate that all components of the algorithms are present, working, and meet basic scientific standards based on TRMM results and GPM requirements. Post-launch testing will focus more on incremental adjustments to the algorithm code, databases, and a priori information to further improve scientific aspects of the precipitation products and will be reported independently of this document. A summary of Appendix M is below.

7.4.1.1   **Algorithm Requirements**

In general, algorithm deliveries for November 2011 (V1) should be running (Baseline) code with all routines and databases included (though some subroutines may be stubs), have all output parameters in the products, use the PPS toolkit, and include algorithm team testing data input and output. Valid (non-missing) output is expected for the majority of a given synthetic GPM orbit. Additionally, the expectation is that the November 2011 codes should perform as least as well as TRMM in the tropics/subtropics and as well as currently possible at higher latitudes.

The November 2012 algorithm (V2/At-Launch) codes should be complete with scientific code and a priori databases. They should demonstrate enhanced performance relative to TRMM under conditions where such performance is possible and produce valid output over all regions (100%) of the GPM core orbit.

7.4.1.2   **Test Data**

In terms of inputs required for algorithm testing, we define (1) *GV* inputs as ground validation measurements from ground or aircraft sensors, (2) *simulation* inputs as those based on CRM models processed through a satellite simulator, and (3) *synthetic* inputs as those from current satellite sensors remapped into the GPM L1 products for use in these L2 algorithm algorithms.

GV data provides actual precipitation measurements at the ground level and some vertical structure (either from in-situ aircraft measurements or high-resolution multi-parameter radar measurements) at specified locations for specified precipitation events. These GV measurements can be collected over time and matched to coincident satellite overpasses to validate the algorithm when GPM-like satellite data is available pre-launch.

The simulation input datasets allow for complete internal consistency between model precipitation profiles and simulated GPM L1 products, but have the drawback that the physics within the models and satellite simulator may not be fully representative of the Earth's precipitation and radiative transfer physics. The satellite simulator team is in various stages of developing and validating simulations from the C3VP, LPVEx, TWP-ICE, MC3E field experiments and a winter storm over California. These simulations use the WRF and GCE models with the spectral-bin microphysics (SBM) scheme developed by Tao's group. In addition, global (Goddard MMF) simulations with GCE embedded within GEOS-5 are being run for 2008.

The synthetic data have the advantage of being actual satellite data, but will require some modeling of additional channels or merging of multiple satellite data since no single satellite has all the radar and radiometer channels of the GPM core satellite.

As described in Appendix M, each algorithm team has decided to use different input datasets for pre-PPS delivery testing of their algorithm. These different inputs will be used in initial PPS post-delivery tests to ensure that no coding errors have been introduced in the algorithm team-to-PPS transition, however common datasets will also be used post-delivery to assess code performance with sample GPM L1 inputs.

7.4.1.3   Summary

In Appendix M, the individual algorithm team testing plans are provided and include input testing datasets, tests to be performed, and measures of success, prior to PPS delivery. After each algorithm delivery to PPS, PPS undergoes it's own process of validating the algorithm code with both algorithm team-provided test data and common input datasets.

7.5   *Multi-Satellite Algorithms*

The advances planned for GPM inter-satellite radiometric calibration and the constellation sensors at Level 2 as part of GPM should substantially improve the reliability and accuracy of precipitation estimates produced by individual high-quality satellite microwave instruments. Other work, both within GPM and under other funding, continues to develop multi-spectral precipitation estimators for use with geosynchronous-orbit imagers, and to develop high-latitude estimates based on satellite sounding retrievals from TOVS, ATOVS, and AIRS. The drawback to all but the geosynchronous estimates is that they depend on low-orbit satellites, meaning that each satellite's estimates are available very intermittently; both the geosynchronous and sounding-based estimates have very modest skill at full resolution.

While frequent coverage afforded by these radiometers is important, there are, and always will be, applications such as hydrology that require even greater temporal and spatial resolution. The purpose of Level 3 combined multi-satellite precipitation algorithms is to collect as many of these individual estimates from the constellation of precipitation-capable satellites as is feasible, determine when and where they provide useful information, and then create a time series of precipitation estimates that is consistently calibrated, fine-scale, uniformly gridded, global, multi-decadal, and tagged with appropriate error and metadata information. This general concept has been developed over the last 15 years, with a proliferation of alternative approaches in the last five, and is the basis for the most-requested dataset in the TRMM suite of products, the TRMM Plus Other Satellites product set (products 3B42 and 3B43).

This 15-year heritage of algorithms includes the Adjusted GPI (Adler et al. 1994), TMPI (Huffman et al. 2001), PERSIANN (Sorooshian et al. 2000), NRL (Turk et al. 2003), SCaMPR (Kuligowski et al. 2002), TMPA (Huffman et al. 2007, the basis for the current TRMM 3B42/3B43 products), CMORPH (Joyce et al. 2004) and GSMaP (Okamoto et al. 2005). The combination techniques do not depend upon the details of the microwave algorithms – merely the instantaneous rainfall product and the estimate of its quality at the time of the overpass. The objective is to create a rain product with uniform temporal and spatial resolution, inter-calibrated to a reference microwave rain estimate. The merged microwave/infrared methods will thus benefit immediately from the constellation algorithms being developed for GPM in that GPM will ensure that the microwave products being used for bias correction are consistent with one another – an essential ingredient to make these algorithms perform optimally.

The U.S. GPM team's next-generation combination algorithm, called I-MERG, was delivered to GPM's Precipitation Processing System (PPS) in 2012. The methodology incorporates PERSIANN, CMORPH, and TMPA. Details of the algorithm, testing, and resulting product listing are in the ATBD found at (http://pps.gsfc.nasa.gov/atbd/atbd.html).

7.6 *Latent Heating Algorithms*

Five different TRMM Latent Heating (LH) algorithms designed for application with satellite-estimated surface rain rate and precipitation profile inputs have been developed, compared, validated, and applied in the past decade (see reviews by Tao *et al.* 2001, 2006, 2013). They are the: (1) Goddard Convective-Stratiform Heating (CSH) algorithm, (2) Spectral Latent Heating (SLH) algorithm, (3) Goddard TRAIN (Trained Radiometer) algorithm, (4) Hydrometeor Heating (HH) algorithm, and (5) Precipitation Radar Heating (PRH) algorithm. The strengths and weaknesses of each algorithm are discussed in Tao *et al.* (2006). Table 7-1 gives a summary of the five algorithms, including the type(s) of TRMM input data used to generate their associated heating product(s), the type of heating product(s) produced, and the key references describing their design. The TRMM-GPM joint science team has decided to have two standard LH algorithms: the Goddard CSH algorithm and the SLH algorithm. Table 7-2 lists the required data and type of heating products for these two algorithms. Note that one of the major inputs for these standard products is the improved rainfall estimate.

Algorithm Name	Data Required	Heating Products	Key References in Algorithm Description
CSH (Convective-Stratiform Heating)	PR, TMI, PR-TMI	Q_1, LH, Q_R, EHT, Q_2	Tao *et al.* (1990, 1993, 2000, 2001, 2010)
SLH (Spectral Latent Heating)	PR	LH, Q_1-Q_R Q_2	Shige *et al.* (2004, 2007, 2008, 2009)
TRAIN (Trained Radiometer Algorithm)	TMI (PR training)	Q_1-Q_R, LH	Grecu and Olson (2006), Olson *et al.* (2006), Grecu *et al.* (2009)
HH (Hydrometeor Heating)	PR-TMI	LH	Yang *et al.* (1999, 2006)
PRH (Precipitation Radar Heating)	PR	LH	Satoh and Noda (2001)

Table 7-1   Summary of the five LH algorithms (see Tao et al. 2006 for further details and salient references). Data inputs, retrieved products, and salient references are included. The conventional relationship between Q_1 (apparent heat source), LH, and Q_R (radiative heating) is expressed by Q_1-Q_R = LH + EHT, where the final term represents eddy heat transport by clouds (vertically integrated EHT is zero, i.e., it provides no explicit influence on surface rainfall). TMI is the TRMM Microwave Imager and PR the TRMM precipitation radar. Note that CSH, SLH and TRAIN explicitly use CRM-simulated latent heating profiles in their heating algorithm look up tables. Both HH and PRH also implicitly use CRM-simulated results (i.e., cloud vertical velocity).

	Spatial scale	Temporal scale	Algorithm	Products
Gridded	0.5 x 0.5 degrees 19 vertical layers	Monthly	SLH-PR CSH-Combined	LH, Q_1-Q_R, Q_2 LH, EHT, Q_R, Q_2
Orbital*	Pixel 19 vertical layers	Instantaneous	SLH-PR CSH-Combined	LH, Q_1-Q_R, Q_2 LH, EHT, Q_R, Q_2
Gridded Orbital	0.5 x 0.5 degrees 19 vertical layers	Instantaneous w/ time stamps on each grid	SLH-PR CSH-Combined	LH, Q_1-Q_R, Q_2 LH, EHT, Q_R, Q_2

Table 7-2   Summary of TRMM cloud heating products from the CSH and SLH algorithms. To obtain total Q_1 estimates from the CSH algorithm, the three individual heating components (i.e., LH, EHT, and Q_R) must be summed together. Also, Q_2 estimates from the CSH algorithm are separated into eddy and microphysical components and must be summed to obtain the total Q_2. *Orbital heating is not a standard TRMM product.

The purpose of Level 3 heating algorithms is to use as many of the Level 2 GPM rainfall estimates as possible to create a time series of heating estimates that is consistently calibrated, fine-scale, uniformly gridded, global, multi-seasonal, and tagged with appropriate error and metadata information. The advances planned for Level 2 products as part of GPM should substantially improve the reliability and accuracy of precipitation estimates produced by individual high-quality satellite microwave and DPR instruments. Given that these different heating algorithms use different Level 2 products with various temporal and spatial resolutions,

the objective of Level 3 heating products is to create an ensemble of such products with detailed documentation on the strengths and weaknesses of each product. These heating products, together with GPM precipitation products, can be used to advance the understanding of the global energy and water cycles. In addition, this information can be used for global circulation and climate models for validating and improving their parameterizations.

It is worth noting that a global heating data set represents a product that was considered beyond reach less than a decade ago. The distributing of heating products to the research community will facilitate new investigations into the thermo-hydro-dynamical complexities of storm life cycles, diabatic heating (latent heating and radiation) controls and feedbacks related to meso-synoptic circulations, and the influence of diabatic heating on the Earth's general circulation, weather, and climate.

Finally, the Level 3 activity will pursue joint work with the Level 4 activity to establish the best use of heating products with numerical models, assimilations (Rajendran *et al.*, 2004; Hou and Zhang 2007), and global model re-analyses. A recent review paper on applications of TRMM LH products was presented by Tao *et al.* (2013).

7.7   *Plans for Model-Assimilated Precipitation Products*

GPM Level 4 data products comprise precipitation estimates that combine information from satellite observations and numerical models. The GPM Mission is establishing agreements or collaborations with domestic and international research and operational agencies to develop GPM Level 4 products. Currently, three types of Level 4 products are under development:

7.7.1 *Global Precipitation Forecast Product*

The European Centre for Medium Range Forecasting (ECMWF), a premier operational numerical weather forecast center sponsored by a consortium of European countries, has agreed to make their global precipitation forecast products available (with 1-day delay) to the research and education community as a GPM Level 4 data product. The ECMWF, which has been leading center in assimilating satellite observations (including rain-affected microwave radiances) into numerical models to improve operational weather prediction (Bauer et al. 2006a, 2006b), expects to benefit from having ready access to GPM radiometer data in near realtime.

7.7.2 *Global Dynamic Precipitation Analysis Product*

The Global Modeling and Assimilation Office (GMAO) at NASA Goddard Space Flight Center has agreed to produce a 4-dimensional global precipitation reanalysis for the GPM Mission as a Level 4 data product. Global analyses that combine satellite precipitation observations with other observations and model information within the framework of statistical estimation can replicate certain intra-seasonal phenomena such as the Madden-Julian Oscillation with greater fidelity than model simulations (Hou et al. 2007). Such dynamically consistent observation-model estimates of the atmosphere are expected to offer a valuable tool for climate process studies.

7.7.3 Regional Model-Downscaled High-Resolution Precipitation Product

For certain hydrological applications that demand precipitation analyses at very high spatial and temporal resolution, GPM is exploring the feasibility of developing a high-resolution regional precipitation analysis using a CRM to dynamically downscale satellite precipitation information to sub-satellite pixel scale (1-2 km) precipitation analysis. A joint pilot project under the direction of the GPM Project Scientist has successfully developed a WRF-based ensemble data assimilation system to dynamically downscale satellite precipitation data to 1 km analysis. This system ingests the full suite of NCEP operational conventional data stream plus rain-affected radiances from microwave radiometers. Initial results from assimilation experiments using AMSR-E radiances show positive impact on analysis and short-term forecasts of storm intensity and precipitation related fields over the central United States (Zupanski et al. 2009). This pilot study offers a promising cornerstone for development of model-downscaled high-resolution precipitation products for GPM.

8. Ground Validation

8.1 Overview

The GPM Ground Validation Program is designed to support pre-launch algorithm development and post-launch product evaluation. The traditional approach to ground validation is to use ground-based observations to directly assess the quality of satellite products. Among the lessons learned from TRMM GV is that while such comparisons are useful and necessary, ground measurements have their own set of uncertainties that must be carefully monitored and quality-controlled. For GPM, precipitation validation centers upon characterizations of uncertainties in satellite retrievals and GV measurements in order to estimate the "true" precipitation rate through the convergence of satellite and ground-based estimates. Moreover, in order to improve physically-based satellite retrieval algorithms, ground observations must go beyond the collection of surface precipitation data to provide ancillary information within a precipitating column to identify sources of errors in retrieval algorithms and their associated assumptions under a variety of environmental conditions. Ground validation should also use hydrological measurements (e.g. streamflow data, snowpack depths, etc.) and water budget analyses as time/area-integrated constraints to quantitatively assess multi-satellite precipitation products and downscaled high-resolution precipitation analyses using models.

Based on recommendations of the GPM GV Advisory Panel, GPM is establishing joint GV activities and/or sites with partner institutions and a series of pre- and post-launch field campaigns to carry out components of the following three types of validation approaches:

• *Direct statistical validation via use of national networks:* Contributions of calibrated ground observations from operational and research instruments, regional and continental scale precipitation and hydrological products with associated error models, the development of downscaling models, and other related activities on large regional or continental scales;

- *Physical validation via process studies and field campaigns:* Contributions of targeted ground and aircraft measurements of cloud microphysical properties, precipitation, multi-frequency radar reflectivity, and radiances; modeling activities related to atmospheric simulation and retrieval algorithm testing; other relevant observations on local to regional scales
- *Integrated validation via assessment of hydrometeorological application:* Contributions related to assessment of satellite precipitation products using stream flow and other hydrologic measurements, formulation and application of downscaling methodologies, and analysis of the utility of satellite precipitation products for basin-scale water budget studies.

Within the framework of the above three approaches, five interdependent satellite, algorithm, modeling, and validation activities are targeted in order to quantify and understand measurement and algorithm uncertainties, propagation of those uncertainties through the product development chain, and ultimately the impact on applications (i.e., end-to-end validation). These five activities are: (1) core satellite error characterization focused on validation of DPR reflectivity, attenuation correction, drop size distribution, and rain rate retrievals; (2) constellation satellite validation focused on detailed statistical comparisons of retrieved rainfall rates; (3) assessment of radar/radiometer retrieval algorithm uncertainties; (4) CRM validation, supported through detailed measurements of cloud and precipitation properties as applied to the retrieval algorithm(s) physical framework; and (5) coupled atmosphere/land surface model validation set in the end-to-end framework of hydro-meteorological analysis, water-budget, and forecast system application.

This chapter provides a high-level overview of GPM GV implementation strategy and plans. Technical implementation details are provided in the GPM Ground Validation Science Implementation Plan (Petersen and Schwaller 2008) http://pmm.nasa.gov/science/ground-validation/ground-validation-library.

8.2   *Integrated PMM Science and GPM Flight Project GV Implementation Approach*

In order to provide robust measurement metrics and to test/improve retrieval algorithm physics, the GV system must provide four-dimensional precipitation measurement capabilities (time and space) spanning a broad spectrum of precipitation rates (i.e., light to heavy), types (liquid and frozen) and meteorological regimes. To accomplish these tasks the GVS will rely on a complementary set of NASA PMM-managed facilities, ground assets provided by the GPM Flight Project, and externally leveraged instrument assets. Here the term "externally leveraged" is defined as including both national and international, research and operational assets, explicitly recognizing that the global nature of the mission requires collaboration with international partners (see Figure 8-1).

Figure 8-1. Locations of GPM ground validation activities worldwide.

On regional scales select national (e.g., interagency) and international resources such as existing calibrated radar and rain gauge networks will provide basic datasets that enable direct statistical validation of GPM core-satellite reflectivities and core/constellation rain rate measurements. The resultant statistical comparisons provide a means for algorithm developers to assess algorithm performance at regional and/or regime scales, thus identifying potential problems in the algorithms or instruments that require further investigation (calibration, algorithm physics, etc.).

To support detailed validation of algorithm physical assumptions in both the pre and post launch periods, and to assure sampling across a range of regimes, GVS first-tier efforts will rely heavily on the use of both transportable and fixed site research-grade multi-frequency, dual-polarimetric radars. Here *first-tier* is defined as a research radar with flexible operation and scanning capabilities, established engineering calibration practices, and an open and/or documented calibration record. The current suite of U.S. *first-tier* radars being coordinated for GPM GV use include transportable platforms such as the NASA N-POL S-band and NASA D3R (Dual-frequency, Dual-polarimetric Doppler) Ka-Ku band radars to be based at NASA GSFC/Wallops Flight Facility, the DOE ARM X-SAPR X-band radar array located in northern Oklahoma, and the NSF CSU-CHILL Radar (S/X band) located in Greeley, Colorado. Current international partner-led first-tier platforms include the Environment Canada King City C-band radar, the Italian Polar 55C radar, the Univ. of Helsinki/FMI Kumpala C-band radar, and the Australia Bureau of Meteorology CP-2 (S/X) and C-POL radars. This suite of radars will be used in both pre and post-launch field studies and coordinated post-launch scanning with select GPM Core and constellation satellite overpasses.

The combined use of S, X, and Ka-Ku band first-tier radars will provide a means to sample the entire spectrum of precipitation rates and types (i.e., the required detection range of 0.2 mmh^{-1} – 110 mmh^{-1}), while platform mobility and geographic distribution facilitate sampling of precipitation in a plethora of meteorological regimes. During focused field efforts, the multi-parameter radar measurements will be referenced and calibrated in many cases using networks of ground-based point-measurement capabilities such as high density disdrometer networks and rain gauge arrays, existing W-band cloud-radars (ground, air and space-based), wind-profiling radars, and instrumented aircraft (NASA and external organizations). First-tier radars will also be tasked in a target of opportunity mode to scan in concert with GPM Core satellite overpasses using a set of flexible sector volume, Range Height Indicator (RHI), and/or rapid Plan Position Indicator (PPI) rain scan modes. Importantly, the first-tier radars provide a calibrated scale-bridge that extends point measurements provided by platforms such as rain gauges to the scale of instantaneous satellite fields of view and regional product scales. Collectively this multi-frequency combination of radars and supporting instrumentation will provide an internally consistent, calibrated means to retrieve precipitation particle type, size, and content in three dimensions.

Concurrent with the performance of direct/statistical validation efforts and supporting the first-tier research radars are larger "national network" systems such as the U.S. National Weather Service WSR-88D polarimetric radar network. These operational network radars comprise the critical *second-tier* of GPM GV radar resources to be used for direct statistical validation (cf. Sec. 8.3). Here "second-tier" is defined as conforming to the same calibration and quality standards expected of first-tier research radar platforms, but it is acknowledged that scanning flexibility and radar control constraints exist due to operational weather decision support requirements.

As a means to assess GPM Products in a hydrologic framework the aforementioned direct and physical validation activities are also leveraged in formal collaborations with external programs such as the Iowa Flood Center (IFC) and NOAA Hydrometeorological Testbed (HMT) activities. These collaborations will be exploited to address GV objectives related to integrated hydrologic validation. Here GVS radar and supporting observational resources will be deployed to supplement existing high quality precipitation, hydrologic and related measurement networks to examine full end-to-end propagation of both ground and satellite-based precipitation measurement and measurement errors through hydrologic prediction systems.

8.2.1 PMM Science Role in the GVS

The PMM Science Team (PST) develops GPM precipitation retrieval algorithms that provide the underlying framework for conducting validation activities. The PST is expected to interact with the GVS in several ways. First and foremost, PST algorithm developers and working groups provide explicit guidelines to the GPM Project Scientist and the GV Science Manager (GVSM) regarding measurements needed for characterizing specific geophysical processes or algorithm "ingredient" parameters. The GVSM will work with the PST to identify potential ground and airborne instrumentation complements, or existing datasets needed to satisfy measurement requirements. Second, the PST works with the GVSM to define a prioritized set of science objectives for each GV field campaign undertaken to address a specific physical validation need. As part of this interaction, the PST may also provide suggestions related to field campaign site location, assist in field campaign planning, and deploy during field

operations as appropriate. Third, and from a programmatic standpoint, as the current TRMM mission transitions to the GPM era, it is expected that the PMM program will provide GVS access to the NASA N-POL S-band dual-polarimetric radar (currently being upgraded/refurbished), access to TRMM-era GV disdrometers and rain gauges, and where/when possible partially fund deployment of aircraft instrumentation and/or platforms for GPM GV field campaigns. Collectively, the interaction between the PST, PMM management, GPM Project Scientist and GVSM help to drive GVS development of the requisite instrumentation and data products within the GPM Flight Project.

8.2.2 GPM Flight Project Role in the GVS

The GPM Flight Project implements the validation activities recommended by the PST and GPM GV Science Panel as communicated to the Project GVS Manager (GVPM) via the Project Scientist and GVSM. These activities include funding the management, development and coordinated deployment of GVS instrumentation, and creation and archival of associated validation data products. Specifically, the GPM Flight Project will lead and/or provide: a) development, procurement, oversight, integration, and testing of the NASA D3R Ka-Ku band radar; b) development, procurement, management, and deployment of a high density disdrometer network (e.g., acquisition of two or more next generation 2D video disdrometers, and ten or more Parsivel disdrometers or their equivalent); c) as required, provide for field deployment of leased S-band wind profilers; d) partial funding contributions to be combined with PMM financial support for the lease of airborne platforms and instrumentation in association with GPM GV field efforts; and e) production of direct validation tools such as data mining software architectures, associated data products, and data archives designed to provide a reduced set of national network precipitation and hydrometeorological observations (e.g., radar, rain gauge, stream flow etc.) relevant to direct validation activities.

8.3 National Validation Networks for Direct Product Evaluation

Statistical comparisons of GPM satellite data and products to similar ground-based measurements are facilitated through the use of national network measurement infrastructure. This infrastructure includes networks of operational weather radar platforms, rain gauge networks, and high quality operational merged radar-rain gauge products. These ground-based datasets can be readily combined with coincident satellite overpass data into a multi-dimensional linked-parameter database. The database provides matches of collocated ground, DPR radar and/or constellation radiometer measurements such as columns of reflectivity, brightness temperatures, precipitation type, and rain rate/accumulations from which statistical comparisons/measures can be derived. Collectively the database and statistical comparisons constitute what is hereafter referred to as the "GPM GV Validation Network (VN)" infrastructure.

The overarching objective of VN statistical comparisons is to identify, understand, and resolve first order variability and bias in precipitation retrievals over large scales (i.e. regional) and different meteorological/hydrological regimes. As such the VN architecture is comprised of three related components. First, GV will use national network radars to conducts orbit by orbit direct statistical validation of DPR radar reflectivities in the vertical column—the fundamental (i.e., Level 1) parameter used in DPR retrieval algorithms of rainfall rate, precipitation diagnostics, and calibration of GMI retrieval algorithms. The second VN component involves

orbit by orbit pixel-based comparisons between core and constellation radiometer and ground-based radar or gauge network-measured precipitation rate/type (e.g., liquid, frozen). The third VN component compares time-integrated and spatially-gridded GV precipitation accumulation datasets to Level-3 products.

8.3.1 DPR-Ground Radar Reflectivity Inter-comparisons

To facilitate development of VN software, a software prototype has been developed to process a subset of U.S. operational radar and coincident TRMM PR overpass data. Here, the VN can acquire data from the operational WSR-88D (NEXRAD) radar network in near-real-time. During the GPM-era, accompanying DPR satellite products will be ingested in near real time via direct interfaces established with the NASA PPS. The current VN software prototype is very flexible and has been used to process other U.S. radar datasets including those from the TRMM GV site on Kwajalein and the ARMOR radar in N. Alabama.

Because *global* validation of precipitation occurring in a myriad of meteorological regimes is required to fully evaluate the global error structure of GPM precipitation retrievals, the VN software is being developed so that it is exportable, providing a means for international partners in host countries to install the software and ingest and process data using their own operational radar and IT infrastructure. Indeed, the current VN prototype has already been applied to radar data collected in other countries. For example, in collaboration with international partners the VN software has been used to process operational ground and TRMM PR radar datasets collected in Australia and Korea, and the software has recently been provided to the U. Barcelona for use in Spain. As the software is further developed, it will be freely available to any GPM international partners who operate radar networks with the only requirement being that the statistical results of the comparisons and some measure of ground radar network performance and calibration are shared with the broader GPM community.

In terms of statistical products, the VN currently generates a full suite of statistical summaries and graphs (profiles, time series, PDFs, cross-sections etc.) for comparisons between TRMM and ground radar reflectivity. Future expansion of the VN will also consider the impending dual-polarimetric upgrade of the WSR-88D network (2009-2012) and inclusion of dual-polarimetric diagnostics provided by the Kwajalein radar, and the NPOL radar based at GSFC/Wallops Flight Facility. The upgraded network will yield internally consistent reflectivity calibrations, generate superior rain rate estimates, and provide the possibility of obtaining broad area drop-size distribution (DSD) statistics.

8.3.2 VN Rainrate Statistics

Rainrate and rainfall validation in the VN architecture will rely heavily on the use of existing high resolution, quality controlled U.S. national network rain rate products such as the NOAA National Mosaic and Multi-Sensor QPE (NMQ: http://nmq.ou.edu/). In collaboration with NOAA and the U. Oklahoma, NMQ products will be used to provide instantaneous gridded, rain gauge-adjusted radar estimates of rainfall rate at 1 km grid scales. These data will be up-scaled and directly compared to coincident DPR rain rate estimates at DPR pixel scales.   The products will also be available for use in footprint-scale comparisons with passive microwave instruments such as the GMI on the core satellite, and where/when necessary, other select GPM constellation members. Finally, hourly-accumulated NMQ rainfall will be available for use in coarser-grid (e.g., 0.1° to 0.25°) direct validation of GPM Level 3 products on temporal and

spatial scales of user choice. Collectively, these comparisons will provide a robust statistical means to verify/validate GPM core/constellation instantaneous and accumulated rain rate products in different climate regimes.

8.4 *Field Campaigns for Physical Validation*

A key lesson learned from TRMM is that precipitation algorithm retrieval errors have a strong dependence on meteorological regimes and physical processes specific to those regimes. The global sampling of GPM and in particular, the extension of sampling into colder polar latitudes and over larger continental regions (relative to TRMM) places even more importance on the ability of GV to support sampling in markedly different "regimes". As such, detailed measurements supporting the development and validation of the retrieval algorithms will emphasize adaptive/transportable field measurements focused on particular meteorological regimes where large uncertainties are known to exist a priori (i.e., retrievals over land, snow and light precipitation, etc.) and/or are discovered after launch. These efforts will focus on the following:

(1) Collection of cloud microstructure, microphysics (cloud water, cloud ice, liquid, mixed and solid precipitation phases), particle sizes, shapes and distributions (PSD), high resolution melting layer characteristics, rainfall rates, and aerosol characteristics (e.g., CCN and IN concentrations to the extent possible). These data are to be collected in coordination with an overflying high-altitude aircraft instrumented with a GPM-like dual-frequency radar and suite of microwave radiometers.

(2) Collection of high-resolution PSDs and rain rate information at the surface and in the column to statistically quantify sub satellite-pixel precipitation characteristics.

(3) Quantification of surface multi-channel microwave emissivity as a function of the land surface state/type, sensible and latent heat fluxes (including soil moisture). This is most easily accomplished using the same airborne radiometer instrumentation cited in (1).

(4) Provision of accurate large-scale forcing environments for CRM simulations (i.e., to remove the issue of quality forcing datasets as an issue for the accuracy of the CRM)

(5) Testing of CRM simulation fidelity via intensive statistical comparisons of simulated to observed cloud properties and latent heating fields.

(6) Further establishment of CRM space-time integrating and data assimilation capability for quantitative precipitation estimation.

Also note that in the course of applying GV physical process measurements to the algorithm validation problem, constant evaluation of the core complement of GPM GV instrumentation and retrieval methods will also be assessed and modified as needed.

The reference architecture for GV physical process studies is based on a series of PMM Principal Investigator-led Extended Observation Periods (EOPs) and Intensive Observation Periods (IOPs). EOP activities are best interpreted as targeted sets of field observations designed to function for an extended period- e.g., 6-12 months or more. In general EOPs leverage *existing* research and/or network operational instrumentation and datasets (e.g., radar, gauges, disdrometers, etc.) to conduct longer duration sampling of precipitation physical processes and/or conduct coordinated sampling of precipitation with GPM Core and Constellation platform overpasses.

Several geographically and meteorological diverse EOP activities are planned for the GPM Core and Constellation missions. For example, radar infrastructure and associated scanning conducted at the first-tier radar locations mentioned in Sec. 8.1 comprise several of the planned EOP activities. Other activities include continuous data collections via the ultra-dense GPM GV gauge and disdrometer networks currently operating at the coastal site of NASA Wallops Island, Virginia, planned reference falling snow measurements made at four densely-instrumented sites across Canada (winter 2013 and onward), radar and gauge-based snowfall measurements made at a high-latitude reference field site in Sodkanklya, Finland, and TRMM-Legacy GV measurements to be continued at the subtropical Melbourne, Florida WSR-88D and tropical oceanic Kwajalein radar sites (K-POL radar and associated gauge/disdrometer infrastructure). Note that the number and makeup of EOP sites is dynamic, but activities are expected to increase beyond that already mentioned. In contrast to EOPs, IOPs are relatively short duration (4-6 week), targeted field campaigns conducted with a dense complement of ground and airborne instrumentation that may or may not occur in conjunction with an EOP. Notwithstanding the shorter operations time frame and dense ground instrumentation, perhaps the most distinguishing characteristic of an IOP is the inclusion of coordinated aircraft sampling; e.g., the inclusion of a high-altitude satellite simulator aircraft such as the NASA ER-2, carrying airborne multi-frequency radar/radiometer instrumentation, and a coordinated under-flying in-situ aircraft carrying microphysical probes.

A total of five GPM GV-lead IOPs are planned, occurring with a periodicity of approximately 18-24 months (3 pre-launch and 2 post-launch, Table 8-1). Of these field efforts, two very successful campaigns have already taken place (cf. http://pmm.nasa.gov/science/ground-validation/field-campaigns), the first addressing mid-latitude warm-season precipitation processes over land (MC3E), the second addressing in situ and remote sensing of snowfall physical processes/characteristics (GCPEX). Importantly, the deployments mentioned in Table 8-1 are designed to solve specific high priority problems in the retrieval algorithms, as identified by algorithm developers who directly participate in IOP/EOP planning and execution.

Table 8-1. GPM GV-lead field campaign deployment schedule

Science Objective	Date/Location
Physical basis for GMI and DPR rainfall retrievals over land surfaces	April-June 2011, MC3E, N. Central Oklahoma
Physical basis for retrieval of frozen and mixed-phase precipitation over land surfaces	Winter Jan – Feb 2012, GCPEx, Ontario Canada.
Physical/Integrated hydrological validation over flat terrain subject to flooding	April-July 2013, IFlooDS, northeastern Iowa
Physical/Integrated hydrologic validation over topography	2014, May-June 2014, IPHEX, N. Carolina, Appalachians/Piedmont region
Physical/Integrated hydrologic validation in extreme coastal and topographic gradients	2015, Nov-Dec, OLYMPEX, Washington, Olympic Peninsula (TBC)

8.4.1 *Mid-latitude Continental Convective Clouds Experiment (MC3E) - 2011*

Pre-launch GPM GV activities must address the development of physically-based passive microwave, DPR, and combined radar-radiometer precipitation retrievals over land. This activity requires a) the collection of new observational datasets that better characterize the 3-D

distribution and character (e.g., size distributions, phases, precipitation rates etc.) of both cloud and precipitation particles; b) observational datasets suitable to initialize, force and physically validate CRM microphysics which provide insights into cloud variables that are difficult to directly observe but critical to algorithm performance (e.g., cloud water and mixed phase); and c) some measure or foreknowledge of the surface character (vegetation, moisture etc.) controlling the upwelling radiative characteristics (i.e., surface emission) for suitable coupled CRM-land surface modeling. To meet these requirements GPM collaborated with the DOE ARM program in the MC3E field campaign from April to June 2011 at the ARM Southern Great Plains Central Facility Cloud and Radiation Testbed (CART) located in north-central Oklahoma. DOE-ARM interests in MC3E revolve around the validation of coupled cloud models via detailed descriptions of convective cloud kinematics, precipitation and feedbacks between kinematics and precipitation.

GPM sampling priorities for MC3E focused on the collection of coincident high altitude Ka-Ku band radar and multi-frequency radiometer data (10-183 GHz), airborne in-situ microphysical observations, and accompanying ground-based polarimetric radar and disdrometer datasets in a *wide variety* of continental precipitation types (Fig. 8-2). Collectively these datasets provide "reference" constraints for the development and testing of both DPR and radiometer retrieval algorithms. Detailed tables of the linkages between algorithm development unknowns (assumptions) and measurements needed to instrumentation requirements were used to define the field campaign efforts. These linkage (science traceability matrices), the science objectives and archived data can be found at http://pmm.nasa.gov/science/ground-validation or http://gpm.nsstc.nasa.gov/mc3e/ .
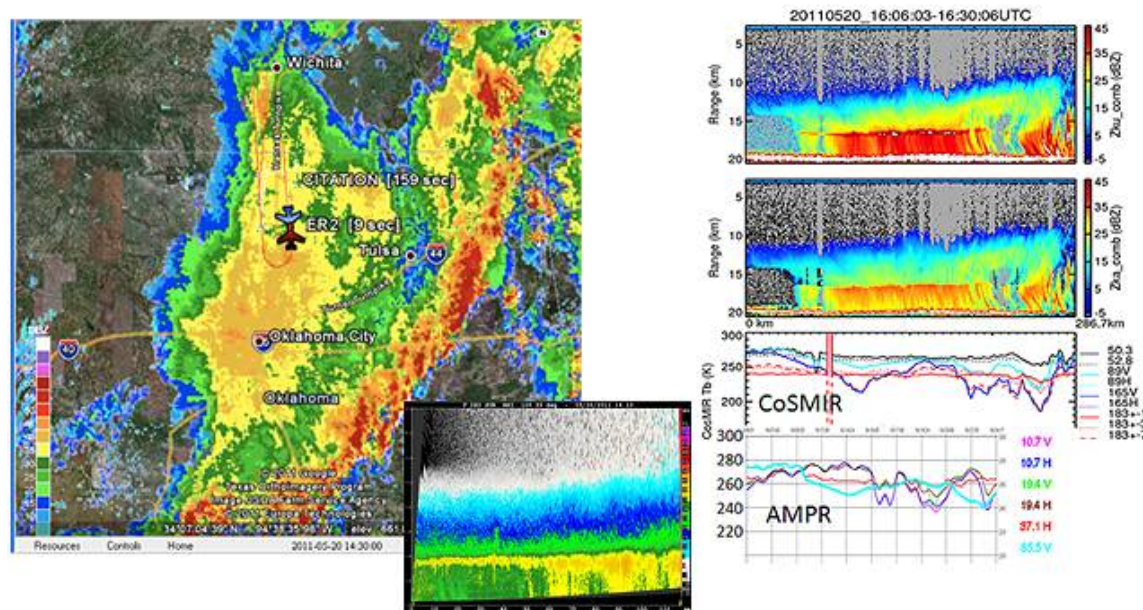
Figure 8-2. MC3E coordinated airborne sampling at 14:30 UTC, May 20, 2012. Left: Example of ER-2 (red) and Citation (white) flight leg coordination overlaid on radar reflectivity. Left inset: A vertical cross-section (RHI; 1419 UTC) of radar reflectivity from the C-SAPR radar oriented approximately along the UND/ER-2 flight tracks. Right: 1606-1630 UTC ER-2 transect of coincident HIWRAP Ku-band (top) and Ka-band (middle) reflectivity, with CoSMIR and AMPR radiometer brightness temperatures.

8.4.2   GPM Cold-season Precipitation Experiment (GCPEx) - 2012

The GPM Cold-season Precipitation Experiment (GCPEx) occurred 70 km northwest of Toronto in Ontario, Canada during the winter season (Jan 17- Feb 29, 2012). GCPEx was designed to address shortcomings in GPM snowfall retrieval algorithm by analysis of collected microphysical properties, associated remote sensing observations, and coordinated model simulations of precipitating snow. GCPEx expanded upon the successful Canadian CloudSat/CALIPSO Validation Programme (C3VP) held the winter of 2006-2007. The GCPEx experiment provided GPM snowfall algorithm developers and satellite simulator models (coupled cloud-resolving and radiative transfer models) with a basic set of observations and modeling simulations to use for algorithm development with science/measurement traceability tables similar to the MC3E field campaign. GCPEx data sets were collected toward achieving the overarching goal of characterizing the ability of multi-frequency active and passive microwave sensors to detect and estimate falling snow. Figure 8-3 shows some examples of collected data. More details about the GCPEx field campaign including science objectives, operation plan, and archived data availability are at http://pmm.nasa.gov/science/ground-validation or http://gpm.nsstc.nasa.gov/gcpex/.
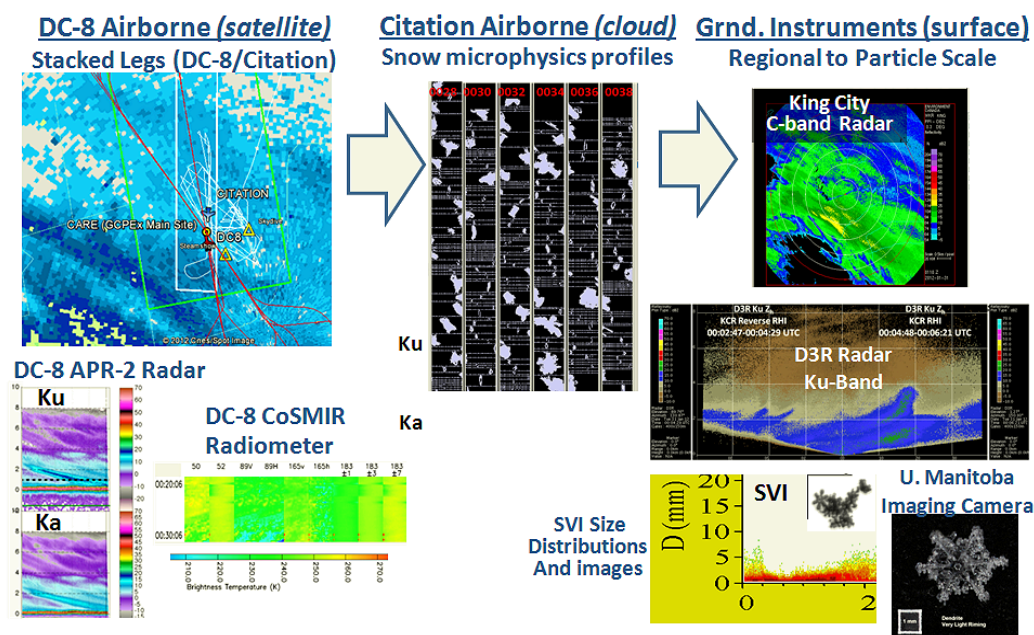
Figure 8-3 Example of data collection on January 30-31, 2012, illustrating the progression of domain-wide high-altitude and *in situ* sampling provided by aircraft. Left: Aircraft tracks overlaid on radar reflectivity and data from instruments including the APR-2 radar (reflectivity, Z) and CoSMIR radiometer (T_B). Center: Example of microphysical profiles collected on six different stacked legs. Right: Top, ground-based measurements of C-band radar reflectivity; center, cross-section of K_u-band reflectivity from he D3R radar, and bottom, particle images provided by NASA Snow Video Imager and University of Manitoba Snow Camera

8.4.3 *Leveraged Field Campaigns of Opportunity*

In order to cast a wider "regime net", GPM GV will also participate in target of opportunity IOPs/EOPs with other partners (national or international). In these cases GPM does not assume the lead for the experiment as in Table 8-1, but both contributes to and leverages external organization resources and synergies in science and field campaign objectives to study science problems relevant to GPM retrieval algorithm needs. Several opportunities that GPM GV has either already participated in or is planning participation in shown in Figure 8-1. In this figure, red text indicates locations of field campaigns in partnerships, blue text indicates locations of TRMM heritage ground validating measurements, while black text indicates general domestic and international partners of GPM for ground validating observations.

Table 8-2: Examples of Leveraged GPM GV field efforts

Science Objective	Date/Location
Cold-season retrieval of frozen and mixed precipitation over land surfaces	Jan-Mar, 2007, C3VP, Ontario, Canada (CloudSat/Environment Canada led)
Retrieval of tropical warm-rain over land, coast, ocean	Feb-Mar, 2010, Pre-CHUVA, Alcantara, Brazil. (Brazil-GPM CHUVA led)
Database for cool-season, high latitude light rain over land and sea	Sept-Oct, 2010, LPVEX, Helsinki, Finland (CloudSat/Finnish Met. Institute led)
Physical/Integrated hydrologic validation over topography	2012, Sept-Nov, HyMEX, Mediterranean France/Italy; EU HyMEX Led

8.5 *Field Campaigns for Integrated Hydrological Validation*

Integrated field efforts supporting hydrologic validation (HGV) are expected to advance satellite-based QPE and our understanding of uncertainties and the propagation of errors into various aspects of hydrologic prediction. The basic plan is to leverage existing HGV observational networks while deploying additional gap-filling observational assets in "Physical/Integrated Hydrologic" field campaigns (Table 8-1). The targets of these field campaigns include a mix of physical and integrated HGV objectives specific to large-scale flooding and orographic regime types.

The Iowa Flood Studies (IFloodS) campaign to take place in northeastern Iowa during spring 2013 is an example of an "integrated" HGV field campaign archetype. Specifically, IFloodS will combine intensive multi-frequency polarimetric radar and dense rain gauge/disdrometer measurements for physical process studies and high resolution rainfall mapping, with soil moisture datasets, hydrologic stream flow measurements, and prototype GPM constellation Level 2 and 3 products. The overarching objective of IFloodS is to use the aforementioned datasets with coupled land surface and hydrologic models to assess uncertainties in GPM precipitation products, and the impact of those uncertainties on hydrologic applications related to flood forecasting as a function of scale and basin morphology. Post-launch "integrated" field efforts (cf. Table 8-1) with similar HGV objectives to IFloodS include the Integrated Precipitation and Hydrology Experiment (IPHEx; joint with the NOAA HMT-Southeast program) and Olympic Peninsula Experiment (OLYMPEX), both in formulation. However, both IPHEX and OLYMPEX represent a shift in GV emphasis to precipitation and hydrologic processes occurring over highly complex terrain. For both campaigns high altitude

remote sensing and in situ microphysics aircraft data collection will be conducted as in MC3E and GCPEX. Coordinated data collections with GPM Core platform overpasses will also be attempted where/when feasible.

8.6 *International Collaboration*

Leveraging of GPM international partner research activities and infrastructure enables coordinated global ground validation activities to be conducted (Table 8-2 and Figure 8-1). Here, "global" refers to more than just geography—it also refers to precipitation regime. Because the problem of identifying observational gaps, organizing relevant datasets, and finally validating satellite products over a global domain is so daunting, a great degree of focus, coordination and organization are required. Set in this framework, specific and targeted collaborations between the PMM Science Team and international partners have been sought.   These collaborations are outlined in Table 8-3 below and in Fig. 8-1.

Table 8-3: Current international projects for GPM Ground Validation collaboration

Country	Project Theme
Argentina	Impact of deep moist convection on rainfall, development of techniques to calibrate and check rainfall estimates
Australia	Australian Calibration and Validation Activities in Support of GPM
Brazil	Convective systems lifecycle, physical processes in warm-clouds, direct validation, hydrologic validation over the Iguacu river basin
Canada	Winter Precipitation Studies in the Greats Lakes area, the High Arctic, and in Mountainous Terrain
Cyprus	Direct and hydrologic validation activities to support GPM
Ethiopia	The Blue Nile River Basin in Ethiopia as the Regional GPM GV site in Africa
European Union	EUMETSAT Satellite Application Facility (SAF) to support operational hydrology and water management (H-SAF) activities.
Finland	Winter precipitation – Calibration and validation activities in Finland for GPM mission
France	Contribution of the French component of the Megha-Tropiques Mission to the Precipitation Measurement Missions Science Team
Germany	Ancillary Active and Passive Polarimetric Studies and Observations providing a better insight in Rain and Precipitation Processes
Israel	Statistical and integrated hydrometeorological validation
Italy	Mediterranean precipitation - Calibration and validation activities in Italy for the GPM mission
Korea	Seasonal direct and physical validation activities using Korean national network and research radar, disdrometer and rain gage resources.
Spain	High-density mobile disdrometer measurements in Spain and GPM GV field campaigns in order to analyze the DSD variability
Switzerland	Precipitation processes and size distributions in complex terrain (liquid and frozen); dense mobile disdrometer measurement datasets
United Kingdom	Quantification of the uncertainties and errors associated with measurements of light precipitation in the northern latitudes

9.   Data Processing Requirements

The Precipitation Processing System (PPS) is a generic, measurement-based, multi-satellite data processing and science information system that will have the processing capability and communications capacity to handle data from the GPM Observatory and partner assets to create science products in three categories: immediate (or near real-time), research, and user-oriented outreach data. A key function of the PPS is to inter-calibrate brightness temperatures from GPM partner radiometers using GMI/DPR measurements as the reference standard to produce consistent brightness temperatures and precipitation rates for the generation of multi-satellite global precipitation products. The PPS will process Level-1 (radiometric brightness temperatures), Level-2 (geophysical), and Level-3 (gridded) products with appropriate data latencies.

9.1 *Background*

The GPM data processing approach evolves from the approach used for TRMM. While the TRMM approach provides the core of the processing approach, GPM is by its nature more complex in data processing because of the requirements to inter-calibrate all the available radiometer data, use the combined radiometer-radar product to create the databases for the enhanced radiometer retrieval algorithms, receive data from widely distributed partner data systems, and establish a meaningful, properly synchronized reprocessing cycle.

For the purposes of this chapter processing is split into two basic types. Near-realtime processing at the IFOV for Tb and precipitation retrievals accomplished as quickly as data are received at the PPS. For GPM GMI near-realtime IFOV will be in 5 min granules. The second type of product is the research products. These will be processed upon receipt of all required input data to ensure the most complete product. Research products at IFOV are processed as orbits. Additional details are contained at http://pps.gsfc.nasa.gov/.

The GPM data processing approach is coordinated between the algorithm development teams and the PPS. Currently all processing will be accomplished within the PPS. PPS will provide a Linux based clustered computing environment for processing. This will maximize the throughput and ensure some algorithm growth capacity. PPS is sized to support concurrent processing of near-realtime data, initial processing of research products and 10x sustained reprocessing of the research products.

The ultimate responsibility for establishing, modifying or adding standard products to the processing stream lies with the Joint PMM Science Team (JPST). Individual partner products are the responsibility of the GPM Project Scientist.

9.2 *Levels of Processing*

Data processing is categorized according to the standard levels of processing according to the Earth Observing System (EOS) categories. See also Fig. 7-1.

- Level 0 processing is raw data in CCSDS scan packets with telemetry effects removed and Reed-Solomon decoded.
- Level 1 (L1) processing
- L1A processing produces orbitized packet data

- L1B processing produces geolocated, calibrated data at the IFOV containing T_a or T_b, or geolocated, calibrated radar powers at IFOV for DPR.
- L1C processing produces inter-calibrated T_b at the IFOV.
- Level 2 processing produces geolocated geophysical data and DPR reflectivities at IFOV.
- Level 3 processing produces time and space sampled geophysical data

During GPM Level 4 products will also be produced (see Section 7.5). These are defined to be products that directly merge remote sensed data with model data. These are generally time and space sampled data.

PPS is responsible for implementing the algorithms for L1A and L1B processing for the GMI instrument. PPS also has responsibility for assisting the science inter-calibration algorithm team to implement the inter-calibrated partner radiometer data (L1C) and the L2 and L3.

9.3 *Acquisition of Data*

Data for GPM comes from two core sources: GPM instruments and GPM partners L1 T_a or T_b data. GPM GMI and DPR data are received from the GPM Mission Operations Center (MOC) using TDRSS via White Sands. PPS has the responsibility for carrying out the first step in the processing of the GPM raw science data, which are desegmented into 5 minute files. The step creates 5-minute science scan packets. The second step in the process for GMI is to package the scan packets into orbit files.

The second source of data is radiometer data from GPM partner data systems. The preferred product is a T_a product at the IFOV. However, in the event the data system does not produce a T_a product, a T_b product at IFOV will be retrieved. These products will be inter-calibrated using GPM core GMI and DPR data to create a level 1C product for all subsequent stages of processing. The method of retrieval and the restrictions as they pertain to the retrieval of these products are different for each partner contribution and are negotiated separately with each partner.

For Tb data of interest for inclusion in merged products that are not produced by official GPM partners but are still of interest and value for GPM, PPS will retrieve these data via the standard distribution mechanism implemented by the provider. Such data will be retrieved on a best effort basis rather than through a negotiated vehicle or via GPM retrieval protocols.

9.4 *Algorithm Code*

PPS has the responsibility for implementing the L1A and L1B code for GMI. In addition the PPS has responsibility to assist the PMM inter-calibration algorithm team to implement and test the partner radiometer inter-calibrated 1C temperature.

All other algorithm codes are developed by PMM algorithm teams. The PPS assists in testing and performance evaluation for these algorithms as they are developed. In addition the PPS must deliver an input/output toolkit which is used to produce the products in standard formats and isolate the production and the development environments.

PPS is also responsible for receiving various versions of the algorithm code and testing it in a production like environment. The PPS builds are specifically designed to receive scientist developed algorithm code at particular levels of completeness (algorithm versions) test these and

interact with the developers in regards to issues whether running or performance. The details of the PPS builds are contained in Appendix B, of the PPS Project Plan, (draft dtd Aug. 26, 2009).

9.5 *Near-realtime and Research Products*

The details of the data management of GPM products are contained in the GPM Science Data Management Plan (GPM-PPS-PLAN-0091). For completeness a summary of this process is outlined in the following paragraphs.

Two types of near-realtime data will be produced. The first is the IFOV brightness temperature or precipitation retrievals. These will be produced and made available to users as the 5min GMI files are processed first to L1B and then to L2. Products are put on ftp servers for retrieval as soon as produced. This allows L1B products to be available without waiting for the L2 products to be produced. This is considered an important step as some users prefer to deal with the brightness temperatures rather than with the precipitation retrieval.

The second type of data is merged swath data at L1C and L2 from all the partner radiometer data. The ultimate goal is the production of a global 3 hour merged swath product from all the radiometers. These data will be in orbital files. However, because of latency of partner data, some partner data may be received before other partner data. PPS will produce the same 3 hour product multiple times. The first product will not be as globally complete as the last product but will be more timely. The last product produced for a 3 hour period will be the most complete product possible in near-realtime. This permits users who prefer timeliness over completeness to choose an appropriate earlier product. For those users for whom completeness is more important, the final merged swath product will be produced.

PPS will also produce a level 3 merged precipitation product as a global gridded product. The same processing approach described above for the L1 and L2 merged products will be used for the globally gridded/time sampled product.

Research products are those produced with 48 hours of data collection, generally. Research product processing will always be held until all possible partner input data has been received. This ensures that the research products will always be the best, most accurate and complete data products available from GPM.

9.6 *Reprocessing*

Reprocessing is planned for GPM data. The exact scheduling for reprocessing and the determination of readiness for reprocessing is the responsibility of the JPST. At each reprocessing cycle the following activities are planned:

- Required format and toolkit changes
- Algorithm code changes by science algorithm team and/or PPS
- Submittal of algorithm package to the PPS
- Science and content testing with designated months of data
- Multi-month testing (period to be established by JPST)
- Distribution of multi-month output data to algorithm developers and test working group
- Certification of readiness to proceed (by JPST)
- PPS starts reprocessing from the beginning of mission

Currently, there are no plans to reprocess data when a partner contributor starts reprocessing of their L1B product. When the JPST has determined that GPM should reprocess its mission data, PPS will begin processing at the L1B/L1C stage. PPS will ensure that the latest reprocessed version has been retrieved from partners and is used in the L1C step of the reprocessing. This allows JPST to determine when GPM data should be reprocessed and not be driven by asynchronous reprocessing requirements of the GPM partners.

9.7 *Distributing and Archiving Data*

Near-realtime data are openly distributed to users with no restrictions. However, near-realtime data are not archived. As the research products are produced they represent the best product producible by GPM. The research products for a designated processing period replace those created in near-realtime.

All research products are archived on a RAID online storage device in duplicate. Raw data, orbit-based scan packet data are stored on the RAID device but are also stored on a PPS management offsite (different building than PPS) RAID facility. Partner L1B data are not archived but PPS produced L1C data will be treated as "raw" and also stored on the offsite RAID facility as well as in the PPS archive.

PPS will distribute all GPM standard products via open ftp facilities, via http protocols and via server tools such as OpenDAPS. Several of these types of servers are currently being prototyped under the GEOSS initiative and GPM will provide access via GEOSS designated standards.

9.8 *NASA PPS Data Products*

The GPM Standard Products comprise the suite of data products approved by the NASA-JAXA Joint PMM Science Team (JPST), which are expected to include all products through at least level 2 processing. As an international satellite mission with multiple partners contributing microwave sensor measurements, each partner may choose to produce a level 3 constellation-based radiometer products. For NASA's level 3 global precipitation products, PPS will produce inter-calibrated multi-satellite global precipitation products built upon the level 2 radar-enhanced radiometer products discussed in Sec. 7.

For the GPM Mission, PPS will produce and distribute the GPM Standard Products approved the JPST as well as all GPM data products sanctioned by the NASA PMM Science Team (see Table 9-1). GPM level 4 model-assimilated data products, which will be processed and distributed by arrangement with modeling centers such as the ECMWF and NASA/GMAO, are not included in Table 9-1.

Product Level	Description	Coverage
Level 1B GMI Level 1C GMI *Latency ~1 hour*	Geolocated Brightness Temperature and intercalibrated brightness temperature	Swath, instrument field of view (IFOV)
Level 1B DPR	Geolocated, calibrated radar powers	Swath, IFOV (produced at JAXA)
Level 1C, partner radiometers	Intercalibrated brightness temperatures	Swath, IFOV
Level 2 GMI *Latency ~1 hour*	Radar enhanced (RE) precipitation retrievals	Swath, IFOV
Level 2 partner radiometers	RE precipitation retrievals from 1C	Swath, IFOV
Level 2 DPR *Latency ~3 hours*	Reflectivities, Sigma Zero, Characterization, DSD, Precipitation with vertical structure	Swath, IFOV (Ku, Ka, combined Ku/Ka)
Level 2 combined GMI/DPR *Latency ~3 hours*	Precipitation	Swath, IFOV (initially at DPR Ku swath and then at GMI swath)
Level 3 Latent Heating (GMI, DPR, Combined)	Latent Heating and associated related parameters	0.25 x 0.25 monthly grid
Level 3 Instrument Accumulations	GMI, partner radiometers, combined and DPR	0.25 x 0.25 monthly grid
Level 3 Merged Product	Merger of GMI, partner radiometer, and IR	0.1 x 0.1 at a 30 minute grid
Level 4 Products	Model Assimilated with partner data	Fine temporal and spatial scale TBD

Figure 9-1. NASA PPS GPM data products

9.9 *Schedule and Milestones*

PPS is being evolved using an incremental build approach. Each build is a scheduled delivery to the PMM science team and the GPM project. Each build is carefully designed around the delivery of algorithms as outlined in the schedule below. The details of the builds are contained in a Appendix B of the PPS Project Management Plan, PPS-6102-P100. Each subsequent build contains all the features of the previous build plus enhancements, new functionalities and the latest algorithms. The following is a summary of the key components in each build.

Build 1 (November 2010) – TRMM V7 processing, 1st use of the GPM input/output toolkit, base software environment to deal with production, storage, and distribution of data products. It includes dynamic sub-setting by geographical area and parameters.

Build 2 (November 2011) - Initial GMI synthetic data in the suggested GPM format that can be used by Level 2 GMI algorithm developers. Also delivered include improved GMI L1A and L1B algorithm code and Version 1 of the GPM algorithms for L2 and L3 (this is not yet complete code or in final format but allows the validation of sizing and performance requirements in PPS). The Version 1 also provides information about required ancillary data and support files, prototype geolocation and coincidence code.

Build 3 (November 2012) – Delivers final GMI synthetic data in the approved GPM format. This is the initial delivery to PPS of simulated data by the PMM science team and Version 2 of the algorithm code. This code uses the PPS toolkit that contains all required fixes and format changes required by the developers since the Version 1 algorithm development. It is

code that has the majority of all science completed with no major addition planned for the next delivery. This build is used to support all the GPM mission simulations.

Operational Acceptance Testing (OAT Build: Six months prior to GPM Core Observatory Launch)- Version 3 of the algorithms. These contain all the science, all the required formatting, and all ancillary and support files. It will be used to do 120 days of testing in both an initial direction and simultaneous reprocessing. It will be capable of all performance end to end testing for the core satellite and initial partner data.

At-Launch Build-Final version of the algorithm: Only fixes of problems found during the OAT are corrected with no additional science added at this stage. Any additional science will be added during the first post-launch reprocessing cycle. This build verifies readiness of the entire PPS functionality and science algorithms. After verification PPS will be emptied and set to initial state for launch.

10.   GPM Science Deliverables and Schedule

The implementation plans for algorithm development, ground validation, and data processing described in sections 6 through 9 are integrated to ensure the successful delivery of algorithm codes and data products for the GPM Mission. The major deliverables of the PMM Algorithm Teams with the support of the PMM Science Team are the Level 1C algorithms for inter-calibrated radiometer brightness temperatures, Level 2 algorithms for radar reflectivities, radar-based precipitation rates and particle size distribution profiles, combined radar/radiometer precipitation retrievals, and radar-enhanced radiometer retrievals, and Level 3 algorithms for space-time averaged precipitation retrievals and latent heating estimates. The development schedules for the individual satellite algorithms, ground validation field experiments, and data processing system builds are coordinated to ensure the timely delivery of algorithm codes to the PPS, as shown in the top-level integrated development schedule for all these activities in Figure 10-1.

These GPM algorithms will incorporate latest advances in physical-based retrievals of precipitation information through careful integration of algorithm research, pre-launch/post-launch ground validation experiments, and product verification procedures. The GPM Project Scientist will direct, monitor, and coordinate the algorithm development, ground validation, and PPS activities through regular status reports from the designated team leads to ensure the success and timely delivery of algorithms to PPS.
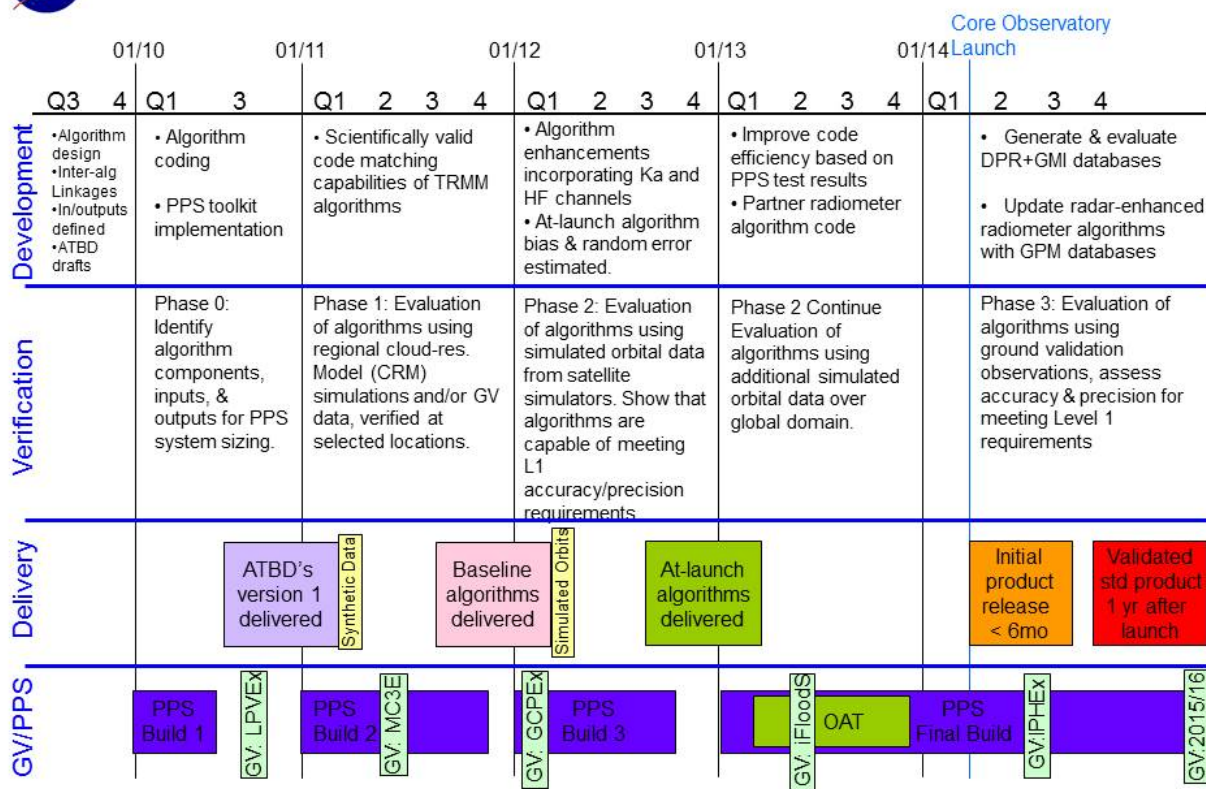
Figure 10-1. Integrated GPM algorithm, GV, and PPS schedule.

11. Mission Success Criteria

As a flagship satellite mission to provide the next-generation global precipitation measurements, GPM will need to meet the following pre-launch baseline performance criteria for full mission success and on-orbit threshold performance criteria for minimum success:

11.1 *Baseline Performance Criteria*

(1)   The capability to provide precipitation measurements of the same geophysical scenes in near-real time using both active and passive microwave sensors on the same space platform in a non-Sun-synchronous orbit at 65° inclination or higher. This permits the development of a common transfer standard based on combined active and passive sensor measurements to unify precipitation estimates from GPM constellation sensors within a consistent framework.

(2)   The capability to measure precipitation intensities ranging from heavy rain rates at 110 mmh^{-1} to light rain rates of approximately 0.2 mmh^{-1} or lower at 5 km horizontal resolution. This represents an advance over the TRMM PR, whose

detection threshold is 0.5 mmh^{-1}. Even though this improvement in sensitivity seems to be small in terms of rain rates, it is important for GPM to capture contributions to the rain volume by light rain events, which are prevalent outside the Tropics. Based on the composite CloudSat-TRMM/PR database (Berg et al. 2009) over ocean as well as ground radar measurements over the continental United States (Lin and Hou 2009), it has been estimated that lowering the detection threshold from 0.5 mmh^{-1} to 0.2 mmh^{-1} reduces the missing global rain volume from 8-9% to 2.5%.

(3)   The capability to detect falling snow at 5 km resolution, which is needed for improving water-flux estimates associated with cold season snowfall events in the middle and high-latitudes. With current progress in surface characterization over frozen terrains and radiometer algorithms for microwave sounders, it is anticipated that quantitative information on snowfall rates can be retrieved during the GPM era.

(4)   The capability to provide quantitative estimates of precipitation microphysical properties such as the mean median mass diameter of particle size distribution to within (±) 0.5 mm.

(5)   The capability to provide calibrated ground-based precipitation measurements and associated error characterizations for comparison with space-based radar and radiometer measurements. The biases in instantaneous rain rates between the ground-based and space-based estimates at 50 km horizontal resolution should not exceed 50% at 1 mmh^{-1} or 25% at 10 mm h^{-1}, while the random errors should not exceed 50% at 1 mm h^{-1} or 25% at 10 mm h^{-1} at designated ground validation sites within ground tracks of the GPM Core Observatory. These bias and random error values represent the present-day remote-sensing capabilities within the Tropics. GPM will extend this measurement capability into middle and high latitudes. With the combined information from DPR and GMI on the Core Observatory, it is anticipated that GPM will likely exceed these baseline accuracy and precision requirements within the Tropics.

(6)   The capability to provide GMI and combined DPR+GMI swath products in near realtime for hurricane monitoring, numerical weather prediction, hydrological model forecast and other operational uses.

11.2 *Threshold Performance Criteria*

As a satellite mission to measure global precipitation, GPM must be able to provide quantitative information on precipitation rates commonly encountered over low, middle, and high latitudes in order to achieve minimum success. The success of TRMM has given the remote sensing community an established track record in measuring heavy to medium rain rates focusing on the Tropics and Subtropics. Since light precipitation accounts for a significant fraction of precipitation occurrences in the middle and high latitudes, it is imperative that GPM is capable of measuring light rain rates - in addition to medium and heavy rain rates – for the mission to be considered minimally successful. Based on the GPM Core Observatory design, this

requires that both frequencies of the DPR and all channels of the GMI be functional to provide the necessary measurement dynamic range and swath coverage.

The minimum success criteria are thus determined by the lowest acceptable performance requirements for both instruments relative to their baseline performance requirements. For the DPR, the acceptable performance degradation is the reduction of the measurement dynamic range from 0.2 mm h^{-1} to 0.3 mm h^{-1} at 5 km resolution, which ensures that Ka-band radar is still capable of quantifying light rain rates. For the GMI, the acceptable degradation is that none of the 13 channels exceed its NEΔT[1] design specification by more than a factor of two, so as to not appreciably affect the accuracy of precipitation retrievals within the Bayesian framework (see Appendix F). At these degraded DPR and GMI performance levels, GPM will be able to provide a common observation-constrained *a priori* cloud database of sufficient quality for unified precipitation retrieval from the constellation radiometers, which is at the heart of the GPM mission and therefore requisite for achieving the minimum mission success. However, these degraded instrument performance levels are expected to translate into larger biases and random errors in instantaneous rain rates between the ground-based and space-based estimates *outside the Tropics*. Specifically, for minimum mission success, in the extra-tropical domain the biases should not exceed 100% at 1 mmh^{-1} or 50% at 10 mm h^{-1}, and the random errors should not exceed 100% at 1 mm h^{-1} or 50% at 10 mm h^{-1}, at 50 km horizontal resolution.

---

[1] The designation NEDT (or NEΔT) is used throughout this document. The scientists assumed NEDT to be the total random (zero mean) error of the brightness temperature channels. The analysis reported in Appendix F, in effect, assumed the combined the effects of the total calibration uncertainty values and the NEDT of Table 5-1 were the random error and that the static error associated with GMI would be easily removable.

12. References

Adler, R.F., G.J. Huffman, P.R. Keehn, 1994: Global tropical rain estimates from microwave-adjusted geosynchronous IR data. *Remote Sensing Rev.*, **11**, 125-152.

Adler, R. F., G. Gu, J.-J. Wang, George J. Huffman, Scott Curtis, and David Bolvin, 2008: Relationships between global precipitation and surface temperature on inter-annual and longer time scales (1979-2006). *J. Geophy. Res.*, **113**, D22104, doi:10.1029/2008JD010536.

Adler, R. F., J.-J. Wang, G. Gu, and George J. Huffman, 2009: A ten-year rainfall climatology based on a composite of TRMM products. *J. Meteorol. Soc. Japan*, 87A, 281-293.

Aires, F., Prigent, C., Bernardo, F., Jiménez, C., Saunders, R. and Brunel, P., 2011: A tool to estimate land-surface emissivities at microwave frequencies (TELSEM) for use in numerical weather prediction. *Q. J. of the Roy. Meteorol. Soc.*, **137**: 690–699. doi: 10.1002/qj.803

Anderson, J. L., 2003: A local least squares framework for ensemble filtering. *Mon. Wea. Rev.*, **131**, 634-642.

Andreae, M.O., D. Rosenfeld, D., Artaxo, P., Costa, A.A., Frank, G.P., Longo, K.M and Silva-Dias, M.A.F., 2004: Smoking rain clouds over the Amazon. *Science,* **303**, 1337-1341.

Anagnostou, E.N., C.A. Morales, and T. Dinku, 2000: The use of TRMM Precipitation Radar observations in determining ground radar calibration biases. *J. Atmos. Ocean. Tech.*, **18**, 616-628.

Aonashi, K., N. Yamazaki, H. Kamahori, and K. Takahashi, 2004: Variational assimilation of TMI rain type and precipitation retrievals into global numerical weather prediction. *J. Meter. Soc. Japan,* **82**, 671-693.

ASM (Asian Surveying and Mapping), cited 2008: China launches Feng Yun-3A. [Available online at http://www.asmmag.com/news/china-launches-feng-yun-3a].

Asrar, G., J. Kaye, and P. Morel, 2001: NASA research strategy for Earth system science: Climate component. *Bull. Amer. Meteor. Soc.*, **82**, 1309-1329.

Avissar, R., and D. Werth, 2005: Global Hydroclimatological Teleconnections Resulting from Tropical Deforestation. *J. Hydrometeor.*, 6, 134–145.

Back, L. E., and C. S. Bretherton, 2006: Geographic variability in the export of moist static energy and vertical motion profiles in the tropical Pacific. *Geophys. Res. Lett.*, **33** (17): Art. No. L17810.

Bauer, P., P. Amayenc, C. Kummerow, and E. Smith, 2001: Over-ocean rainfall retrieval from multi-sensor data of the Tropical Rainfall Measuring Mission. *J. Atmos.   Ocean Tech.*, **18**, 1838-1855.

Bauer, P., P. Lopez, A. Benedetti, D. Salmond, and E. Moreau, 2006a: Implementation of 1D+4D-var assimilation of precipitation-affected microwave radiances at ECMWF. I: 1D-Var. *Q. J. R. Meteoro. Soc.*, **132A**, 2277-2306.

Bauer, P., P. Lopez, A. Benedetti, D. Salmond, and E. Moreau, 2006b: Implementation of 1D+4D-var assimilation of precipitation-affected microwave radiances at ECMWF. II: 4D-Var. *Q. J. R. Meteoro. Soc.,* **132A**, 2307-2332.

Bell, T. L., D. Rosenfeld, K.-M. Kim, J.-M. Yoo, M.-I. Lee, M. Hahnenberger , 2008: Midweek increase in U.S. summer rain and storm heights suggests air pollution invigorates rainstorms, *J. Geophys. Res.*, **113**, D02209, doi:10.1029/2007JD008623.

Berg, W., T. L'Ecuyer, and C. Kummerow, 2006: Rainfall Climate Regimes: The relationship of TRMM rainfall biases to the environment, *J. Appl. Meteor.,* **5**, 434-454.

Berg, W., T. L'Ecuyer, and J. M. Haynes, 2009: The Distribution of Rainfall over Oceans from Spaceborne Radars. *J. Appl. Meteor. Climatol.* Submitted.Bolen, S.M. and V. Chandrasekar, 2000: Quantitative cross validation of space-based and ground-based radar observations. *J. Appl. Meteor.,* **39**, 2071-2079.

Boukabara, S.-A.; Garrett, K.; Wanchun Chen; Iturbide-Sanchez, F.; Grassotti, C.; Kongoli, C.; Ruiyue Chen; Quanhua Liu; Banghua Yan; Fuzhong Weng; Ferraro, R.; Kleespies, T.J.; Huan Meng; , "MiRS: An All-Weather 1DVAR Satellite Data Assimilation and Retrieval System," *Geoscience and Remote Sensing, IEEE Transactions on* , vol.49, no.9, pp.3249-3272, Sept. 2011, doi: 10.1109/TGRS.2011.2158438

Bhatt, C. B., and K. Nakamura, 2005: Characteristics of monsoon rainfall around the Himalayas revealed by TRMM precipitation radar. *Mon. Wea. Rev*., **133**, 149-   165.

Brown, S., C. Ruf, S. Keihm and A. Kitiyakara, 2004: Jason Microwave Radiometer performance and on-orbit calibration, *Marine Geodesy*, **27**(1-2), 199-220.

Brown, S. and C.S. Ruf, 2005: Determination of a Hot Blackbody Reference Target over the Amazon Rainforest for the On-orbit Calibration of Microwave Radiometers, *AMS J. Oceanic Atmos. Tech*., **22**(9), 1340-1352.

Bunin, Stacy L., D. Holmes, T. Schott, and H. J. Silva, 2004: "NOAA/NESDIS Preparation for the NPOESS Era," Preprints, 20th International Conference on Interactive Information and Processing Systems (IIPS) for Meteorology, Oceanography, and Hydrology, Amer. Meteorolo. Soc., Seattle, Washington.

Chen, F.W. and D.H. Staelin, 2003: AIRS/AMSU/HSB Precipitation Estimates, *IEEE Trans. Geoscience and Remote Sensing*, **41**, 410-417.

Cherny, I. V., G. Chernyavsky, V. Nakonechny, and S. Pantsov, 2002: Spacecraft "Meteor-3M" Microwave Imager/Sounder MTVZA: First results. Avaliable online http://ieeexplore.ieee.org/iel5/7969/22040/01026733.pdf?arnumber=1026733.

Cotton W. R., and R. A. Pielke, 2007: *Human Impacts on Weather and Climate*. 2nd Edition, Cambridge University Press, 308 pp.

Dabberdt, W., T. Schlatter, F. Carr, J. Friday, D. Jorgensen, S. Koch, M. Pirone, M. Ralph, J. Sun, P. Welsh, J. Wilson, and X. Zou, 2005: Multifunctional mesoscale observing networks., *Bull. Amer. Meteor. Soc.*, **86**, 961–982.

Del Genio, A.D., W. Kovari, M. -S. Yao and J. Jonas, 2005: Cumulus microphysics and climate sensitivity. *J. Climate*, **18**, 2376-2387.

Desbois, M., R. Roca, L. Eymard, N. Viltard, M. Viollier, J. Srinivasan, S. Narayanan, 2003: The Megha-Tropiques mission., *Proceedings Soc. Photo-Optical Instrumentation Engineers (SPIE)*, **4899**, 172-183.

Douglas E., A. Beltrán-Przekurat, D. Niyogi, R. Pielke, Sr., and C. Vörösmarty, 2008: The impact of agricultural intensification and irrigation on land-atmosphere interactions and Indian monsoon precipitation - A mesoscale modeling perspective, *Global Planetary Change*, accepted.

Ebert, E., J. Janowiak, and C. Kidd, 2007: Comparison of near real time precipitation estimates from satellite observations and numerical models. *Bull. Amer. Meteor. Soc.*, **88**, 47-64.

Edward, P., and D. Pawlak, 2000: MetOp: The space segment for EUMETSAT's polar system, *ESA Bull.,* **102**, 6-18.

Evans, K.F., J. Turk, T. Wong, and G. Stephens, 1995: A Bayesian approach to microwave precipitation profile retrieval. *J. Appl. Meteorol.* **34**, 260–279.

Fekete, B., C. Vörösmarty, J. Roads, and C. Willmott, 2004: Uncertainties in precipitation and their impacts on runoff estimates. *J. Climate,* **17**, 294-304.

Foufoula-Georgiou, E., 1997: On stochastic theories of space-time rainfall: Some recent results and open problems, in *Stochastic Methods in Hydrology: Rain, Landforms and Floods*, Gupta et al. (eds.), *Advanced Series on Statistical Sciences and Applied Probability*, **7**, 25-72.

Gopalan, K., L. Jones, S. Biswis, S. Bilanow, T. Wilheit and T. Kasparis, 2009: A time-varying radiometric bias correction for the TRMM microwave imager, *IEEE Trans on Geosci and Remote Sens*, in press.

Grecu, M. and W. S. Olson, 2006: Bayesian estimation of precipitation from satellite passive microwave observations using combined radar-radiometer retrievals. *Applied Meteor. Climatol.*, **45,** 416-433.

Grecu, M. W. Olson, C.-L. Shie, T. L'Ecuyer, and W.-K. Tao, 2009: Combining Satellite Microwave Radiometer and Radar Observations to Estimate Atmospheric Latent Heating Profiles. *J. Climate* (submitted).

GPM (Global Precipitation Measurement), cited 2012: Global Precipitation Measurement Ground Validation. [Online at http://pmm.nasa.gov/science/ground-validation].

GPM GV-2008, 2008: The 3rd International Workshop on GPM Ground Validation. [Available online at http://pindara.cptec.inpe.br/gpm/workshop/index.html].

Gu, G., R. Adler, G. Huffman, S. Curtis, 2007: Tropical rainfall variability on interannual-to-interdecadal and longer time scales derived from the GPCP monthly product. *J. Climate,* **20**, 4033-4046.

Grecu, M., W. Olson, and E. Anagnostou, 2004: Retrieval of precipitation profiles from multiresolution, multifrequency, active and passive microwave observations. *J. Appl. Meteorol.*, **43**, 562-575.

Haddad Z., E. Smith, C. Kummerow, T. Iguchi, M. Farrar, S. Durden, M. Alves, and W. Olson, 1997: The TRMM 'day-1' radar/radiometer combined rain-profiling algorithm. *J. Meteor. Soc. Japan.,* **75**, 799-809.

Hong, L., W.L. Jones, T. Wilheit, and T. Kasparis, 2009: Two Approaches for Inter-Satellite Radiometer Calibrations between TMI and WindSat. to be published in *J. Met. Soc. Japan*, **87A**, 223-235.

Hou, A. Y., S. Zhang, A. da Silva, W. Olson, C. Kummerow, and J. Simpson, 2001: Improving global analysis and short-range forecast using rainfall and moisture observations derived from TRMM and SSM/I passive microwave sensors. *Bull. Amer. Meteor. Soc.,* **81**, 659-679.

Hou, A. Y., S. Zhang, and O. Reale, 2004: Variational continuous assimilation of TMI and SSM/I rain rates: Impact on GEOS-3 hurricane analyses and forecasts. *Mon. Wea. Rev.*, **132**, 2094-2109.

Hou, A. Y., and S. Q. Zhang, 2007: Assimilation of precipitation information using column model physics as a weak constraint. *J. Atmos. Sci.*, **64**, 3865-3879.

Hou, A. Y., G. Skofronick-Jackson, C. D. Kummerow, and J. M. Shepherd, 2008: Global precipitation measurement. In *Precipitation: Advances in Measurement, Estimation, and Prediction* (Ed. Silas Michaelides), Springer-Verlag, 131-169.

Hossain, F., and E. Anagnostou, 2004: Assessment of current passive microwave and infra-red based satellite rainfall remote sensing for flood prediction, *J. Geophys. Res.,* **109**(D7), D07102. (DOI 10.1029/2003JD003986).

Hossain, F., and D. Lettenmaier, 2006: Flood prediction in the future: Recognizing hydrologic issues in anticipation of the Global Precipitation Measurement mission. *Water Resour. Res.*, **42**, W11301, doi: 10.1029/2006WR005202.

Hudak, D., H. Barker, P. Rodruguez, and D. Donovan, 2006: The Canadian CloudSat/CALIPSO Validation Project. The 4th European Conference on Radar in Hydrology and Meteorology, Barcelona, Spain, 18-22 Sept. 2006, 609-612.

Hudak, D., P. Rodriguez, G.W. Lee, A. Ryzhkov, F. Fabry, and N. Donaldson, 2006b: Winter precipitation studies with a dual polarized C-band radar. 4th European Conf. on Radar in Hydrology and Meteorology, Barcelona, Spain, 9-12 Sept., 2006, 9-12.

Tokay, A. and coauthors, 2007: Disdrometer derived Z-S relations in south central Ontario, Canada. Preprints, 33rd International Conference on Radar Meteorology, American Meteorological Society, 6-10 August 2007, Cairns, Australia.

Huffman, G.J., R.F. Adler, D.T. Bolvin, G. Gu, E.J. Nelkin, K.P. Bowman, Y. Hong, E.F. Stocker, D.B. Wolff, 2007: The TRMM multi-satellite precipitation analysis: quasi-global, multi-year, combined-sensor precipitation estimates at fine scale. *J. Hydrometeor.*, **8(1)**, 38-55.

Huffman, G.J., R.F. Adler, M. Morrissey, D.T. Bolvin, S. Curtis, R. Joyce, B McGavock, J. Susskind, 2001: Global precipitation at one-degree daily resolution from multi-satellite observations. *J. Hydrometeor.,* **2**(1), 36-50.

Iguchi, T., T. Kozu, R. Meneghini, J. Awaka, and K. Okamoto, 2000: Rain-profiling algorithm from the TRMM precipitation radar. *J. Appl. Meteor.*, **39**, 2038-2052.

IFNET (International Flood Network), cited 2008: International Flood Network. [Available online at http://www.internationalfloodnetwork.org].

Joyce, R. J., J. E. Janowiak, P. A. Arkin, and P. Xie, 2004: CMORPH: A method that produces global precipitation estimates from passive microwave and infrared data at high spatial and temporal resolution. *J. Hydrometeor.*, **5**, 487-503.

Joyce, R. J., J. E. Janowiak, P. A. Arkin, and P. Xie, 2004: CMORPH: A method that produces global precipitation estimates from passive microwave and infrared data at high spatial and temporal resolution. *J. Hydrometeor.*, **5**, 487-503.

Katsumata, M., S. Mori, T. Ushiyama, Y.-M. Kodama, S. Satoh, 2009: An improved version of the PRH latent heating estimation algorithm based on the observed vertical structure. *J. Climate* (submitted).

Kelley, O., J. Stout, and J. Halverson, 2004: Tall precipitation cells in tropical cyclones eyewalls are associated with tropical cyclone intensification. *Geophys. Res. Lett.*, **31**, L24112.

Kelley, O. A., and J. B. Halverson, 2011: How much tropical cyclone intensification can result from the energy released inside of a convective burst? *J. Geophys. Res.* 116, D20118.

Kidd, C. K., D. R. Kniveton, M. C. Todd, and T. J. Bellerby, 2003: Satellite rainfall estimation using combined passive microwave and infrared algorithms. *J. Hydrometeor.*, **4**, 1088-1104.

Kongoli, C., P. Pellegrino, R.R. Ferraro, C. Grody, and H. Meng, 2003: A new snowfall detection algorithm over land using measurements from the Advanced Microwave Sounding Unit (AMSU), *Geophys. Res. Lett.*, **30**(14), 1756-1759.

Kubota, T., S. Shige, H. Hashizume, K. Aonashi, N. Takahashi, S. Seto, M. Hirose, Y. N. Takayabu, K. Nakagawa, K. Iwanami, T. Ushio, M. Kachi, and K. Okamoto, 2007: Global Precipitation Map using Satelliteborne Microwave Radiometers by the GSMaP Project: Production and Validation, *IEEE Trans. Geosci. Rem. Sens.* **45**, 2259-2275.

Kuligowski, R. J., 2002: A self-calibrating real-time GOES rainfall algorithm for short-term rainfall estimates. *J. Hydrometeor.*, **3**, 112-130.

Kumar, S., C. Peters-Lidard, Y. Tian, P. Houser, J. Geiger, S. Olden, L. Lighty, J. Eastman, B. Doty, P. Dirmeyer, J. Adams, K. Mitchell, E. Wood, and J. Sheffield, 2006: Land information system - An interoperable framework for high resolution land surface modeling. *Environ. Modelling & Software*, **21**, 1402-1415.

Kummerow, C., and L. Giglio, 1994: A Passive Microwave Technique for Estimating Rainfall and Vertical Structure Information from Space. Part I: Algorithm description. *J. Appl. Meteoro.*, **33**(1), 3-18.

Kummerow, C., W. Olson, and L. Giglio, 1996: A simplified scheme for obtaining precipitation and vertical hydrometeor profiles from passive microwave sensors, *IEEE Trans. Geosci. Rem. Sens.,* **11**, 125-152.

Kummerow, C., et al., 2000: The status of the Tropical Rainfall Measuring Mission (TRMM) after two years in orbit. *J. Appl. Meteoro.*, **39**, 1965-1982.

Kummerow, C., cited 2007: Radiometer Level 1C Data. [Available online at http://mrain.atmos.colostate.edu/LEVEL1C/].

Kummerow, C., C. Ruf, and T. Wilheit, 2007: The GPM inter-satellite calibration study. Quarterly Newsletter of Global Space-based Inter-Calibration System (GSICS) (R. Lacovazzi and J. Sullivan, Co-Editors), **1** (2), 2-3. [Available online at http://www.orbit.nesdis.noaa.gov/smcd/spb/calibration/icvs/GSICS/index.html].

Kummerow, C., S. Finn, J. Crook, D. Randel and W. Berg, 2009: An observationally based a-priori database for Bayesian rainfall retrievals," to be submitted to *J. Clim. and Appl. Meteorol*. 2009.

Kummerow, C. and W.A. Petersen, 2006, GPM Ground Validation: Strategy and Efforts.. http://gpm.gsfc.nasa.gov/ground_advisory.html

Kunkee, D. B., G. Poe, D. Boucher, S. Swadley, Y. Hong, J. Wessl, and E. Uliana, 2008: Design and evaluation of the first Special Sensor Microwave Imager/Sounder., *IEEE Trans. Geosci. Rem. Sens*., **46**, 863-883.

Liao, L., R. Meneghini, T. Iguchi, and A. Detwiler, 2005: Use of dual-wavelength radar for snow parameter estimates, *J. Atmos. Ocean Tech*., **22**, 1494-1506.

Liao, L., R. Meneghini, and T. Iguichi, 2001: Comparisons of rain rate and reflectivity factor derived from the TRMM Precipitation Radar and the WSR-88D over the Melbourne, Florida, site. *J. Atmos. Ocean. Tech.*, **18**, 1959-1974.

Lin, X., and A. Y. Hou, 2008: Evaluation of coincident passive microwave rainfall estimates using TRMM PR and ground-based measurements as references. *J. Appl. Meteoro. Climate*, **47**, 3170-3187.

Lin, X., and A. Y. Hou, 2009: Estimation of rain intensity spectra over the continental United States using ground radar-gauge measurements. *J. Climate*, in preparation.

Macduff, M.C., R.C. Eagan, 2004: ARCF Data Collection and Processing Infrastructure. U.S. Department of Energy. Office of Science, Office of Biological and Environmental Research. ARM TR-046.

Marecal, V. and J.-F. Mahfouf, 2003: Experiments on 4D-var assimilation of rainfall data using an incremental formulation. *Q. J. R. Meteorol. Soc*., **129**, 3137-3160.

Marzano, F., A. Mugnai, G. Panegrossi, N. Pierdicca, E. Smith, and J. Turk, 1999: Bayesian estimation of precipitating cloud parameters from combined   measurements of spaceborne microwave radiometer and radar. *IEEE Trans.   Geosci. Rem. Sens*, **37**, 596-613.

Masunaga, H., and C. Kummerow, 2005: Combined radar and radiometer analysis of precipitation profiles for a parametric retrieval algorithm. *J. Atmos. Ocean Tech*., **22**, 909–929.

Masunaga, H., T.S. L'Ecuyer, and C.D. Kummerow, 2006: The Madden–Julian Oscillation recorded in early observations from the Tropical Rainfall Measuring Mission (TRMM). *J. Atmos. Sci*., 63, 2777–2794.

Mitchell, K., et al., 2004: The multi-institution North American Land Data Assimilation System (NLDAS): Utilizing multiple GCIP products and partners in a continental distributed hydrological modeling system. *J. Geophys. Res*., **109**, D07S90, doi: 10.1029/2003 JD003823.

Montaigne, F., 2002: Water pressure. *National Geographic*, September issue, 2-33.

Morita, J., Y. N. Takayabu, S. Shige, and Y. Kodama, 2006: Analysis of rainfall characteristics of the Madden-Julian oscillation using TRMM satellite data. *Dyn. Atmos. Oceans*, **42**, 107-126.

Mote, T., M. Lacke, and J. M. Shepherd, 2007: Radar signatures of the urban effect on precipitation distribution: A case study for Atlanta, Georgia. *Geophy. Res. Lett.*, **34**, L20710, doi:10.1029/2007GL031903.

Munchak, S.J. and G. Skofronick-Jackson, "Evaluation of Precipitation Detection over Various Surfaces from Passive Microwave Imagers and Sounders," in press Atmospheric Research, as of October 10, 2012.

Mugnai, A., et al., 2007: Snowfall measurements by the proposed European GPM Mission. In *Measuring Precipitation from Space: EURAINSAT and the future*. Eds. V. Levizzani, P. Bauer and J. Turk. Springer-Verlag, 750 pp.

NASA (National Aeronautics and Space Administration), cited 2007: NASA Science Plan 2007, 169 pp. [Available online at http://science.hq.nasa.gov/strategy/].

Negri, A.J., R.F. Adler, L. Xu, and J. Surratt, 2004: The Impact of Amazonian Deforestation on Dry Season Rainfall. *J. Climate*, **17**, 1306–1319.

Nesbitt, S.W., E. J. Zipser, and D. J. Cecil, 2000: A Census of Precipitation Features in the Tropics Using TRMM: Radar, Ice Scattering, and Lightning Observations. *J. Climate*, **13**, 4087–4106.

Nesbitt, S.W., E.J. Zipser, and C.D. Kummerow, 2004: An examination of Version-5 rainfall estimates from the TRMM Microwave Imager, Precipitation Radar, and rain gauges on global, regional, and storm scales. *J. Appl. Meteor.,* **43**, 1016-1036.

Nijssen, B., and D. P. Lettenmaier, 2004: Effect of precipitation sampling error on simulated hydrological fluxes and states: Anticipating the Global Precipitation Measurement satellites. *J. Geophys. Res.*, **109**, D02103, doi:10.1029/2003JD003497.

NOAA (National Oceanic and Atmospheric Administration), cited 2009: The NOAA Hydrometeorological Testbed Program. [Available online at http://hmt.noaa.gov/].

NRC (National Research Council), 2005: *Assessment of the Benefits of Extending the Tropical Rainfall Measuring Mission*, National Academies Press, Washington, DC, 103 pp.

NRC (National Research Council), 2007a: *NOAA's Role in Space-Based Global Precipitation Estimation and Application*, National Academies Press, Washington, DC, 131 pp.

NRC (National Research Council), 2007b: *Earth Science and Applications from Space: National Imperatives for the Next Decade and Beyond*, National Academies Press, Washington, DC, 428 pp.

NSF (National Science Foundation), 2005: *Water: Challenges at the Intersection of Human and Natural Systems*. 50 pp. [Available from the National Science Foundation, AC-ERE].

NSTC (National Science and Technology Council), 2004: *Science and Technology to Support Fresh Water Availability in the United States*. 19 pp.

Okamoto, K. T. Iguchi, N. Takahashi, K. Iwanami, T. Ushio, 2005: The global satellite mapping of precipitation (GSMaP) project. 25th IGARSS Proceedings, 3414-341.

Olson, W. S., C. D. Kummerow, S. Yang, G. W. Petty, W.-K. Tao, T. L. Bell, S. A. Braun, Y. Wang, S. E. Lang, D. E. Johnson and C. Chiu. 2006: Precipitation and latent heating distributions from satellite passive microwave radiometry. Part I: Improved method and uncertainties. *J. Appl. Meteor. and Climatol.*, **45**, 702-720.

Petersen, W. A., D. Hudak, V. Bringi, P. Siquiera, A. Tokay, V. Chandrasekar, L. F. Bliven, R. Cifelli, T. Lang, S. Rutledge, and G.-S. Jackson, 2007: NASA GPM/PMM Participation in the Canadian CloudSat/Calipso validation project (C3VP): Physical process studies in snow. *33rd International Conference on Radar Meteorology*, American Meteorological Society, Cairns, Australia, August 6-10, 2007.

Petersen, W. A., and M. R. Schwaller, 2009: Global Precipitation Mission Ground Validation Science Implementation Plan. Draft available at http://gpm.gsfc.nasa.gov/documents/GPM_GVS_imp_plan_Jul08.pdf.

Petty, G. and K. Li, 2013: Improved Passive Microwave Retrievals of Rain Rate Over Land and Ocean. 1. Algorithm description, under review fall 2012 by Journal of Atmospheric and Oceanic Technology.

Petty, G. 2013: Improved Passive Microwave Retrievals of Rain Rate Over Land and Ocean. 2. Validation and Intercomparison, under review fall 2012 by Journal of Atmospheric and Oceanic Technology.

Prigent, C., C., W. B. Rossow, and E. Matthews, 1997: Microwave land surface emissivities estimated from SSM/I observations. *J. Geophys. Res.*, **102**, 21 867 – 21 890.Prigent, C., E. Jaumouille, F. Chevallier, and F. Aires, 2008: A parameterization of the microwave land surface emissivity between 19 and 100 GHz, anchored to satellite-derived estimates*, IEEE Transaction on Geoscience and Remote Sensing* , **46**, 344-352, doi:10.1109/TGRS.2007.908881.

Rajendran, R., T. N. Krishnamurti, V. Misra, and W.-K. Tao, 2004: An empirical cumulus parameterization scheme based on TRMM latent heating profiles. *J. Meteor. Soc. Japan*, **82**, 989-1006.

Rodell, M., P. Houser, U. Jambor, J. Gottschalck, K. Mitchell, C.-J. Meng, K. Arsenault, B. Cosgrove, J. Radakovich, M. Bosilovich, J. Entin, J. Walker, D. Lohmann, and D. Toll, 2004: The global land data assimilation system. *Bull. Amer. Meteor. Soc.*, **85**, 381-394.

Rosenfeld, D., Y. Rudich, and R. Lahav, 2001: Desert dust suppressing precipitation – a possible desertification feedback loop. *Proceedings of the National Academy of Sciences U.S.A.*, **98**, 5975-5980.

Ruf, C. S. 2000: Detection of calibration drifts in spaceborne microwave radiometers using a vicarious cold reference. *IEEE Trans. Geosci. Remote Sens.*, **38**(1), 44-52.

Ruf, C.S., Y. Hu and S.T. Brown, 2006: Calibration of WindSat Polarimetric Channels with a Vicarious Cold Reference. *IEEE Trans. Geosci. Remote Sens.*, **44**(3), 470-475.

Satoh, S., and A. Noda, 2001: Retrieval of latent heating profiles from TRMM radar data. Proceedings of 30th International Conf. on Radar Meteorology, [Munich, Germany; 19-24 July 2001], 340-342.

Satoh, S., A. T. Noda, and T. Iguchi, 2009: Retrieval of latent heating profiles in various cloud systems from TRMM PR data. *J. Meteor. Soc. Japan*, (submitted).

Shepherd, J. M., H. Pierce, and A. Negri, 2002: On rainfall modification by major urban areas: Observations from space-borne radar on TRMM. *J. Appl. Meteorolo.,* **41**, 689-701.

Shige, S., Y. N. Takayabu, W.-K. Tao and D. E. Johnson, 2004: Spectral retrieval of latent heating profiles from TRMM PR data. Part I: Development of a model-based algorithm. *J. Applied Meteor.,* **43**, 1095-1113.

Shige, S., Y. N. Takayabu, W.-K. Tao and C.-L. Shie, 2007: Spectral retrieval of latent heating profiles from TRMM PR data. Part II: Algorithm improvement and heating estimates over tropical ocean regions. *J. Applied Meteor.,* **46**, 1098-1124.

Shige, S., Y. N. Takayabu, and W.-K. Tao, 2008: Spectral retrieval of latent heating profiles from TRMM PR data. Part III: Estimating apparent moisture sink profiles over tropical oceans. *J. Applied Meteor. Climatol.,* **47**, 620-640.

Shige, S., Y. N. Takayabu, S. Kida, W.-K. Tao, X. Zeng and T. L'Ecuyer, 2009: Spectral retrieveal of latent heating profiles from TRMM PR data. Part IV: Comparisons of lookup tables from two- and three-dimensional simulations. *J. Climate* (in press).

Shige, S., T. Watanabe, H. Sasaki, T. Kubota, S. Kida, and K. Okamoto, 2008: Validation of western and eastern Pacific rainfall estimates from the TRMM PR using a radiative transfer model, *J. Geophys. Res.,* **113**, D15116, doi:10.1029/2007JD009002.

Shimoda, H., 2005: "GCOM Missions," *Proc. IEEE/IGARSS* 2005, July 2005.

Simpson, J., J. Halverson, B. Ferrier, W. Petersen, R. Simpson, R. Blakeslee and S. Durden, 1998: On the role of "hot towers" in tropical cyclone formation. *Meteor. Atmos. Phys.,* **67**, 15-35.

Skofronick-Jackson, G., B. Johnson, A. Tokay, W. Petersen, Observational data set in support of falling snow retrieval algorithm development Geoscience and Remote Sensing Symposium, 2007. IGARSS 2007. IEEE International 23-28 July 2007 Page(s):3903 - 3906 Digital Object Identifier 10.1109/IGARSS.2007.4423697

Smith, E., C. Kummerow, and A. Mugnai, 1994: The emergence of inversion-type profile algorithms for estimation of precipitation from satellite passive microwave measurements. *Rem. Sens. Rev.,* **11**, 211-242.

Sorooshian, S., K.-L. Hsu, X. Gao, H. V. Gupta, B. Imam, and D. Braithwaite, 2000: Evaluation of PERSIANN system satellite-based estimates of tropical rainfall. *Bull. Amer. Meteor. Soc.,* **81**, 2035-2046.

Steiner, M., T. Bell, and E. Wood, 2004: Sampling-related uncertainty of satellite rainfall averages and implications for hydrologic applications. *8th International Conference on Precipitation -- Quantifying Uncertainties in Precipitation   Measurements,   Estimates, and Forecasts*, Vancouver, Canada, 3-3.

Stephens, G., and C. Kummerow 2007: The remote sensing of clouds and precipitation from space: A review. *J. Atmos. Sci.,* **64**, 3742-3765.

Surussavadee, C. and D. Staelin, 2008: Global Millimeter-Wave Precipitation Retrievals Trained with a Cloud Resolving Numerical Weather Prediction Model, Part 1: Retrieval Design, *IEEE Trans. Geoscience and Remote Sensing*, **46**, PAGE NUMBERS.

Tao, W.-K., S. Lang, J. Simpson, and R. Adler, 1993: Retrieval algorithms for estimating the vertical profiles of latent heat release: Their applications for TRMM. *J. Meteor. Soc. Japan*, **71**, 685-700.

Tao, W.-K., S. Lang, J. Simpson, W.S. Olson, D. Johnson, B. Ferrier, C. Kummerow, and R. Adler, 2000: Retrieving vertical profiles of latent heat release in TOGA COARE convective systems using a cloud resolving model, SSM/I and radar data. *J. Meteor. Soc. Japan*, **78**, 333-355.

Tao, W.-K., S. Lang, W.S. Olson, S. Yang, R. Meneghini, J. Simpson, C. Kummerow, E. Smith and J. Halverson, 2001: Retrieved vertical profiles of latent heating release using TRMM rainfall products for February 1998. *J. Appl. Meteor.,* **40**, 957-982.

Tao, W.-K., E.A. Smith, R.F. Adler, Z.S. Haddad, A.Y. Hou, T. Iguchi, R. Kakar, T.N. Krishnamurti, C.D. Kummerow, S. Lang, R. Meneghini, K. Nakamura, T. Nakazawa, K. Okamoto, W.S. Olson, S. Satoh, S. Shige, J. Simpson, Y. Takayabu, G.J. Tripoli, and S. Yang, 2006: Retrieval of latent heating from TRMM measurements. *Bull. Amer. Meteor. Soc.,* **87,** 1555-1572.

Tao, W.-K., R. Houze, Jr., and E. Smith, 2007: Summary of the 4th TRMM Latent Heating Workshop, *Bull. Amer. Meteor. Soc.,* **88**, 1255, 1259.

Tao, K., and A. Barros, 2008: Fractal downscaling of satellite precipitation products for hydrometeorological applications. *J. Oceanic Atmos. Tech.*, submitted.

Tao, W.-K., S. Lang, X. Zeng, S. Shige, and Y. N. Takayabu, , 2009: Convective and stratiform rainfall and their relationship to latent heating. *J. Climate* (submitted).

Tao, W.-K., J. Shi, S. Chen, S. Lang, S.-Y. Hong, G. Thompson, C. Peters-Lidard, A. Hou, S. Braun, and J. Simpson, 2007: New, improved bulk-microphysical schemes for studying precipitation processes in WRF: Part I: Comparison with different microphysical schemes, *Mon. Wea. Rev.*, (submitted).

Tao, W.-K., Y. N. Takayabu, S. Lang, W. Olson, S. Shige, A. Hou, X. Jiang, W. Lau, T. Krishnamurti, D. Waliser, C. Zhang, R. Johnson, R. Houze, P. Ciesielski, M. Grecu, S. Hagos, R. Kakar, N. Nakamura, S. Braun, and A. Bhardwaj, 2013: TRMM Latent Heating Retrieval and Comparison with Field Campaigns and Large-Scale Analyses, *AMS Meteorological Monographs - Multi-scale Convection-Coupled Systems in the Tropics* (submitted).

Treadon, R.E., H.-L. Pan, W.-S. Wu, Y. Lin, W. Olson, and R. Kuligowski, 2002: Global and regional moisture analyses at NCEP. *Proceedings of an ECMWF/GEWEX Workshop on Humidity Analysis. 8-11 July, ECMWF,* 33-47. [Available from the European Centre for Medium Range Weather Forecasts, Shinfield Park, Reading,   RG2 9AX, UK.]

Turk, F.J., E.E. Ebert, B.-J. Sohn, H.-J. Oh, V. Levizzani, E.A. Smith, R. Ferraro, 2003: Validation of a global operational blended-satellite precipitation analysis at short time scales. Preprints, *12th Conf. Sat. Meteor. Ocean.*, Long Beach, CD-ROM, JP1.2.

Turk, F. J., and S. D. Miller, 2005: Toward improving estimates of remotely-sensed precipitation with MODIS/AMSR-E blended data techniques. *IEEE Trans. Geosci. Remote Sens.*, **43**, 1059-1069.

Validation Network Data Product User's Guide. Available online at: http://gpm.gsfc.nasa.gov/ground_direct.html

Wang, J., R. Bras, and E. Eltahir, 2000: The impact of observed deforestation on the mesoscale distribution of rainfall and clouds in Amazonia. *J. Hydrometeor.*, **1**, 267–286.

Yang, S., and E.A. Smith, 1999: Four dimensional structure of monthly latent heating derived from SSM/I satellite measurements. *J. Clim.*, **12**, 1016-1037.

Yang, S., W.S. Olson, J.-J. Wang, T.L. Bell, E.A. Smith, and C.D. Kummerow, 2006: Precipitation and latent heating distributions from satellite passive microwave radiometry.

Part II: Evaluation of estimates using independent data. *J. Appl. Meteor. Climatol.*, **45**, 721-739

Zipser, E. J., D. J. Cecil, C. T. Liu, S. W. Nesbitt, and D. Yorty, 2006: Where are the most intense thunderstorms on earth? *Bull. Amer. Meteor. Soc.*, **87**, 1057-1071.

Zupanski, M., D. Zupanski, D. Parrish, E, Rogers, and G. DiMego, 2002: Four-dimensional variational data assimilation for the blizzard of 2000. *Mon. Wea. Rev.*, **130**, 1967-1988.

Zupanski, D., S.Q. Zhang, M. Zupanski, A.Y. Hou, and S.H. Cheung, 2009: Development of an ensemble-based data assimilation algorithm for high-resolution dynamically balanced precipitation analysis. Geophys. Res. Abstracts, **11**, EGU2009-2605-2, EGU General Assembly 2009, Vienna, Austria.

List of Acronyms

AGRMET: AGriculture METeorology model
AIRS: Atmospheric Infrared Sounder
AMSU: Advance Microwave Sounder Unit
AMSR-E: Advanced Microwave Scanning Radiometer - EOS
ATBD: Algorithm Theoretical Basis Document
ATMS: Advanced Technology Microwave Sounder
ATOVS: Advanced TIROS Operational Vertical Sounder
CAPE: Convective Available Potential Energy
C3VP: Canadian CloudSat/CALIPSO Validation Project
CEOP: Coordinated Energy Observation Project
CEOS: Committee on Earth Observation Satellites
CGMS: Coordination Group for Meteorological Satellites
CoSSIR: Conical Scanning Submillimeter-wave Imaging Radiometer
CoSMIR: Conical Scanning Millimeter-wave Imaging Radiometer
CPW: Cloud Precipitatable Water
CRM: Cloud-Resolving Model
DMSP: Defense Meteorological Satellite Program
DOE-ARM: Department of Energy – Atmospheric Radiation Measurement
DPR: Dual-frequency Precipitation Radar
DWSS: Defense Weather Satellite System
ECMWF: European Center for Medium Range Forecasting
ENSO: El Nino/Southern Oscillation
ESA: European Space Agency
FOV: Field of View
GCOM-W1: Global Change Observation Mission - Water 1
GDAS: Global Data Assimilation System
GEO: Group on Earth Observations
GEOSS: Global Earth Observing System of Systems
GEWEX: Global Energy and Water Cycle Experiment
GMAO: Global Modeling and Assimilation Office
GMI: GPM Microwave Imager
GPM: Global Precipitation Measurement
GSICS: Global Space-based Inter-Calibration System
GV: Ground Validation
GVS: Ground Validation System
GWEC: Global Water and Energy Cycle
HIWRAP: High-altitude Imaging Wind and Rain Profiler
HMT: Hydrometeorological Testbed
IFNET: International Flood Network
IFOV: Instantaneous Field-of-View
IGOS: Integrated Global Observation Strategy
IGWCO: Integrated Global Water Cycle Observations
IPWG: International Precipitation Working Group
IR: Infrared

JAXA: Japan Aerospace Exploration Agency
JMA: Japan Meteorological Agency
JPST: Joint PMM Science Team
JPSS: Joint Polar Satellite System
LDAS: Land Data Assimilation Systems
LH: Latent heating
LIO: Low-Inclination Observatory
LSM: Land Surface Model
LST: Land Surface Temperature
LUT: Look-Up Table
MADRAS: Multi-Frequency Microwave Scanning Radiometer
MHS: Microwave Humidity Sounder
NAO: North Atlantic Oscillation
NEΔT (or NEDT): Noise Equivalent Delta Temperature
MJO: Madden-Julian Oscillation
NASA: National Aeronautics and Space Administration
NCEP: National Center for Environmental Prediction
NICT: National Institute of Information and Communications Technology (of Japan)
NOAA: National Oceanic and Atmospheric Administration
NPOESS: National Polar-orbiting Operational Environmental Satellite System
NPP: NPOESS Preparatory Project
NRC: National Research Council
NSF: National Science Foundation
NSTC: National Science and Technology Council
NWP: Numerical Weather Prediction
PMM: Precipitation Measurement Missions
PNA: Pacific-North America
PPS: Precipitation Processing System
PR: Precipitation Radar
PST: Precipitation Science Team
SSM/I: Special Sensor Microwave/Imager
SSMIS: Special Sensor Microwave Imager/Sounder
SST: Sea Surface Temperature
TMI: TRMM Microwave Imager
TDRSS: Tracking and Data Relay Satellite System
TOVS: TIROS Operational Vertical Sounder
TPW: Total Precipitable Water
TRMM Tropical Rainfall Measuring Mission
VN: Validation Network
WCRP: World Climate Research Program
WMO: World Meteorological Organization
WRF: Weather Research and Forecasting

Appendix A. GPM Level 1 and Level 2 Science Requirement Traceability for Radar and Radiometer Measurements

GMI Level 1 and Level 2 Requirements Table

Level 1 Science Requirements	Level 2 Science Requirements
Radiometer **Section 4.6.1.1** The GPM Core and Low-Inclination satellites shall carry a multi-channel, wide-band (10-183 GHz) GPM Microwave Imager (GMI). **Section 4.6.1.4.2** The GPM Project, using measurements from the GMI, shall quantify rain rates between 0.2 and 60 millimeter (mm) per hour (hr) and demonstrate the detection of snowfall at an effective resolution of 15 kilometer(s) (km).	**Section 3.1.1.1** The GPM GMI shall have two channels at 10.65 GHz, one with Vertical (V) polarization and one with Horizontal (H) polarization. The antenna beamwidth (as defined by 3-dB width) shall not exceed 1.75 degree, and the Beam Temperature Sensitivity (Beam-NEDT) shall not exceed 0.53 K. **Rationale**: The 10 GHz channels are needed for retrieving heavy precipitation rates (>10 mm/hr) encountered in the tropics. Dual polarizations are needed to differentiate surface emissivity effects from precipitation signals over oceans. The TMI instrument added these channels after noticing that SSMI, its predecessor, suffered from severe attenuation in the heavy tropical rain events. With the Core Spacecraft at 407 km, even though the 10 GHz GMI footprints are larger than the 15 km resolution of GMI retrieval products, information from these channels are used in a multi-channel retrieval algorithm. The channel specifications are based in part on the TMI heritage. The Beam-NEDT is comparable to that for TMI when normalized with respect to the bandwidth and integration time (see GPM Science Implementation Plan (SIP) Appendix D) and is suitable for precipitation retrieval (see GPM SIP Appendix F). (Note: The Beam-NEDT is defined for an integration time equal to the scan-time of one full beamwidth. At the standard GMI sample-interval of 3.6 ms, a Beam-NEDT of 0.53 K corresponds to a Sample-NEDT of 0.96 K.) **3.1.1.2** The GPM GMI shall have two channels at 18.7 GHz, one with V polarization and one with H polarization. The 3-dB antenna beamwidth shall not exceed 1.00 degree, and the Beam-NEDT shall not exceed 0.61 K. **Rationale:** The 18.7 GHz channels are needed for retrieving moderate to light precipitation rates over ocean. These channels provide Nyquist-sampled data as an integral part of the multi-channel retrieval algorithm. The channel specifications are based in part on the heritage instruments of SSM/I, TMI, AMSR-E, WINDSAT and SSMIS. The Beam-NEDT specification is comparable to that for TMI when normalized with respect to the

bandwidth and integration time (see GPM SIP Appendix D) and is suitable for precipitation retrieval (see GPM SIP Appendix F). A Beam-NEDT of 0.61 K corresponds to a Sample-NEDT of 0.84 K at the standard GMI sample-interval of 3.6 ms.

3.1.1.3
The GPM GMI shall have a 23.8 GHz channel with V polarization. The 3-dB antenna beamwidth shall not exceed 0.90 degree, and the Beam-NEDT shall not exceed 0.82 K.

Rationale: The 23.8 GHz channel is needed to correct for the absorption of water vapor in the other channels in multi-channel retrievals. Only V polarization is needed because the polarization signature is not very pronounced at frequencies around 22 GHz. The channel specifications are based in part on the heritage instruments of TMI, SSM/I, AMSR-E, and SSMIS. The Beam-NEDT specification is comparable to that for TMI when normalized with respect to the bandwidth and integration time (see GPM SIP Appendix D) and is suitable for precipitation retrieval (see GPM SIP Appendix F). A Beam-NEDT of 0.82 K corresponds to a Sample-NEDT of 1.05 K at the standard GMI sample-interval of 3.6 ms.

3.1.1.4
The GPM GMI shall have two 36.5 GHz channels, one with V polarization and one with H polarization. The 3-dB antenna beamwidth shall not exceed 0.90 degree, and the Beam-NEDT shall not exceed 0.52 K.

Rationale: The 36.5 GHz channels were used originally by SSM/I and later by TMI, AMSR-E, WINDSAT and SSMIS in tandem with 19 GHz channels to measure moderate and light precipitation over ocean. These channels are critical in the multi-channel retrieval algorithm to estimate moderate rain rates at 15 km resolution and are used in conjunction with the 35.5 GHz channel of the KaPR to produce combined radar-radiometer precipitation retrievals. The channel specifications are based in part on the TMI heritage. The Beam-NEDT specification is comparable to that for TMI when normalized with respect to the bandwidth and integration time (see GPM SIP Appendix D) and is suitable for precipitation retrieval (see GPM SIP Appendix F). A Beam-NEDT of 0.52 K corresponds to a Sample-NEDT of 0.65 K at the standard GMI sample-interval of 3.6 ms.

3.1.1.5
The GPM GMI shall have two 89.0 GHz channel, one with V polarization and one with H polarization. The 3-dB antenna beamwidth shall not exceed 0.40 degree, and the Beam-NEDT

shall not exceed 0.65 K.

Rationale: The 89 GHz channels are used in the multi-channel retrievals, where their small FOVs are essential to separate convective from stratiform precipitation and thus correct for nonlinearities introduced by rainfall inhomogeneity. Given the specified beamwidth, the IFOV will be ~7.5 km for the Core Observatory. It was the main channel for TRMM retrievals over land, where only ice scattering can be detected over radiometrically warm backgrounds. The small IFOVs take precedence over contiguous sampling considerations for these channels. TMI has shown that footprint gaps in the cross-scan direction of up to 60% of the scene are acceptable for precipitation retrievals. The Beam-NEDT specification is comparable to that for TMI when normalized with respect to the bandwidth and integration time (see GPM SIP Appendix D) and is suitable for precipitation retrieval (see GPM SIP Appendix F). A Beam-NEDT of 0.65 K corresponds to a Sample-NEDT of 0.57 K at the standard GMI sample-interval of 3.6 ms.

3.1.1.6:
The GPM GMI shall have two channels at 165.5 GHz, one with V polarization and one with H polarization. The 3-dB antenna beamwidth shall not exceed 0.40 degree, and the Beam-NEDT shall not exceed 1.72 K.

Rationale: The 166.5 GHz channels (in conjunction with the 89 and the 183 GHz channels) are needed for determining light precipitation rates encountered in frontal situation outside the tropics. The resolution of these channels is chosen to match that of the 89 GHz channels based on trade considerations between spatial resolution and coverage. TMI has shown that footprint gaps in the cross-scan direction of up to 60% of the scene are acceptable for precipitation retrievals. The Beam-NEDT specification is comparable to that for SSMIS when normalized with respect to the bandwidth and integration time (see GPM SIP Appendix D) and is suitable for light rain retrieval and snowfall detection (see GPM SIP Appendices F and G). A Beam-NEDT of 1.72 K corresponds to a Sample-NEDT of 1.50 K at the standard GMI sample-interval of 3.6 ms.

3.1.1.7:
The GPM GMI shall have one channel at 183±3 GHz and one at 183±8 GHz, both with V polarization. For each channel, the beamwidth shall not exceed 0.40 degree, and the Beam-NEDT shall not exceed 1.72 K.

	Rationale: The 183 GHz channels are needed for detecting scattering signals from small ice particles, which are used to estimate light rain and snowfall rates over snow-covered land (radiometrically cold backgrounds). Only V polarization is needed because the surface polarization signature is not very pronounced at frequencies around 183 GHz (mainly because of the water vapor absorption). The resolution of these channels is chosen to match that of the 89 GHz channels based on trade considerations between spatial resolution and coverage. TMI has shown that footprint gaps in the cross-scan direction of up to 60% of the scene are acceptable for precipitation retrievals. The Beam-NEDT specification is comparable to that for SSMIS when normalized with respect to the bandwidth and integration time (see GPM SIP Appendix D) and is suitable for light rain retrieval and snowfall detection (see GPM SIP Appendices F and G). A Beam-NEDT of 1.72 K corresponds to a Sample-NEDT of 1.50 K at the standard GMI sample-interval of 3.6 ms.
Radar **Section 4.6.1.1** The GPM Core Observatory shall provide microwave measurements of microphysical properties and 3-dimensional structures of precipitation systems in near real-time from 65 degrees north latitude to 65 degrees south latitude. The GPM Core Observatory shall carry a Dual-frequency Precipitation Radar (DPR) with Ku/Ka-bands (13.6 and 35.5 GHz). **Section 4.6.1.4.1** The GPM Core	**Section 3.1.2.1 Ku-Band** The GPM DPR shall have a 13.6 GHz channel to measure 3-dimensional precipitation structure with a horizontal resolution of 5.2 km, a range resolution of 250 m, an echo top up to an altitude of at least 19 km, a minimum measurable rain rate of 0.5 mm/hr, and an accuracy of +/-1 dBZ. **Rationale:** Active radar at 13.6 GHz is required for measuring moderate to heavy precipitation rates. The Ku-band is heritage from the PR on TRMM which has shown that rain rates up to 110 mm/hr and down to 0.5 mm/hr can be estimated with a reflectivity sensitivity of 18 dBZ. A 250 m range resolution provides vertical information at scales needed to resolve cloud structures (e.g., the melting layer). The DPR needs to be able to measure hurricane updrafts (hot towers) that penetrate into the lower stratosphere, hence the 19km echo top requirement. The 1 dBZ accuracy is based on TRMM heritage. **3.1.2.2 Ka-Band** MRD192 The GPM DPR shall have a 35.5 GHz channel to measure 3-dimensional precipitation structure within the Ku swath with a horizontal resolution of 5.2 km, a range resolution of 250 m, an echo top to an altitude of at least 19km, a minimum measurable rain rate of 0.2 mm/hr, and an accuracy of (+/-) 1 dBZ. **Rationale:** The Ka-band provides greater measurement

Observatory shall make measurements of the same geophysical scenes using both active and passive techniques. These are needed for development of a reference standard for calibrating and retrieving precipitation information from microwave sensors on GPM partner satellites.

Section 4.6.1.4.2
The GPM Project shall use DPR measurements to quantify rain rates between 0.22 and 110 millimeter (mm) per hour (hr) and demonstrate the detection of snowfall at an effective resolution of 5 kilometer(s) (km).

Section 4.6.1.4.3
The GPM Project, using measurements from the Core observatory, shall estimate the median mass diameter of precipitation particle size distribution to within +/- 0.5 mm.

sensitivity to signatures of light rain rates (down to 0.2 mm/hr) and snowfall relative to the Ku-band. The sensitivity of the Ka-band is designed to 0.2 mm/hr which exceeds the L1 requirement. Also, with overlapping dual frequency coincident observations, the DPR will provide quantitative information on rain and snow particle size distributions (including the median mass diameter to within ±0.5mm or another comparable measure of diameter) and other microphysical properties over the mid-range of precipitation intensities. The Ka and Ku bands are selected because they are both sensitive to particle size distributions that occur from light to moderate rain rates, thus providing two degrees of freedom for defining particle size distributions for these rain rates over the inner swath of the dual frequency channels. The dual frequency information on precipitation microphysics properties is needed for improving radiometer retrieval algorithms and representations of precipitation processes in numerical models. The 1 dBZ accuracy requirement matches the accuracy for the Ku-band.

Appendix B. Enhanced GPM Sampling with a Low Inclination Observatory

Xin Lin and Arthur Hou
(May 2009)

This appendix describes the enhanced global coverage and sampling capabilities if a Low Inclination Observatory (LIO) carrying a GMI or other microwave precipitation sensor at a 40° non-sun-synchronous orbit were added to the GPM constellation satellite suite. The appendix shows GPM mission enhancement in terms of science afforded by additional samples in the $\pm 40^{\circ}$ latitude band where polar orbiting satellites have fewer overpasses per day. Note that this analysis was performed for a baseline GPM algorithm development plan that uses microwave sounder observations only over land surfaces, hence the GPM constellation samples are different between the ocean and land.

1) Analysis of impact of LIO data on the sampling interval by the GPM constellation:

An analysis was performed to determine the probability density function (PDF) of the sampling interval between visits by the GPM constellation of satellites with and without the LIO for the years of 2014 and 2017.

The 2014 constellation consists of: Core, LIO, GCOM-W1, F18, F19, plus (NPP, NOAA-19, NPOESS-C1 [Now JPSS], MetOp-B) over land. The possible extension of the Megha-Tropiques satellite (which is to be launched in 2010 for a 3-year baseline mission) into 2014 or beyond is not considered in this analysis. For 2017 the constellation comprises the Core, LIO, F-20, GCOM-W1, plus sounders over land from NPP, MetOp-C, NPOESS-C1, and NPOESS-C2. The analysis is based on one year of hourly data in each case. Figures 1 and 2 show the averaged number of observations per month as a function of sampling interval in hourly bins for 0 degree longitude from 60 N to 60 S.
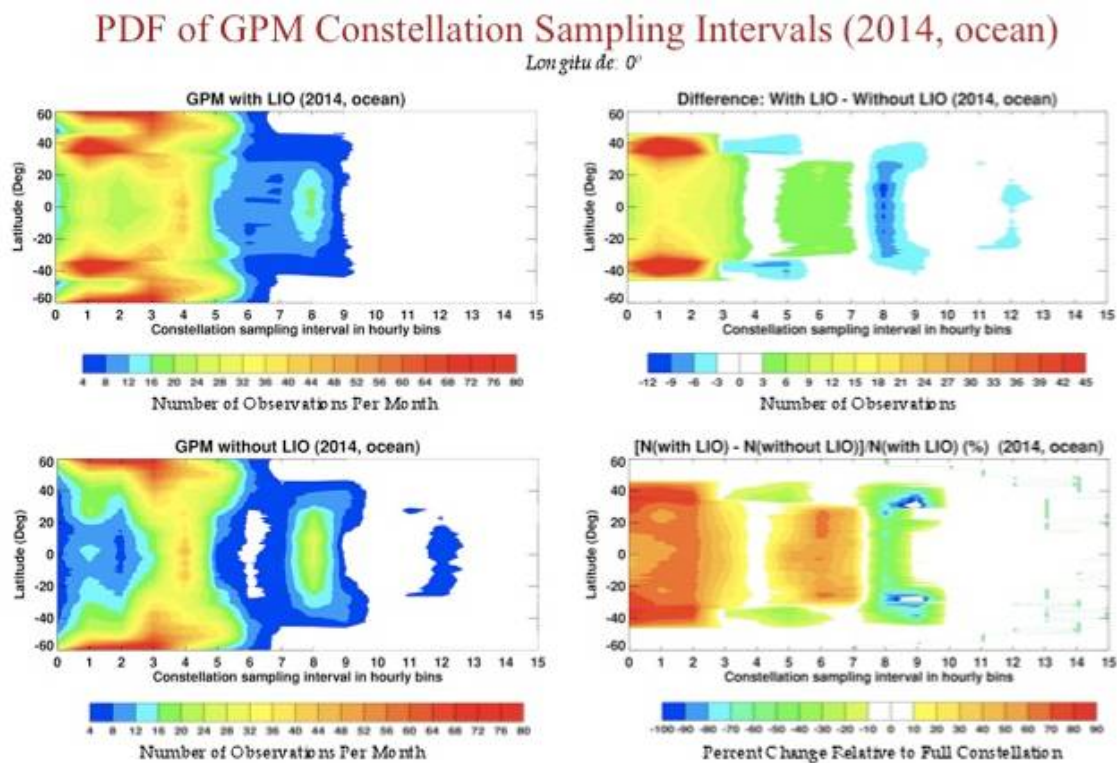
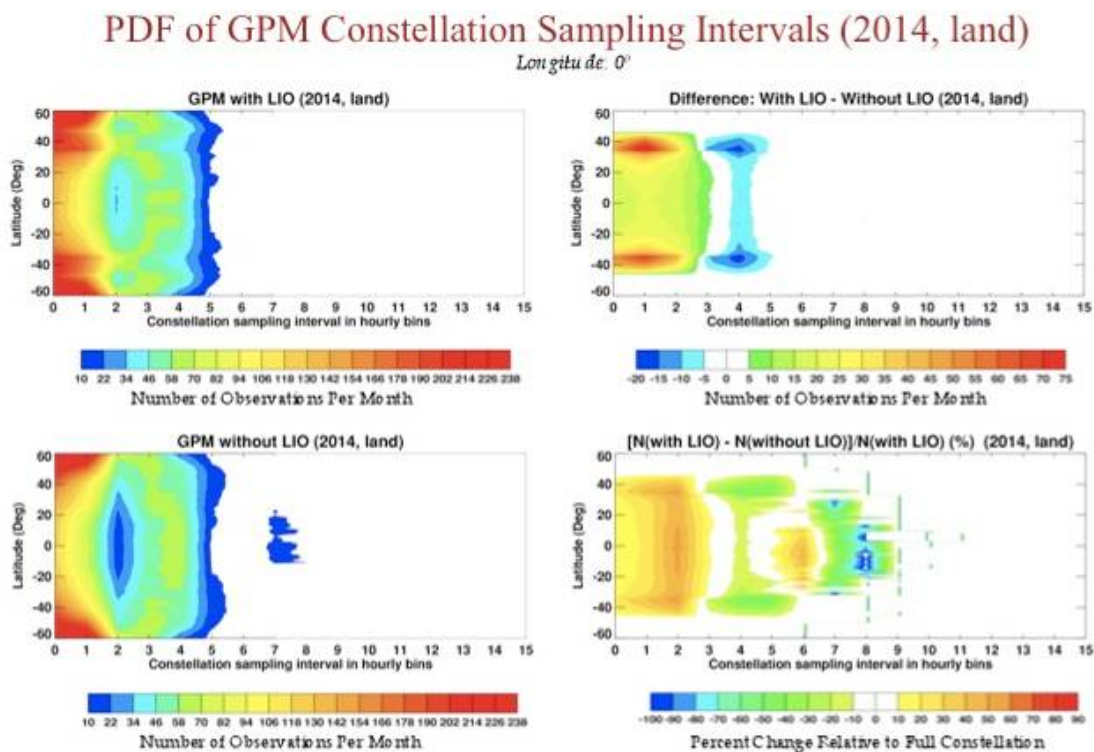Figure 1a. GPM sampling interval PDF for 2014 (ocean)

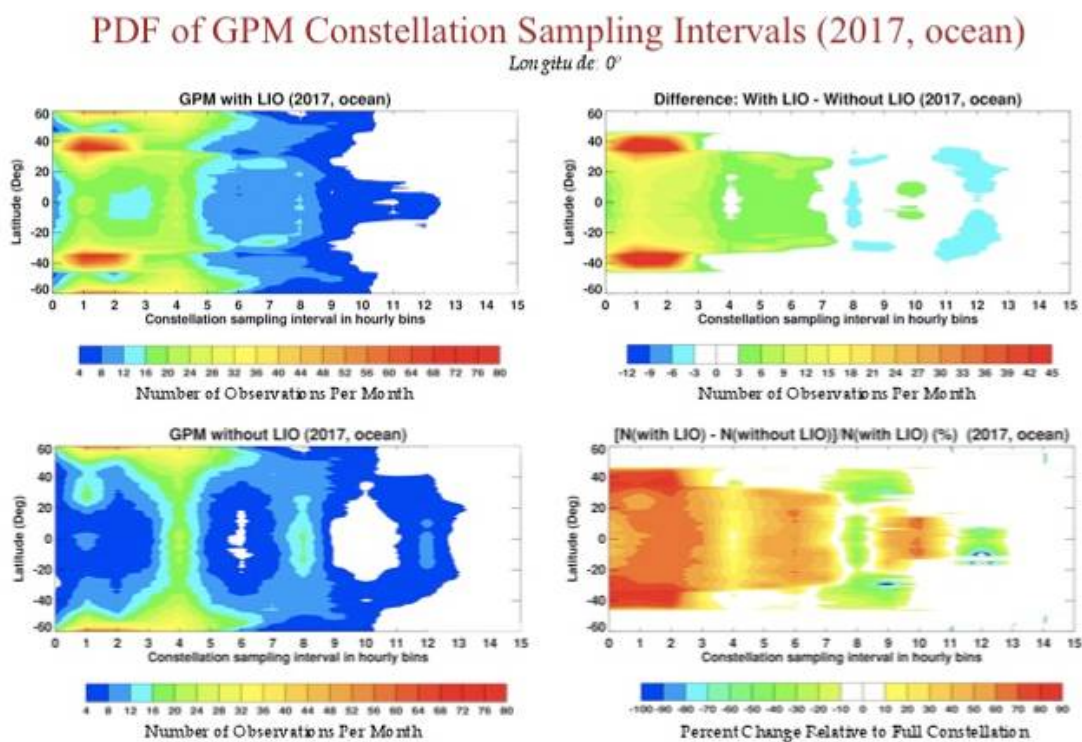Figure 1b. GPM sampling interval PDF for 2014 (land)

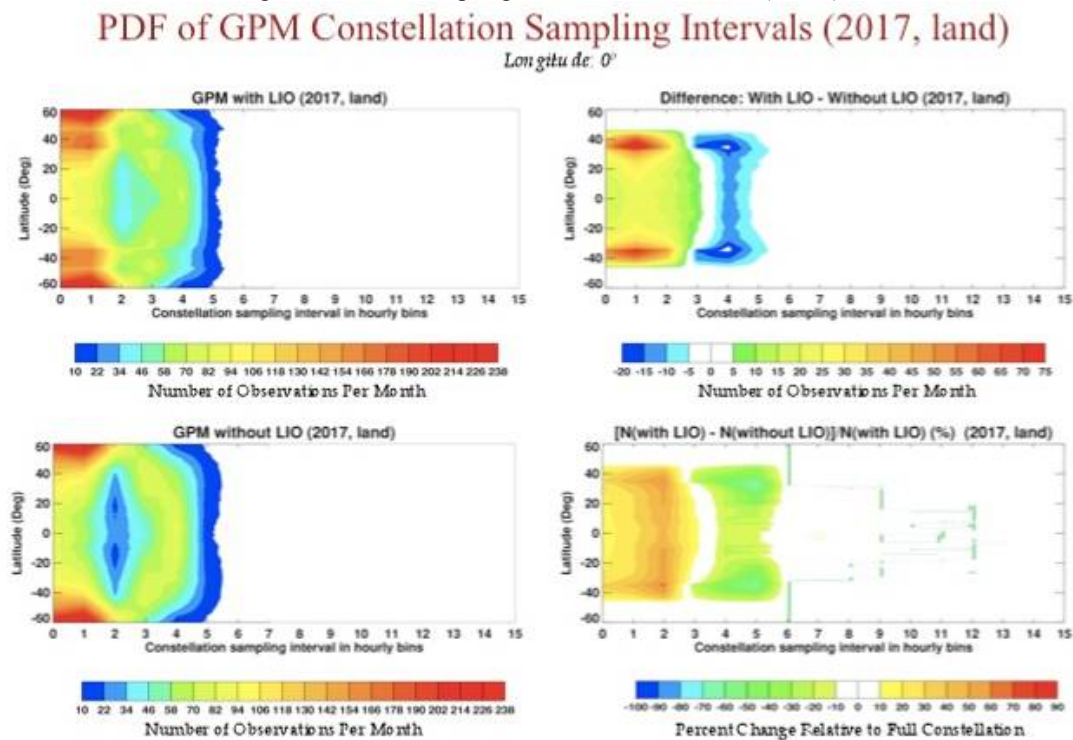Figure 2a. GPM sampling interval PDF for 2017 (ocean)

Figure 2b. GPM sampling interval PDF for 2017 (land)

In summary, the above results show that without the LIO, GPM's ability to provide < 3 h sampling (a requirement for hydrological applications, Hossain and Lettenmaier 2006) will be reduced by 60-70% over ocean and 20-50% over land.

2) Impact of LIO sampling on time-integrated rain accumulation over continental United States:

An analysis of GPM sampling errors in monthly rain accumulation over the continental US was performed for January and July 2014 using composite surface radar-gauge data as the truth. Results are shown in Figures 3a and 3b. In each figure, the upper left panel shows true rain accumulation in mm as given by the combined surface radar+gauge data. The upper right panel shows errors (in mm) due to discrete sampling by the GPM constellation with LIO. The lower left panel shows increase in error (in mm) without LIO. (Note that in terms of monthly averaged rain rate, these errors are on the order of 1 mm/day, or 30 Wm^{-2} at 0.5-deg resolution.) The lower right panel shows percent error without LIO relative to the full constellation over areas where the true rain accumulation exceeds 10 mm. Note that the large percentage errors are not an artifact of small denominators.

      In summary, this analysis shows that the impact of not having the LIO in the GPM constellation is to increase errors in rainfall accumulation by 40-60% in localized areas over the continental United States, significantly degrades the utility of GPM data for basin-scale water resource management and other hydrological applications.
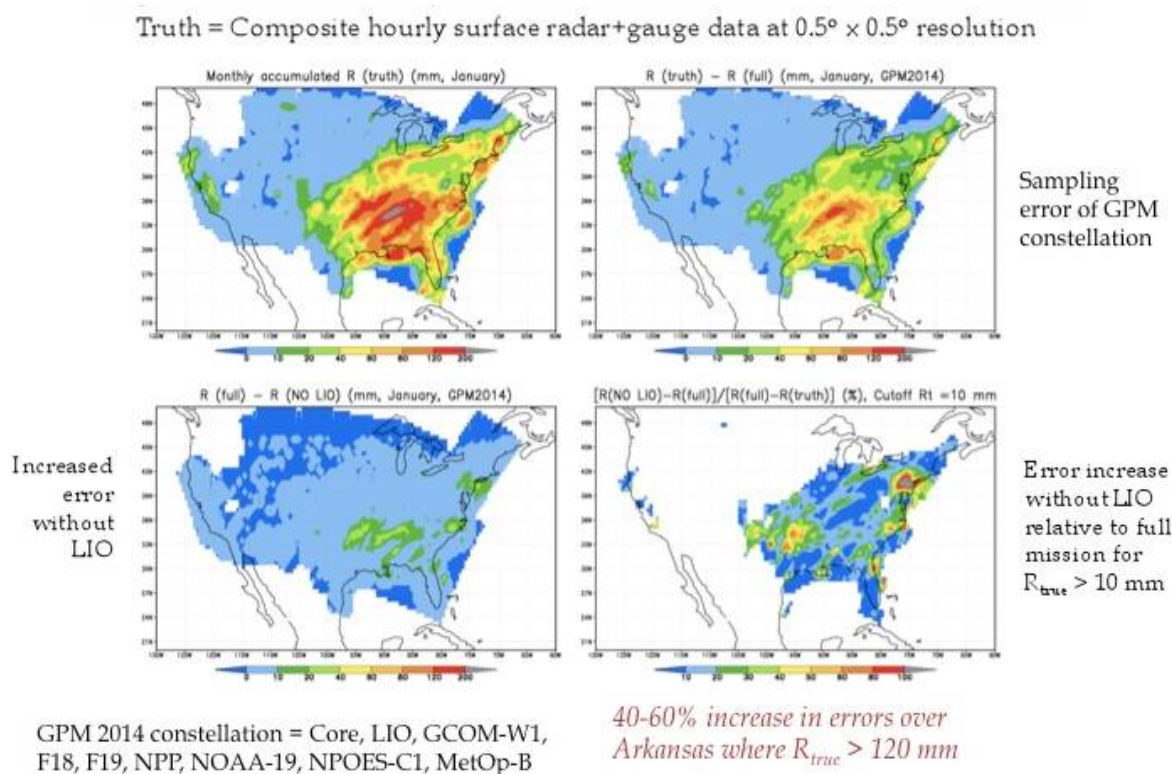
Figure 3a. Degradation in monthly rain accumulation without LIO: January 2014
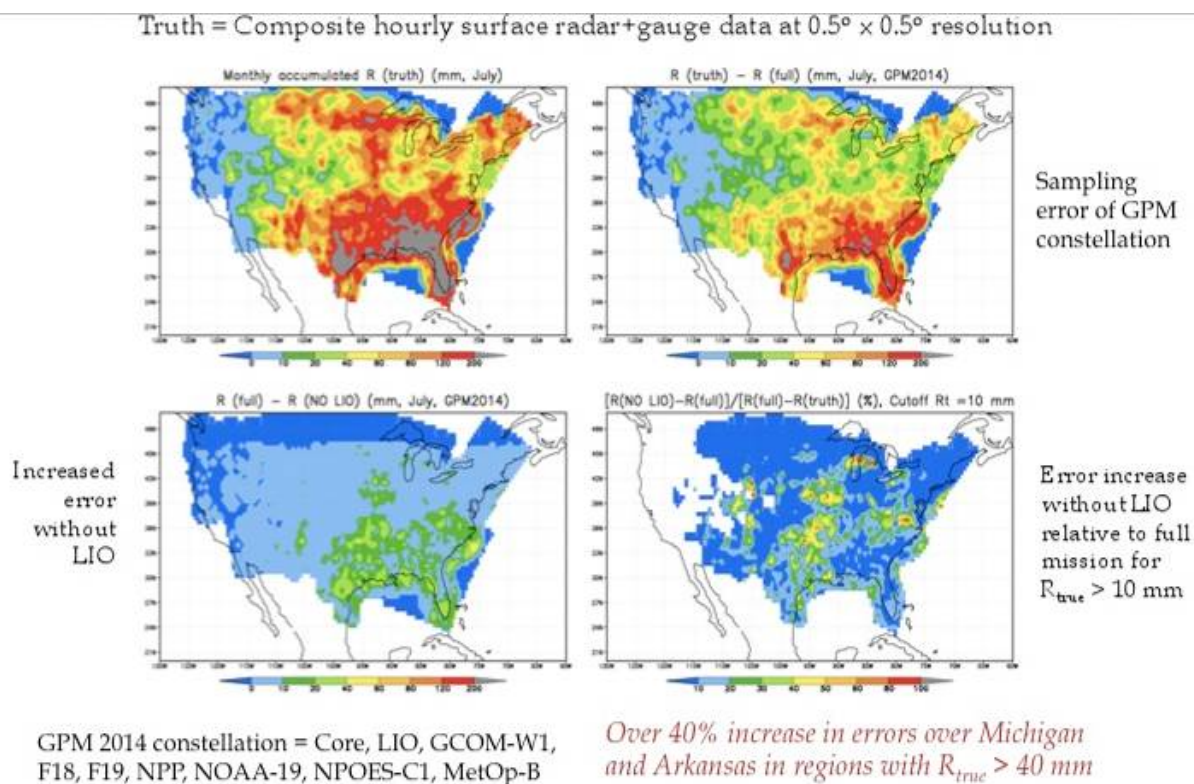
Figure 3b. Same as Figure 3a except for July 2014

3) Impact of LIO sampling on tropical rainfall estimation:

Unlike the mesoscale convective rain systems over the continental U.S. examined in the previous section, convective events in the Tropics (e.g. over the ITCZ) are small in scale and short-lived by comparison. To assess the impact of LIO in estimating rainfall accumulation from rapidly-varying localized convective events, we performed an analysis using high-resolution (2 km) model-simulated TOGA-COARE rain events as the truth.
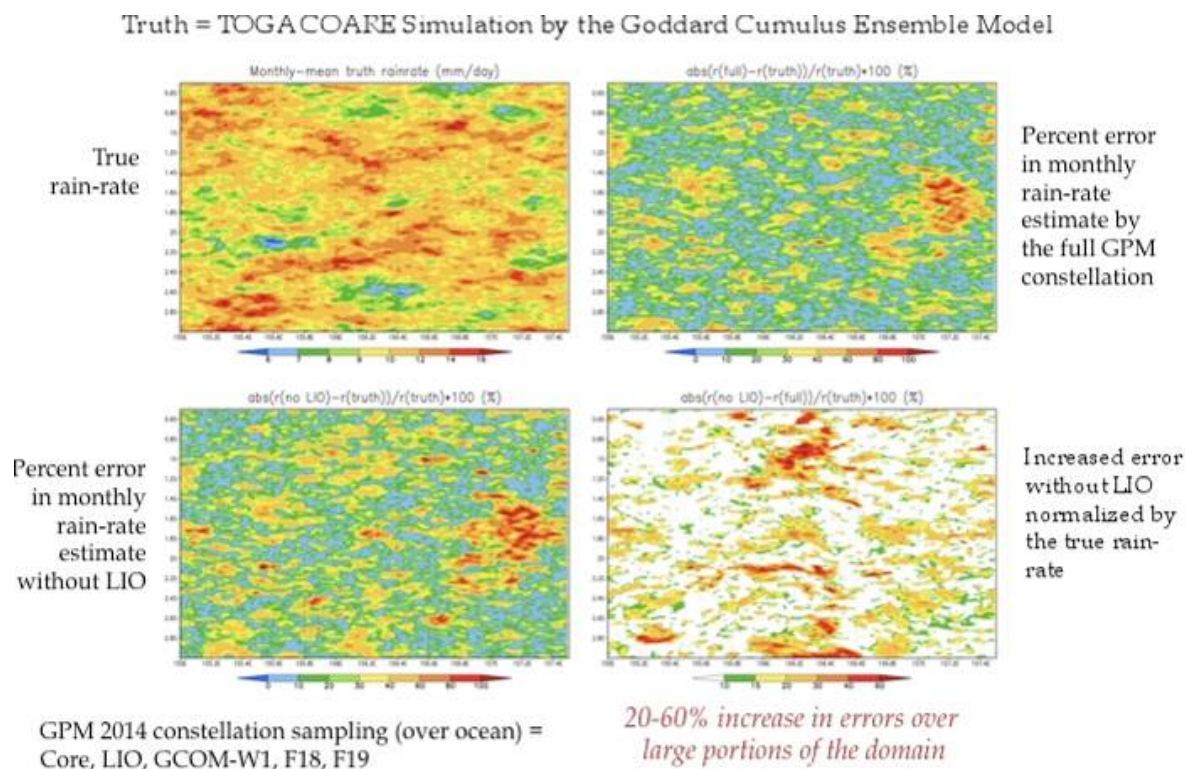
Figure 4. Degradation in monthly-mean rain rate estimate without LIO: January 2014

Figure 4 shows that without the LIO, errors in the monthly-mean rain rate would increase by 20-60 over large portions of the domain. The switching from rain accumulation (which was used for the continental US study) to rain rate is necessitated by the fact that monthly rain accumulations cannot be directly constructed from the limited conical-scanning radiometers (rainfall estimates from microwave sounders have significant biases over oceans hence not included in the GPM sampling). Traditionally, the monthly rain amount is estimated by multiplying the mean rain rate (mm/day) by the number of days. This underscores the dire situation over oceans, where more radiometers with emission channels, especially one such as the LIO in a non-Sun-synchronous orbit, are needed.

Appendix C. Scientific Considerations for the 183 GHz Channel Selection

Preamble

In April 2002, Gousheng Liu (Florida State University) and Eric A. Smith (then the GPM Project Scientist) produced a white paper for the GPM Project stating the channel sets appropriate for snow detection over ocean versus over land. The white paper states that for ocean snow detection, the primary channels are 166 V and H, while 22, 183±1, ±3, ±6, ±9 GHz can play a role in accounting for atmospheric moisture. For detecting snow over land, they define a "sweetness factor" that maximizes brightness temperature sensitivity to falling snow in the atmosphere while minimizing sensitivity to surface contamination. The channels favored by the sweetness factor were 183±3 for typical atmospheric environments, 183±6 for atmospheric environments 10°C colder than typical, and 183±9 for atmospheric environments 20°C colder than typical. While 183±8 GHz was not explicitly recommended in this white paper, there is sufficient analysis to state that 183±8 GHz will provide scientifically valid observations to meet GMI requirements.

This appendix reproduces the Liu-Smith white paper (without edits) in the following pages.

**Final GMI High Frequency Channel Options for Measuring
Over-Ocean & Over-Land Snowfall**

Guosheng Liu and Eric A. Smith, April 2002

Minimum: 166V or 150V
Baseline: 166V&H
Better: 166V&H, 183±3V, 183±9V
Best: 166V&H, 183±1V, 183±3V, 183±6V, 183±9V

Over-Ocean (Figures 1-3)

Suggested primary channels for snow detection are 166 GHz at V-pol & H-pol. Dual polarization allows use of PCT which is more sensitive to snowfall than any single polarization. If only one polarization is possible, use V-pol instead of H-pol, because dynamic range is much greater at V-pol (i.e., background is much warmer).

Suggested ancillary channels to account for moisture are 22 & 183±1,±3,±6,±9 GHz, all at V-pol.
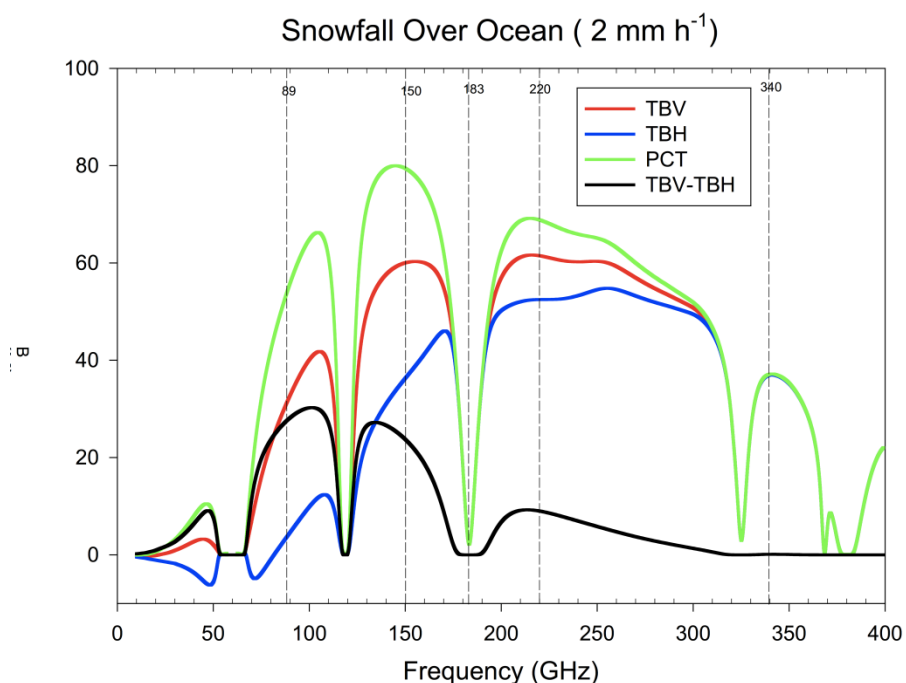
Figure 1: Spectral distribution of brightness temperature decrease (ΔT_B) due to over-ocean snowfall of 2 mm h^{-1} (water equivalent) for typical snow profile and typical atmospheric profile observed over Sea of Japan. PCT is polarization-corrected-temperature.
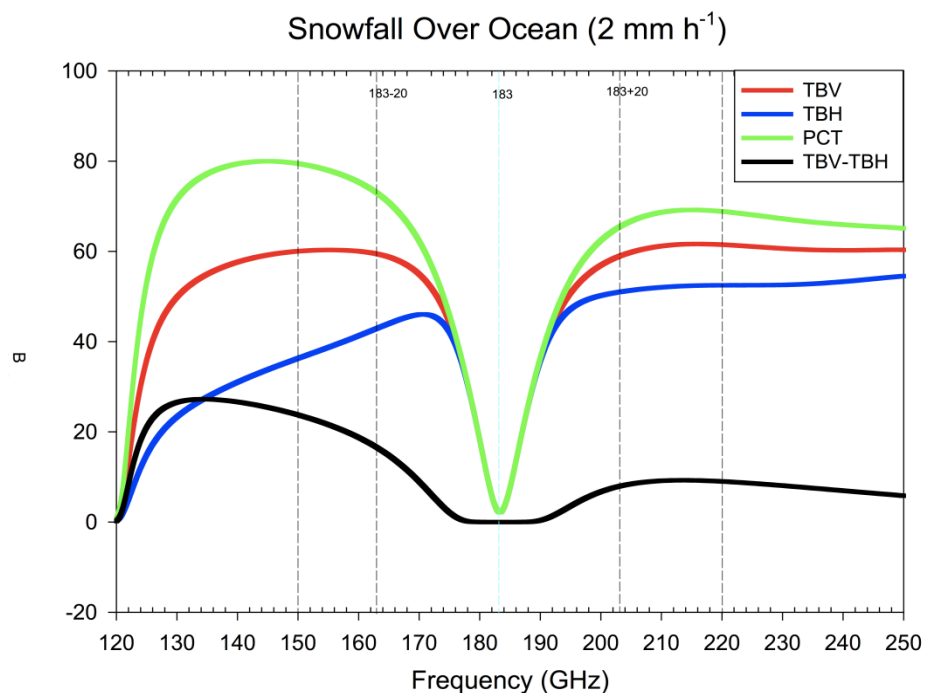
Figure 2: Same as Fig. 1, except for restricting abscissa to 120-250 GHz.
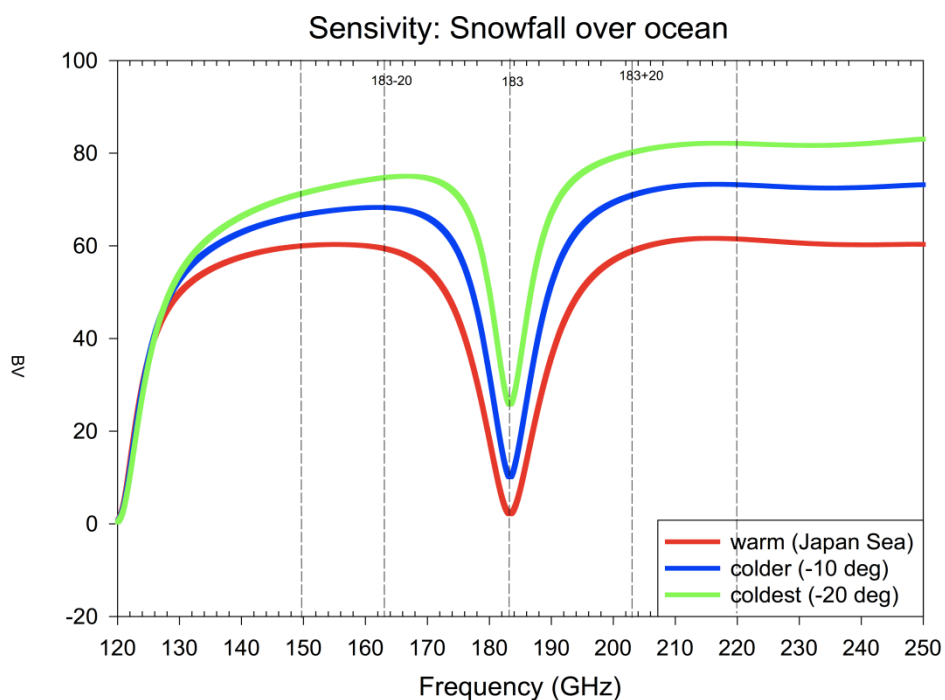
Figure 3: Spectral distribution of sensitivity (ΔT_B) of vertical polarized brightness temperature for 3 atmospheres: (1) red for typical environment (Sea of Japan); (2) blue for 10°C colder than typical; (3) green for 20°C colder than typical. Because relative humidity is invariant for three profiles, colder temperatures translate to less water vapor. Because water vapor has masking effect on snow scattering, lower water vapor concentrations lead to higher sensitivities.

Over Land (Figures 4-5)

<u>Suggested primary channels for snow detection are 183±3 & 183±9, both at V-pol</u>. First channel is for low water vapor densities while second is for high water vapor densities.
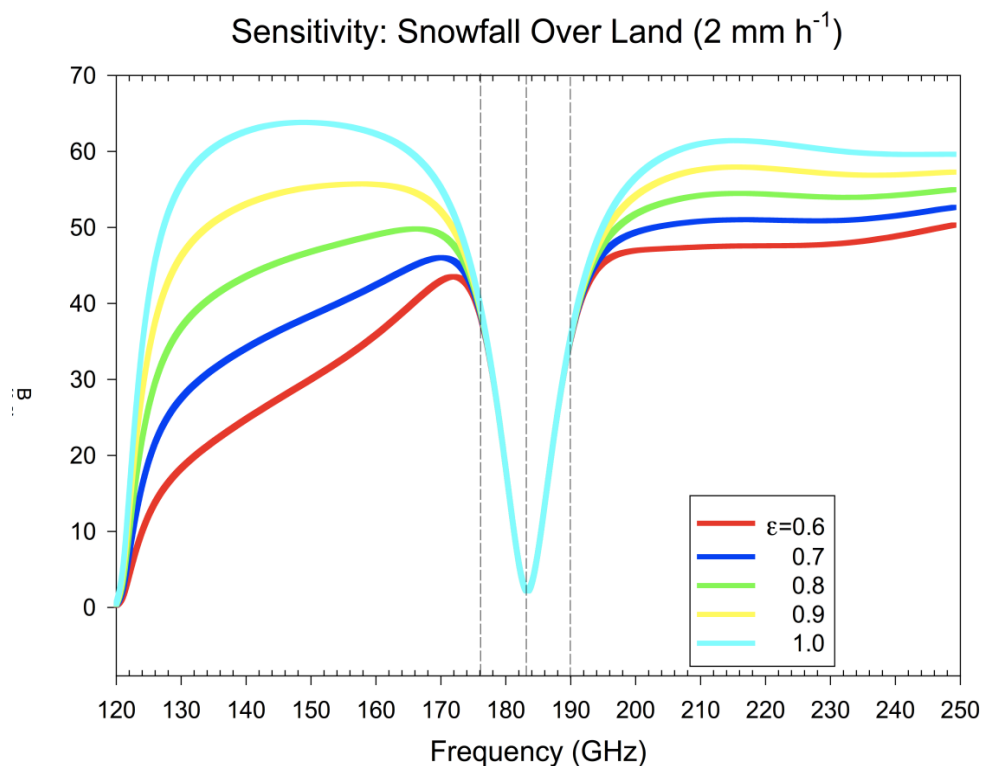
Figure 4: Influence of surface emissivity on brightness temperature change (ΔT_B) for snowfall rate of 2 mm h^{-1} (water equivalent). Typical snow profile and typical atmospheric profile observed over Sea of Japan are used in calculations. Surface emissivity varies from 0.6 to 1.0 assuming Lambertian surface.

Define "sweetness factor" (SF) as:

$$SF = \frac{\Delta TB_{\varepsilon sur}}{max_1} \times (1 - \frac{\Delta TB_{\varepsilon sur,max} - \Delta TB_{\varepsilon sur,min}}{max_2})$$

where first term is "sensitivity" to snowfall and second term is "insensitivity" to surface. This factor reflects signal to noise ratio (surface noise), such that greater SF value yields better snowfall retrieval over land.

$$SF=\Delta T_{B0.6}/max1*[1-(\Delta T_{B1.0}-\Delta T_{B0.6})/max2]$$
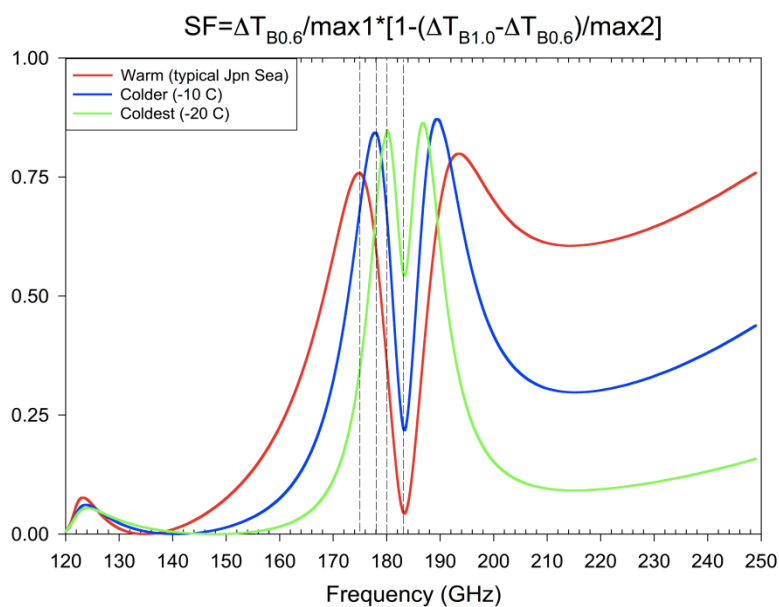
Figure 5: Spectral distributions of SF for 3 atmospheres for surface emissivities of 0.9 (upper panel) and 0.6 (lower panel): (1) red for typical environment (Sea of Japan); (2) blue for 10°C colder than typical; (3) green for 20°C colder than typical. Snowfall rate is taken as 2 mm h^{-1} (water equivalent). Peaks of SF appear at approximately 183±3, 183±6, 183±9 GHz for 3 atmospheres, respectively.

Typical Atmospheric and Snowfall Profiles
Typical Atmospheric Profiles (Sea of Japan in Winter)
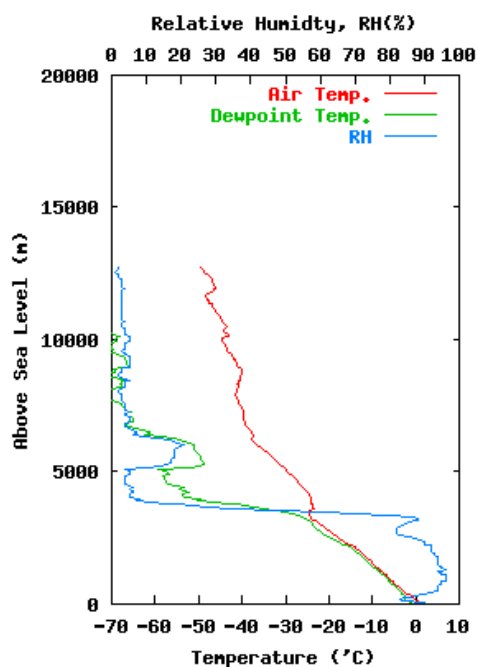
Typical Snowfall Profiles (Sea of Japan in Winter)
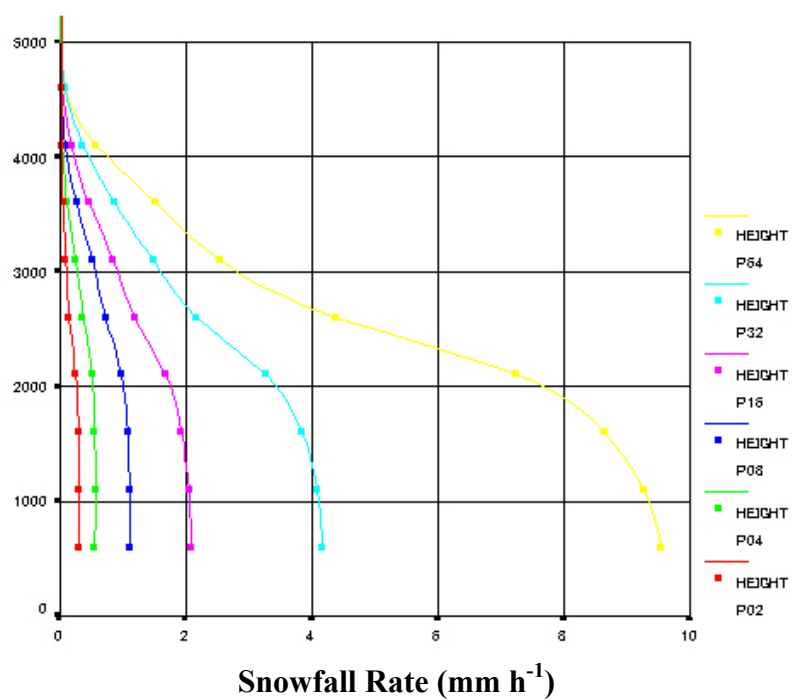
Snowfall Rate (mm h^{-1})

Appendix D. Radiometer NEDT Specifications: GMI versus TMI and SSMIS (conical-scanning imagers)

Jim Shiue
Date: 3/9/09

1. Introduction

The Temperature Sensitivity (ΔT), also known as NEDT, is a measure of the radiometer's precision, usually expressed in temperature units. The dominant part of the NEDT can be represented by the expression in (1):

$$\Delta T = Ts / Sqrt [BW \times t_i] \qquad (1)$$

where Ts is the System noise temperature (including both the Antenna Temperature and the radiometer receiver's internal noise temperature), BW is the pre-detection bandwidth, ti is the integration time, and Sqrt is the square-root operation.

The System noise temperature term, Ts, is indicative of how "quiet" the radiometer is. The smaller the Ts, the better are the radiometer. In other words, it has a better precision.

To compare the ΔTs of two different microwave radiometers for the purpose of comparing their precision, one must first "normalize" their integration- time and bandwidth, because these parameters are frequently different. Furthermore, the integration time ti is somewhat arbitrary (frequently it is the engineering considerations that determine ti).

Let the tb value set to be equal to ΔTs which is "the time it takes for a scanning radiometer to scan across one full beam width" in along-scan direction, then the value of ΔT from equation (1) is called Beam Temperature Sensitivity, or ΔTb.

For multi-frequency microwave radiometers with several different beamwidths, the value of tb will be different from one channel to another, and for engineering reasons, frequently only one single integration time is set for all the channels. This single integration time is called Sample time, or ts, and the ΔT values obtained from equation (1) with this sample time is called Sample NEDT, or ΔTs. For example, the GMI has a single sample time of 3.6 ms for all its 13 channels.

Temperature Sensitivity, or Radiometric Precision, is only one of the figures of merit, with which one judges a microwave radiometer. There are other figures of merit, e.g., the spatial resolution, particularly for the imaging microwave radiometers, and the two are not totally independent from each other. A commonly used figure of merit for spatial resolution is the Footprint size, or Instantaneous Field of View (IFOV), which, in the case of earth remote sensing from a satellite, is the figure cut by a right circular cone, represented by the antenna beam width, intercepting the earth surface. Frequently a major diameter $(IFOV)_M$ and a minor diameter $(IFOV)_m$ are used to represent the Footprint (which is in general a pear-shaped figure). In a conical scanning microwave radiometer, such as the TMI or GMI, the antenna beam is scanning on the surface of a cone, whose axis is the nadir direction, with half-cone angle equal to the off-nadir angle θ_n.

Obviously the size of the antenna beam width is a key figure of merit for the spatial resolution. But it is equally obvious that in terms of the (IFOV)s, the orbital height and off-nadir angle all come into play.

Finally, since the Beam Temperature Sensitivity is dependent on the amount of (integration) time it take to scan one full $(IFOV)_m$. That connects the Beam Temperature Sensitivity, or Radiometric Precision, to the spatial resolution.

2. Normalization Process

In order to fairly compare GMI to other instruments we must normalize the temperature sensitivity equation (1). We normalize with respect to the integration time and bandwidth of the two instruments. Thus we take eqn (1) and multiply by the following factors:

$$\Delta T_{s,b} \text{ (Inst norm)} = \Delta T_{s,b} \text{ (Inst)}*f$$
$$f = \text{sqrt}[(BW(inst)/BW(GMI))*(t_i(inst)/ t_i(GMI)]$$

where $\Delta T_{s,b}$ (Inst norm) is the instrument's NEDT normalized to GMI's NEDT (and subscripts s and b refer to sample versus beam NEDT), $\Delta T_{s,b}$ (Inst) is the non-normalized NEDT of the instrument, and so on for the other variables. In the tables in this document, the highlighted rows indicated NEDT values of GMI and normalized to GMI.

3. Normalization of TMI

In the normalization process below to compare GMI on GPM to TMI on TRMM, we define the bandwidth as the actual bandwidths used by either of the instruments. In a more general situation, really the Specified (or Maximum allowed RF) bandwidth should be used for a more fair comparison, even though sometimes the actual bandwidth used by the designer is smaller than the maximum allowed.

In Table 1, the GMI on GPM is compared to TMI on TRMM. The table shows that GMI low frequency NEDT are comparable to the TMI low frequency NEDT.

Table 1: TMI normalized to GMI

	GMI	TMI	GMI	TMI	GMI	TMI	GMI	TMI	GMI	TMI
Freq (GHZ)	10.7	10.7	18.7	19.4	23.8	21.3	36.5	37.0	89.0	85.5
Sample NEDT (K)	0.94		0.82		0.71		0.54		0.41	
Normalized Sample NEDT (K) ΔT(TMI>GMI)		0.8		0.66		1.46		0.69		1.32
Beam NEDT (K)	0.51		0.60		0.55		0.43		0.47	
Normalized Beam NEDT (K) ΔT(TMI>GMI)		0.42		0.46		1.03		0.68		1.36

The values in Tables 2 and 3 are parameters of GMI on GPM (407 km orbit) and TMI on TRMM (350 km orbit), respectively. These parameters were used in the normalization process to obtain the results shown in Table 1. The TMI has an antenna with 61 cm diameter, and the GMI have an antenna of 120 cm diameter (both projected in the beam boresight direction). Both instruments are conically scanning microwave radiometers.

Table 2: GMI Parameters used to compute values in Table 1

	GMI	GMI	GMI	GMI	GMI
Freq (GHZ)	10.7	18.7	23.8	36.5	89.0
BW (MHZ)	100	200	400	840*	2900*
Integration time (ms)	3.6	3.6	3.6	3.6	3.6
BeamW (deg, pred)	1.73	0.98	0.86	0.83	0.40
BeamW (deg,Spec)**	1.75	1.0	0.90	0.40	0.40
N***	3.34	1.89	1.66	1.60	0.76

Table 3: TMI parameters used to compute values in Table 1

	TMI	TMI	TMI	TMI	TMI
Freq (GHZ)	10.7	19.4	21.3	37.0	85.5
BW (MHZ)	100	200	500	1000*	3000*
Integration time (ms)	6.6	6.6	6.6	6.6	3.3
BeamW (deg) ****	3.72	1.89	1.70	1.00	0.43
Sample NEDT (K)	0.59	0.49	0.71	0.34	0.71
Beam NEDT (K)	0.31	0.34	0.50	0.34	0.73

Table Notes:
(*) Bandwidths here are IF (predetection) bandwidths (for Double-side band heterodyne systems), the rest are RF bandwidths
(**) Values are "specified requirements," (both Beam width, and beam ΔT) for GMI.
(***) N is the number of samples per beam width in along-scan direction
(****) For the TMI, average value is used when the V and H channels are different.

4. Normalization of SSMIS for 166.5 and 183 GHz Channels

Using the same process of normalizing as was used for TMI above, we repeat the analysis for the conically-scanning SSMIS, with the "sample NEDT" results as shown in Table 4.

Table 4: SSMIS normalized to GMI

	GMI	SSMIS	GMI	SSMIS	GMI	SSMIS
Freq (GHZ)	166.5	150	183±3	183±3	183±8	183±6.6
Sample NEDT (K) at 3.6 ms	1.58		1.42		1.44	
Normalized Sample NEDT (K)		**1.57**		**1.05**		**1.43**
ΔT(SSMIS>GMI)						

Tables 5 and 6 provide the parameters used for the analysis to obtain the numbers in Table 4.

Table 5: GMI high frequency parameters

	GMI	GMI	GMI
Freq (GHZ)	166.	183±3	183±8
BW (MHz)	1650	3200	3700
Sample NEDT (K)	1.58	1.44	1.42
Beam NEDT (K) Predicted from sample NEDT	1.87	1.78	1.76

Table 6: SSMIS high frequency parameters

	SSMIS	SSMIS	SSMIS
Freq (GHZ)	150	183±3	183±6.6
BW (MHz)	1500	1000	1500

| *Sample NEDT (K) at 12.6 ms* | *0.88* | *1.0* | *1.2* |
| *Normalized NEDT (K)* | *1.57* | *1.05* | *1.43* |

Comparing the converted SSMIS NEDT values to the corresponding GMI, in Table 4, it is seen that there are two frequencies of GMI and SSMIS have comparable performance; only in the case of 183 (+/-) 3.0 GHz is the GMI worse than the equivalent SSMI (1.44 vs 1.05 K).

The predicted beam-NEDT values of GMI are obtained if the integration time is set to equal to "the time it takes to move one beamwidth," according to the definition of beam NEDT. (The sample-NEDT values are from data presented by Ball, as of PSR package, December 2008.)

Footnotes:

In Table 6, the SSMIS NEDTs are the so-called 3x1 cells, where each cell is equivalent to a footprint size of 3 x (12.5 km) x (14 km), or (37.5 km) x (14 km) size, corresponding to sample integration time of 3 x 4.2 ms = 12.6 ms.

The procedure to obtain the values in Table 4 is reported here. To compare the SSMIS NEDTs to the corresponding GMI values, we must first convert the integration time difference between the two. To covering the 37.5 km sample length, with the corresponding integration time of 3x4.2 sec, or 12.6 ms. The conversion factor for integration time difference is $f = $ Sqr $(12.6/3.6) = 1.87$.

To convert the NEDT of SSMIS to that of equivalent NEDT of GMI, i.e., NEDT (S>G), we have:

$$\text{NEDT (S>G)} = \text{NEDT (S)} \times f \times \text{Sqr [BW(S)/BW(G)]} \qquad (2)$$

We also note that the RF frequency of the GMI is at 166.5 GH, which is higher than that of the corresponding frequency of the SSMIS, which is 150 GHz. It is in general more difficult to achieve the same low noise figure at higher frequency than lower ones.

In addition, there is also more components in the NEDT calculation than the main-component which are dependent to the integration time ratio factor f, in equation (2). NEDT also contains other components that do not follow the formula of inverse-square relationship to the product of bandwidth and integration time. There are also some FIXED components, e.g., video noise, quantization error, etc., whose effects are not considered here in (2). (assuming that they are relatively small by comparison to the main component)

5. Concluding remarks:

Table 1 shows that the predicted GMI NEDTs are either comparable or better than converted TMI; only the two lower frequencies, 10.7 GHz, and 18.7 GHz, where the equivalent TMI NEDTs are better (lower) than the GMI.

Comparing the converted SSMIS NEDT values to GMI values (Table 4), it is seen that there are two frequencies of GMI and SSMIS have comparable performance; only in the case of 183 (+/-) 3.0 GHz is the GMI worse than the equivalent SSMI (1.42 vs 1.05 K).

Tables 1 and 4 show that TMI normalized NEDT are comparable to GMI, with all channels greater than 19 GHz of TMI having a smaller normalized NEDT and the 10 and 19 GHz channels having of TMI and GMI NEDTs within 0.15K of each other. For the high frequencies, the SSMIS 183+/-3 GHz channel is about 0.39K better than the similar GMI channel. This is probably due to a better Ts on the SSMIS instrument for this channel and related to the fact that it will be more difficult to get a low Ts for 166 GHz (on GMI) versus 150 GHz on SSMIS.

Appendix E. Comparison of High-Frequency Channel Characteristics: GMI versus Cross-Track Scanning Sounders

Jim Shiue
Date: 3/05/09

1.   Introduction

Using the process described in the GMI NEDT comparison appendix for conically-scanning radiometers to normalize other instruments to GMI, we compare to cross-track scanning instruments. We first compare NEDT values between the two instruments and then we compare gaps and footprints between the two instruments. Highlighted rows indicate NEDT values of interest.

2a. Comparison of NEDT values

A comparison of the NEDTs of GMI vs ATMS is as follows:

Table 1: GMI versus ATMS at high frequencies

	GMI	ATMS	GMI	ATMS	GMI	ATMS
Freq (GHZ)	166.0	165.5	183±3	183±3	183±8	183±7
BW (MHZ)	1650	1100	3200	950	3700	1900
Integration time (ms)	3.6	18	3.6	18	3.6	18
Sample NEDT (K)	1.58	0.59	1.42	0.56	1.44	0.45
Normalized NEDT (K) ΔT(ATMS>GMI)		**1.07**		**0.68**		**0.73**

 Remarks of Table 1.

$\Delta T(A{>}G)$ is the converted ATMS equivalent NEDT; they are to be compared to the corresponding GMI NEDTs in the row above. The conversion from ATMS to GMI is scaled by:

$$\Delta T(A{>}G) =$$
$$\Delta T(A) \times SQRT[\ (f) \times (BW_a\ /\ BW_g)\ ]$$

where: $\Delta T(A)$ = NEDT of ATMS, (f) = 18/3.6, BW_a is the bandwidth of ATMS, BW_g is the bandwidth of GMI, and SQRT is square-root operation. The comparison in Table 1 shows that the GMI NEDT worse than the ATMS. The reason for this result is probably rooted in the fact that GMI receiver has higher "system noise" temperature than ATMS.

According to ITT, the system noise temperature of GMI for the 166 GHz channels is 3052 K, while the corresponding system noise of the ATMS is 2073 K, or a ratio of r=1.47. If we multiply the 1.07 K (of the converted equivalent value of ATMS frequency) by r, then the result is 1.58 K, which matches that of the GMI. (Note: System noise temperature of a radiometer-receiver is the key figure of merit of such a system.)

2b. Comparison of footprints and gaps within footprints

1.The GMI:

The GMI for GPM is a multi-channel conically scanning microwave radiometer with channel frequencies ranging from 10.7 to 183 GHz, and concomitant variable beamwidths, ranging from 1.7 to 0.4 degree.

Channel 13 of GMI receives energy from two bands, centered at 183.3 (+/-) 8.0 GHz, each with a bandwidth of 3.7 GHz. These two bands are centered symmetrically about the strongly opaque water vapor absorption line at 183.3 GHz.

The GMI antenna at this frequency has a (3 dB) beamwidth of 0.361 deg., pointing at an off-nadir angle of 45.34 deg. From an (the core-spacecraft) orbital-height of 407 km, this results in an IFOV of 4.1 km by 6.3 km, in along-scan and cross-scan direction, respectively. (Based on requirements set for in GMI Technical Requirement document (see Ref.1).

However, because the sample-interval of the GMI is set at 3.6 mS for every channel, the sampled-distance in the along-scan direction is 5.8 km, rather than the IFOV in along-scan direction of 4.1 km.

The Radiometric Temperature Sensitivity, (NEDT) of this channel is predicted to be (sample-NEDT) 1.42 K, at the sample-time of 3.6 mS (based on data in Ref. 2), which is equivalent to a beam-NEDT of 1.76 K.

The antenna system of the conical-scanning design provides two important advantages:

(a) It maintains a constant footprint (IFOV) throughout its scanned swath.

(b) It maintains a constant incidence angle throughout the scanned swath, which is an important feature for surface measurement.

2.The ATMS

The ATMS is an instrument slated for future temperature and humidity sounding on the US National Polar Orbiting Environment Satellite System (NPOESS) Preparatory Project (NPP) and the JPSS weather satellites. ATMS has 22 channels, ranging in frequency from 23.8 to 183 GHz, and beamwidths ranging from 5.5 to 1.2 degrees, corresponding to the frequencies of 23.8 and 183 GHz, respectively.

The mission goal for the ATMS is primarily aimed at providing routine measurement of temperature and humidity profiles on a global basis. Because of the need to retrieve (temperature or humidity) profiles, there are many more channels centered about the oxygen and water vapor absorption lines or line complexes.

The ATMS Channel 18 has a beamwidth of 1.2 degree, and a sample-NEDT of 0.38 K, at a sample-time of 18 mS. From a orbit of 800 km, the IFOV of ATMS channel 18, at a off-nadir angle of 43.34 degree, is about 34 km by 25 km, in the along-scan and cross-scan direction, respectively. This footprint is equivalent to about 7x6 or 42 of the GMI IFOVs assembled together. If the GMI were having contiguous coverage along the down-track direction, it would take about 8 scans to collect the needed cells to form a composite ATMS cell. But the GMI has a gap of about equal to its IFOV in the down-track direction, so that the actual number of scans needed will be 4 lines instead of 8 and half of the area under the composite cell will not be sampled. (That means that half of the field of view is not covered within the 3-dB antenna beamwidth.)

3. A comparison between the GMI and ATMS measurements

3.1 Comparison of NEDTs

If we were to form a Composite Cell from 42 of Channel 13 of the GMI data, to be compared to a single-cell of the ATMS at the same off-nadir angle, then the Effective NEDT of the Composite GMI Cell will be equal to [(1.42 K)/sqrt (21)], or *0.31 K.*

If the GMI beam-NEDT is used for comparison, then the Composite GMI cell NEDT will be: [(1.63 K)/sqrt (21)], or *0.36 K.* Either of these two 0.31 K (sample-NEDT), or 0.36 K (beam-NEDT), is comparable or better than the ATMS' 0.38 K, (beam-NEDT). However, the comparison can be made only if:

i)   The meteorological-conditions remain unchanged during the 4 scans, or about 8 seconds period.

ii)   The difference in "surface polarity" at these frequencies (for GMI Channel 13, it is 8 GHz from the absorption line-center; for ATMS Channel 18, it is 7 GHz from the line-center), is small and can be neglected.

Then the brightness temperature of the composite GMI cell above can be compared to that of the ATMS. From instrumental viewpoint, the precision of the equivalent composite GMI cell is comparable or slightly better than the ATMS single cell.

3.2 Calibration Accuracy comparisons

The ATMS probably has better overall calibration accuracy than GMI. The potential reasons are as follows.

a). The on-board calibration system of the ATMS is inherently better than that of the GMI.

This is because of the fact that the cross-track scanning design of the ATMS allows its antenna to view the two calibration reference points, the "cold-space" and the "warm-load," directly, (simply with the rotation of the antenna reflector), whereas for the GMI, a different calibration "circuit" has to be substituted for each of the two calibration measurements. (A cold-sky calibration sub-reflector is introduced for the cold-calibration, and the feedhorn views the warm-load directly--- without the main-reflector--- during the warm-load measurement.) Both of the substitutions tend to introduce more biases, which must be accounted for.

b). The Radiative Transfer (RT) models of opaque absorption lines, together with ground truth (meteorological data), as well as the fact that there are many sounding channels (particularly on the temperature sounding oxygen absorption lines), probably provide a more accurate overall calibration of the top-of-the-air brightness temperature for the ATMS.

The above discussion indicates qualitatively that ATMS is probably better in calibration accuracy than GMI. However, it is rather difficult to establish a quantitative comparison between the two instruments, beyond their respective design analysis and projections. ATMS has posted its calibration accuracy to be 0.4 K (Ref. 3), and GMI Ch. 13 is projected to be 1.34 K (Ref.2).

From the above discussions, it is reasonable to conclude that while the composite GMI cell is comparable to or slightly better in its measurement precision than the ATMS, but the ATMS has better calibration accuracy than GMI. The fact that GMI is missing data in about half of the area within the composite cell of the ATMS will also introduce more uncertainty in the calibration.

References:

Ref. 1.GPM GMI Technical Requirements, GPM 422-30-00-001, GPM Project, NASA GSFC.
Ref. 2. Project Status Rev., data package, p. 80, presented at the December 2008 GPM-   PSR, by Ball Aerospace and Technology Corporation.
Ref. 3. ATMS-NPOESS data, from STAR, Center for Satellite Applications and   Research,   a NOAA website.

Appendix F. Sensitivity of Rain Retrieval to NEDT

Mircea Grecu and Bill Olson
Updated: 3/31/2009

Introduction

The impact on noise equivalent delta T (NEDT) magnitude on precipitation retrievals from GMI observations can be best assessed through numerical simulations. That is, numerical simulations can be employed to generate databases of candidate solution precipitation profiles and associated brightness temperatures. The alternative, i.e. the generation of a precipitation – brightness temperature database directly from observations is not feasible yet, given the unavailability of GMI-like observations. The augmentation of TMI observations with high frequency (150 GHz and above) observations from other sensors is not feasible either, because the quality of this kind of extended set of observations may be significantly inferior to that of GMI observations due to resolution differences and collocation errors. Therefore, the most rigorous assessment of the impact of NEDT characteristics on retrievals can be achieved through analysis of synthetic data.

Simulated Data

Cloud resolving model simulations are used to generate a large database (consisting of a half million entries) of precipitation profiles and associated GMI brightness temperatures. The cloud resolving model simulations include high-quality realistic realizations of tropical (Tao et al. 2003; Tao et al. 2004) and mid-latitude (Chaboureau et al. 2008) events. While the simulation and analysis of tropical events for remote sensing purposes have been motivated by TRMM, realistic simulations of mid-latitude events have been lacking until recently. The work of Chaboureau et al. (2008) properly addresses this issue.

Figure 1 shows simulated 183.3±7GHz brightness temperatures for a case, referred to as the millennium storm, which occurred over the United Kingdom on 30 October 2003. Comparisons of the simulated brightness temperatures with actual observations indicate the realism of the storm simulation (Chaboureau et al. 2008). To ensure that tropical precipitation is properly represented, we augmented the database with precipitation profiles and associated GMI brightness temperatures derived from the application the combined algorithm of Grecu et al. (2004) to two days worth of TRMM observations from July 2000.
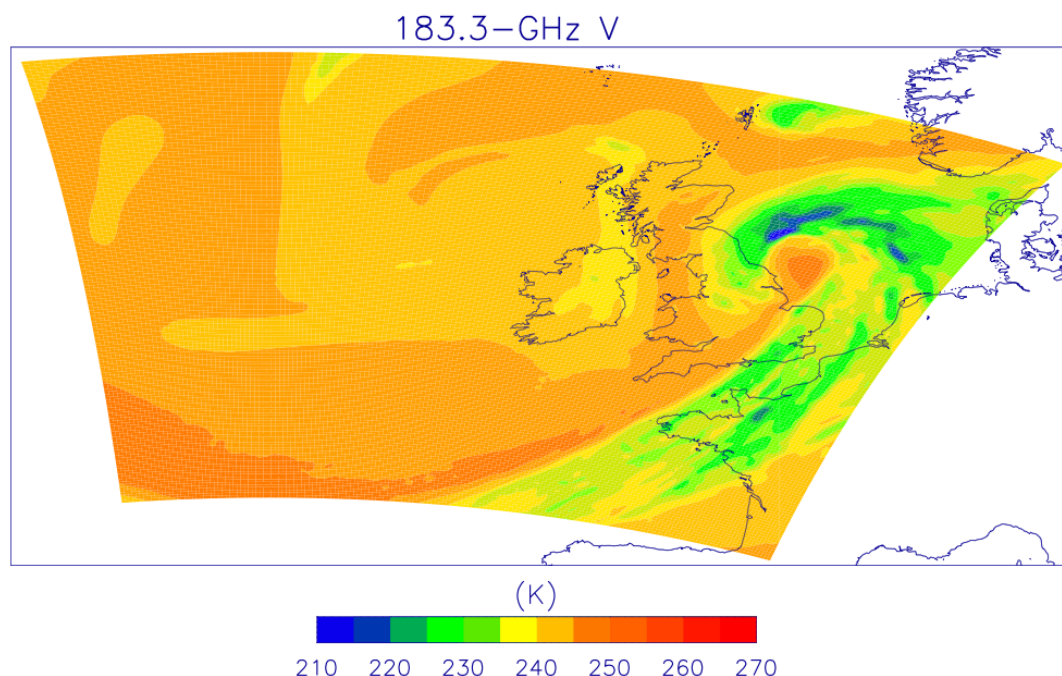
Fig 1. Simulated 183.3±7 GHz GMI observations for a simulation of the millennium storm (UK, 30 October 2003).

Methodology and Results

An efficient methodology (Grecu and Olson 2006) that provides precipitation retrievals based on the exploration of a large database of precipitation profiles and associated brightness temperatures is used. The database is split into two equal parts. The entries in the two parts are different, but statistically similar. The first half is used in the retrievals, while the second half is used for validation. That is, for any given entry in the second part, the first part is explored and a surface rain rate estimate is determined. Because these entries are part of contiguous areas of precipitation, the estimates can be aggregated to a 50 km x 50 km resolution. The evaluation is done at this resolution. The retrievals are done based on the following four scenarios. In the first scenario, random noise with the nominal GMI NEDT[2] characteristics is added to the simulated observations. In the second, third, and fourth scenarios, two, four, and eight times the nominal value NEDT are added to the observations. Shown in Fig 2 are the relative mean squared retrieval errors for the four scenarios.

---

[2] The designation NEDT is used throughout this document. The scientists assumed NEDT to be the total random (zero mean) error of the brightness temperature channels. The analysis reported herein, assumed nominal random errors of 0.96 K, 0.84 K, 1.05 K, 0.65 K, 0.57 K, 1.5 K, and 1.5 K for 10, 18, 23, 36, 89, 165, and 183 GHz channels, respectively (see also Table 5-1).
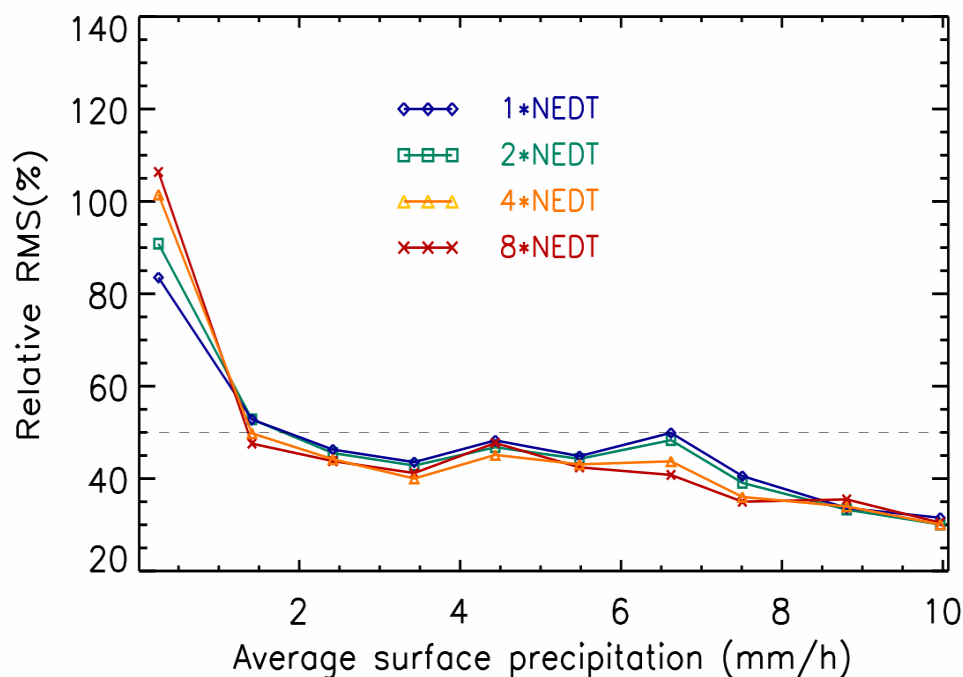
Fig.2 Relative mean squared retrieval errors as a function of rain intensity for rain rates between 0 and 10 mm/h at 50 km resolution.

One may notice in Fig 2, that a four times increase in the NEDT magnitude still yields a relative RMS smaller than 50% for average rain rates between approximately 1 and 10 mm/h. The low sensitivity of high rain rate retrievals to increases in NEDT characteristics is due to ambiguities in brightness temperature - precipitation relationships. That is, for any given set of observations, multiple precipitation profiles are consistent with those observations. The optimal retrieval is just a weighted average of these possible solutions. Noise in the observations leads to a slightly different weighting of the possible solutions, but subsequent averaging over the set of possible solutions tends to overwhelm errors induced by noise. In the end, the retrievals from observations altered by noise are not significantly different from those derived from perfect observations (provided that the NEDT is smaller than the brightness temperature - rainfall relationship variability, which is the case for higher rain rates). For small rain rates less than 1 mm/h (Figure 3), the limiting rain rate error (no noise) is about 0.12 mm/hr, and in this regime, any appreciable noise may be interpreted by the algorithm as rain signal. Therefore, the relative RMS error increases with NEDT. Results for rain rates larger than 5 mm/h are less robust due to limited numbers of intense rain events (less than 100 at a given rain rate) in both observations and the *a priori* database.
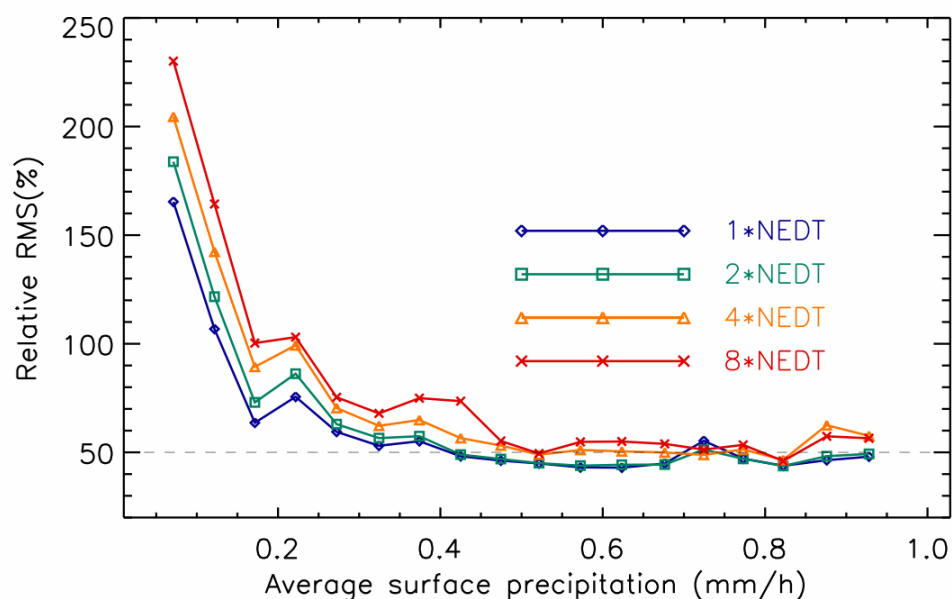
Fig.3 Relative mean squared retrieval errors as a function of rain intensity for rain rates between 0 and 1.0 mm/h.

The overall bias of the retrievals is zero. However, due to averaging involved in the retrieval process, low rain rates are slightly increased (through averaging with larger intensity possible solutions) while high rain rates are reduced (through averaging with lower intensity possible solutions). Rain rates larger than 2.0 mm/h are much less frequent than lower rain rates (between 0 and 1.0 mm/h) and occasionally underestimated high rain rates are compensated by very small, but very frequent, overestimation of low rain rates, resulting in zero global bias.

Summary

The GPM requirements state random errors of no more than 25 to 50% for 1 to 10 mm/h with respect to ground validation data (Level 2, MRD 192). If we assume that the truth from ground validation data is the simulated "truth", then we meet this 50% error when NEDT is no more than 2*NEDT. There are no direct GPM requirements on rain rates less than 1 mm/h for the radiometer. However, GPM requirements (Level 2, MRD 771) state that rain rates as low as 0.2 mm/h should be retrieved from GMI. In order to meet this goal, we can only tolerate 2*NEDT[3] such that extremely low rain rates are close to the 50% random error requirements.

---

[3] Two times the nominal NEDT numbers are 1.92, 1.68, 2.1, 1.3, 1.14, 3.0, 3.0 K for 10, 18, 23, 36, 89, 165, and 183 GHz channels, respectively. These numbers are mostly larger than the GMI required uncertainty values of 1.35 and 1.5 K for 10- 89, and 165-183 GHz channels, respectively, with only 2*NEDT of 89 GHz exceeding the 1.35 uncertainty requirement. This indicates that if GMI uncertainty is random and includes NEDT then science requirements are met if GMI performance meets GMI calibration uncertainty requirements. This is especially true if the pre-launch performance calibration uncertainty values reported in Table 5-1 are valid post-launch.

References

Chaboureau, J.-P., N. Söhne, J.-P. Pinty, I. Meirold-Mautner, E. Defer, C. Prigent, J. R. Pardo, M. Mech, and S. Crewell, 2008: A midlatitude cloud database validated with satellite observations. J. Appl. Meteorol. Clim. 47, 1337–1353.

Grecu, M., W. S. Olson, and E. N. Anagnostou, 2004, Retrieval of Precipitation Profiles from Multiresolution, Multifrequency Active and Passive Microwave Observations. Journal of Applied Meteorology, 43, 562–575.

Grecu, M., and W. S. Olson, 2008: Bayesian Estimation of Precipitation from Satellite Passive Microwave Observations Using Combined Radar–Radiometer Retrievals, JAMC, 45, 416–433.

Tao, W.-K., C.-L. Shie, R. Johnson, S. Braun, J. Simpson, and P. E. Ciesielski, 2003: Convective Systems over South China Sea: Cloud-Resolving Model Simulations. J. Atmos. Sci., 60, 2929-2956.

Tao, W.-K., D. Johnson, C.-L. Shie, and J. Simpson. 2004: Atmospheric energy budget and large-scale precipitation efficiency of convective systems during TOGA COARE, GATE, SCSMEX and ARM: Cloud-resolving model simulations, J. Atmos. Sci., 61, 2405-2423.

Appendix G. On the Performance of Snowfall Detection versus Variable NEDT at GMI High Frequency Channels

Benjamin T. Johnson
UMBC/JCET and Code 613.1
Updated: 3/31/2009

1. Introduction
The minimum success requirement for GPM with respect to snowfall is defined to be "detection" of snowfall.   Here, "detection" is defined to be when the retrieval algorithm (described herein) correctly identifies snowing pixels, subject to some minimum threshold.

In this appendix, we describe the sensitivity of snowfall detection to increases in the observation noise equivalent delta temperature (NEDT).

2. NEDT Definition
From Section 3.1.4 of GMI TRD Rev. H 10/10/08 [hereafter TRD]:

"The radiometric sensitivity (NEDT) is the *minimum detectable change* of the microwave power (in brightness temperature units) incident at the antenna aperture. It is the end-to-end resolution of the radiometer, including all contributing factors, defined for a single operational sample. NEDT is defined as *the standard deviation* of the radiometer measurement."

With this definition in mind, we treat the NEDT as a single standard deviation. We use the NEDT values in the table below, reproduced from TRD tables 3-1, 3-2:

Channel Frequency & Polarization	NEDT [K] (Max.)
89.0 V	0.57
89.0 H	0.57
165.0 V	1.5
165.0 H	1.5
183.31 +/- 3 V	1.5
183.31 +/- 7 V	1.5

3. Simulation
In the present study, we employ simulated data obtained from the WRF model for a modeling case study involving lake effect snowfall in the Great Lakes region (Matsui, et al.).   The WRF domain is 456 km x 456 km, at 1 km horizontal resolution.   Each one of these 1 km x 1 km "pixels" contains 30 vertical layers, for a total of 456 * 456 * 30 = 6238080 grid boxes.   Within each grid box, temperature, relative humidity, and pressure are defined. The amount of rain, snow, graupel (rimed snow), cloud ice, and cloud liquid water are also provided (even if zero).

Given this simulated physical domain, we seek to simulate what the GMI sensor would sense if flying over this domain.   A forward model (Johnson, 2007) is run for each 1-D vertical column (456 x 456 columns) to compute the top-of-the-domain passive microwave brightness temperatures (TBs) at the frequencies listed in the table above.   These channels are the most sensitive to ice-phase precipitation.   The computed TBs, with *randomly added NEDT noise*, combined with their respective vertical profiles comprise the "full"-database that will be used for retrievals.   The high-resolution multi-channel TBs (prior to adding NEDT noise) are then degraded to the GMI scan pattern and IFOV size using an approximate scan pattern and assuming 2-D Gaussian antenna beam pattern, loosely following Bennartz, 2000.   This results in approximately 4710 sets of 6-channel TBs for the simulated domain.   This set represents our base (or mean) "observed TBs", with no NEDT noise added yet.

In the present study, we seek to understand how increases in NEDT can influence the detectability of snow.   The basic approach is as follows:
1. Simulate brightness temperatures in the domain using the forward model, splitting them into database TB and observed TB groups.
2. Add random noise to the "observed" TBs, constrained to be within [-NEDT to +NEDT] multiplied by a scaling factor.
3. Examine the effect on snowfall detection by employing increasing NEDT scaling factors: 1,2,3,4,5, and 10.   A factor of 2 would be random noise in the range [-2*NEDT to +2*NEDT] added to the base "observed" TBs.

For comparison with the retrieval methodology described in section 4, the true snow and graupel ice-water-contents are vertically summed together at each grid box (obtaining the total IWC), and then integrated over the vertical layers to obtain the total ice water path (IWP) for that column.   The IWP is the column-integrated snow and graupel IWC for each of the 456 x 456 columns in the domain.   Because the retrieval results are obtained at the GMI resolution, we also degrade the domain IWP to the GMI scan pattern so a 1-to-1 pixel comparison can occur. This will be referred to as the "true IWP", although some inaccuracies (relative to the original model resolution) are expected due to the degradation method.

4. Retrieval and Detection
The present retrieval technique is described by Kim, et al. 2008.   In short, the method employs Bayes Theorem to infer information regarding the IWP given a set of observed TBs.   Using the database outlined in the previous section, observed TBs (i.e., those degraded to GMI resolution) are compared to the "full" database TBs (i.e., the database contains the observed TBs -- the trivial case).   For each of the comparisons, the associated database profile makes a *weighted contribution* to the final retrieved profile. The weighting depends on the TB difference, with smaller TB differences having higher weighting.   Therefore the final "retrieved" profile is a normalized weighted average profile. Once this profile is obtained, it is vertically integrated to obtain the "retrieved IWP".

Because passive microwave observations are sensitive to column-integrated quantities, we feel that the IWP (an integrated quantity) is a better variable to retrieve rather than the more "traditional" surface precipitation rate, which presumably the observed brightness temperatures

are less directly sensitive.   In the present retrieval scheme, we use retrieved IWP as the criterion for detection, which are:

1. Does the retrieval correctly retrieve *any* value of IWP at the same pixel location as the "true IWP"? That is, is it correctly identifying a pixel with precipitation in it?   For detection to be satisfied, we do not care what the amount of retrieved IWP, but rather that is it above the minimum detection threshold (defined below).   This is termed a "correct detection".
2. Does the retrieval incorrectly detect a pixel as having some IWP above the threshold when the true IWP shows a value below the threshold?   That is, is it a "false positive"?

There are two other categories of binary classification that we do not consider in this brief study: false negatives, and true negatives -- that is, incorrectly detecting "no snow", and correctly detecting "no snow" respectively.

It should be noted that because we are using simulations for both observation and database, we also have "perfect" knowledge of the surface properties, cloud properties, temperature and water vapor profiles, etc -- parameters not always well specified in actual retrievals.

For the purposes of understanding the retrieval, a minimum detection threshold was set at an IWP of 1 g/m^2.   This means that any retrieved IWP below this value is considered to be "no snow". This value came about after preliminary analysis of the retrieval statistics -- it appears that this is a minimum threshold for reasonably accurate retrievals (under the assumption that we have perfect knowledge of the surface properties, cloud properties, temperature and water vapor profiles, etc).   More work remains to be done with respect to determining any final minimum retrievable IWP. However for the purposes of this study it is not an unreasonable assumption to set this lower limit and allows for some flexibility in what defines "detection" versus what we can reasonably retrieve given the current datasets and retrieval methodology.

5. Results
Since everything is done in simulation space (due to a lack of actual data) we know when the retrieval should correctly detect snow, so we can construct the binary classification described in the previous section.

Figure 1 illustrates the fractional changes in the detection of snowing pixels (compared to the true number of snowing pixels: 3197) -- in panel (a) the fraction of correct detections is shown with respect to increases in the NEDT.   Panel (b) shows the fraction of incorrect snow detections (i.e., false positives).   In panel (a), at NEDT factor of x1, we see that the fraction "correct detections" is near 0.96, and in panel (b) the fraction of false positives is around 0.4. However, as the NEDT factor increases, we see that the fraction of correct detections decreases linearly with NEDT factor, while the fraction of false positives also increases linearly with NEDT factor. With each factor of NEDT increase, the fraction of correct detections decreases by about 1.4%.
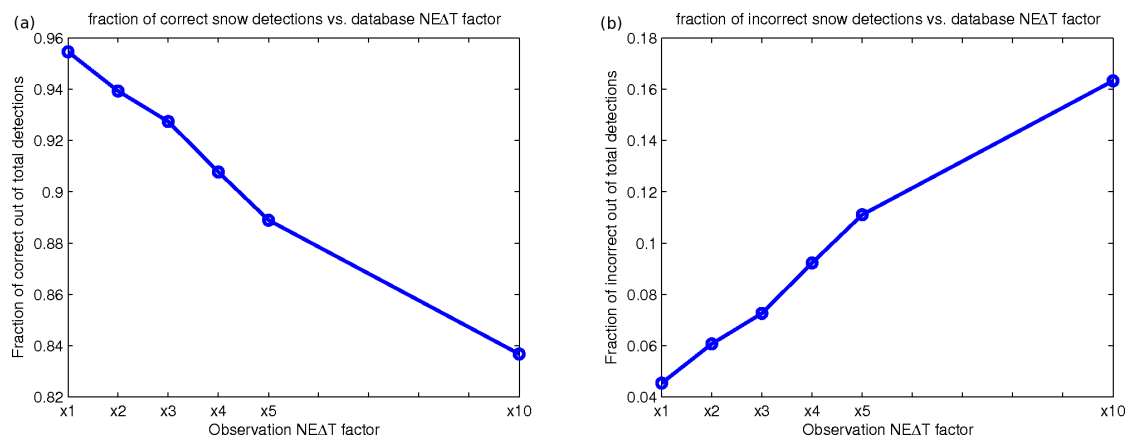
Figure 1. (a) Fraction of correctly detected snow pixels out of the total number of snowing pixels vs. NEDT factors, and (b) fraction of incorrect detection out of the total number of snowing pixels vs. NEDT factors.

Figure 2 (below) illustrates the sensitivity of mean retrieved IWP (mean over all 4710 observations) to changes in the NEDT factor.   Note: *This is a preliminary result intended to highlight the effect of increasing NEDT on the physical properties of the retrieval.*   It is apparent that at a factor of 1x, the retrieved mean IWP (blue circle line) is quite close to the true mean IWP (black dashed line), but as noise is added to the observed TBs, the retrieved IWP deviates from the true value. The mean of the standard deviations of all points are shown as error bars.

Figure 2. Mean retrieved ice water path (IWP) versus increasing NEDT.   The black dashed line indicates the "true" mean IWP.   Errorbars show the mean of the standard deviation.

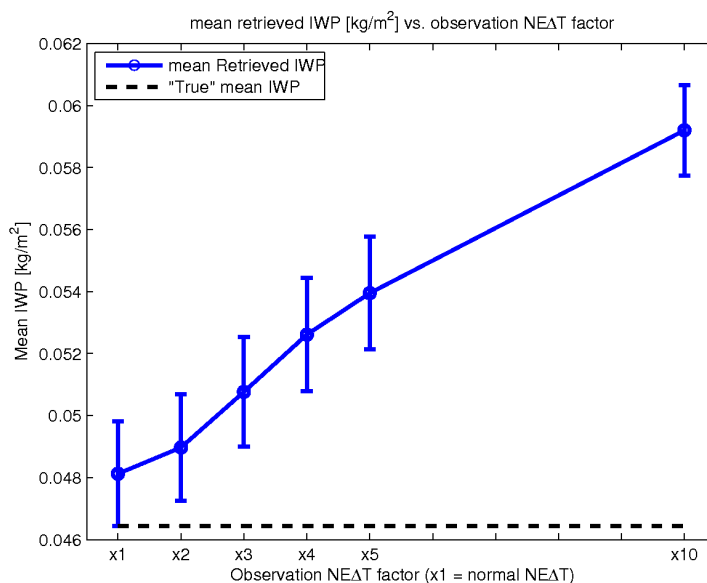Figure 3 illustrates the preliminary sensitivity of mean retrieved surface snowfall rate (melted equivalent, and mean is taken over all 4710 observations) to changes in NEDT factor. *This is a preliminary result intended to highlight the effect of increasing NEDT on the physical properties of the retrieval.* Similar to the trend shown in figure 2, we see a general increase in the difference between the mean true precipitation rate and the mean retrieved precipitation rate as the NEDT factors increase.
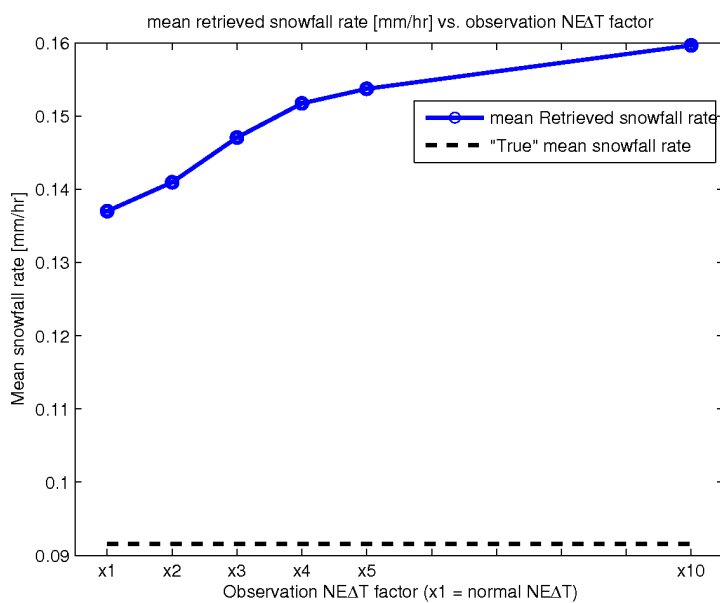

Figure 3. Mean retrieved snowfall precipitation rate (liquid equivalent) [mm/hr] versus increasing NEDT. The black dashed line indicates the "true" mean precipitation rate.

6. Discussion

The present study describes the basic sensitivity of a novel snowfall detection/retrieval technique to changes in observed high frequency passive microwave brightness temperatures. These changes are imposed by increases in the NEDT beyond the specified reference state. The basic detection testing indicates that increases in NEDT noise do not appreciably influence the detection of snowfall in the current model. However, the retrieval of mean IWP and mean precipitation rate indicate that there may be relatively strong influences on the retrieved quantities if the NEDT values are increased significantly.

Final comment: Due to the very limited nature of this study and the lack of real observational data, it is expected that the true sensitivity of the detection and retrieval of snowfall to changes in NEDT (using the GMI sensor) will be quite different from what we have indicated here. However, given the current state of the snowfall retrieval algorithm, which is still being developed and refined, this serves as our "best guess" as to how noise will potentially influence the detection of snowfall using radiometer only observations. On GPM, the addition of the radar frequencies will provide strong constraints on the passive-only retrieval.

7. Selected References

Johnson, B. T. 2007: Multi-frequency passive and dual-frequency radar remote sensing of snowfall, Ph.D. dissertation, Univ. of Wisconsin -- Madison, Madison, WI.

Bennartz, R., 2000: Optimal convolution of AMSU-B to AMSU-A. J. Atmos. Ocean. Technol., 17, 1215-1225.

Kim, M.J., 2008: A physical model to estimate snowfall over land using AMSU-B observations. J. Geophys. Res. 113

Matsui, T., Tao, W.-K., Shi, J., Lang, S., Tokay, A., Skofronick-Jackson, G. Hou, A., 2008: "Development of the Goddard Weather Research and Forecasting Model over Canadian CloudSat/CALIPSO Validation Project (C3VP) Site, Eos Trans. AGU, 89(23), Jt. Assem. Suppl., Paper A41A-07.

Appendix H: Brightness Temperature Sensitivity to 183 GHz Bandwidth

Gousheng Liu
Florida State University
Updated: April 2, 2009

Introduction:

In an effort to determine the scientific impact of the width of the bandpass filter used for 183±3 and 183±7 GHz, an analysis was performed that numerically computes brightness temperatures using various bandwidths.

Procedure:

Brightness temperatures were calculated using both mid latitude winter and arctic winter atmospheres, with snowfall profiles from 2-year CloudSat retrievals. The two-years worth of CloudSat vertical profiles were categorized into various surface snowfall rates based on near-surface radar reflectivity values and then averaged within those categories. There are 9 snowfall profiles (near-surface snowrate categories) used in the calculations. They are averaged profiles derived from 2-year CloudSat data. Profiles #1 to #7 are deep snowfall, #8 and #9 are shallow but heavy snowfall. Brightness temperatures are first calculated every 0.1 GHz around the center frequency, and then are weighted averaged within the bandwidth (assume the weights reduce to half from the center to the edge of the bandwidth obeying a normal distribution). The surface type (land with emissivities 0.7, 0.8 and 0.9, and ocean) are also varied.

Results:

Figures 1-3 show the response of the brightness temperatures for the 9 snowrate categories for 166, 183±3, and 183±7 GHz, respectively. These figures compare brightness temperatures for the GMI specified bandwidth to a smaller (as specified in the figures). To understand the figures, Table 1 provides the heights of the weighting function' peaks for each channel.

Table 1: Weighting function peaks for the frequencies and atmospheric winter types.

	166 GHz	183±3 GHz	183±8 GHz
Arctic Winter	0.0 km	3.0 km	1.0 km
Mid-Lat Winter	0.0 km	3.5 km	1.5 km

These weighting function heights indicate that 166 GHz sees all the way to the surface (hence any snowing profile will be fully "observed" by the radiometer in space). On the other hand, the 183±3 GHz channel peaks near 3 to 3.5 km. Thus snow at lower altitudes will be obscured by the heavy water vapor attenuation in the vertical profile. If the bandwidth of this channel is increased the weighting function peak effectively broadens. For 183±8 (which we should state is very similar to 183±7 GHz) the response is in between that of 183±3 and 166 GHz.
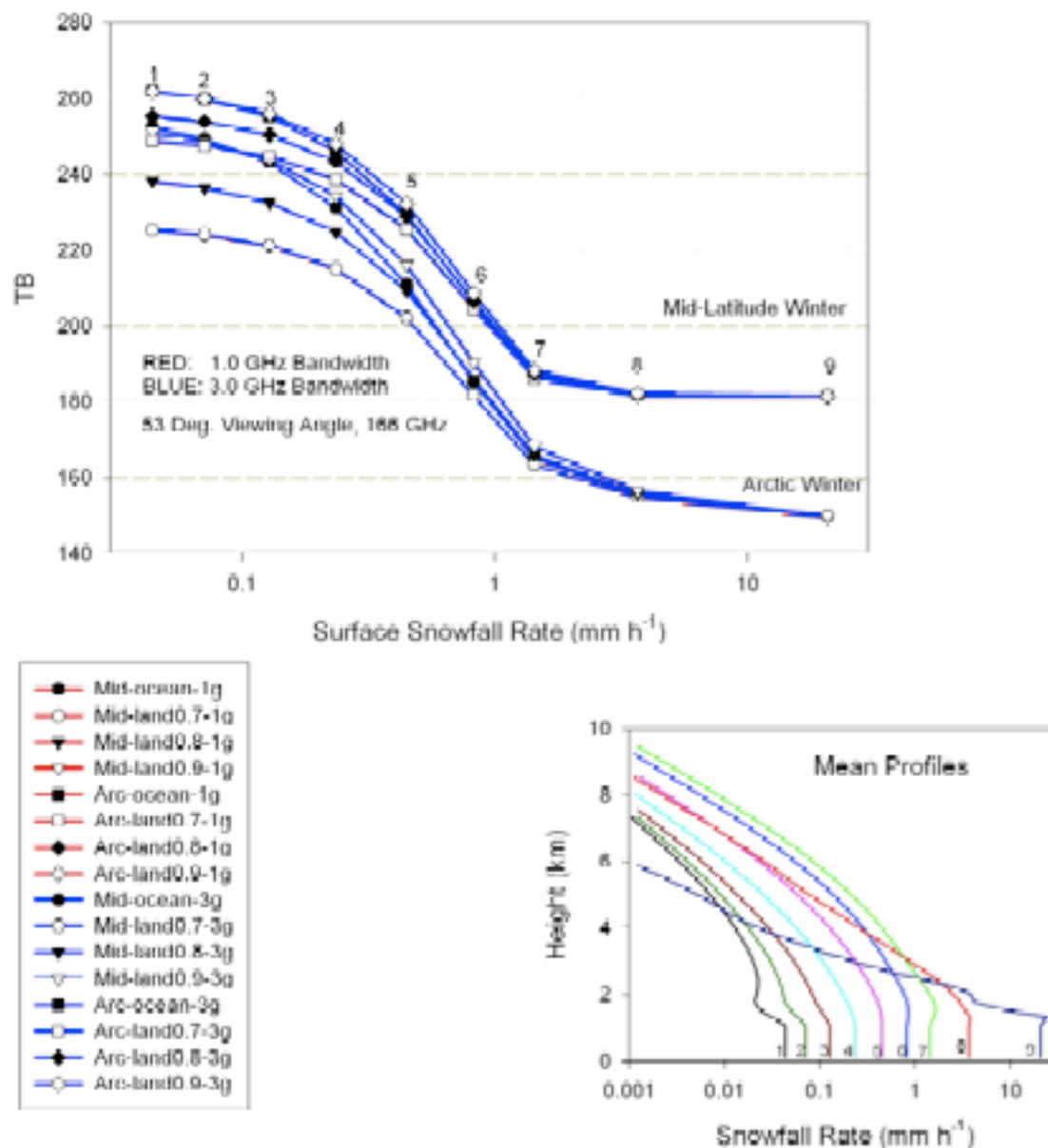
Figure 1: Response for 166 GHz.

Figure 1 shows the response for 166 GHz. Here red lines are for the smaller 1.0 GHz bandwidth, while blue lines are for a 3.0 GHz bandwidth. Symbols on the plot indicate which type of winter atmosphere and surface type is used (as identified in the lower left of the figure). The lower right image shows the 9 snowfall profiles categorized and averaged from CloudSat. The blue (wide bandwidth) lines completely obscure the red (narrow bandwidth) lines effectively stating that bandwidth does not affect brightness temperatures at 166 GHz.
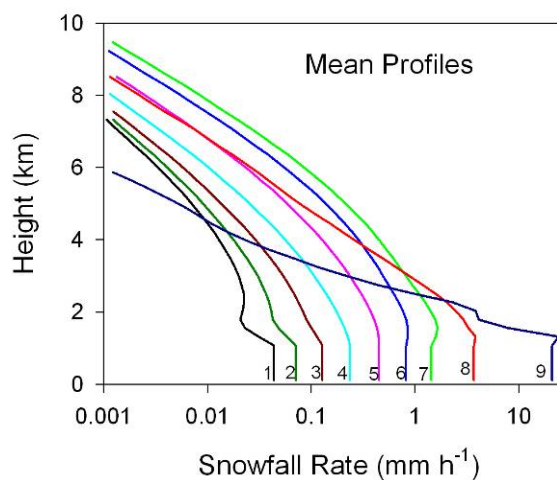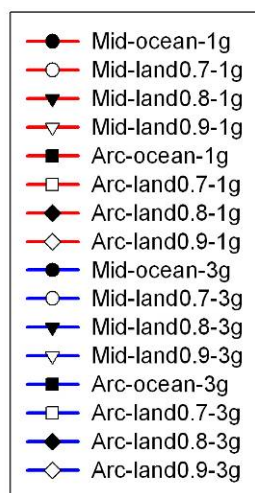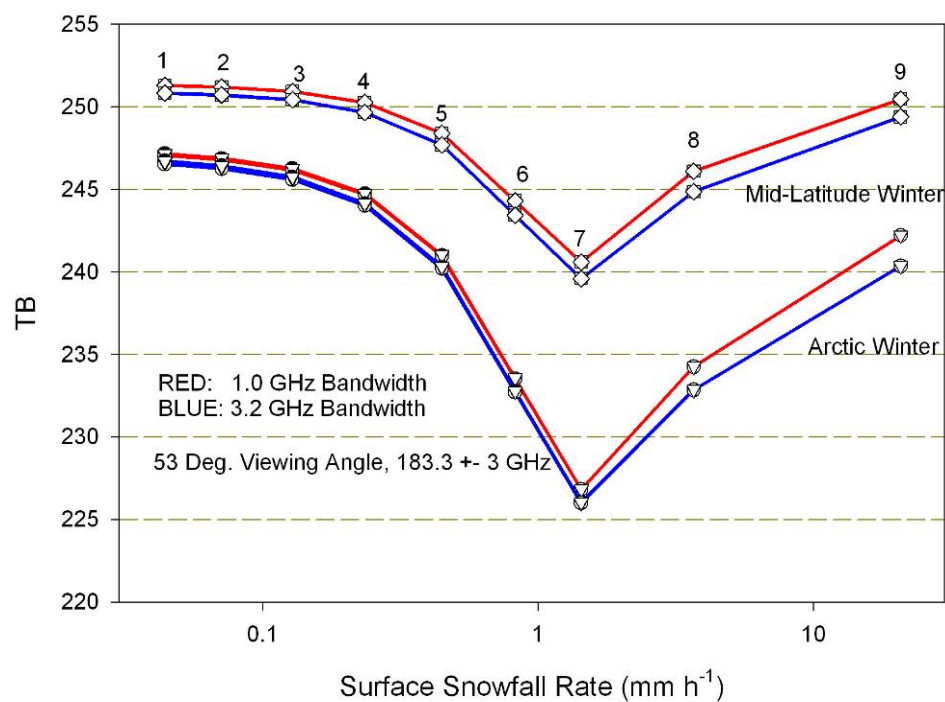
Figure 2: Response for 183±3 GHz.

Figure 2 shows the response for 183±3 GHz. Here the red lines are for the smaller bandwidth and show that there is about a 2 Kelvin difference between the narrow and wide bandwidths. It is expected that this difference in BW between radiometers can be reconciled through modeling, though the GPM Project plans to pursue a 1-GHz BW filter for GMI HF channels as an enhancement to the current design.
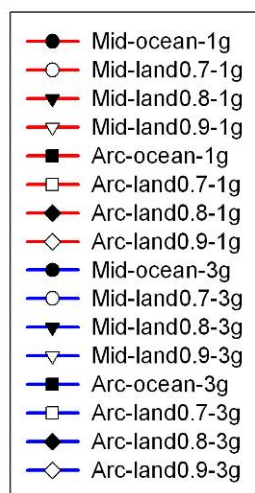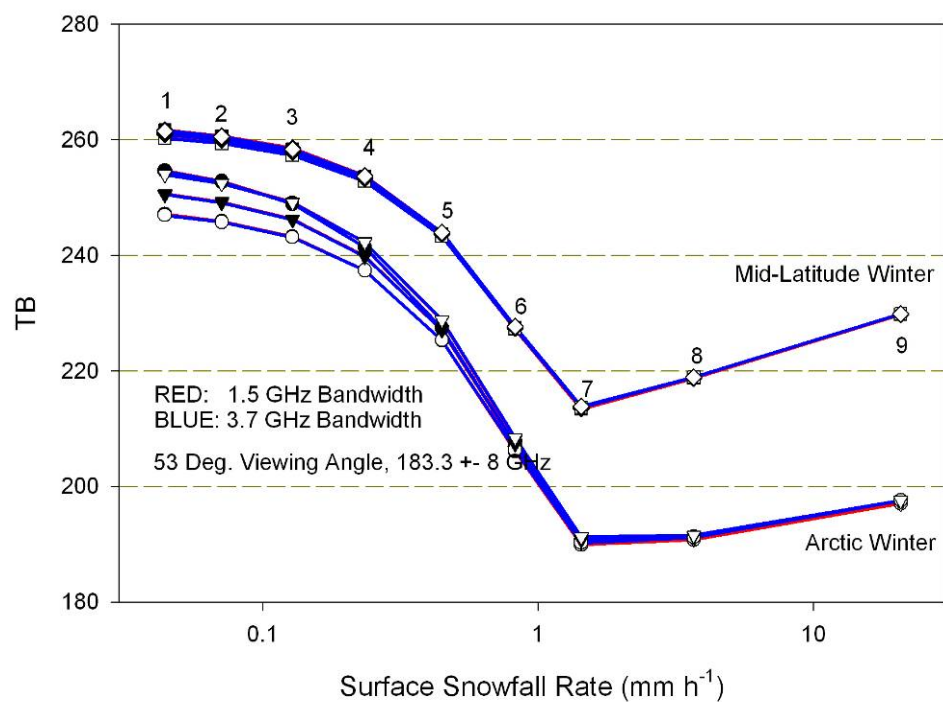
Figure 3: Response for 183±8 GHz.

Figure 3 shows the response for 183±8 GHz. For this plot the red and blue lines overlap such that no bandwidth differences are noted.

Conclusions:

The sensitivity to snow does not change much due to changes in the bandwidth. There is some impact on 183±3 GHz, but the other two frequencies seem to be immune and 183±3 GHz can be modeled properly for inter-calibration independent of bandwidth.

From the snow sensitivity point of view, the wide bandwidth does not seem to be a problem under these controlled conditions. For uncontrolled or noisy conditions (e.g., varying the amount of water vapor) the brightness temperature variability will increase, but analysis has not yet been done to see the effects of variability in environmental conditions with respect to a narrow versus a wide bandwidth.

Appendix I. Analysis of DPR Performance Requirements for Particle Size Distribution Measurements

Robert Meneghini
NASA Goddard Space Flight Center
November 2009

1. Introduction

A key component of the particle size distribution is the median mass diameter, D_0, which is defined as the diameter that divides the particle-size spectrum into two parts, with each part representing 50% of the total water content of the full spectrum. With overlapping dual frequency Ka and Ku-band coincident observations, the DPR will provide quantitative information on rain and snow particle size distributions (including the median mass diameter) over the mid-range of precipitation intensities (from 0.5 mm hr^{-1} to moderate rain rates). A quantitative analysis has been performed to examine the DPR performance requirements for estimating the D_0 in particle size distributions. The analysis (as summarized herein) shows that for particle size distributions in liquid rain and frozen precipitation the median mass diameter D_0, can be estimated to within ±0.5 mm.

2. D_0 Calculation by Dual-Wavelength Radar and Error Assessment

An estimate of D_0 can be obtained by means of the dual-wavelength ratio, DFR, or, in dB, the difference of the attenuation-corrected radar reflectivity factors, dBZ, at the two wavelengths. In the following, the DFR will be taken to be equal to dBZ(13.6 GHz)- dBZ(35.5 GHz). There are three principal error sources that determine the accuracy of DFR in rain: the relative radar calibration error, the variability from measurement noise, and the attenuation correction error.

Although the performance requirements of the absolute calibration accuracy of the DPR instrument is given as ±1 dB, the relative calibration can be determined to a much higher accuracy by considering the returns near the storm top where the scattering is primarily Rayleigh. For Rayleigh scattering, the reflectivity factors at the two wavelengths are approximately the same, the small difference arising from the fact that the dielectric factor for the backscattering cross sections of the particles changes slowly with frequency. Assuming, as in the TRMM PR, that the radar calibrations are very stable, a scatter plot of dBZ values less than 20 dBZ taken near the storm top should provide a reliable check of the relative calibration accuracy. The occasional cases of non-Rayleigh scattering at small Z should not affect this statistical procedure since the focus is on the dBZ difference as it approaches zero or some constant value.

Measurement noise is caused by the random nature of the returns from ensembles of scatterers. For the logarithmic receiver used by the DPR, the standard deviation in dB of the sample mean derived from N samples is $5.57/\sqrt{N}$. For the DPR, N changes slightly with incidence angle; using N=110 as a typical number, we obtain a standard deviation of 0.531 dB. Since the reflectivity factor measurements at the two wavelengths are independent, the variance is additive

and the standard deviation of the difference is $\sqrt{(0.531)^2 + (0.531)^2} = 0.751$ dB. This variability can be reduced by averaging in range and in the along-track direction but at the expense of vertical or horizontal resolution. For example, if a uniform window average is used over 3 consecutive range gates, where each range gate represents a 125 m interval, the standard deviation of the DFR estimate can be decreased from 0.751 dB to about 0.434 dB.

The third source of error arises from errors in the attenuation correction procedure. The associated errors are difficult to quantify because they depend on factors such as the rain intensity, distance into the storm and the attenuation correction algorithm itself. In dry snow regions, the attenuation is small and the difference in the measured reflectivity factors is close to the attenuation-corrected value. For small values of attenuation, a forward recursion procedure has been shown to be adequate. In this procedure, the attenuation is updated by adding a new increment to the attenuation as derived from the parameters of the drop size distribution in the previous gate. This procedure, however, tends to become unstable as the attenuation increases. An alternative is a backward recursion which is more stable but requires a path-integrated attenuation (PIA) estimate. In the case of the TRMM PR, the PIA is derived from the surface reference technique (SRT) which is estimated from a difference in the radar return powers from the surface outside and inside the rain. A dual-wavelength version of the method is expected to be more accurate because it takes advantage of the correlation in the surface cross section with wavelength. Despite this advantage, there will remain certain surface types and incidence angles, such as nadir incidence over land, where the method is unreliable. In these cases, iterative solutions of the recursion equations or a 'weak-constraint' approach that uses the difference of the measured reflectivity factors at the closest range above the surface can be used. Other approaches that use simplifying assumptions regarding the behavior of D_0 and number concentration as a function of height have the advantage of being robust with errors that appear to be small for most rain events. Although the error characterization of these alternative approaches are now being explored, it appears that a combination of these and other methods can be used to obtain, in most cases, an attenuation correction to within an accuracy of ±1 dB.

3. D_0 Calculation for Liquid Rain Drops

For rain the accuracy of the D_0 estimate can be derived from the accuracy of the DFR and the variability in the shape parameter, μ, of the drop size distribution. In Figure 1, an example is shown for an overall 4 dB error (y-axis) from the ±1 dB of attenuation correction, the ±0.75 dB from the measurement noise of N samples, and an extra ±0.25 dB for margin. The figure assumes that the shape factor is uniformly distributed between 0 and 8 resulting in a D_0 range of 1.2mm or an error of ±0.6mm. However, μ is ultimately expected to be known with less error than a uniform distribution between 0 and 8, thus the lighter shading in Figure 1 shows a more likely error in D_0 which is closer to ±0.3mm. Most studies of measured size distributions using disdrometers estimate the μ parameter to be between 0 and 6. For the TRMM PR rain retrievals, μ=3 is assumed. Other studies have proposed a μ-D_0 relation in which case the DFR-D_0 relations reduce to a single curve. How universal this μ-D_0 relation is and how much variability can be expected with rain type and climatology are areas of continuing research. As the curves in Fig. 1 make clear, a decrease in the variability associated with the shape parameter (μ) can have a significant impact on the accuracy by which D_0 can be inferred from the DFR. With the DPR on the GPM Core Observatory along with the GMI radiometer, the GMI can be used to limit

unknowns of the shape parameter to further reduce the D_0 errors. In addition, if the error sources contributing to the DFR are larger, knowledge about the shape factor will help reduce the overall D_0 error.
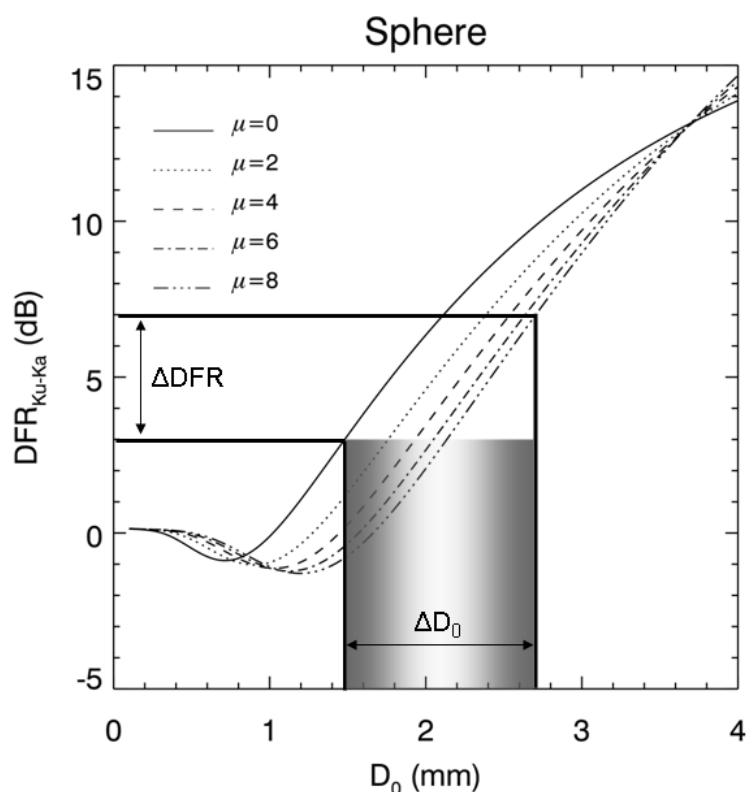
Fig. 1. Curves of DFR versus D_0 (mm) for spherical rain at 10^oC for values of the shape factor from 0 to 8. Shown is how an uncertainty in the DFR (ΔDFR) of 4.0 dB translates into an uncertainty in D_0 of approximately ±0.6 mm assuming the shape factor of the gamma distribution, μ, is uniformly distributed between 0 and 8. The lighter shading represents the error in D_0 when more is known about the shape factor, μ, which shows an error of $\sim\pm0.3$mm.

4. D_0 Calculation for Frozen Precipitation

For snow, the basic procedure of inferring D_0 from an estimate of DFR is the same as that in rain. However, the error sources for the two cases are different. Measurements in snow suggest that the shape parameter is typically near 0 and that the distribution is approximately exponential. Another advantage to the snow estimation problem is that the attenuation in dry snow is much less than in rain and the errors arising from the correction procedure are correspondingly smaller than in rain. On the other hand, the snow density is an unknown that adds uncertainty to the estimate. As shown in Fig. 2a, if we are interested only in the median mass diameter of the unmelted snow, the uncertainty introduced from the unknown mass density is small. These results imply, however, that if we are interested in the median mass diameter of the melted size distribution (Fig. 2b), then the unknown snow density is a major source of error.

As shown in Figure 2, for the estimation of D_{0s}, a 4.0 dB error in DFR translates into an error in D_{0s} of about ± 0.4 mm whereas the same error in DFR translates into about a ± 0.55 mm error in D_0 assuming snow densities ranging from 0.05 to 0.2 g/cm^3.
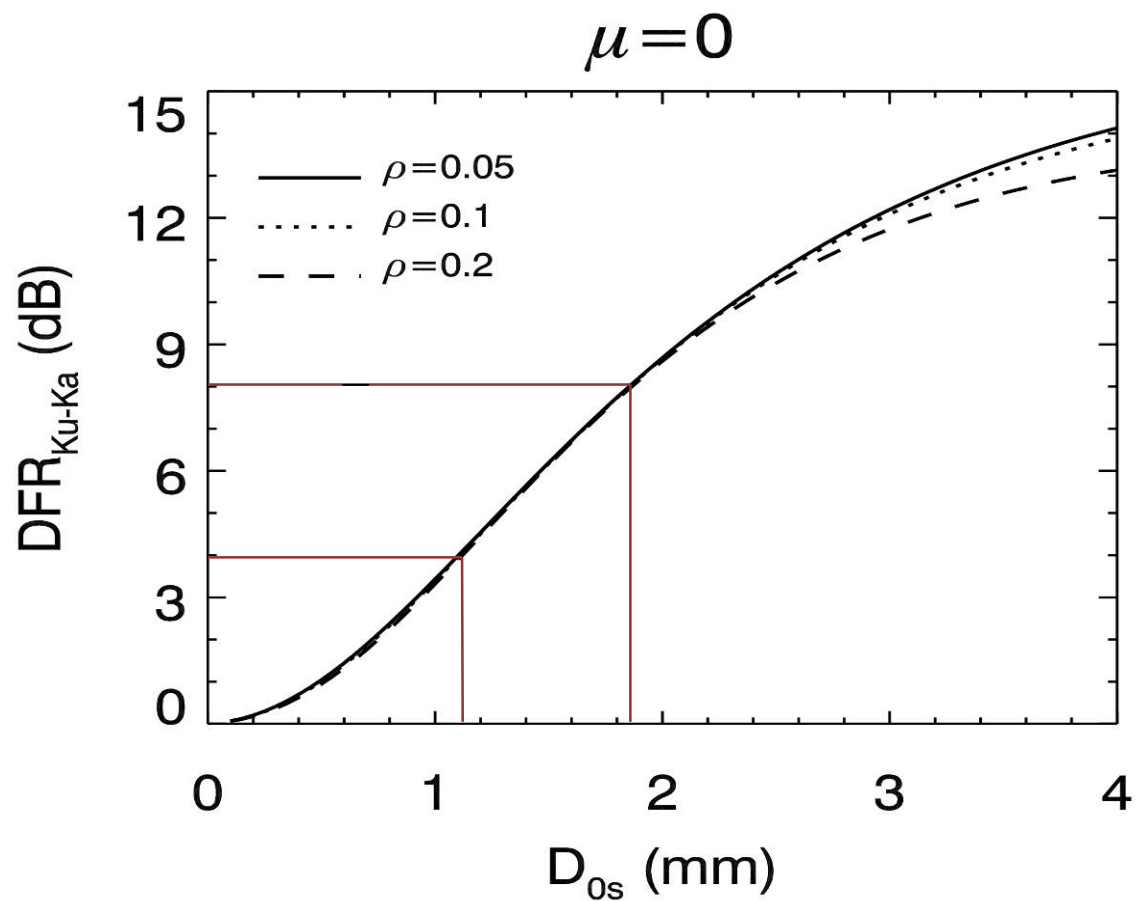
Fig. 2a. Relationship between DFR and the median mass diameter, D_{0s}, of the unmelted snow size distribution for 3 values of the mass density (g/m^3).
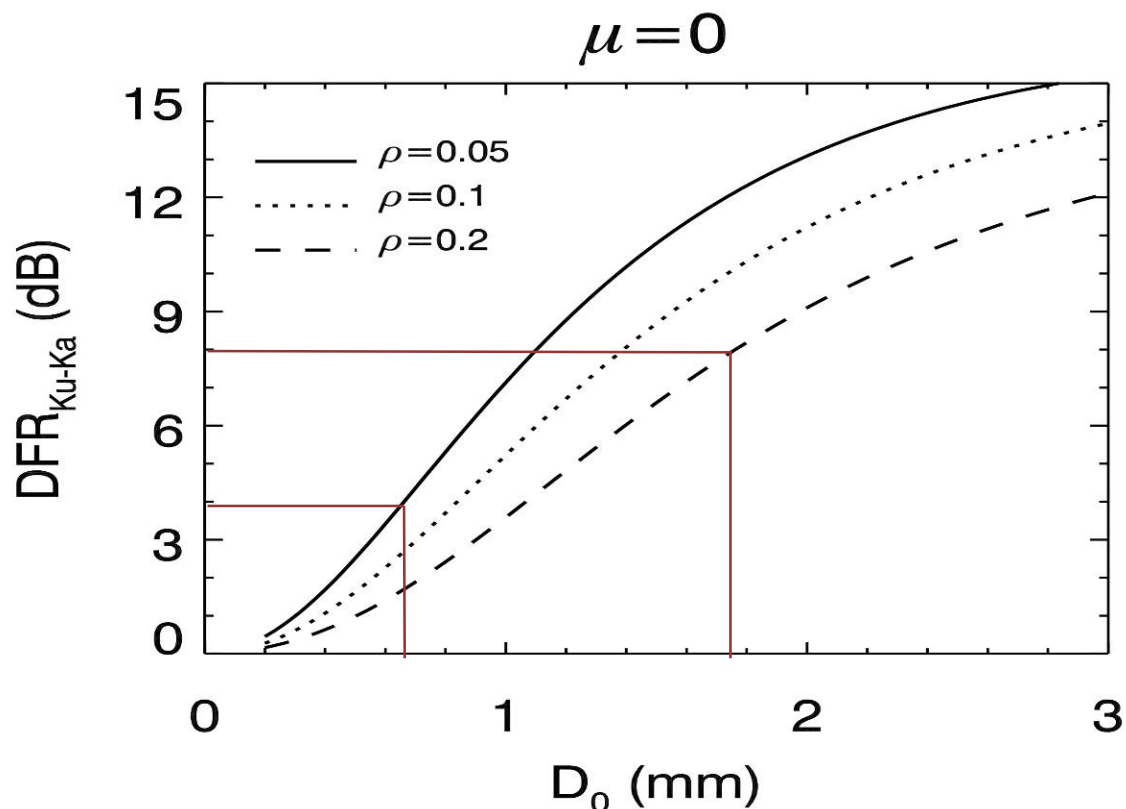
Fig. 2b. Relationship between DFR and the median mass diameter, D_0, of the melted snow size distribution for 3 values of the mass density (g/m^3).

5. Concluding Remarks

This analysis shows that based on the expected range of DPR error sources, the resultant uncertainty in D_0 is less than ± 0.5 mm. In reality, this ± 0.5 mm error margin represents a conservative estimate since GMI radiometer data and/or ground validation data can be used to define the unknowns such as the shape parameter and snow densities to further refine the D_0 estimate.

Appendix J. Bias and Random Error Estimates Using Pre-GPM Satellite Products and Ground Validation Rain Rate Estimates

Walter Petersen, Robert Meneghini, David Wolff, Mircea Grecu, George Huffman, Liang Liao, Gail Skofronick-Jackson, Arthur Hou

December 2009

0.   Introduction

This study presents a discussion of bias and random errors relevant to measurements made from the GPM core satellite as illustrated using theory, results in the literature, and direct comparisons between the Tropical Rainfall Measuring Mission (TRMM) instrument and calibrated ground validation (GV) data. We discuss these errors in the framework of demonstrating that that the collective total error (embedded bias + random) in current (TRMM) estimates meet or exceed those stated in the GPM requirements. We present a bias and random error analysis for rain rates at a 50 km resolution and also inter-compare instantaneous rain rates observed by the two rain sensors aboard the TRMM satellite (Precipitation Radar (PR) and TRMM Microwave Imager (TMI)) with ground data from two regional sites established for long-term GV: Kwajalein Atoll (KWAJ) and Melbourne, Florida (MELB) (Wolff et al. 2005). Reasons for differences in the bias results between these two locations are also provided. The bias and random error results represent current state of the art in space-based precipitation retrievals; however we reasonably assume that GPM estimates will be significantly superior to those of TRMM, given the inclusion on GPM of the dual frequency radar (DPR), an improved passive microwave GPM Microwave Imager (GMI), and expected improvements in retrieval algorithms employed during the GPM era.

2. Error Sources

Bias error is defined as a systematic shift (above or below) from a 1:1 correspondence between measured values and some other *a priori* reference. Random error is defined as the standard deviation or biased-removed root mean square error of the measured values. There are three primary sources for the errors which stem from (1) uncertainties in the reference or comparison measurement (e.g., ground validation), (2) satellite instrument measurement uncertainty, and (3) precipitation retrieval algorithms. Given the nonlinear and under-constrained character of the rain retrieval problem, it is expected that any error above could induce both systematic (biases) and random components. The instrument designs of DPR and GMI (as well as PR and TMI) are such that the instrument errors are typically much smaller than the errors associated with errors in the retrieval algorithms and errors in the GV data. Within each of the three categories we discuss the principal errors sources. In Section 4 we also describe potential improvements in these errors for the GPM-era.

2.1 Satellite Error Sources

Broadly speaking, the satellite measurements have errors in raw data such as reflectivity for the radar and NEDT and calibration for the radiometers. For the radar, reflectivities are affected by instrument calibration, noise, quantization, beam matching, and beam filling (Iguchi et al., 2009). For the radiometers, the NEDT is mostly driven by the noise of the receiver, the integration sample time and bandwidth of the receiver. (See SIP Appendices F and K for information on how instrument errors propagate through the radiometer and radar retrievals, respectively.) As shown in Section 4, instrument error sources for GPM will be as good as or better than the TRMM instrument errors.

2.2 Retrieval Algorithm Error Sources

The satellite retrieval algorithms inherently have errors because the estimation is under-constrained and assumptions must be made about the unknowns. These errors are more difficult to assess since instantaneous detailed knowledge of cloud-scale physical processes throughout the entire precipitating column is impractical to obtain. Some of the radar error sources include: sub-pixel and beam to beam drop size distribution (DSD) variability, attenuation correction (a priori DSD and cloud-water assumptions), and surface backscatter cross-section variability. For the radiometer, Bayesian database representativeness and assumptions therein cause bias and random errors. For example, snow density parameterizations can induce both bias and random errors because the natural variability of snow density can be captured only in a mean sense. At low or very high rain rates errors are further introduced by the changes in the drops themselves that affect the relationships between the microphysical properties and their active and passive radiative properties. Despite the large number of retrieval unknowns, the internal random error uncertainty between the PR estimates and the TMI estimates is roughly 50% at 1 mm/h and 25% at 10 mm/h at 0.5 degree resolution (SIP Figure 5-1).

2.3 GV Error Sources

The GV error source is due mainly to the uncertainty in ground radar calibration. Uncertainty in the ground radar calibration results from logistical difficulties in performing absolute calibrations, which require external targets of known cross-sections (i.e. tethered spheres, horns, etc.). For TRMM GV (non-absolute) calibration requires a large sample of rain gauge data matched with collocated radar data to determine Z-R relationships. The other primary source of random error in the GV rainfall retrieval is due to the natural variability of DSD parameters and their degree of representation at any given time or location in a given Z-R equation (Lee and Zawadzki, 2005). In the literature this error has been assessed by comparing reflectivity and rainfall rates for a large number (i.e., thousands) of naturally-occurring DSDs, to a least-squares fit of the DSD-ensemble Z-R relationship. Using this technique Bringi and Chandrasekar (2001) have demonstrated that random errors in instantaneous Z-R estimates can approach 70% for

rainfall rates < 5 mm/hr (lower error for heavier rain rates). This "parameterization" random error is clearly much larger than those associated with instrument error (70 vs. 10% or 15%, respectively). Similarly, Lee and Zawadzki (2005; amongst others) used a "climatological" average Z-R relationship constructed from a multi-year DSD sample to demonstrate that a random error of ~40% represents the theoretical "best case" for estimating instantaneous rain rate over a typical radar pulse volume (assuming a constant DSD within the pulse volume). Importantly, Lee and Zawadzki point out that any *a priori* information on the precipitation regime/DSD physics in a pulse volume can reduce this error. For the most part, this error will be larger than that associated with the instrument error (true for GV, TRMM or GPM DPR).

3. Bias and Random Error Analysis

In this section we present two sets of analyses to show that current TRMM products already meet or are close to meeting GPM Level 1 requirements on biases and random errors over a wide range of rain rates. The first analysis computes the biases and random errors in TRMM PR rain rates at 5 km resolution relative to ground radar estimates and uses an empirical formula to scale random errors from 5 km to 50 km. The second analysis computes the biases and random errors in TRMM PR and TMI rain rate products averaged to 0.5º x 0.5º horizontal resolution relative to ground-based estimates.

3.1 TRMM PR Biases and Random Errors at 5 km Resolution Relative to Ground Radar Estimates and Implications for Random Errors at 50 km Resolution

To establish the basis for GPM L1 requirements at the 0.5º x 0.5º scale, let us first consider biases and random error (RE) sampled at the native resolution (5 km pixel) of a current satellite sensor such as the TRMM PR. Figure 1 shows that the pixel-scale bias (RE) for the PR is 100% (175%) and positive at the lowest rainfall rates (1 mm hr^{-1}), rapidly decreases to values < 10% (<90%) when rainfall rates reach ~10 mm hr^{-1}, and eventually reaches values of ~ -20% (50%) at a rainfall rate of ~20 mm hr^{-1}. Note that the biases at 5 km pixel scale at relative high rain rates (>5 mm/hr^{-1}) already meet the 50 km bias requirements for GPM. With the addition of a Ka-band, the DPR is expected to significantly reduce the biases at the very low rain rates at the 5 km scale.
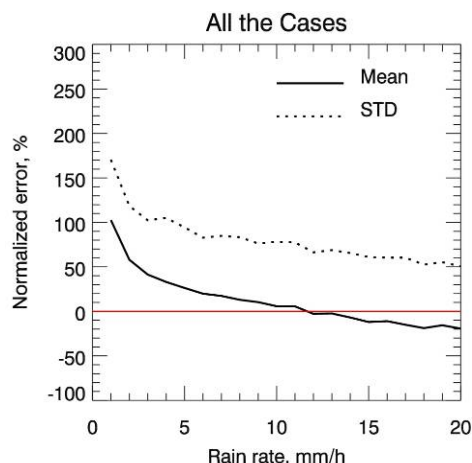
Figure 1. Plots of PR bias (solid line, indicated as "mean") and RE (dotted line, indicated as STD) expressed in % relative to GV (ordinate) as a function of rain rate bin (abscissa) for the Melbourne, Florida region.

For random errors (RE), it is possible to upscale the results at 5 km resolution (A_5) to estimate the RE at 50 km (A_{50} over a 0.5º x 0.5º grid area) using an empirical relation developed in observational sampling studies by Steiner et al. (2003) based on WSR-88D radar data in the central U.S. A key result of the Steiner et al. study was that random errors between two different-sized sampling regions (or length scales) at fixed temporal sampling and rain rate bins should scale as the ratio of the smaller to larger length scales raised to the 0.7 power (with non-trivial variability possible due to different weather regimes):

$$\frac{\sigma_E}{R}100\% = f(T, \Delta t)\left(\frac{R_0}{R}\right)^{0.20}\left(\frac{L_0}{L}\right)^{0.70}$$

where σ_E is the uncertainty, R is the precipitation rate averaged over the averaging area, f is a function of averaging time (T) and observation interval (Δt) that doesn't enter this discussion, L is the spatial scale of the averaging area, and R_0 and L_0 are constants (1 mm/h and 500 km, respectively). The precipitation factor accounts for increased spottiness in the occurrence of light precipitation compared to heavy, since the latter tend to be embedded in larger-scale systems. The spatial factor accounts for multi-scale time/space correlations in the precipitation, summarizing the tremendous power that a spectral analysis shows at all observed scales.

Fixing all variables but L,

$$\frac{\sigma_{E1}}{\sigma_{E2}} = \left(\frac{L_2}{L_1}\right)^{0.70}$$

where 1 and 2 denote different averaging scales. In particular, for $L_1 = 50$ km and $L_2 = 5$ km, $\sigma_{50} = 0.2\ \sigma_5$.

Based on this scaling relationship, we can estimate the expected change in random error from A_5 to A_{50} scales; i.e., the expected random error at A_{50} will be approximately 20% of that observed at A_5, namely 35% at 1 mm hr^{-1} and 15% at 10 mm hr^{-1}, which would exceed GPM L1 bias and RE requirements.

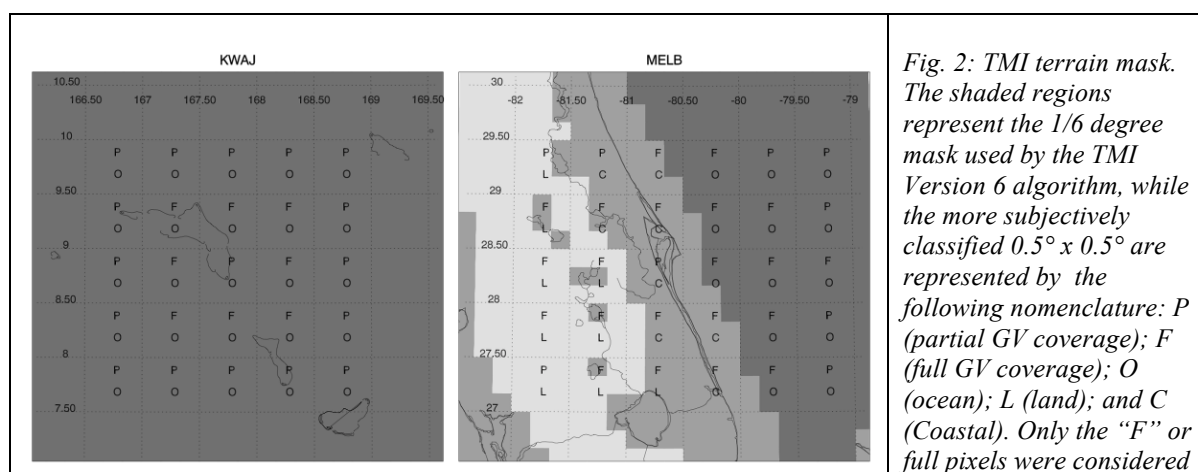Note that unlike random errors, the bias results at 5 km cannot be scaled to 50 km, except in the unrealistic scenario of uniform rain rate over a 50 km x 50 km domain. However, both biases and random errors at 50 km can be directly computed from satellite retrievals and ground-based measurements, which are presented in Section 3.2.

3.2 Estimation of Biases and Random Errors in TRMM PR and TMI Products at 50km Resolution Relative to Ground-based Measurements

We compare instantaneous rain rates from the TRMM 3G68[4] product with instantaneous GV program rain rates, both gridded at a horizontal scale of 0.5° x 0.5°. Figure 2 (from Wolff and Fisher, 2008) provides a depiction of the GV sites, illustrating the land–coast–ocean 1/6° terrain mask used by the Version-6 TMI algorithm to delineate geographical type: dark gray is "ocean," medium gray denotes "coast" (both coastal land and coastal water), and light gray denotes "land." Also shown are the more subjectively classified terrain types within each of the 0.5° grid locations of the TRMM 3G68 product employed in this study. In these figures, "L" is for land, "C" for coast, and "O" for ocean. Additionally, a GV coverage notation is provided ("F" for full coverage and "P" for partial). The purpose of the coverage flag is to identify pixels that are both fully observed by the GV radar and that contain a supermajority of one geographical type (i.e., mostly ocean, coast, or land, subjectively set at about 60%). For this analysis, only the F pixels were considered.

Fig. 2: TMI terrain mask. The shaded regions represent the 1/6 degree mask used by the TMI Version 6 algorithm, while the more subjectively classified 0.5° x 0.5° are represented by the following nomenclature: P (partial GV coverage); F (full GV coverage); O (ocean); L (land); and C (Coastal). Only the "F" or full pixels were considered

---

[4]3G68 is an hourly gridded text (ASCII) product containing TRMM Radiometer (2A12) [Kummerow etal., 2001], TRMM Radar (2A25) [Iguchi et al., 2000], and TRMM Combined (2B31) [Haddad et al., 1997a, 1997b], rain estimates. The 3G68 product includes 24 hour of hourly grids into a single daily file. The combination of the rain estimates on a common 0.5 x 0.5 degree grid provides an easy way to compare instantaneous results from the three retrieval algorithms.

in this analysis.

In an effort to provide robust statistical comparisons, coincident satellite and GV data covering the period 1999-2004 were used. After coincident pixels were matched in both time (instantaneous) and space (0.5° x 0.5°), satellite data outliers exceeding two standard deviations (+/- 2σ) of the mean rain rate in each rain rate bin were removed (outliers evident in scatter plot shown in Fig. 3).
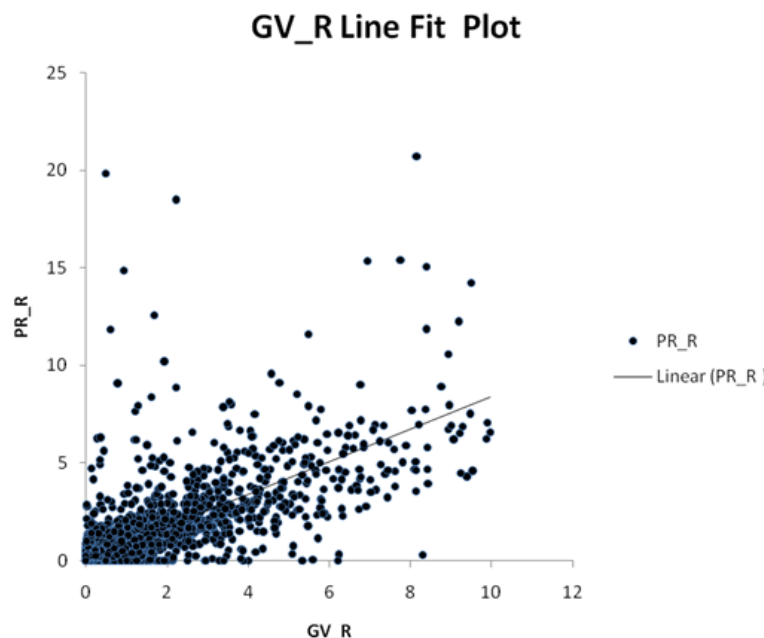
Figure   3.   Coincident   sample pairs of GV (abscissa) and TRMM PR rainfall rates (ordinate) for A_{50} grid boxes surrounding Melbourne. Note outliers.

Next, vectors of bias and (bias-removed) RE were calculated relative to GV-observed rain rates, centered on 1 mm hr^{-1} bins (bin width +/- 0.5 mm hr^{-1}) for bins ranging from 1-10 mm hr^{-1}. The bias was defined by the following equation:

$$Bias = \frac{\overline{E} - \overline{G}}{\overline{G}} \times 100\%$$

where $\overline{E}$ represents the mean instantaneous satellite rain rate over the period and $\overline{G}$ represents the mean GV rain rate.

The RE (%) was defined for the satellite estimates (e.g., PR, TMI) and as the RMSE between the individual satellite (E_n) and GV (G_n) estimates normalized by the GV mean rain rate in each bin.

$$RE\ (\%) = \frac{\left[\frac{1}{N} \sum_n (E_n - G_n)^2 \right]^{0.5}}{\overline{G}} \times 100$$

Here it is important to note a couple of things: First, the total number of sample pairs (N) at A_{50} is much lower than A_5, trending toward larger values at the lower end of the rain rate spectrum (because of averaging over a larger area). Secondly, the number of GV-satellite sample pairs for Kwajalein is even lower than that of Melbourne due to a combination of reduced scanning frequency of the Kwajalein radar (every 10 minutes at Kwajalein vs. 6 minutes at Melbourne) and the occurrence of more frequent convection near Melbourne. As a consequence, the number of samples of significant area-average rain rate in TRMM data covering a 0.5º x 0.5º for the period studied tends to fall well below a total of 10-20 total samples at rain rates in excess of 4-5 mm/hr. Therefore, bias and RE plots (e.g., Fig. 4-5) were truncated at rain rates where the sample number decreased to less than 10.

3.2.1 Bias

Fairly low biases exist at A_{50} over Kwajalein (Fig. 4) with the TMI rain rate estimate exhibiting primarily a positive bias relative to GV, peaking at a value of ~19%. The PR bias over Kwajalein is slightly negative, with values ranging from -13% to -19%. Over Melbourne (Fig. 5) the TMI and PR exhibit similar A_{50} bias behavior. The Bias values for both the PR and TMI range from near 0% at a rain rate of 1 mm hr^{-1} for the PR (TMI closer to -20%), to -20% or better at rain rates of 5 mm hr^{-1}. For the Melbourne area note that the rainfall rate sample pairs represent those occurring over coast, land and ocean. Most importantly, Figs. 4 and 5 reveal that the TRMM biases at A_{50} either meet or are very close to meeting the GPM requirements- at least over a portion of the rain rate spectrum where enough coincident samples exist (e.g., 1-4 or 5 mm hr^{-1}).

3.2.2 Random Error

With regard to RE, the results of Fig. 4 and 5 show that over Kwajalein (Melbourne) the current TRMM PR random error is ~50 % (58%) at 1 mm hr^{-1} and ~26 % (40%) at 4 mm hr^{-1}. Results beyond about 4 mm hr^{-1} are not statistically robust in Figs 4-5 due to reduced sample numbers. The TMI errors for Kwajalein (Melbourne) are similar to slightly higher than those of the PR at ~61% (76%) and ~25% (45%) at 1 and 4-5 mm hr^{1}. The PR random error values for A_{50} can be compared to those of the upscaled PR A_{50} results from Fig. 1, which are of order 35% at 1 mm hr^{-1} and 20% at 4-5 mm hr^{-1}, respectively (see Section 3.1). With the improved sampling and measurement capabilities of GPM as well as improved GV radar networks (i.e., dual-polarimetric, reducing GV errors), the expectation is that GPM products will meet the Level 1 accuracy and precision requirements.
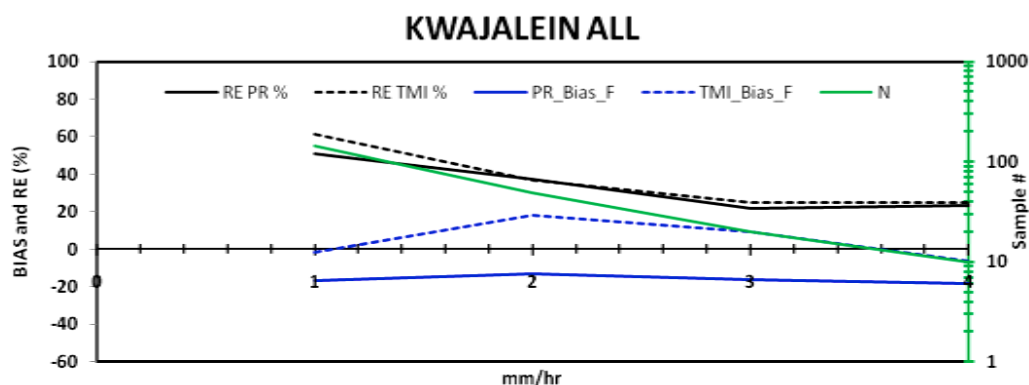
KWAJALEIN ALL

Figure 4. TRMM PR (solid lines) and TMI (dash lines) Bias (blue) and Random Error (RE: black) in % (ordinate) for 0.5 x 0.5° grid boxes in the vicinity of Kwajalein as a function of rain rate (abscissa). Note that sample numbers (green; right ordinate) decrease to below 10 for rain rates in excess of 4 mm hr^{-1}.

MELBOURNE ALL

Fig
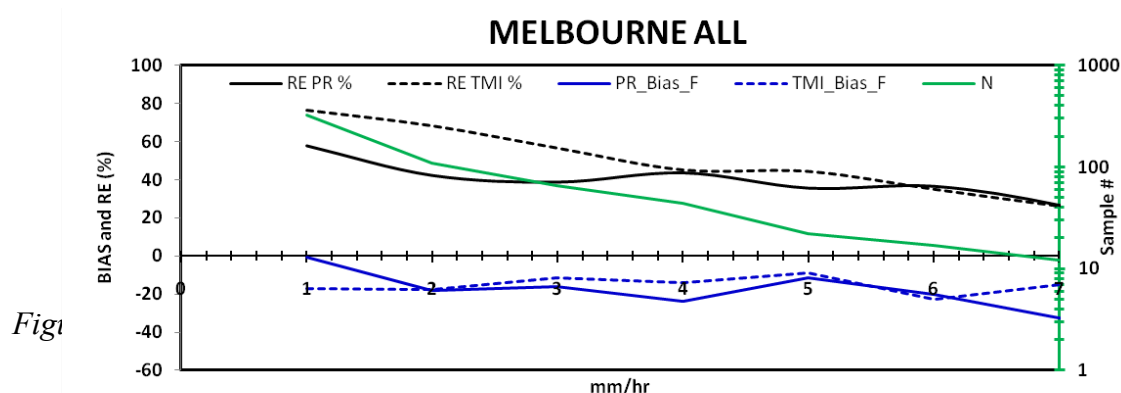
3.3 On Bias Differences between Kwajalein and Melbourne

The Kwajalein and Melbourne sites are characterized by different climatic regimes. While Kwajalein is a purely oceanic tropical site, Melbourne is a (at least partly) continental subtropical site. The retrieval algorithm and ground based measurements contribute to the differences. In terms of the retrievals, both PR and TMI algorithms rely on observations as well as climatology (which is built in the associated assumptions in databases) to derive estimates. For the ground based measurements, these differences are attributable to (1) different numbers and geographical distributions of rain gauges, (2) ocean versus land/coast-contaminated fields of view, and (3) uncertainty in the ground radar calibration.

3.3.1 Limited gauges at Kwajalein for developing appropriate Z-R relations (only seven sites, as compared to over 100 at MELB).

The current TRMM GV rain rate estimates are derived from probability matched reflectivity-rainrate (Z-R) relationships (PMM; Rosenfeld et al. 1995). In order to develop robust relationships, a large sample of gauge data matched with collocated radar data must be used. At

Kwajalein (Fig. 6a) given the limited available land area for deployment of gauges (total of six sites outside the radar "cone of silence"), a longer series of gauge observations (seasonal or annual) is necessary. At Melbourne (Fig. 6b), however, there are several gauge networks (more than 100 total gauges) available for developing these relationships, and the PMM relationships are derived monthly. It should be emphasized that during the GPM era, use of dual-polarimetric radars over Kwajalein, CONUS, and Europe etc. will provide for more robust rain rate estimates, which do not require gauges for input. Of course, multi-platform rain rate products will still be created operationally in CONUS by NOAA (for example), and these products will employ a combination of dual-polarimetric estimators plus gauge bias adjustments.
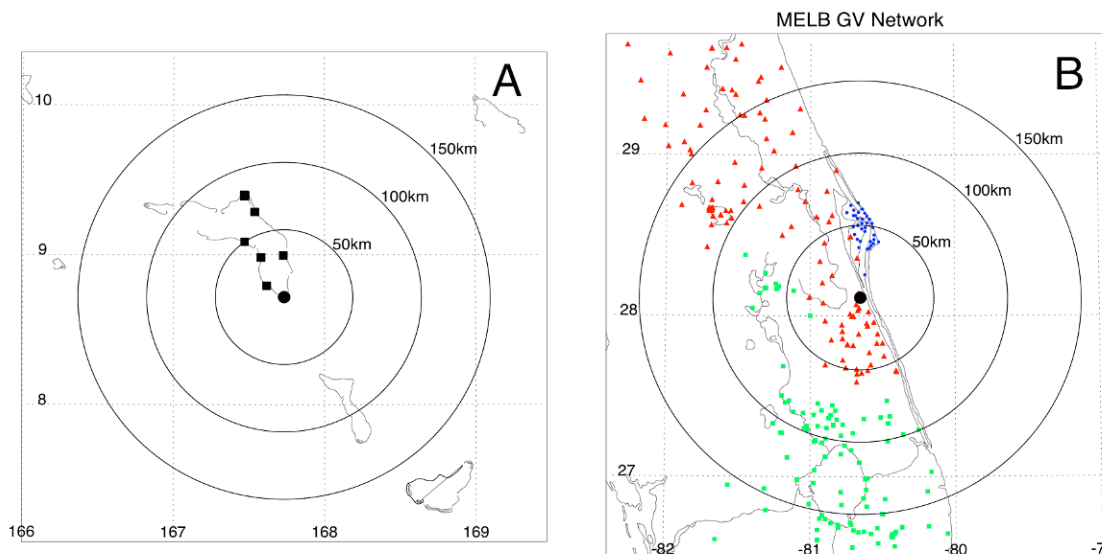
Fig. 6: Maps illustrating the TRMM GV rain gauge and radar networks at Kwajalein (left panel) and Melbourne, FL (right panel). At MELB, there are several available networks: NASA Kennedy Space Center (Blue), St. John's River Water Management District (Red); and South Florida Water Management District (Green). At Kwajalein, there are only six sites that are outside of the radar "cone of silence" and can thus be used for development of PMM Z-R relationships.

As an example, with recent data from Kwajalein, the dual-polarization data was used to develop polarimetrically-tuned Z-R relationships (Bringi et al. 2004). These relationships were then used to create instantaneous rain maps, which in turn were integrated monthly and compiled over a six month period. Figure 7 shows a scatter plot of gauge vs. radar monthly accumulations for July-December 2008. We note that no gauge data was used to develop the polarimetrically-tuned Z-R relationships, which relied solely on the radar observations of reflectivity, differential reflectivity, and specific differential phase.

The Goddard Profiling (GPROF) algorithm estimates instantaneous TMI rain rates over ocean, land and coastal areas using precipitation information obtained remotely from the observed emissions and scattering of hydrometeors in the atmosphere. The information collected in the available channels represents a radiometric temperature sounding at different depths of the precipitating cloud (Kummerow et al. 1998). To estimate the cloud liquid water content, the rain signal must be distinguished from the microwave background upwelling from the surface. This is

most easily accomplished over the radiometrically cold oceans, which cover three-quarters of the earth's surface. Over the oceans, GPROF applies a physical algorithm utilizing the radiometric information of all nine TMI channels (Kummerow et al. 1996, Kummerow et al. 2001).
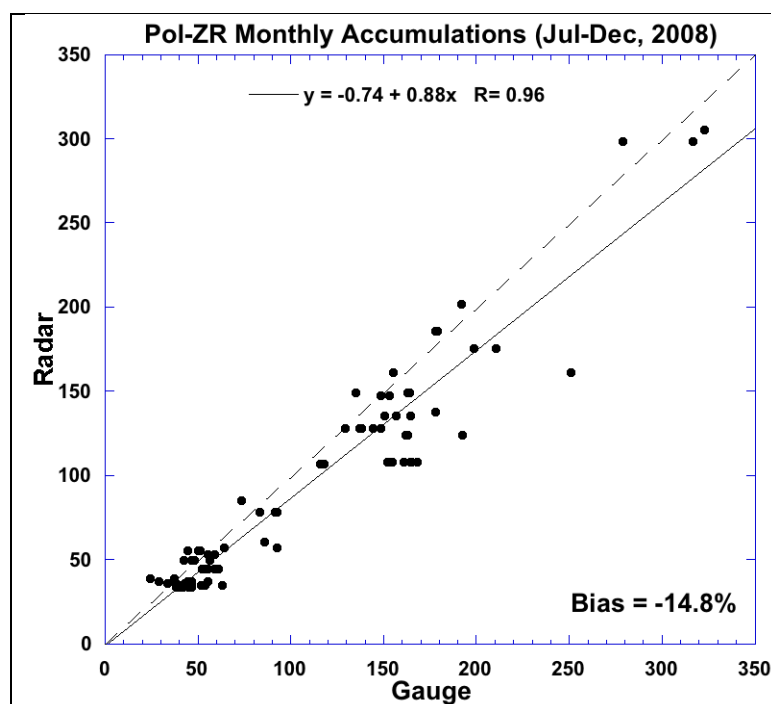
Fig.7: Monthly radar accumulations for July – December 2008 derived from the S-band dual-polarimetric radar at Kwajalein radar observations using the polarimetrically-tuned Z-R relationships of Bringi et al. 2004. It should be noted that no gauge data was used to develop these relationships, but rather they are based solely on radar observations of reflectivity, differential reflectivity and specific differential phase.

3.3.2 Ocean vs. land/coast retrievals and possible contamination of multiple-terrain types in a single 0.5 deg (50 km) pixel.

The rain retrievals are considerably more complicated over the radiometrically warm land surface due to variations in soil moisture, vegetation and transpiration, surface roughness, and topography. Difficulty in handling the microwave background over land has precluded the usage of the lower frequency emission channels. Spencer et al. (1989) showed that at 85.5 GHz, a reduction in the detected signal related to the scattering of radiation from frozen hydrometeors above the freezing level can be used as an empirical estimator of rain rate. Rain rates over land are subsequently determined empirically from the scattering information in the two 85.5 GHz channels (Spencer 1989, Ferraro 1997, Conner and Petty 1998, McCollum and Ferraro 2003). However, brightness temperature-rain rate relations are not directly related to surface rainfall, since they characterize scattering processes in the higher regions of the cloud (Wilheit et al 2003). Currently, GPROF applies an empirically based rain algorithm originally developed by Ferraro (1997) and McCollum and Ferraro (2003) over land.

The problems over land are further exacerbated near coastal regions due to the sharp contrast between land and ocean surfaces of the TMI footprint. In this case, the radiometrically warm land and cold ocean surfaces are both present in the TMI footprint. Coastal pixels are treated using a decision tree that first determines whether rain exists in the pixel. If a determination of rain existence cannot be made then the pixel is classified as ambiguous and a rain rate is not

assigned. If rain exists, then the rain rate is determined using empirical relations described in McCollum and Ferraro (2005) and others.

To address the specific GPM requirements, it is noted that if one combines the land, coast and ocean areas at MELB (i.e. Fig. 3; SIP_Appendix_J) it seems reasonable to conclude that the same result as Kwajalein (an ocean site) should not be expected. Nevertheless, the resultant TRMM biases for MELB are already reasonably small and well behaved and approach (even exceed in some cases) those required for GPM.

3.4 Bias and Uncertainty in GV radar calibration

Using conventional radars, such as those currently deployed for TRMM GV efforts, calibration (which results in bias errors) is a very difficult issue to handle effectively. The TRMM GV program developed a methodology to assess the relative calibration (i.e. hour-to-hour and day-to-day changes) of the Kwajalein radar using the distribution of ground clutter area reflectivities (Silberstein et al. 2007); however, absolute calibration with conventional radars can only be done using external targets of known cross-sections (i.e. tethered spheres, horns, etc.). Logistical limitations often limit that capability, especially with operational radars such as the NWS WSR-88D systems. Calibration is extremely important for quantitative rain rate estimation, given that a calibration offset of 2 dB can result in rainfall estimation error of 30%, as measured by the default WSR-88D reflectivity rain rate relationship ($Z=300R^{1.4}$). It is well documented that polarimetric properties of the rain medium can be used to determine the absolute calibration of a radar system. Techniques to capitalize on these relations range from the comparison of rainfall rates derived from power and phase measurements (Gorgucci et al. 1992), to comparing observed and estimated differential propagation phase (Goddard et al. 1994, Vivekanandan et al. 2003, Ryzhkov et al. 2005, and others). The self-consistency of Z_H, Z_{DR}, and K_{DP} measurements was quantified by Scarchilli et al. 1996 and Gorgucci et al. 1999 using a gamma distribution model that described many of the natural variations in the raindrop size distribution (DSD). It is envisaged that GPM era absolute radar calibrations will be within ± 1 dB, and recent TRMM GV analyses have shown that this expectation is well founded.

4. Expected GPM Measurement and Retrieval Improvements Relative to TRMM

The fundamental premise assumed herein is that GPM measurements will exceed the quality, accuracy and precision of the current TRMM measurements. Accordingly, analyses using TRMM data can serve as a benchmark for demonstrating that we can meet the GPM bias and random error requirements. If it is accepted that GPM measurement quality will meet (at a minimum) or exceed the quality of the TRMM measurements and that current TRMM measurements produce bias and random error values that approach or exceed GPM requirements, then we can reasonably expect GPM measurements to meet or exceed the L1 requirements.

4.1 GPM Instrument Performance Requirements

Table 1 shows a comparison of the Ku-PR and the TRMM (Iguchi et al. 2009). It should be noted that in the table some of the TRMM PR specifications, such as swath width and horizontal resolution at nadir, apply to the pre-boost conditions when the satellite was at an altitude of 350 km. At its present altitude of approximately 400 km, the horizontal resolution has increased from 4.3 km to approximately 5 km while the swath width has increased from 215 km to about 245 km. In other words, the resolution and scan geometry of the Ku-band channel of the DPR should closely match those of the TRMM PR at its present altitude.

Table 1: Comparison of DPR and PR Instrument Specifications

Item	Ku PR	Ka PR	TRMM PR
Antenna Type	Active Phased Array [128]	Active Phased Array [128]	Active Phased Array [128]
Frequency	13.597 & 13.603 GHz	35.547 & 35.553 GHz	13.796 & 13.802 GHz
Swath Width	245 km	120 km	215 km
Horizontal Resolution	5 km (at nadir)	5 km (at nadir)	4.3 km (at nadir)
Tx Pulse Width	1.6 μs (x2)	1.6/3.2 μs (x2)	1.6 μs (x2)
Range Resolution	250 m @ 1.67 μs	250/500 m @ 1.67/3.34 μs	250 m @ 1.6 μs
Obs. Range	18 km to -5 km [mirror image near nadir]	18 km to -3 km [mirror image near nadir]	15 km to -5 km [mirror image @ nadir]
PRF	VPRF (4206 ± 170 Hz)	VPRF (4275 ± 100 Hz)	Fixed PRF (2776 Hz)
Sampling #	104 - 112	108 - 112	64
Tx Peak Power	> 1013 W	> 146 W	> 500 W
Minimum Detect. Z [Rain Rate]	< 18 dBZ [~ 0.5 mm hr^{-1}]	< 12 dBZ (500 m res) [~ 0.2 mm hr^{-1}]	< 18 dBZ [~ 0.7 mm hr^{-1}]
Meas. Accuracy	within ± 1 dB	within ± 1 dB	within ± 1 dB
Data Rate	< 112 Kbps	< 78 Kbps	< 93.5 Kbps
Mass	< 365 kg	< 300 kg	< 465 kg
Power Consumption	< 383 W	< 297 W	< 250 W
Size	2.4 x 2.4 x 0.6 m^3	1.44 x 1.07 x 0.7 m^3	2.2 x 2.2 x 0.6 m^3

*Minimum detectable rainfall rate is defined by $Z_e=200R^{1.6}$ (TRMM PM $Z_e=37.24R^{??}$)

A comparison of the data in columns 1 and 3 shows that the performance of the Ku-DPR and the TRMM PR can be expected to be very similar because the instrument specifications are nearly the same. Some minor differences in the radar's frequencies (13.8 GHz for the TRMM PR versus 13.6 for the Ku-band DPR), and peak transmit powers (TRMM PR transmit power exceeds 500 W while the Ku-band DPR transmit power will exceed 1 kW). This 3 dB improvement in the Ku-band DPR sensitivity relative to the TRMM PR because of the higher transmit power is offset somewhat by the increase in altitude from 350 to 400 km (-1.16 dB) and by the slight decrease in frequency (-0.25 dB). Nevertheless, the sensitivity of the Ku-band DPR should be better than the TRMM PR sensitivity at 350 km and the 18 dBZ minimum sensitivity shown in the table appears to be a conservative estimate.

The primary difference between the two radars arises from the difference in the number of samples. By using a variable pulse repetition frequency (VPRF), where the range window is restricted to that part of the atmosphere most likely containing precipitation, the number of samples will increase from 64 in the TRMM PR case to a number between 104 and 112, depending on incidence angle. This implies that the standard deviation in the estimate of Z will decrease from $5.57/\sqrt{64} = 0.696$ dB to $5.57/\sqrt{108} = 0.536$ dB or about a 23% reduction in the standard deviation. This, in turn, will improve the effective signal-to-noise ratio and the effective minimum detectable signal level.

In conclusion, the performance of the Ku-DPR is expected to be nearly identical to that of the TRMM PR with modest reductions in the variance of the Z estimates and modest improvements in the effective signal-to-noise ratio. As such, the comparisons between the ground-validation (GV) data and the Ku-DPR-only retrievals should be comparable to or better than the comparisons presently obtained between the TRMM PR and GV data. However, in the inner swath where dual-wavelength radar data will be available, the comparisons between the dual-wavelength DPR rain retrievals and those from the ground-validation sites are expected to improve significantly relative to the present TRMM PR-GV results. This inner swath data of the Ka+Ku+GMI provides additional constraints on the path-integrated attenuation, DSD assumptions, and overall retrieval estimates. Additionally, the improved resolution of the GMI instrument and the existence of additional high frequency channels will reduce the degree of indeterminacy in radiation-precipitation databases and facilitate the derivation of significantly more accurate radiometer-only precipitation retrievals.

For the radiometer on GPM, the GPM Science Implementation Plan (SIP) Appendices D and E (Appendix D. Radiometer NEDT Specifications: GMI versus TMI and SSMIS (conical scanning imagers) and Appendix E. Comparison of High-Frequency Channel Characteristics: GMI versus Cross-Track Scanning Sounders) all demonstrate the instruments onboard GMI will have NEDT as good as or better than current radiometer instruments. Further, special instrument features for GMI (e.g., noise diodes, hot load tray) are designed to reduce calibration errors.

4.2 Expected Improvements in GPM GV Measurements

Of course, GPM satellite measurements are not the only measurements that will improve in the GPM era. For GV measurements during GPM operations, dual-polarized ground radars will provide more robust rain rate estimates that do not require gauges as input. Use of DP radars leveraged/calibrated with the sub-satellite pixel dense networks of disdrometers will also allow for estimation of the key parameters of the DSD, which can be used to help validate the physics of the satellite algorithms. At least two approaches can be taken to reduce "parameterization" random error in GV estimates. First, if the DSD "regime" parameters can be identified a priori (i.e., if the dominant physical process driving associated DSD characteristics is properly inferred and/or parametric characteristics of the DSD can be measured) the random error in estimating the precipitation rate due to DSD variability can be reduced to less than 10% for instantaneous estimates (Lee and Zawadzki, 2005*). Importantly, some a priori inference of the DSD regime will be possible with both GPM dual-frequency and GV polarimetric radar measurements because both sets of measurements implicitly provide extended/intrinsic information on DSD* characteristics through multi-parameter techniques. Secondly, even if "climatological" or fixed Z-Rs were to be used by the GV radars or GPM DPR (pixel-scale random errors of 40-70% expected), spatial averaging of the radar pixels to produce a 0.5º x 0.5º grid should reduce the random error as demonstrated in Figs 1, 4 and 5 and Sec. 3.3.

4.3 Expected Improvements in GPM Retrievals

Satellite retrieval algorithms have been steadily improving over the 12 years of TRMM observations and the dual frequencies of the DPR and the additional channels of the GMI will

constrain the unknowns via estimation of the drop size distribution (DSD) and reduce uncertainties associated with the retrievals. Radiometer-only algorithms are likely to further improve because the existence of coincident radiometer-dual frequency radar observations will facilitate the development of more accurate and statistically representative databases of precipitation and associated brightness temperatures. Such databases have been proved to have a significant positive impact on precipitation retrieval from radiometer-only observations (Grecu and Olson 2006).

Retrievals at low rain rates (less than 1 mm/hr) are where we expect the biggest improvement from GPM with the addition of Ka-band and GMI HF channels. The PR algorithms have difficulties separating light rain from non-precipitating cloud droplets and also the path integrated attenuation (PIA) retrievals at light rain rates are comparable to natural variations in surface return, thus making it difficult to refine drop size distributions. The situation will change in GPM when the DPR Ka-band radar will assist with PIA retrievals and separating cloud drops from light rain drops. We expect more accurate estimates from the DPR observations, that will then improve the combined and radiometer observational cloud databases. Therefore, the new algorithms will be as robust as the current algorithms, while being able to make effective use of the additional information. We expect improvements in the GMI estimates as well mainly because of the addition of new channels, more representative cloud database, and improvement in the instrument resolution which will narrow the distribution of possible precipitation profiles that can be associated with a given set of observations.

5. Summary

The Level 1 requirements on rain rate biases and random errors are defined in terms of the systematic and uncorrelated discrepancies between satellite and ground-based estimates. Instrument measurement uncertainties, retrieval algorithm uncertainties and GV measurement uncertainties, as provided in Section 2, all contribute to the "total errors" between satellite and GV estimates. We show that the GPM Level 1 requirements are already met by current TRMM rainfall products (except for very light rain rates) at two research-quality tropical sites established for long-term TRMM ground validation (GV): one at Kwajalein Atoll and another at Melbourne, Florida (Section 3). At low rain rates is where we expect the biggest improvement from GPM with the addition of Ka-band and GMI HF channels. Since the DPR and GMI performance requirements are comparable to or better than those of TRMM (Section 4), the errors of current TRMM products represent an upper bound for the errors in GPM products, which are expected to be significantly reduced as a result of an host of improvements including the use of DSD estimates provided by the DPR and improved retrievals.

The above expectation is rooted in the fact that the current generation of radiometer retrievals suffers from having an inadequate and limited tropical cloud database generated by cloud-resolving models. An anticipated major advance from GPM is the construction of an observation-constrained cloud database consistent with the DPR and GMI measurements made by the GPM Core. This will enable GPM to significantly improve radiometer retrievals over the globe, especially outside the tropics. The linkage of the Level 1 requirements on rain rate biases and random errors to instrument requirements is, in effect, that DPR and GMI must provide measurements of the same geophysical scenes to enable the development of an observation-

based cloud database for radiometer retrievals, which is met by accommodating both sensors on the Core spacecraft.

In conclusion, based on the analysis of errors in current TRMM products, coupled with the anticipated advances in retrievals using DSD estimates provided by the DPR and an observation-constrained global cloud database, GPM precipitation products are fully expected to meet the Level 1 rain rate accuracy and precision requirements with the current DPR and GMI performance specifications.

References

Bringi V. N., T. Tang, and V. Chandrasekar, 2004: Evaluation of a New Polarimetrically Based *Z–R* Relation. J. Atmos. Ocean. Tech.*,* **21**, 612–623

Bringi, V. N., and V. Chandrasekar, *Polarimetric Doppler Weather Radar—Principles and Applications*, 636pp., Cambridge Univ. Press, New York, 2001.

Conner M. D., and G. W. Petty, 1998: Validation and intercomparison of SSM/I rain-rate retrieval methods over the continental United States. *J. Appl. Meteor*., **37**, 679-700.

Ferraro, R. R., 1997: Special sensor microwave imager derived global rainfall estimates for climatological applications. J. Geophys. Res., **102**, 16,715-16,735.

Grecu, M., and W.S. Olson, 2006: Bayesian Estimation of Precipitation from Satellite Passive Microwave Observations Using Combined Radar–Radiometer Retrievals. *J. Appl. Meteor. Climatol.*, **45**, 416–433.

Goddard, J., J. Tan, and M. Thurai, 1994: Technique for calibration of meteorological radars using differential phase. *Electron. Lett*., **30**, 166-167.

Gorgucci, E., G. Scarchilli, and V. Chandrasekar, 1992: Calibration of radars using polarimetric techniques. *IEEE Trans. Geosci. Remote Sens*., **30**, 853-858.

Gorgucci, E., G. Scarchilli, and V. Chandrasekar, 1999: A procedure to calibrate multiparameter weather radar using properties of the rain medium. *IEEE Trans. Geosci. Remote Sens.*, **34**, 269-276.

Haddad, Z. S., E. A. Smith, C. D. Kummerow, T. Iguchi, M. R. Farrar, S. L. Durden, M. Alves, and W. S. Olson, 1997a: The TRMM `Day-1' Radar/Radiometer Combined Rain-Profiling Algorithm", *J. Meteor. Soc. Japan*, **75**, 799-809.

Haddad, Z. S., D. A. Short, S. L. Durden, E. Im, S. Hensley, M. B. Grable and R.A. Black, 1997b: "A New Parametrization of the Rain Drop Size Distribution", *IEEE Trans. Geosci. Rem. Sens.*, **35**, 532-539.

Iguchi, T., T. Kozu, R. Meneghini, J. Awaka, and K. Okamoto, 2000: Rain-profiling algorithm for the TRMM precipitation radar, *J. Appl. Meteor.*, **39**, 2038-2052

Iguchi T., R. Oki, K. Nakamura, S. Seto, H. Hanado and R. Meneghini, 2009: Dual-frequency Precipitation Radar (DPR) in the Global Precipitation Measurement (GPM) Mission. *34th Conf. on Radar Meteorology*, Oct. 5-9, Williamsburg, VA

Kummerow, C. Y. Hong, W. S. Olson, S. Yang, R. F. Adler, J. McCollum, R. Ferraro, G. Petty, D. B. Shin, and T. T. Wilheit, 2001: The evolution of the Goddard profiling algorithm (GPROF) for rainfall estimation from passive microwave sensors, *J. Appl. Meteor.*, **40**, 1801-1840.

Kummerow, C. W. Barnes, T. Kozu, J. Shiue, J. Simpson, 1998: The tropical rainfall measuring mission (TRMM) sensor package. *J. Atmos. Oceanic Technol.*, **15**, 809-817.

Kummerow, C. W., W. S. Olson, L. Giglio, 1996: A simplified scheme for obtaining precipitation and vertical hydrometeor profiles from passive microwave sensors. *IEEE Trans. Geo. Remote Sens.*, **34**, 1213-1232.

Lee G. W. and I. Zawadzki, 2005: Variability of Drop Size Distributions: Time-Scale Dependence of the Variability and Its Effects on Rain Estimation, *J. Appl. Met.*, **44**, 241-255

McCollum, J. R. and R. R. Ferraro, 2003: Next Generation of NOAA/NESDIS TMI, SSMI/I, and AMSR-E microwave land rainfall algorithms. *J. Geophys. Res.*, **108**,

Rosenfeld, D., D. B. Wolff and E. Amitai, 1995: The Window Probability Matching Method (WPMM) for rainfall measurements with radar. *J. Appl. Meteor.*, **33**, No. 6, 682-693.

Scarchilli, G., E. Gorgucci, V. Chandrasekar, and A. Dobaie, 1996: Self-consistency of polarization diversity measurement of rainfall. *IEEE Trans. Geosci. Remote Sens.*, **34**, 22-26.

Silberstein, D. S., D. B. Wolff, D. A. Marks, D. Atlas, and J. L. Pippitt, 2008: Ground clutter as a monitor of radar stability at Kwajalein, RMI. *J. Atmos Oceanic Technol.*, 25, 2037-2045.

Spencer, R., W. H. Goodman, and R. E. Hood, 1989: Precipitation retrieval over land and ocean with the SSM/I: identification and characteristics of the scattering signal. *J. Appl. Meteor.*, **6**, 254-273.

Steiner, M., T. L. Bell, Y. Zhang, and E. F. Wood, 2003: Comparison of two methods for estimating the sampling-related uncertainty of satellite rainfall averages based on a large radar dataset. *J. Climate*, **16**, 3759-3778.

Vivekanandan, J., G. Zhang, S. Ellis, D. Rajopadhyaya, and S. Avery, 2003: Radar reflectivity calibration using differential propagation phase measurement. *Radio Sci.*, **38**, 8049,

Wolff, D. B., D. A. Marks, E. Amitai, D. S. Silberstein, B. L. Fisher, A. Tokay, J. Wang, and J. L. Pippitt, 2004: Ground validation for the Tropical Rainfall Measuring Mission. *J. Atmos. Ocean. Tech,* **22,** No. 4, 365-380.

Wolff, D. B. and B. L. Fisher, 2008: Comparisons of Instantaneous TRMM Ground Validation and Satellite Rain Rate Estimates at Different Spatial Scales, *J. Clim. Appl. Meteor., 47, 2215-2237*.

Appendix K. Sensitivity of Rain Retrievals to DPR Reflectivity Errors

Mircea Grecu

December 2009

Introduction

This study presents a discussion of bias and random errors in precipitation retrievals resulting from DPR radar instrument errors as manifest in reflectivities. Two types of instrument errors are considered. These are intermediate-term errors due to gain/loss variations caused by various changes in the system state (e.g. temperature) and instantaneous errors due to instantaneous variations in the backscattered signal. The intermediate-term error is within ±1dB (Kozu et al., 2001) and varies slowly in time (therefore, it can be considered observation bias in this analysis), while the instantaneous error varies range gate by range gate and can be considered a random variable with 0.0 mean and a fixed standard deviation (0.53 dB herein based on the DPR specifications - see SIP Appendix I). The analysis presented in this study relies on the radar dual frequency observations collected by the Airborne Precipitation Radar-2 (APR-2) in the NASA Monsoon Multidisciplinary Analyses (NAMMA) experiment (http://namma.msfc.nasa.gov/). The APR-2 is a dual frequency (Ka and Ku band) instrument and can serve as a proxy for the DPR. Here we take the APR-2 aircraft measurements and randomly add the two errors described above. The errors added to the two frequency observations are considered independent, although the reflectivity biases may be correlated. Because uncorrelated reflectivity biases (intermediate-term errors) impact the retrievals more severely than correlated biases, this analysis can be considered a worst-case scenario. For this analysis, retrieval bias error is defined as a systematic shift from a 1:1 correspondence between retrieved values and some other *a priori* reference. Retrieval random error is defined as the root mean square error of the retrieval (with bias removed) about the reference values.

2. Analysis

To understand the impact of random errors in reflectivity measurement on the estimates of rain rate from the GPM DPR, a Monte Carlo experiment was conducted. For this experiment, random errors were added to real radar dual frequency observations collected by the Airborne Precipitation Radar -2 (APR-2) in the NASA Monsoon Multidisciplinary Analyses (NAMMA) experiment and precipitation retrievals were derived. The process of precipitation retrieval from noise corrupted APR-2 observations was repeated a large number of times (i.e. 50) and the results were compared to precipitation retrievals using the nominal APR-2 observations (here the nominal non-noisy APR-2 retrievals are considered as *a priori* "truth"). Random noise added to the APR-2 observations was generated from a Gaussian distribution with 0.0 mean and 0.53 dB standard deviation, while the reflectivity bias was generated from a Gaussian distribution with 0.0 mean and 1.0 dB standard deviation.

The precipitation rates derived from the 50 realizations were compared to nominal precipitation rates (e.g., Fig. 1).   As evidenced in Fig. 1 the precipitation rates derived from observations subject to random error are highly correlated to those derived from nominal observations. Moreover, the systematic differences are relatively small, i.e. the retrievals from noisy observations are generally within 4% of the retrievals from nominal observations. Even in conditions of random errors larger than those considered here, propagation of the random error through the DPR retrievals are not likely to be biased because systematic differences from the nominal retrievals can be rigorously assessed and corrected through Monte Carlo procedures such as the one described herein. Moreover, filtering of errors due to noise can be achieved through inclusion of climatologic information into the retrieval functional (Grecu and Anagnostou 2006) and strategies to mitigate gain/losses variations can be incorporated into retrieval algorithms (Marzoug et al. 1994).
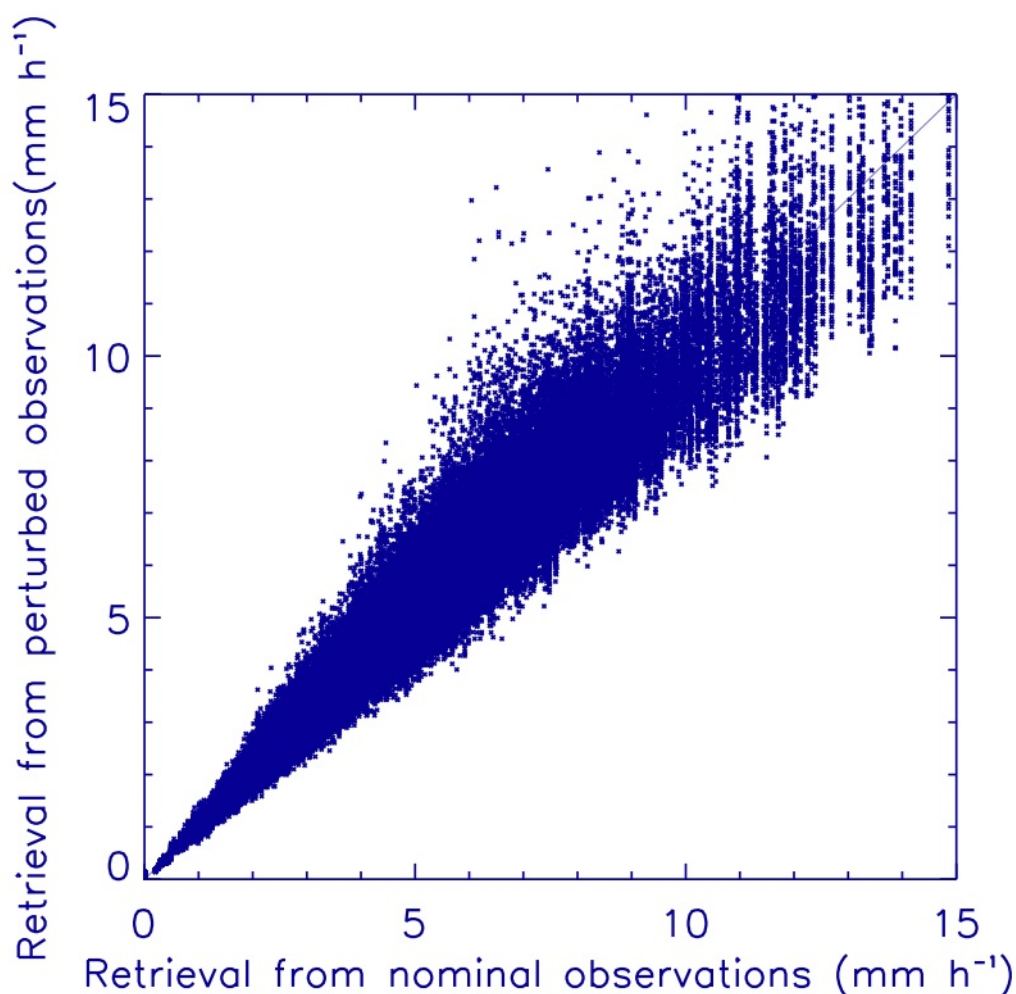

Fig. 1. Scatterplot of precipitation retrieved from nominal APR-2 observations vs. that corrupted with random noise.

The retrieval algorithm used in this experiment is based on a least square approach.   The retrieved DSD are expressed as a function two parameters, i.e. the mean drop size diameter and

the total drop concentration. A gradient-based iterative procedure is used to retrieve vertical profiles of mean drop sizes and total drop concentrations by minimizing a weighted sum of squared differences between model predicted attenuated reflectivities and observed reflectivities. The information from surface return estimates of path integrated attenuation (PIA) is incorporated into retrieval by adding weighted squared differences between model predicted and surface estimated PIAs to the reflectivity functional. That is, the following functional

$$F = \frac{1}{2}\left(Z_{13}(N,D) - Z_{13}^{ob}\right)^{T} W_{13}^{-1}\left(Z_{13}(N,D) - Z_{13}^{ob}\right) + \frac{1}{2}\left(Z_{35}(N,D) - Z_{35}^{ob}\right)^{T} W_{35}^{-1}\left(Z_{35}(N,D) - Z_{35}^{ob}\right) +$$

$$\frac{1}{2}\left(PIA(N,D) - PIA_{SRT}\right)^{T} W_{PIA}^{-1}\left(PIA(N,D) - PIA_{SRT}\right)$$

is minimized as a function of $\mathbf{N, D}$, where $\mathbf{N, D}$ are the total drop concetration and mean diameter profiles. $\mathbf{Z(N,D)}$ and $\mathbf{PIA(N,D)}$ are model predicted reflectivities and PIAs while $\mathbf{W}$ are uncertainty matrices (set to $1dBZ^2$ for reflectivities and $1.0dB^2$ for PIAs). The functional minimization is achieved through the procedure described in Grecu and Anagnostou (2002). When Ka band observations are not available, $\mathbf{N}$ is parameterized vertically as a function of a single variable (Grecu and Anagnostou, 2002). This makes the least square approach fully consistent with the Hitschfeld-Bordan formulation used by the 2A25 algorithm.

3. Bias and Random Error Results

One can take Figure 1 and restate the data in terms of bias (Figure 2a) and random error (Figure 2b) resulting from errors in the radar reflectivities alone. Figure 2a shows relative biases between retrievals from noisy observations and retrievals from nominal observations as a function of rain rate. Note that these biases are generally small for all rain rates. However, for both small and large rain rates, the number of points involved in the analysis is small, see Figure 3, which may affect the representativeness of the results. Figure 2b shows the relative standard deviation (or random error) of differences between retrievals from erroneous observations and retrievals from nominal observations as a function of rain rate. It is apparent from Figure 2 that the biases and random errors as contributed from the instrument reflectivity errors described above are small. Comparisons between GV and PR retrievals at PR resolution exhibit standard deviations significantly larger than those in Fig. 2b (see Appendix J). It should be emphasized that the results in Figs. 1 and 2 are derived for retrievals at PR-2 resolution (600 meters horizontal resolution). Although evaluation of these results at $0.5^0x0.5^0$ resolution is impossible due to limited amount of data available (all APR-2 data ever collected would not fill more than a few $0.5^0x0.5^0$ grid boxes), it is expected that at such resolution the standard deviations, scaled by the ratio of grid box lengths raised to the 0.7 power, would be even smaller (Steiner et al. 2003, also SIP Appendix J).
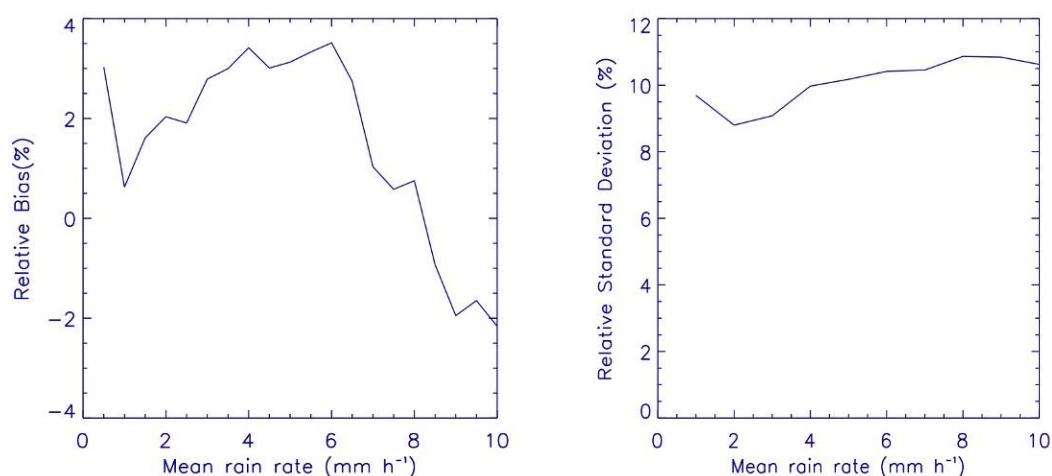
Figure 2: (a) Relative biases as a function of rain rate, (b) relative standard deviations (random error) as a function of rain rate.
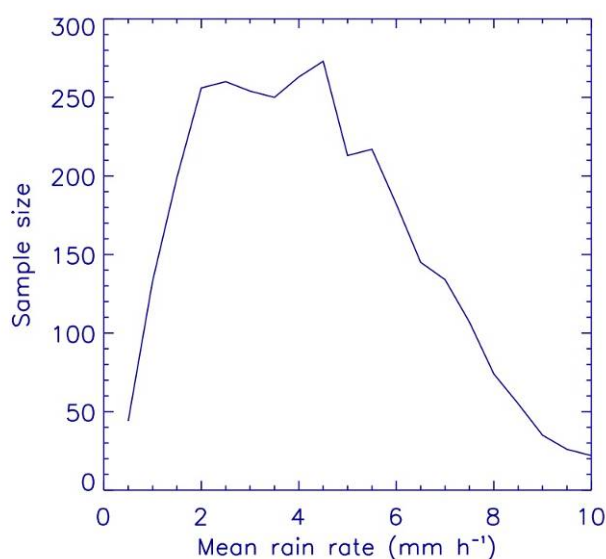
Figure 3: Sample size (number of points involved in the statistical analysis) as a function of rain rate. Smaller sample sizes affect the representativeness of the results.

4. Concluding Remarks

The study shows that the random error and bias associated with errors in DPR reflectivities are expected to be small relative to the overall bias and random error requirements for GPM. For aircraft data at a 600 meter horizontal resolution, the bias ranges from -2 to 4% over the rain rate range of 0.5 mm/hr to 10 mm/hr, while the random error is approximately 10% over the same rain rate range. When upscaled to 50 km using the rain variability model Steiner et al. (2003), the

random error reduces to the order of 0.5%, which is much smaller than errors from other sources (e.g., the retrieval algorithm and ground based measurements).

References

Grecu, M., and E.N. Anagnostou, 2002: Use of Passive Microwave Observations in a Radar Rainfall-Profiling Algorithm. *J. Appl. Meteor.*, **41**, 702–715.

Kozu, T., T. Kawanishi, H. Kuroiwa, M. Kojima, K. Oikawa, H. Kumagai, K. Okamoto, M. Okumura, H. Nakatsuka and K. Nishikawa, 2001: Development of precipitation radar onboard the tropical rainfall measuring mission (TRMM) satellite. *IEEE Geosci. Remote Sens.*, **39**, (1), 102-116.

Marzoug, M., and P. Amayenc, 1994: A Class of Single- and Dual-Frequency Algorithms for Rain-Rate Profiling from a Spaceborne Radar. Pad I: Principle and Tests from Numerical Simulations. *J. Atmos. Oceanic Technol.*, **11**, 1480–1506.

Steiner, M., T. L. Bell, Y. Zhang, and E. F. Wood, 2003: Comparison of two methods for estimating the sampling-related uncertainty of satellite rainfall averages based on a large radar dataset. *J. Climate*, **16**, 3759-3778.

Appendix L. Comparison of AMSR-E and Operational Radar Rain Rate in Western Europe

Chris Kidd (Univ. of Birmingham, U.K.)
Summarized by George Huffman (SSAI; NASA/GSFC)
25 November 2009

Precipitation estimates computed from AMSR-E data with a recent version of the Goddard Profiling Algorithm (GPROF) at the National Snow and Ice Data Center (NSIDC) were compared to the operational radar network in Western Europe. Nearest-time radar data were matched to satellite overpasses for 2005-2009 and accumulated to a 50-km grid.

Total	**0.4158**
U.K. & Ireland	0.3424
France	0.3956
Germany	0.4271
Atlantic	0.8033
North Sea	0.8370

Table 1. Bias ratio, computed as [satellite/radar]. In general the satellite underestimates precipitation compared to the radar, with relatively good performance over ocean, and the worst performance in the cold season over land.
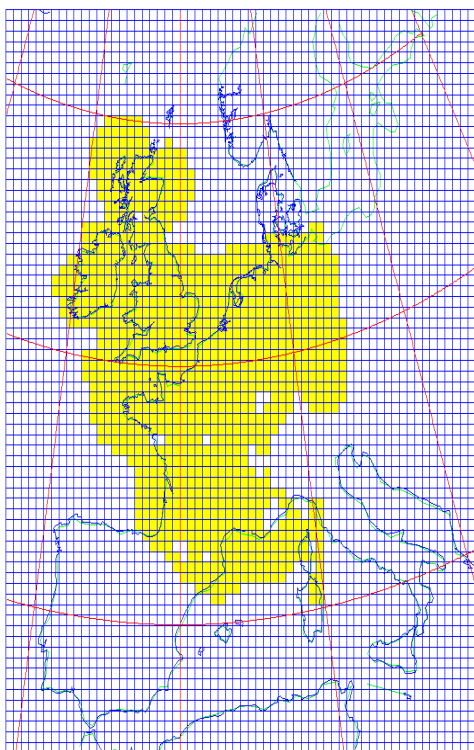

Figure 1. Region of coverage. The yellow-highlighted area shows the detailed extent of radar coverage. The outer reaches of the radar coverage and coastal satellite estimates are considered unreliable and are not included in the statistics.

RR (mm/h)	MAM samples	All	Land	Ocean	JJA samples	All	Land	Ocean
0	10926	0.14	0.34	0.18	10160	0.18	0.63	0.22
1	1685	0.99	1.64	0.92	2012	0.98	2.51	0.96
2	505	0.95	1.47	0.72	623	0.86	1.91	0.69
3	199	0.92	1.18	0.75	299	0.82	1.63	0.68
4	77	0.93	1.10	0.81	153	0.85	1.37	0.73
5	57	0.91	1.26	0.75	87	0.87	1.28	0.75
6	22	0.92	0.79	0.80	53	0.82	1.36	0.82
7	20	0.97	1.00	0.95	38	0.84	1.03	0.84
8	14	0.96	0.82	1.00	25	0.83	0.88	0.73
9	13	0.85	0.97	1.00	20	0.89	0.71	0.87
10	4	0.95	0.77	0.89	12	0.86	0.84	

RR (mm/h)	SON samples	All	Land	Ocean	DJF samples	All	Land	Ocean
0	9910	0.15	0.28	0.24	10223	0.13	0.09	0.21
1	1849	0.98	1.55	0.95	1601	1.01	1.04	0.94
2	474	0.90	1.29	0.72	410	0.97	1.00	0.75
3	186	0.88	1.21	0.71	146	0.97	0.99	0.75
4	87	0.89	1.00	0.73	45	0.98	0.99	0.78
5	44	0.92	0.89	0.88	30	0.99	0.97	0.81
6	25	0.91	0.87	0.93	24	0.99	1.00	0.67
7	20	0.93	1.06	0.74	9	0.97	1.00	0.82
8	21	0.90	0.85		8	1.00	1.00	0.81
9	8	0.93	0.71	0.92	2	0.99	1.00	0.92
10	4	0.97	0.72	0.83	3	1.00		0.82

Table 2. Bias-corrected normalized Root-Mean-Square Error (RMSE) by rainrate and surface type. Given the relatively large bias over land, we choose to display the RMSE about the de-biased satellite mean, and divide by the rainrate bin average to get a relative error. These results show that the standard deviations range from 100 to 250% at 1 mm/h. Results for rainrates higher than 2 mm/hr are only qualitative, since the number of samples is so small.

This analysis must be considered a preliminary assessment of the current state of the art. On the radar side, the radars included are operational and suffer the usual drop-outs and operational expediencies. Planned GPM GV activities will focus on research radars. On the satellite side, the GPROF algorithm used in this study was developed for use in tropical and subtropical regions. The underlying database lacks any real representation of cold-season precipitation systems. The forthcoming GPROF-2008 will take a step forward in improving this situation, but is only now being implemented. The real advance will come after the launch of GPM, when the GMI and DPR data will be used to populate the database, even as GPROF-2008 is doing now with TRMM TMI and PR case.

Appendix M: Algorithm Readiness Test Plan for PPS Delivery

Joe Munchak (ESSIC)
with Robert Meneghini, William Olson, and Chris Kummerow
September 2011

1.0 Introduction

The Radar, Combined, and Radiometer Level 2 algorithms being developed by the algorithm teams will require acceptance testing both before and after delivery to the Precipitation Processing System (PPS). This document reports the testing plans for each PPS delivery (V1; November 2011 and V2; November 2012) and algorithm (radar, combined, radiometer). Testing plans include datasets used to validate the algorithm, tests performed, and measures of success/checklists of performance requirements.

This section focuses on GPM pre-launch algorithm testing. While there will be ongoing post-launch evaluation of GPM DPR and GMI products resulting from the delivered algorithms (and updated post-launch versions), this section's priority is to ensure that test plans for pre-launch algorithm code delivery are adequate to demonstrate that all components of the algorithms are present, working, and meet basic scientific standards based on TRMM results and GPM requirements. Post-launch testing will focus more on incremental adjustments to the algorithm code, databases, and a priori information to further improve scientific aspects of the precipitation products and will be reported independently of this document.

1.1 Algorithm Requirements

In general, algorithm deliveries for November 2011 (V1) should be running (Baseline) code with all routines and databases included (though some subroutines may be stubs), have all output parameters in the products, use the PPS toolkit, and include algorithm team testing data input and output. Valid (non-missing) output is expected for the majority of a given synthetic GPM orbit. Additionally, the expectation is that the November 2011 codes should perform as least as well as TRMM in the tropics/subtropics and as well as currently possible at higher latitudes.

The November 2012 algorithm (V2/At-Launch) codes should be complete with scientific code and a priori databases. They should demonstrate enhanced performance relative to TRMM under conditions where such performance is possible and produce valid output over all regions (100%) of the GPM core orbit.

1.2 Test Data

In terms of inputs required for algorithm testing, we define (1) *GV* inputs as ground validation measurements from ground or aircraft sensors, (2) *simulation* inputs as those based on CRM models processed through a satellite simulator, and (3) *synthetic* inputs as those from current satellite sensors remapped into the GPM L1 products for use in these L2 algorithm algorithms.

GV data provides actual precipitation measurements at the ground level and some vertical structure (either from in-situ aircraft measurements or high-resolution multi-parameter radar measurements) at specified locations for specified precipitation events. These GV measurements can be collected over time and matched to coincident satellite overpasses to validate the algorithm when GPM-like satellite data is available pre-launch.

The simulation input datasets allow for complete internal consistency between model precipitation profiles and simulated GPM L1 products, but have the drawback that the physics within the models and satellite simulator may not be fully representative of the Earth's precipitation and radiative transfer physics. The satellite simulator team (led by Toshi Matsui) is in various stages of developing and validating simulations from the C3VP, LPVEx , TWP-ICE, MC3E field experiments and a winter storm over California. These simulations use the WRF and GCE models with the spectral-bin microphysics (SBM) scheme developed by Tao's group. In addition, global (Goddard MMF) simulations with GCE embedded within GEOS-5 are being run for 2008.

The synthetic data have the advantage of being actual satellite data, but will require some modeling of additional channels or merging of multiple satellite data since no single satellite has all the radar and radiometer channels of the GPM core satellite.

As described herein, each algorithm team has decided to use different input datasets for pre-PPS delivery testing of their algorithm. These different inputs will be used in initial PPS post-delivery tests to ensure that no coding errors have been introduced in the algorithm team-to-PPS transition, however common datasets will also be used post-delivery to assess code performance with sample GPM L1 inputs.

1.3 Summary

In this document in sections 2-4, we discuss the individual algorithm team testing plans to include input testing datasets, tests to be performed, and measures of success, prior to PPS delivery. After each algorithm delivery to PPS, PPS undergoes it's own process of validating the algorithm code with both algorithm team-provided test data and common input datasets. The PPS testing process is described in Section 5, followed by a summary.

2.0 Radar Testing Plan

The Japanese will be the primary algorithm developers for the DPR radar algorithms, which will retrieve precipitation profiles using Ku-only, Ka-only, and Ku+Ka-band data from DPR. In contrast to TRMM, the DPR radar algorithms are modular (Figure 2.1). The US PMM radar lead has the responsibility to deliver the surface reference technique (SRT) code and to investigate experimental algorithms that can supplement or provide alternatives to the standard algorithms. The remaining modules are being developed by the Japanese GPM PIs.

Framework of DPR L2 Algorithm

- Preparatio
- Vert.
- Classificati
- SRT
- DSD
- Solver

Echo Power (L1)
GANAL
Rain/no-
σ^0
Z
T. W Clou
σ^0 Z
Tv Brigh
PIA
pha k-Z
N(D) V(D) ρ
Scatt
PIA Z D
Precinitation
Precinitation

Figure 2.1: Flow chart of DPR Level 2 algorithms with modules indicated. Courtesy of T. Iguchi, NICT.

2.1 November 2011

2.2 Input Testing Datasets 2011

Three types of test data are being created at JAXA to test the DPR algorithms. The first type is simulated data from simple assumptions (e.g., Qr = 0.2(g/kg) below 4km, and Qr=0 above 4km) with random noise and known properties of ocean surface scattering. The second type is synthetic DPR data generated from TRMM. One month (July 2001) of this data has been created. The Ka-band reflectivities were simulated from DSD estimates by the TRMM/PR standard algorithm. No measurement error, noise, clutter effects were simulated. The third type is simulated data from numerical models. Alternative datasets (aircraft-, TRMM-, and model-based) are being created by US members of the PMM team and may be considered for future testing.

2.3 Tests 2011

Testing is done at the module level before the code is integrated. The integrated code is then tested. Testing at both levels uses the datasets described above, where appropriate.

2.4 Measures of Success 2011

The primary performance metric of the integrated code is that it performs comparably to TRMM in the tropics. This can be demonstrated most directly with the results of tests performed using

the DPR data simulated from TRMM PR output. With the same DSD and vertical model assumptions, the DPR algorithm output is to match the TRMM PR output in terms of rain rate.

2.5 November 2012
2.6 Input Testing Datasets
Because a requirement for this version of the code is that performance exceeds TRMM when possible, synthetic data with realistic assumptions is required to demonstrate that errors and biases are within the limits specified by GPM Project criteria (the ability to retrieve rain rates between 0.2 and 110 mm/hr with error and bias less than 25-50% for rain rates between 1 and 10 mm/hr and to detect snowfall at 5km resolution). Therefore, input testing datasets based on numerical simulations as well as Ka-band data synthesized from PR data with alternate DSD assumptions will be a focus of testing for this version.

2.7 Tests 2012
Same as 2.1.2, but for the following three situations:
1. Ku band only (outer swath)
2. Ku+Ka band
3. Ka band only (high sensitivity mode)

2.8 Measures of Success 2012
1. Ku band algorithm shows same performance as TRMM.
2. Dual-frequency algorithm better than Ku-only relative to validation (simulated or APR2 aircraft data with GV).
3. High-sensitivity Ka-band algorithm provides valid (non-missing) output in cold environments/frozen precipitation.

3.0 Combined Testing Plan

First it is expected that the ultimate combined (radar+radiometer) algorithm will have the following characteristics-
 • reasonably complete and accurate physics representation
 • to the extent known, parameter *a priori* information properly represented
 • instrument characteristics properly represented
 • a robust, modular inversion method
 • operates within PPS framework and computational constraints
 • estimates the precipitation profile (PSD parameters), environmental parameters, and uncertainties of these quantities.

The algorithm advancements beyond TRMM include the additional channels on the DPR and GMI, along with new algorithm mechanics. This means testing will need to focus on the performance of the new algorithm along with the use of the new channel sets and additional information they provide beyond those used in TRMM.

3.1 November 2011

3.2 Input Testing Datasets 2011

The primary source of test data will be existing TRMM orbits. These will be carefully selected to include mid-latitude cold season precipitation as well as the tropics and subtropics to ensure adequate performance in environments that GPM will sample. Simulated data will be used if available, but are not required to meet the objectives for this deadline.

In addition to comparisons with existing TRMM products (2A25 and 2B31), comparisons with the TRMM Ground Validation sites at Kwajalein and Melbourne may also be used for validation of the combined algorithm.

3.3 Tests 2011
The beta version of the combined algorithm code has been run on the following cases from TRMM:
1. Hurricane
2. Shallow convection
3. Mid-latitude cold front

3.4 Metrics for success 2011
Absent direct validation, it is expected that the new code perform comparably to V7 2A25 and 2B31 products in the tropical test cases, and perform similarly or better than these products relative to well-calibrated ground validation.

The sensitivity of the algorithm to initial assumptions can also be used as a performance metric in the absence of direct validation. It has been demonstrated that the combined algorithm always reduces the bias relative to Ku-band radar only solutions when a biased initial assumption of the DSD parameter N_w is assumed (Figure 3.1).
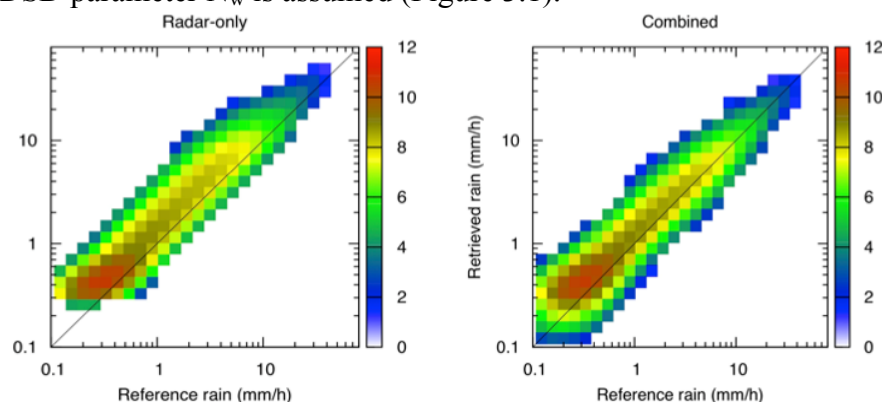

Figure 3.1: Combined retrievals with positive bias in initial N_w
Ku-only 43% bias; 41% rms
Ku+TMI 18% bias; 14% rms

3.5 November 2012
3.6 Input Testing Datasets
Regarding Nov. 2012, it is hoped that the cloud-resolving simulations will be available next year with most of the bugs worked out such that we can use GPM data simulated from the CRMs to provide a testbed. The less favorable alternatives are to continue to use augmented TRMM

observations or ground-based radar reconstructions of precipitation fields (at higher latitudes) to provide testbed data.

3.7 Tests 2012
a. Mechanical – test if introduction of GMI frequencies and DPR Ka data causes failure.
Test compatibility with DPR L2 inputs (prep, vertical profile, classification, srt)
Test algorithm with TRMM and CRM data
Test PPS compatibility
b. Performance – using available simulator data or APR2+COSMIR if in-situ GV is also available

3.8 Measures of Success 2012
a. Show that addition of Ka band and/or high frequencies improves precipitation estimates relative to Ku+TMI channels

4.0 Radiometer Testing Plan

The radiometer algorithm team will rely on the Bayesian technique successfully used for many years by TRMM. TRMM's Version 7 algorithms rely on "observational" TRMM-provided Bayesian (a priori) databases that combine the precipitation estimates from the PR and the brightness temperatures from the TMI.

For GMI, the plan is to build similar observational databases. For the at-launch algorithms we will need to rely on TRMM observations in the tropics, and proxy databases using CloudSat, AMSR-E, SSMIS, AMSU-B, and MHS, supplemented with global model simulations. Six months to a year after launch, the GMI algorithm database can start incorporating the combined retrievals in place of the TRMM, CloudSat, etc proxy database. Alternatively, if the algorithm team feels comfortable using DPR Ku-band algorithm (expected to be stable at launch due to TRMM heritage), profiles from the instrument checkout period can be used for the release of post-launch algorithm versions.

The primary testing issues associated with the radiometer algorithm include: land versus ocean, tropics versus mid and high latitudes, empirical versus physical surface characterizations for the Bayesian database, and extending the GMI retrievals to constellation radiometer partners.

4.1 November 2011

Nov. 2011: Deliver the first full algorithm that ingests various radiometer datasets, ancillary data and produces realistic rain rate distributions from the empirical database. Bayesian retrieval will look in appropriate lat/lon/month grid for database entries. Input and outputs will be binary.

4.2 Input Testing Datasets 2011
Since the same algorithm will be run on constellation radiometers, data from existing imaging radiometers (TMI, AMSR-E, SSMI/S, etc.) can be used as-is for algorithm testing. Since no existing radiometer has all the channels on GMI, synthetic or simulated data will need to be

constructed to test the GMI implementation. Validation of existing satellite and synthetic (coincident overpass-based GMI constructions) will use the following datasets:

Tropical Oceans
- *TRMM & GPROF2010*
- *Kwajalein*

Extra-tropical Oceans
- *Alaska WSR-88*

Tropical Land
- *TRMM*
- *NMQ*

Extra-tropical Land
- *NMQ with snow cover data from NSIDC*
- *AMeDAS*

4.3 Tests 2011

The algorithm components include a classification (database selection) and retrieval step. During the classification step, the sensitivity to the choice of ancillary dataset used (e.g., ECMWF vs. MERRA) needs to be established. Land retrievals will also be a focus of these tests as the GPM code will be substantially different than TRMM V7.

4.4 Measures of Success 2011

For this algorithm delivery to objective is to ensure that rainfall rates are comparable to 2A12 V7 over the tropical oceans, and look reasonable over land/high latitudes.

4.5 November 2012

4.6 Input Testing Datasets 2012

All satellite simulator datasets should be available at this time, and can be used to create synthetic GMI data for testing. Additionally, the sounding radiometer code/databases will be ready for this delivery, so existing and simulated sounding radiometer datasets will be used.

4.7 Tests 2012

Same as 7.7.4.3, but also include sounders. Additional tests with simulated data to establish performance metrics.

4.8 Measures of Success 2012

The various ground validation datasets listed in section 4.1 will be used to demonstrate the following metrics established by the GPM Project:

1. GMI quantifies rain between 0.2 and 60 mm/hr and detect snowfall at effective resolution of 15 km
2. GPM shall have bias of less than 25-50% for rain rates of 1-10 mm/hr at 50km resolution
3. GPM shall have random errors less than 25-50% for rain rain rates of 1-10 mm/hr at 50km resolution

5.0 PPS Testing Procedure

PPS's perspective is that for the November 2011 (V1) deliveries the algorithm code should have the following characteristics:
- Running code with the bulk of the science retrieval, but changes may still be made.
- All routines included, although some subroutines are allowed to be stubs.
- Use of PPS Toolkit for input and output using GPM formats
- Output products contain all parameters although some may not be filled.

This November 2011 code is used for input/output testing, format verification, flow testing, and limited end-to-end testing.

For the November 2012 (V2) deliveries, the code will be full algorithms with all science code, reading and writing GPM product formats and utilizing all ancillary data. This code is used for end-to-end testing, mission simulations, and performance testing.

The At-launch (V3) code delivered in Jan 2013 (and so not undistinguished from the Nov 2012 code in the text above), fixes major bugs in the 2012 delivered code, has no changes in science, and is used in the PPS Operational Acceptance Testing (OAT). OAT is a 90-day period during which end-to-end testing of At-launch code will be done. This will require 30+ days of unique orbits that will be generated from simulated data. Scans within orbits need to be unique as long as precipitation coverage is realistic.

When code is delivered to PPS, the package should include the code, input data, and output products. To verify the code in the PPS system, PPS will compare PPS generated results (output products) with algorithm developer submitted output products. PPS may end up converting some types of code into a common (FORTRAN) version.

6.0 Summary

November 2011 PPS Code Delivery
Requirement: Equivalent performance to TRMM in tropics, and existing products (e.g. AMSR-E) in high latitudes

	Radar	**Radiometer**	**Combined**
Datasets	-Simple synthetic -TRMM (PR)	-TMI (as-is or with synthetic high frequencies) -AMSR-E, SSMIS (high latitude)	-Awaiting Toshi's simulations [5] -TRMM as-is
Testing	-Module-level -Full algorithm on TRMM orbit subsets	-TRMM: Compare to TRMM V7 -Others: compare to QPE products	-Compare to 2A25 and 2B31 -Compare to TRMM GV data (Melbourne/Kwaj)

---

[5] Expected availability of synthetic datasets (January 2012)

November 2012 PPS Code Delivery
Requirement: Superior performance to TRMM in tropics when possible, and existing products (e.g. AMSR-E) in high latitudes, over land

	Radar	**Radiometer**	**Combined**
Datasets	-APR2 (aircraft) -Simulator	-TMI (as-is or with synthetic high frequencies) -AMSR-E, SSMIS (high latitude), sounders (AMSU-B/MHS/AMPR)	-Simulator
Testing	-Module-level on APR2 data -Full algorithm on TRMM orbit subsets and simulator "truth"	-TRMM: Compare to TRMM V7 -High latitudes/land: compare to QPE products	-Compare to simulator "truth" -Validate microphysics with synthetic datasets -Establish information content of GMI channels